University of Southampton

Faculty of Medicine

Clinical and Experimental Sciences

Optical Coherence Tomography Imaging and Quantification of Corneal Inflammation

Aristides Konstantopoulos MBChB MSc FRCOphth

Thesis for the degree of Doctor of Philosophy

May 2016

UNIVERSITY OF SOUTHAMPTON

ABSTRACT

FACULTY OF MEDICINE
Clinical and Experimental Sciences

Doctor of Philosophy

OPTICAL COHERENCE TOMOGRAPHY IMAGING AND QUANTIFICATION OF CORNEAL INFLAMMATION

by Aristides Konstantopoulos

Infection and inflammation of the cornea are common clinical presentations that are potentially blinding. Evaluation of the presenting condition and assessment of the treatment response are subjective and rely greatly on examiner experience. In-vivo quantification of the extent of ocular surface inflammation could lead to objective criteria for diagnosis and monitoring of infective and inflammatory conditions of the cornea. It could also transform research on the treatment or prevention of these conditions.

In this thesis, the capabilities of Anterior Segment Optical Coherence Tomography (AS-OCT) as an imaging and quantification modality in ocular surface inflammation and infection are investigated. AS-OCT is applied to research on prevention, diagnosis and monitoring of bacterial keratitis; the in-vivo quantification findings are verified with laboratory investigations, including cytokine quantification, immunohistochemistry and bacterial counts.

This work has shown that a range of AS-OCT parameters, including corneal thickness, infiltrate thickness and infiltrate width, can be used for quantitative objective assessment of patients with bacterial keratitis. Greater corneal parameters of acute inflammation in Gram-ve compared to Gram+ve infection at presentation, specifically corneal thickness and infiltrate thickness, are indicative of Gram-ve keratitis. A reduction in these AS-OCT parameters between presentation and day 3 of treatment is identified as a criterion that indicates a successful treatment response. Finally, AS-OCT quantification of acute corneal inflammation in an animal study has shown that current bacterial keratitis prophylaxis strategies following keratoprosthesis surgery may not be effective.

CONTENTS

LIST OF FIGURES

LIST OF TABLES

PUBLICATIONS ARISING DURING THIS PhD WORK

Konstantopoulos A, Kuo J, Anderson DF and Hossain PN. Assessment of the use of anterior segment optical coherence tomography in microbial keratitis. Am J Ophthalmol 2008; 146:534-542.

Konstantopoulos A and Hossain PN. Limitations of Fourier Domain OCT. J Cataract and Refractive Surgery 2010; 36:534.

Konstantopoulos A, Yadegarfar G, Fievez M, Anderson D, Hossain P. In-vivo quantification of bacterial keratitis with optical coherence tomography. Invest Ophthalmol Vis Sci 2011; 52:1093–1097.

Konstantopoulos A, Yadegardar M, Yadegarfar G, Stinghe A, Macleod A, Jacob A, Hossain P. Deep sclerectomy versus trabeculectomy: a morphological study with anterior segment optical coherence tomography. Br J Ophthalmol 2013;97:708-14.

Konstantopoulos A, Tan XW, Goh GT, Saraswathi P, Chen L, Nyein CL, Zhou L, Beuerman R, Tan DT, Mehta J. Prophylactic Vancomycin Drops Reduce the Severity of Early Bacterial Keratitis in Keratoprosthesis. PLoS One. 2015;10(10):e0139653. doi: 10.1371/journal.pone.0139653.

Ang M, Konstantopoulos A, Goh G, Htoon HM, Seah X, Lwin NC, Liu X, Chen S, Liu L, Mehta JS. Evaluation of a Micro-Optical Coherence Tomography for the Corneal Endothelium in an Animal Model. Sci Rep. 2016 Jul 15;6:29769. doi: 10.1038/srep29769.

STATEMENT OF ORIGINALITY

The work presented in the thesis was carried out by me. During this PhD the help of experts was enlisted for specific laboratory techniques, as detailed below.

- Jonathan Ward and Clair Barber of the University of Southampton assisted in preparation and reading of cytospin slides.
- Liyan Chen of the Singapore Eye Research Institute carried out the liquid chromatography - mass spectrometry, as detailed in chapter 6.

ACKNOWLEDGEMENTS

It is my pleasure to thank everyone who helped me during the years of this tortuous long journey.

Associate Professor Parwez Hossain has been of great influence in my career and research development over the past decade. He has provided enormous support, guidance and enthusiasm! He has not only been an excellent supervisor for this work, he has also become a good friend and colleague. I would also like to thank Professor Andrew Lotery for his soft kind words of encouragement and motivation at difficult times.

Associate Professor Jod Mehta supervised my research and clinical fellowship in Singapore. He provided a homely feeling during my studies abroad and became a good friend. He was extremely generous with his support and time, both at work and socially. I would like to thank all the laboratory staff at Singapore Eye Research Institute, particularly Gwen and Chan, who helped me achieve so much during my visit.

I would like to thank my family and friends who have put up with my selfish and anti-social behaviour during my clinical and research training over the past decade. Finally and most importantly I would like to recognise the contribution of my wife, Marina, towards this work. She not only assisted in recruitment and follow-up of patients, but also provided the conditions that enabled me to concentrate on carrying out and writing-up this work!

LIST OF ABBREVIATIONS

AC	anterior chamber
ANOVA	analysis of variance
AS-OCT	anterior segment optical coherence tomography
BK	bacterial keratitis
CT	corneal thickness
CTS	corneal tissue swelling
CTL	corneal tissue loss
CV	coefficient of variation
DSEK	Descemets stripping endothelial keratoplasty
ED	epithelial defect
FD-OCT	fourier-domain optical coherence tomography
GM-CSF	granulocyte macrophage colony stimulating factor
Gram+ve	Gram positive
Gram-ve	Gram negative
GT	graft thickness
H&E	haematoxylin and eosin
ICC	intra-class correlation coefficient
ID	infiltrate diameter
IFN	interferon
IT	infiltrate thickness
IVCM	in-vivo confocal microscopy
IW	infiltrate width
Kpro	keratoprosthesis
LC-MS	liquid chromatography – mass spectrometry
LPS	lipopolysaccharide
MHC	major histocompatibility complex

MIC	minimum inhibitory concentration
MMPs	matrix metalloproteinases
MSD	Meso Scale Discovery
MyD88	myeloid differentiation primary response 88
NLRP	nucleotide-binding oligomerization domain, leucine rich repeat and pyrin domain containing
NPV	negative predictive value
PAMPs	pathogen associated molecular patterns
PBS	phosphate buffer solution
PCR	polymerase chain reaction
PG	peptidoglycan
PMNs	polymorphonuclear neutrophils
PPV	positive predictive value
PUK	peripheral ulcerative keratitis
RA	rheumatoid arthritis
SAS	Statistical Analysis Software
SCUT	steroids for corneal ulcers trials
SL-OCT	slit-lamp optical coherence tomography
SLP	slit-lamp photography
SPSS	Statistical Package for Social Sciences
Sw	standard deviation of absolute difference
TD-OCT	time-domain optical coherence tomography
TLR	toll-like receptor
TNF	tumour necrosis factor
TRIF	toll/interleukin-1 receptor-domain-containing adapter-inducing interferon-β
VA	visual acuity

1. Introduction

1.1 Prologue

Corneal infection and inflammatory disorders are significant causes of global visual impairment and blindness.[1] According to the World Health Organisation, corneal disease predominantly in association with infection and scarring is a major cause of blindness in the world, second only to cataract.[2] In the United Kingdom, bacterial keratitis (BK) is a frequent and serious corneal infection; it is estimated that at least 4000 cases per year may develop in contact lens wearers.[3,4] The infection combined with the host immune response contribute to ulceration, tissue melting and scarring of the cornea with poor vision as a consequence.[5,6]

Clinical assessment of corneal infection and inflammation is difficult and relies greatly on the experience of the examining clinician, especially regarding the depth and extent of pathology. Evaluation of the response to treatment is also subjective and is traditionally carried out by serial measurement of the epithelial defect dimensions on the slit-lamp,[7] and less commonly with the aid of serial anterior segment photography. Objective clinical grading and quantification of the extent of corneal inflammation and infection is currently not possible, and thus not part of routine clinical assessment.

Animal research studies that require quantification of corneal infection use a semi-quantitative grading system that is based on assessment of slit-lamp features, such as conjunctival injection, conjunctival chemosis, corneal oedema and corneal infiltration.[8,9] Similar to patient examination, assessment of these features is subjective. Objective assessment and quantification of the state of the cornea in BK, or any inflammatory condition, with a suitable imaging modality may assist the initial examination at patient presentation and also the monitoring of the response to treatment.

Current understanding of the clinical profile and inflammatory response during the course of human BK is lacking, due to poor in-vivo quantification methodologies and inherent limitations in obtaining corneal specimens for serial study. Improvements in imaging technology may facilitate the in-vivo

study of the human condition and improve our understanding of its clinical course and inflammatory response. This may lead to improved treatment protocols and better outcomes for patients with corneal infection and other ocular surface inflammatory conditions.

New anterior segment imaging devices aim to overcome current limitations and improve our diagnostic and research capabilities. New modalities include rotating Scheimpflug imaging, such as the Pentacam® (Oculus Inc, Lynnwood, WA, USA), and Anterior Segment Optical Coherence Tomography (AS-OCT), such as the Visante® OCT (Carl Zeiss Meditec Inc, Dublin, CA, USA,) and Slit-lamp OCT (SL-OCT™, Heidelberg Engineering GmbH, Heidelberg, Germany). They provide more quantitative information and, particularly AS-OCT, a novel perspective in corneal and anterior segment imaging.

AS-OCT produces high-resolution cross-sectional images of the cornea, making it a promising modality for imaging corneal anatomy and pathology. It has been used to analyze the architecture of clear corneal incisions following cataract surgery and to assess the depth of intrastromal corneal rings in keratoconic eyes.[10,11] The imaging capabilities displayed in these early studies suggest that AS-OCT has the potential to provide objective assessment and quantification of corneal infection and inflammation. Due to the non-contact nature of examination and ease of scanning, it may be the ideal imaging modality for evaluating and monitoring infection and inflammation of the cornea and ocular surface.

The aim of this research thesis is to evaluate the imaging capabilities, quantification capabilities, and clinical and research application of AS-OCT in ocular surface inflammation and corneal infection.

1.2 Corneal and conjunctival anatomy

1.2.1 Gross anatomy of the ocular surface

The human eye is spherical in shape and approximately 25mm in diameter. It sits within a pyramidal bony socket of the skull, the orbit. It contains structures that convert light energy from the external environment to a nerve impulse that is transmitted via the optic nerve to the brain where vision is perceived. The wall of the eye consists of segments of two spheres, an anterior smaller sphere that is the cornea and a posterior larger sphere that is the sclera. The two sphere segments meet at a junction called the limbus.

The cornea is the transparent, most anterior structure of the eye. Transparency is its most important property. The cornea provides two thirds of the refractive power of the eye, on average 43 dioptres, and the lens 21 dioptres on average.[12] The human cornea is approximately 520 μm thick in the centre and becomes progressively thicker towards the periphery. The anterior surface has on average a radius of curvature of 0.78 mm and the posterior surface a curvature of 0.64.[13] The horizontal dimension of the cornea is larger than the vertical dimension. Externally, the horizontal axis measures 11.7 mm and the vertical axis 10.6 mm.[14]

The external eye consists not only of the cornea but also of the conjunctiva and eyelids. The cornea and the conjunctiva form the ocular surface that is in contact with the external environment. Due to its location, the ocular surface is vulnerable to exogenous infection and trauma. Although conjunctival infection is common, it is only occasionally sight threatening.[15] On the other hand, infection of the cornea is sight threatening and occasionally may threaten the integrity of the eye.[16,17]

The eyelids provide an important protective role to the ocular surface. With the aid of the eyelashes they form a structural barrier to trauma, and also contribute greatly to the composition of tears. In addition, the blinking effect of the eyelids distributes and spreads the tear film over the ocular surface. There are three distinct populations of glandular cells in the lids and conjunctiva that produce tear components. These are the meibomian glands, the glands of Moll and the glands of Zeis. In addition, two populations of

accessory lacrimal glands are found within the conjunctiva, the glands of Krause and Wolfring. The meibomian glands are sebaceous glands found in the tarsal plate, secreting sebaceous lipid material that forms the anterior layer of the tear film. The glands of Moll are specialised sweat glands that are situated anterior to the lashes; they discharge into the lash follicle.[18] In addition, they produce some lipoprotein. The glands of Zeis are rudimentary sebaceous glands located close to the lid margin and lash follicle.[19]

The tear film is approximately 40 μm in thickness and consists, in a posterior to anterior direction, of the mucin, aqueous and lipid layers. The mucin layer, that is produced by conjunctival goblet cells, the lacrimal glands and epithelial cells of the ocular surface, is in contact with the epithelial surface and predominantly consists of glycoproteins.[20] The aqueous layer is produced by the main lacrimal and accessory glands. The most anterior layer, the lipid layer, stabilizes and prevents excessive evaporation of the aqueous layer. It contains hydrocarbons, sterol esters, wax esters, triglycerols, free cholesterol, free fatty acids and polar acids.

The tear film has multiple important functions. It has significant refractive properties, as the greatest change in refractive index occurs at the interface between air and tear film.[21] The tear film supplies oxygen and other nutrients to the anterior cornea and is responsible for the removal of particulate debris from the ocular surface. It acts as a lubricant, preventing dehydration, desiccation and breakdown of the ocular surface epithelium. It also contains important anti-microbial agents, such as lysozyme, lactoferrin, β-lysin, complement and immunoglobulins, including IgA and IgG.[19] Defensins, specifically the α-defensins (HNP 1–3) and β-defensins (hBD 1–3 and 109), are small proteins in tears that kill invading pathogen; carriers of risk alleles of hBD-1 have been found to exhibit a tendency toward increased susceptibility and severity of contact lens–related keratitis.[22]

The conjunctiva is a thin transparent mucous membrane that is continuous with the cornea at the limbus and the skin at the lid margin. It is reflected off the eye at the superior and inferior fornices onto the inner, tarsal, surface of the eyelids. This layout of the conjunctiva results in formation of the conjunctival sac, when the lids are closed. As discussed above, the conjunctiva

plays an important role in the production of the tear film and in protection of the ocular surface from infection.[23]

The conjunctiva can be divided into three parts, the palpebral, forniceal and bulbar conjunctiva. The palpebral conjunctiva lines the inner surfaces of the eyelids. Via the canaliculi and nasolacrimal duct, it is in communication with the nasal and nasopharyngeal mucosa. A small subtarsal sulcus is present close to the lid margin and this traps and removes debris that is present on the ocular surface. The forniceal conjunctiva lines the upper and lower fornices and is much looser than the palpebral conjunctiva. The bulbar conjunctiva, a continuation of the forniceal conjunctiva, lines the anterior part of the eyeball. It is tightly bound to the globe near the limbus, but becomes looser peripherally. Beneath the bulbar conjunctiva lies the Tenon's capsule or bulbar fascia, a thick fibrous sheath that envelopes the globe.[23]

1.2.2 Ultrastructure of the cornea

The cornea is an avascular structure that traditionally has been described to consist of five layers, the epithelium, Bowman's layer, stroma, Descemet's membrane and endothelium. Recently, a novel sixth pre-Descemet's layer was described.[24]

The corneal epithelium is a stratified squamous non-keratinised epithelium. It consists of 5-6 cell layers and is approximately 50-60 µm thick. The anterior surface of the epithelium displays numerous microvilli and microplicae that interact with and stabilise the mucin layer of the tear film. Desquamating surface epithelial cells are replenished by cells migrating centrally from the limbus and anteriorly from the basal layers of the epithelium.[25] The basal epithelial cells sit on the basal lamina, a basement membrane that is attached to Bowman's layer via anchoring collagen fibrils. The central epithelium is devoid of melanocytes and immunocompetent cells, including major histocompatibility complex (MHC) class II antigen positive dendritic cells (Langerhans cells).

Bowman's layer is an acellular region of the stroma, 8-12 µm thick. The anterior surface is well delineated, while the posterior surface merges with the stroma. The stroma forms the majority of the corneal thickness. It consists of

200-400 layers of collagenous lamellae that are parallel to the corneal surface.[26] The lamellae are highly organised and arranged at 90 degrees orientation to the lamellae above and below. In the anterior third of the stroma the lamellae have a more oblique orientation. The predominant collagen in the stroma is type I, with small amounts of type III, V and VI. The regular spacing of the collagen fibres is of paramount importance to the transparency of the cornea. This is maintained by glycosaminoglycan and proteoglycan bridges between the collagen fibrils. Between the lamellae lie extremely flat, modified fibroblasts, the keratocytes.

Keratocytes are sparsely arranged in the stroma, but form an interconnected cellular network through dendritic processes. Upon injury, they either undergo cell death or lose their quiescence and then transition into a repair phenotype. The repair phenotypes promote regeneration or, alternatively, induce fibrotic scar formation. In corneal injuries where Bowman's membrane is breached and the stroma damaged, keratocytes at the injury site die, but a subpopulation of neighbouring keratocytes transition to a repair or "activated" phenotype, exhibiting morphological characteristics of fibroblasts, and subsequently migrate to the site of injury. The myofibroblast is a subpopulation of activated fibroblasts observed in the corneal stroma following injury. It is found directly within the wound and is responsible for extracellular matrix deposition and organization during corneal repair.[27]

Important resident immune cells, including macrophages, dendritic cells and Langerhans cells, are present in the corneal stroma.[28] The macrophage, a professional phagocyte of the innate immunity and an antigen-presenting cell (APC) of the acquired immunity, is an important cell in the combat of infection. It phagocytoses bacteria, but also phagocytoses and removes apoptotic polymorphonuclear neutrophils (PMNs) that are involved in bacterial clearance.[29] Dendritic cells are potent APCs that are present in the stroma and epithelium of the human cornea, mostly in an undifferentiated state.[30,31] Langerhans cells are a subgroup of dendritic cells that are mostly present in the human corneal epithelium.[32] Both cell types are important in regulating immunogenicity in the corneal environment.[30] They may have a significant role in contact lens associated bacterial keratitis (BK), as contact lens wear may

result in central migration of these cells and priming of the cornea to a more rapid initiation of antigen processing.[28]

Between the stroma and the corneal endothelium lies Descemet's membrane. It is a modified basement membrane of the endothelium, approximately 8-12 µm thick. It consists of an anterior third that is banded and a homogenous posterior two thirds that is not banded. It contains of variety of collagen types, including types IV, V, VI and VIII, glycoproteins and laminin. Descemet's membrane is continuous peripherally with the trabecular meshwork and is thickened at its peripheral termination, the Schwalbe's line, which is also the anterior limit of the trabecular meshwork.[33]

The endothelium is a monolayer of squamous epithelium that forms the most posterior layer of the cornea. The cells are hexagonal or polygonal in shape, similar to the honeycomb of beehives. The cells are 5-6 µm in height and 18-20 µm in diameter. The lateral surfaces are highly interdigitated with tight apical junctional complexes that form a relatively leaky barrier, allowing paracellular percolation of aqueous humour and nutrients into the corneal stroma. The endothelial cells have an active metabolic function, as they have a critical role in pumping fluid out of the stroma and maintaining transparency of the cornea.[33]

1.2.3 Ultrastructure of the conjunctiva

The epithelium of the conjunctiva varies in thickness and morphology depending on location. It is organised into basal, intermediate and superficial cells. Close to the lid margin and at the tarsus it is a stratified squamous non-keratinising epithelium, whereas the bulbar conjunctiva has stratified columnar epithelium. The epithelium of the limbal conjunctiva is stratified squamous non-keratinising. Its basal cell layer houses the corneal epithelial stem cells that are important for regeneration of the corneal epithelium.

Important cells within the epithelium include goblet cells, melanocytes, Langerhans cells and intraepithelial lymphocytes. The goblet cells are mucin-secreting cells that are most numerous in the fornices and plica semilunaris. They secrete the majority of the conjunctival mucins. Although melanocytes

are present in all eyes, the degree of conjunctival melanisation depends on race. The Langerhans cells are MHC II positive dendritic cells that are responsible for trapping and internalising antigens and transporting them to the local lymph nodes where a primary immune response can be induced. Intraepithelial lymphocytes are present in normal conjunctiva, but their number tends to increase in inflammatory conditions.

The conjunctival epithelium sits on an underlying substantia propria. The substantia propria contains numerous immunocompetent cells, such as mast cells, eosinophils, plasma cells and lymphocytes, which may form lymphoid follicles as part of the mucosal-associated lymphoid tissue. It also contains the two accessory lacrimal glands, the glands of Krause and Wolfring, which are responsible for basal tear production.[34]

1.2.4 Comparison of the human and rabbit cornea

The rabbit cornea is thinner than the human cornea, as in the adult rabbit it measures approximately 400 µm in thickness, but has a larger diameter of about 15 mm.[35] Similar to humans, the epithelium is a stratified squamous epithelium that sits on a distinct basement membrane and is 35-40 µm thick. The underlying Bowman's layer is very thin, approximately 3 µm in thickness.[36] Below Bowman's layer lies the stroma that, similar to the human cornea, comprises 90% of the corneal thickness. The stroma consists of collagen fibres that form lamellae in a similar arrangement to humans. Keratocytes are also present between the lamellae. The underlying Descemet's membrane is present in the rabbit cornea and is 8-10 µm thick. The endothelium is the innermost layer and is 3.5-5 µm thick. A hexagonal arrangement is demonstrated by the cells and, in sharp contrast to humans, the endothelial cells retain replicative potential.[37,38] The blink rate of the rabbit eye, estimated at a frequency of 1 blink per 3 - 30 minutes,[39,40] is considerably less than the human rate of 1 blink per 0.02 - 0.17 minutes.[41]

The rabbit cornea has, therefore, wide-ranging similarities with the human cornea. It has been extensively used as an animal model of BK, with the involved pathogens ranging from *Staphylococcus aureus* to *Pseudomonas*

aeruginosa and *Streptococcus pneumoniae*.[42-44] Although higher mammals, such as monkeys, are the closest match to humans,[35] their use is expensive and associated with significant ethical considerations, especially in view of the discomfort associated with the study of corneal infection.

1.3 Inflammation of the conjunctiva and cornea

1.3.1 Conjunctival inflammation

Conjunctivitis, an inflammation of the conjunctiva, is a common condition that presents to general practitioners and ophthalmologists. It is usually a mild condition, a superficial bacterial infection, with no long-term consequences. However, occasionally conjunctivitis can be caused by systemic conditions, such as ocular cicatricial pemphigoid, and lead to conjunctival scarring and ocular surface keratinisation with loss of vision.

Infectious conjunctivitis presents with engorgement of the conjunctival vessels and a mucous or watery discharge. Viruses, usually adenovirus and herpes simplex virus, are the most common cause.[45] They tend to cause an acute inflammatory response and, as a result, patients are very symptomatic with profuse watering, photophobia and lid oedema. Viral conjunctivitis can affect the cornea as well, causing corneal inflammation, known as keratitis. The acutely intensive inflammatory response can lead to scarring of the conjunctiva, known as cicatrisation.

Bacterial infection is the second most frequent cause of conjunctivitis, the most commonly implicated bacteria being staphylococci, streptococci, and especially in children *Haemophilus influenzae*. More pathogenic bacteria, such as *Neisseria gonorrhoeae* and pseudomonas, can also precipitate conjunctivitis. Although the mild and moderate cases are self-limiting with a good prognosis, treatment usually involves antibiotic drops; more pathogenic bacteria require systemic treatment. Aggressive pathogens, such as *Neisseria gonorrhoeae* and *Neisseria meningitides*, can infiltrate deeper to the conjunctiva or even involve the cornea, leading to perforation of the globe. Interestingly, bacteria are also commensals of the conjunctiva; common bacteria are *Staphylococcus epidermidis*, Diphtheroids, *Propionibacterium acnes* and in children streptococcus species.

Chlamydial conjunctivitis is a relatively common bacterial infection, caused by *Chlamydia trachomatis*. In the Western world, chlamydial conjunctivitis is a sexually transmitted condition that affects the genital mucosa and is caused by

Chlamydia trachomatis serotypes D, E, F, G, H, I, J and K. In the developing world, *Chlamydia trachomatis* tends to cause trachoma, the leading cause of infectious blindness worldwide, with serotypes A, B and C. Chlamydial conjunctivitis is a low-grade inflammatory response with symptoms similar to bacterial conjunctivitis. It can also affect the cornea, causing subepithelial and marginal inflammatory infiltrates. Treatment involves systemic antibiotic therapy. In trachoma, a chronic low-grade inflammation is elicited by the chlamydial antigens and by recurrent infection, causing conjunctival scarring with shortening of the conjunctival fornices, entropion, trichiasis and corneal vascularisation with scarring, in progressive order.[46]

Conjunctivitis can be caused by systemic conditions and hypersensitivity reaction. Stevens-Johnson syndrome is a systemic acute vasculitis that causes inflammation and epithelial breakdown of the epidermis, conjunctiva, and mucous membranes of the oropharynx, respiratory system and genitourinary system. It is a potentially fatal condition, as it can lead to sepsis and multi-organ failure. The most common aetiology is a hypersensitivity reaction to a drug, such as aminopenicillins and sulphonamides, and less commonly to infectious agents, such as *Mycoplasma pneumoniae* and cytomegalovirus.[47] Although treatment may include systemic steroids, intravenous immunoglobulins and plasmapheresis, their effectiveness has not been convincingly shown.[48] Conjunctival cicatrisation often develops as a sequela. A similar clinical picture can also develop with ocular cicatricial pemphigoid, a systemic autoimmune condition. This presents less acutely than Stevens-Johnson syndrome, but also causes inflammation of the mucous membranes and bulla formation. Conjunctival scarring develops with gradual plical scarring, shortening of the conjunctival fornices, symblepharon, entropion and keratinisation of the ocular surface.[49]

Non-infectious, less acute, causes of low-grade conjunctivitis can also result in conjunctival scarring. Chronic allergic eye disease, such as atopic keratoconjunctivitis and vernal keratoconjunctivitis, can produce scarring with forniceal shortening, symblepharon and conjunctival keratinisation.[50] Chronic use of topical drugs, particularly glaucoma medication such as dipivefine, timolol and pilocarpine, can produce conjunctival cicatrisation that typically manifests as shortening of the inferior conjunctival fornix. Less commonly,

injuries with chemical agents and radiation can also cause conjunctival scarring.[51,52]

Surgery or trauma involving the conjunctiva, such as squint surgery, pterygium excision and glaucoma filtration surgery, also result in conjunctival inflammation and scarring.[53,54] Filtration surgery is one of the commonest operations involving the conjunctiva; an excess of 4000 trabeculectomy procedures are performed in England per year.[55] Excessive conjunctival scarring at the site of glaucoma filtration surgery is the major cause for poor postoperative intraocular pressure and surgical outcome.[56-58] Aiming to reduce the conjunctival inflammation and scarring, postoperative steroid drops are routinely used for a period of three months.

1.3.2 Corneal inflammation

Corneal inflammation, known as keratitis, can affect all corneal layers and can be categorised by aetiology into infectious and non-infectious. It is generally more serious than conjunctivitis, as it tends to result in more visual disability.

In epithelial inflammation, opaque or semi-opaque lesions develop in the epithelium. Viruses, such as adenovirus, herpes simplex and molluscum contagiosum, are the main cause. Other pathogens, such as the Microsporidia protozoa, can cause inflammation of the epithelium.[59] In its early stages, *Acanthamoeba* infection also affects the epithelial layers causing punctate or pseudo-dendritic epithelial lesions.[60] In allergic eye disease, the epithelium becomes inflamed and breaks down, causing epithelial defects known as shield ulcers.[50] Idiopathic conditions, such as Thygeson's keratitis, can also cause epithelial inflammation.[61] The shape and size of epithelial lesions can vary from small round punctate lesions in microsporidial keratitis to large linear or geographic lesions in herpetic keratitis.

Sub-epithelial inflammatory lesions, usually white and round in appearance, may also be present in combination with the epithelial inflammation. These are often termed infiltrates and can develop in adenovirus, herpetic and *Chlamydia trachomatis* infections. *Acanthamoeba* infection and Thygeson's keratitis can also cause sub-epithelial infiltrates.[61,62] In addition, they can develop as a cell-

mediated hypersensitivity reaction to *Staphylococcus aureus* cell wall antigens.[63]

In stromal keratitis the clinical appearance may depend on the factors triggering and driving the inflammatory response. In acute inflammatory conditions that are associated with a rapid influx of leukocytes, such as in BK, a well-defined white opacity, the infiltrate, tends to develop within the stroma. In less acute and more chronic conditions, a ground glass appearance of cornea develops, known as interstitial keratitis, in which the stroma becomes inflamed but the overlying epithelium does not break down.[64] The most common causes are herpes simplex virus, varicella zoster virus, syphilis, tuberculosis, measles and Lyme disease.[64]

BK tends to present with an acute inflammatory clinical picture; a localised area of inflammatory cell infiltration develops in the stroma below an epithelial defect, in response to bacterial invasion. The cornea also becomes oedematous and, as a result, less transparent than normal.[65] The clinical appearance may be similar in fungal keratitis, although the history is usually sub-acute rather than acute.[66] Mycobacteria can also cause a slowly progressive keratitis with a gradually enlarging stromal infiltration and should be considered in the differential diagnosis of suspected fungal keratitis.[66] *Acanthamoeba* keratitis, caused by the protozoon *Acanthamoeba*, affects the epithelial layers and causes a radial neuritis or perineuritis in the earlier stages, but then progresses to stromal infiltration with a salt-like pattern or ring configuration.[61]

Endothelial inflammation is typically caused by viruses, such as the mumps virus and the herpes family viruses, including herpes simplex virus, varicella zoster virus and cytomegalovirus. Corneal oedema develops in the absence of an epithelial defect or stromal infiltration, but keratic precipitates on the endothelial surface in association with anterior chamber inflammation are present. In cytomegalovirus endotheliitis, coin shaped lesions of keratic precipitates are characteristic of the condition.[67] Endothelial inflammation also occurs in immunologic graft rejection, following either full thickness penetrating keratoplasty or lamellar endothelial keratoplasty; the clinical appearance of the two procedures, however, is different, with a characteristic lack of the Khodadoust immune line in endothelial keratoplasty rejection.[68,69]

Introduction

Rosacea and atopic dermatitis are two relatively common skin conditions that can cause non-infectious corneal inflammation. The cornea can also become inflamed in association with systemic autoimmune conditions. Peripheral ulcerative keratitis (PUK) is a relatively painless inflammatory condition of the cornea and limbus; it is not very common and in association with systemic disease it has been estimated to have a UK annual incidence of 3.01 per million per year.[70] PUK involves epithelial breakdown and ulceration of the peripheral cornea. The stroma becomes thin and the affected area tends to acquire a crescent shape.[71] Inflammatory cell infiltration may not be apparent at clinical level and peri-limbal hyperaemia may be subtle and confined to the area of ulceration. The most common causes are connective tissue disorders and systemic vasculitides, such as rheumatoid arthritis, Wegener's granulomatosis and polyarteritis nodosa.[70,72] A similar crescent-shaped peripheral ulceration may develop in the absence of a systemic condition or local infection, termed Mooren's ulceration. Important features that distinguish it from autoimmune PUK are the presence of ocular pain and the absence of scleral inflammation.[71]

Corneal inflammation that involves the stroma results in scarring and may cause loss of corneal tissue. Scar tissue is less optically transparent than healthy cornea. In addition, the irregularity of the corneal surface caused by the tissue loss and the scar compromise the optical properties of the cornea, therefore limiting vision. The transparency of the cornea relies heavily on the regular diameter of the collagen fibrils and their regular spacing.[26] The healthy cornea is composed predominantly of collagen type I and smaller amounts of types III and V.[73] As part of the regeneration process and scar formation, healthy collagen is replaced by less well-organised type I, III and V collagen, resulting in increased light scattering.[26] In addition, the new collagen fibrils are of greater and more variable diameter, with the presence of empty spaces or 'lakes' amongst them. All these factors contribute to the increased light scattering of corneal scars.[74]

1.4 Bacterial keratitis

1.4.1 Clinical importance

Bacterial keratitis, a potentially serious infection of the cornea, is a significant cause of ocular morbidity worldwide that can cause severe visual loss and blindness. The World Health Organisation estimates that corneal ulceration is responsible for more than two million cases of monocular blindness every year.[2] Bacterial infection is the most common corneal infection in the Western world.[75-77] In the United Kingdom, BK is a frequent presentation and at least 4000 cases in contact lens wearers alone may require hospital treatment per year.[3,4] At the Eye Casualty department of University Hospital Southampton NHS Foundation Trust, more than 1500 attendances per year are experienced due to BK. In the United States, United Kingdom and Australia, it predominantly affects the working age population in association with contact lens wear, ocular surface disease and ocular trauma.[77-80]

Bacterial keratitis is associated with significant ocular morbidity. In a large South of England study of 1786 patients with infectious corneal ulcers, despite ulcer resolution, 1311 (73.4%) patients did not improve visual acuity (VA) compared to presentation.[77] Bourcier et al, in a study of 300 cases, found that 120 (40%) developed poorer final vision than at presentation.[17] In a review of 291 cases, 28 (23.3%) experienced loss of 2 or more Snellen lines of VA compared to the fellow eye after treatment completion and 2 (1.6%) a loss of 10 or more lines of VA.[79] In addition, large ulcers or cases that present late with inappropriate or no treatment are associated with a poor outcome and the requirement for keratoplasty.[16]

Bacterial keratitis is diagnosed clinically with a typical history and findings on slit-lamp examination. Patients initially experience a foreign body sensation in the affected eye that develops into more severe pain as the infection becomes established and more advanced. Sensitivity to light, photophobia, associated with watering of the eye, epiphora, and a mucous discharge are present. Patients often have a history of contact lens wear, ocular trauma or eyelid pathology. Clinically, the affected eye shows evidence of conjunctival inflammation, manifesting as of a red, oedematous conjunctiva with engorged

blood vessels. The cornea has an epithelial defect that is associated with inflammatory infiltration of the stroma, often described as a corneal ulcer or infiltrate; this usually appears white on slit-lamp examination. This is typically circular in appearance, but can acquire a more varied shape as the condition becomes more advanced. Inflammatory cells are also present in the anterior chamber of the eye that may precipitate in the inferior irido-corneal angle to form a hypopyon.

Clinical studies, using slit-lamp measures of inflammation and infection, have shown that Gram-negative (Gram-ve) BK tends to present with greater inflammation and corneal ulceration than Gram-positive (Gram+ve) BK. In the study by Bourcier at al, Gram-ve bacteria were associated with severe anterior chamber inflammation, as well as a greater surface of infiltrate.[17] Similarly, Dahlgren et al found a larger corneal infiltrate in pseudomonas keratitis.[81] In clinical practice, however, it is not possible to quantify inflammation accurately or precisely with slit-lamp biomicroscopy, and BK does not always present with a well defined corneal infiltrate, thus limiting measurement of the infiltrate dimensions.

1.4.2 Bacteriology

Bacterial infection is the commonest corneal infection in the developed world. In the large South of England study by Ibrahim et al, 696 (71.1%) of the 979 bacterial isolates were Gram+ve and 283 (28.9%) Gram-ve. Of the 1786 patients, only 86 (4.8%), 12 (0.7%), 11 (0.6%) and 8 (0.4%) patients had a viral, chlamydial, acanthamoebal, and fungal aetiology, respectively.[77] In an Australian study of 266 cases of non-herpetic microbial keratitis, 205 (77.1%) were bacterial (55.0% Gram+ve, 22.1% Gram-ve), 8 (3.0%) acanthamoebal and 14 (5.3%) fungal.[79] In a Dutch study of 156 patients with infectious keratitis, Gram-ve bacteria were identified in 58 (52.3%), Gram+ve bacteria in 46 (41.4%), viruses in 5 (4.5%) and fungi in 2 (1.8%) of the 111 culture positive cases.[82] In a French BK study of 291 patients, Gram+ve bacteria were identified in 167 (83%) of cases and Gram-ve bacteria in 34 (17%) of 201 culture positive cases.[17] The variation in the identification of Gram+ve and Gram-ve bacteria in the above Western studies most likely reflects the different criteria for obtaining corneal scrapes or inclusion in the study. It is well documented, however, that there is

a wide geographic variation in the spectrum of bacteria involved in BK.[83] In South India, for example, the most commonly implicated bacterium is *Streptococcus pneumoniae*,[84] compared to Western countries where pseudomonas and staphylococcus species predominate.[76,77,79,85,86]

Bacteria are unicellular prokaryotic microbes. They can be classified into five groups depending on their shape; cocci are spherical, bacilli are rod shaped, spirochaetes are corkscrew shaped, vibrios are comma shaped and spirilla are spiral. One of the most useful and clinically relevant classifications of bacteria is their phenotypic classification into Gram+ve and Gram-ve. Discovered by Hans Christian Gram in 1884, Gram staining involves staining the sample on the microbiology slide with crystal violet, followed by iodine, then de-staining with alcohol and counter-staining with safranin. The different cell wall structure and thickness of Gram+ve and Gram-ve bacteria produces a different appearance under microscopy with the former staining blue-purple and the latter red.[87,88]

The cell wall of bacteria is principally composed of peptidoglycan (PG) or murein, PG being a glycopeptide olimer of sugars and peptides. Gram+ve bacteria contain a thick PG structure, 20-80nm in thickness, which surrounds the cytoplasmic membrane and accounts for 90% of their dry weight (figure 1). The wall also contains teichoic acid, lipoteichoic acid and teichuronic acid.[89] In Gram-ve bacteria, the PG cell wall is approximately 10nm thick, accounting for 5-10% of the dry weight, and is located between the cytoplasmic membrane and the outer membrane (figure 1).[90] The cell wall is covalently attached to the outer membrane via lipoprotein.[89] The outer membrane of Gram-ve bacteria is an asymmetric bilayer with an inner leaflet consisting of phospholipids and outer leaflet consisting of lipopolysaccharide (LPS).[91]

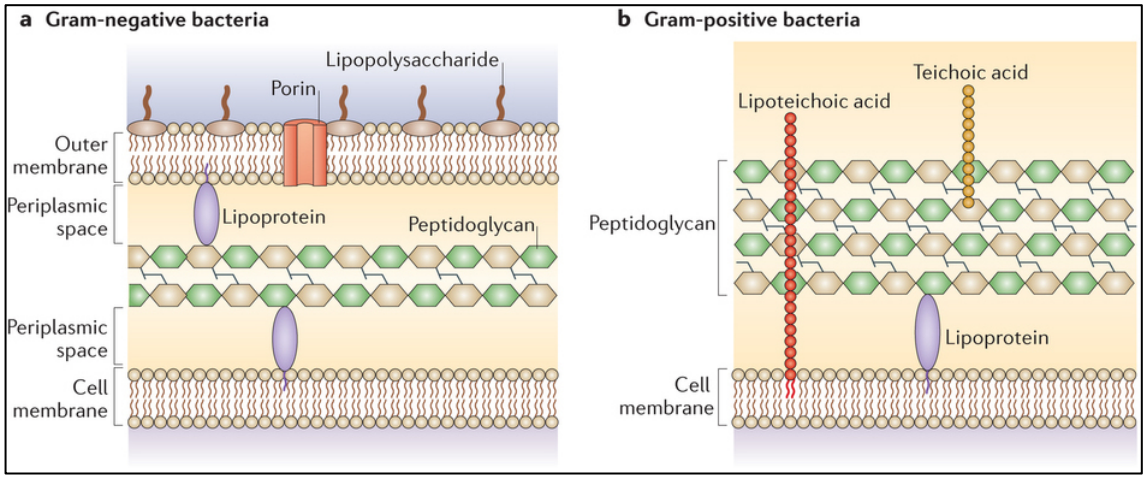

Figure 1. The cell wall structure of bacteria. A. The cell wall of Gram-negative bacteria consists of a thin layer of peptidoglycan in the periplasmic space between the cytoplasmic (cell) membrane and the outer membrane. B. Gram-positive bacteria have a thick cell wall, composed of a thick layer of peptidoglycan and lipoteichoic acid, which surrounds the cytoplasmic membrane (image from Brown L et al.[92]).

1.4.3 Keratoprosthesis and associated infection

Globally, 2.85 million people are estimated to be visually impaired and 1.56 million blind due to corneal opacities.[1] Improvement of vision in patients with corneal opacity most often necessitates corneal graft surgery, whereby the pathological cornea is replaced with a clear cadaveric cornea. However, there is limited worldwide availability of high quality corneal material. In addition, the prognosis of corneal grafts, even in developed countries, is poor in the presence of ocular surface disease, inflammation or failed previous graft.[93,94] Artificial corneas that have the potential to eliminate such immune mediated rejection and failure, especially in higher risk cases, have thus been developed.

Results with fully synthetic corneas have been poor;[95,96] the AlphaCor artificial cornea had a retention rate of 80% and 62% at 1 and 2 years respectively.[95] Devices that use a hybrid of synthetic and biological tissue, such as the Boston keratoprosthesis (Kpro), have recently gained in popularity, as they provide visual improvement with a relatively low extrusion rate.[97-99] In a large multi-centre study, the Boston type 1 Kpro retention rate was 67% at 7 years.[100]

However, the requirement for human cadaveric cornea and the development of glaucoma, retro-prosthetic membrane and infection have limited more widespread use.[97,101-103] Nonetheless, Kpro may be the preferred therapeutic option for cases with high risk of corneal graft failure, such as ocular cicatricial pemphigoid, Stevens-Johnsons syndrome, congenital aniridia or multiple failed grafts.

Infection in Kpro is a devastating complication that can cause acute deterioration of vision and lead to extrusion of the prosthesis. Published rates of infection in Boston Kpro vary, depending on the follow-up and the cohort of the study, ranging between 3.2-17% of eyes.[104-107] In a retrospective review of 126 eyes that had Boston type 1 Kpo by Chan et al, the incidence of microbial keratitis was 7.9% (10 eyes). Of the 10 cases, 3 were culture negative, 5 fungal (3 *Candida*, 1 *Fusarium*, 1 *Dactylaria constricta*), and 2 bacterial (1 *Rhodococcus equi*, 1 non-specific Gram-negative cocci).[107] In a study of 125 Kpro procedures in 110 eyes, 15 (13.6%) eyes developed a corneal infiltrate due to presumed microbial keratitis; the cultured pathogens were *Staphylococcus aureus*, coagulase-negative staphylococci, *Candida parapsilosis* and *Acremonium* species. Corneal infection had a detrimental effect, as more than half of the infected cases required removal of the Kpro and its donor cornea.[106] In the Chan et al study, 4 (40%) of the infected cases had a poor outcome with final vision of counting fingers or worse; however, 4 (40%) cases did relatively well as they maintained vision 20/70 or better.[107]

1.4.4 Diagnosis of bacterial keratitis

Late presentation of BK and large ulcers are associated with a poor outcome and the requirement for keratoplasty.[16] A rapid diagnosis, reliable identification of the responsible organism and initiation of appropriate treatment are, therefore, very important in BK, especially for highly virulent pathogens.[78]

The clinical features that characterise BK were discussed above (section 1.4.1). However, diagnosis of the causative pathogen based on slit-lamp features relies greatly on the clinical experience of the examiner and is at best of modest predictive value. In a study involving 104 cases of ulcerative keratitis, 15 clinicians assessed the patient and decided on the category of microbial keratitis. The positive predictive value for *Pseudomonas* keratitis was 65%, for

other cases of BK 48%, for fungal keratitis 45%, and for *Acanthamoeba* keratitis 89%. Interestingly, corneal specialists carried out 86% of the assessments in this study.[81]

Corneal scrapes for microbiology analysis are considered the 'gold standard' for identification of the causative pathogen, but culture growth is only achieved in 63.8-71.2% of cases.[17,77,81] In addition, microbiology cultures provide the opportunity to assess the in-vitro antimicrobial sensitivities of the pathogen. However, plate cultures typically requires 48 hours to achieve bacterial growth and even longer for fungal or acanthamoebal growth. In practice, many ophthalmologists treat corneal ulcers without obtaining corneal scrapes due to cost, time and availability limitations.[108]

In more advanced cases, or when a poor treatment response is observed, a corneal biopsy may be carried out. This involves a lamellar excision of the cornea that allows histopathological examination and also processing of the material for culture. However, results in BK are limited by poor sensitivity.[109] This may be attributed to the fact that patients have usually been on antibiotics for a long period before the biopsy.

In-vivo confocal microscopy (IVCM) is a non-invasive imaging modality that has been applied to the diagnosis of the causative pathogen in microbial keratitis. It provides images with a magnification of 400X, a transverse resolution of 1.5-6 µm and an axial resolution of 10-20 µm.[109] Due to the small size of bacteria, usually between 0.5 and 10 µm in size, IVCM is of no diagnostic use in BK, but has shown excellent value in the diagnosis of Acanthamoebal and fungal keratitis.[110-113]

Molecular diagnostic techniques have become available that may overcome the low yield and time-delay of culture plates. These are polymerase chain reaction (PCR) based techniques that amplify and examine for the presence of pathogen specific DNA fragments. In a study of 108 samples of microbial keratitis using broad-range PCR, 86% of bacterial and fungal culture-positive samples were positive by PCR, but interestingly 88% of culture-negative samples were also positive by PCR.[114] In a similar study of 88 patient samples, broad-range PCR outperformed cultures and smears for the differentiation of bacterial and

fungal keratitis.[115] More recently, technical progress has allowed the analysis of minute samples, and quantitative PCR using real-time detection of fluorescent amplification products has provided quantification of the starting material. With multiplex PCR, multiple primer sets can be run simultaneously with the potential to diagnose a multitude of pathogens from one initial sample. In contrast to microbiology cultures, though, a major drawback of PCR based techniques remains the fact that they require a strong suspicion of the pathogens that may be involved with appropriate selection of primer sets.[116]

1.4.5 Immune response in bacterial keratitis

Animal studies have shown that the predominant immune cell in BK is the polymorphonuclear neutrophil (PMN). It is crucial to the resolution of infection, but it also mediates tissue damage with the release of free radicals and tissue degrading enzymes, such as matrix metalloproteinases (MMPs).[28,117] The PMNs infiltrate the infected cornea via the tear film, in response to pro-inflammatory cytokines and chemokines, such as MIP-2, the murine functional homologue of human IL-8, IL-6 and KC. [28,117] This process is mediated by IL-1β production by resident corneal cells and infiltrating inflammatory cells.[28]

The PMNs are key effectors of the innate immune response. They migrate rapidly to the site of infection, become activated and initiate a cascade of defence mechanisms. They engulf microorganisms and kill them with the production of reactive oxygen species and the release of antimicrobial and proteolytic granule proteins that are stored in specific organelles.[118] The rapid recruitment of PMNs to the infected cornea is essential for the control of bacterial replication, but their presence or persistence may be associated with extensive stromal damage, scarring or perforation.[119-121] Chusid and colleagues, induced neutropaenia with whole body X-irradiation in guinea pigs before induction of BK and found that greater numbers of bacteria, but reduced PMN numbers were present in the corneas of neutropaenic animals; in addition, less corneal damage was observed in the neutropaenic guinea pigs.[121] In a murine model of pseudomonas keratitis, depletion of PMNs with cyclophosphamide prior to corneal infection resulted in the presence of a more transparent cornea, but also in death of the mice due to bacterial dissemination.[120] Kernacki and colleagues, in an animal study of BK, found that inhibition of PMN

recruitment with a monoclonal antibody against MIP-2 once infection was established, resulted in significantly less corneal damage and perforation.[122] Animal studies on BK, including these discussed above, tend not to use antibiotic treatment once the infection has been induced; this may affect extrapolation of findings to human clinical practice, where antibiotic treatment is started as soon as possible.

The PMN is by far the principal cell in BK, but macrophages, dendritic cells and Langerhans cells of the cornea may also have a role.[28] In mice that had experimental *Pseudomonas aeruginosa* BK, macrophage depletion with subconjunctival clodronate containing liposome injection resulted in increased disease severity with earlier perforation. Greater PMN numbers and higher levels of pro-inflammatory cytokines were measured in the macrophage-depleted mice.[123] Sun et al, in a murine study of pseudomonas keratitis, demonstrated that stromal macrophages were the predominant cells to express toll-like receptors (TLR) 4 and 5 that initiated production of IL-1 and PMN chemokines. These receptors were also detected in dendritic cells, epithelial cells and fibroblasts.[124] The importance of dendritic cells has also been shown in human work that found that their density in the cornea was increased in BK compared to controls.[125] The contribution of the Langerhans cell to the immune response in BK was presented in a murine study, which found that Langerhans cells were detected only in corneas of mice that perforated following pseudomonas keratitis, but not in corneas that healed.[126]

The cascade of cytokine release and PMN recruitment is triggered principally by activation of TLR, but also NOD-like receptor (NLR) pathways in immune cells and corneal resident cells.[127] TLRs are a family of highly conserved glycoprotein pattern recognition receptors that recognize conserved motifs on pathogen associated molecular patterns (PAMPs) on bacteria, viruses, fungi and protozoa. Ten functional TLRs have been identified in humans; TLRs 1, 2, 4, 5, 6 and 10 are located at the cell surface, whereas TLRs 3, 7, 8 and 9 are intracellular.[128]

PAMPs are evolutionary highly conserved structures of pathogens that interact with pattern recognition receptors, such as TLRs and NLRs.[129] In Gram-ve infection, the LPS of the bacterial cell wall stimulates the TLR4 receptor and downstream pathway,[130] whereas flagellin of *Pseudomonas aeruginosa* activates

TLR5 and the corresponding pathway.[131] The TLR4 is also involved in the response to pneumolysin, a virulence factor and toxin that is produced by *Streptococcus pneumoniae*.[132] The cell wall components of Gram+ve bacteria, lipoteichoic acid and lipoproteins, mediate TLR2 responses. However, TLR2 has a broader range of agonists, including lipoproteins from *Borrelia burgdorferi*, *Aspergillus fumigatus* and *Mycoplasma fermentes*.[133] In addition to cell surface structures, internal molecules of pathogens can stimulate an immune response. The RNA of viruses interacts with and activates TLRs 3, 7 and 8,[134-136] and bacterial DNA interacts with TLR9.[137]

The TLRs are expressed in the epithelium and stroma of the cornea. The expression of mRNA for TLRs 1-10 has been detected in the corneal epithelium of patients and also cadaver corneas. Expression at protein level has only been confirmed for TLRs 2, 3, 4, 5 and 7. The TLR4, studied with immunofluorescence, has been found to be expressed in the deeper basal and wing cells of the human corneal epithelium, whilst being absent from the superficial epithelial cells.[138] A similar distribution in the basal and wing cells has been shown for TLR5.[139] The absence of TLRs from the superficial epithelial cells may explain the fact that corneal inflammation is not induced without trauma, as a breach of at least the superficial epithelial layer would be required for bacteria to interact with the deeper TLRs. An immune response may also be triggered by TLRs that are present in the stroma, as mRNA expression for nearly all TLRs (except 8) has been detected in stromal cells.[140] The expression of mRNA for TLRs 2, 3, 4 and 9 has been detected on keratocytes from human cadaver corneas, whereas myofibroblasts expressed only TLR 3 and 9 mRNA.[141]

The TLR 4 and 2 pathways, the principal TLR pathways involved in bacterial infection, are activated by the interaction of PAMPs of Gram-ve and Gram+ve bacteria, respectively, with the TLR 4 and 2 receptors that are present on the surface of corneal cells and PMNs in order to produce IL-1β.[28,127] In addition to the MyD88-dependent pathway that is involved following TLR activation, in Gram-ve infection the TLR4 also engages a TRIF mediated MyD88-independent pathway for IL-1β production.[142] The TLR4-TRIF system synergises with the NLRP3 inflammasome via caspase-11 (caspase-4 & 5 human analogues) to regulate caspase-1 activation and thus production of IL-1β and IL-18.[143,144]

Introduction

Cytokines, such as IL-1 and IFNs, act as primary activators of the immune response. Chemokines are secondary chemotactic factors capable of attracting inflammatory cells, such as PMNs, mononuclear cells and lymphocytes. They are produced by many cells, including PMNs, monocytes, macrophages, epithelial cells, fibroblasts and endothelial cells, in response to a variety of factors, such as bacterial products or the cytokines IL-1 and IFNs.[28,145]

IL-1 is a key cytokine in bacterial infection that has potent pro-inflammatory properties.[146,147] It influences PMN influx into tissues and is produced by resident corneal cells in addition to PMNs, mononuclear cells and macrophages.[146,148-150] IL-1β has been found in high levels in the tears of patients with corneal infection and inflammation.[151] In the human cornea, all layers express IL-1β and experimental in vitro work has shown that adding exogenous recombinant IL-1 to human corneal epithelial and keratocyte cell cultures stimulates synthesis of IL-6 and IL-8, predominantly by keratocytes.[152] Although IL-1β is expressed in human corneal epithelial cells, fibroblasts may not produce IL-1β unless stimulated.[153]

Cytokine IL-1 most likely exerts its pro-inflammatory effect on PMNs indirectly through the induction of chemokines, such as IL-8. Chemokine production, however, can also be triggered directly by the interaction of microbial products, such as LPS, with TLRs.[154] IL-8 is a chemokine that predominantly chemoattracts and activates PMNs to release granule enzymes and respond with respiratory burst. It also has chemotactic properties towards monocytes, but less efficiently than towards PMNs. IL-8 is secreted in response to pro-inflammatory signals, such as IL-1, TNF-α and IFN-γ, by a variety of cell types, including fibroblasts, endothelial cells, lymphocytes, monocytes, and PMNs.[154]

Cytokine TNF-α stimulates IL-8 release from PMNs with greater efficacy than IL-1β. It has been shown to stimulate human epithelial and keratocyte cell cultures to produce IL-8.[152] TNF-α is an important product of PMNs, but PMNs do not respond directly to bacteria.[155] TNF-α production, however, has been found to occur following stimulation with IL-2.[156] In a murine model of BK, TNF-α was found to be constitutively expressed in the epithelium and its

production was increased following infection with pseudomonas. The researchers suggested that TNF-α production might lag production of IL-8 and IL-6 in infection.[157]

IFN-γ is a pro-inflammatory cytokine that is produced by natural killer (NK) cells, T-cells and APCs.[145] Recent work has shown that IFN-γ is also produced by PMNs in response to bacterial and fungal infection.[158,159] It stimulates the bactericidal activity of phagocytic cells, including PMNs, and thus the innate immune response, against pathogens. It is also the main cytokine to stimulate Th-1 helper cells that drive the adaptive cellular immune response.[158] IFN-γ production is stimulated by IL-12 and in turn IFN-γ primes monocytes and PMNs to produce IL-12.[127,160] A study using IL-12 knockout mice found that in the absence of IL-12, there was insufficient production of IFN-γ to control bacterial growth and corneal perforation resulted.[161]

IL-12 is a multifunctional cytokine with a number of activities that may modulate the progress of an infection, including the ability to stimulate production of immunoregulatory cytokines, such as IFN-γ, and enhance proliferation and cytotoxicity of NK and T cells.[162,163] A major function of IL-12 is regulation of the adaptive immune response, as it induces Th-1 helper cell differentiation. It is produced by PMNs, monocytes, macrophages, dendritic cells and B cells.[145] A variety of pathogens induce high levels of IL-12 production, including Gram+ve and Gram-ve bacteria, parasites, viruses, and fungi. Microbial products, such as LPS, lipoteichoic acid and peptidoglycan, stimulate IL-12 production by cells of the innate immune system via TLR signalling.[164,165] On the other hand, IL-12 production is inhibited by IL-10, IL-11, IL-13 and type I IFNs (IFN-α and IFN-β).[145]

IL-6 has been described to have both pro-inflammatory and anti-inflammatory actions.[28,166-168] It is produced by human corneal epithelial cells,[169] macrophages, PMNs and lymphocytes.[170] In a mouse model of lung inflammation, both IL-6 deficient and wild type mice experienced an increase in local TNF-α and PMN levels after exposure to LPS in aerosol, but the IL-6 deficient mice developed greater levels of TNF-α, suggesting a possible anti-inflammatory role for IL-6.[167]

On the other hand, a mouse study of pseudomonas keratitis showed that PMN recruitment into the cornea was dependent on IL-6 production. The IL-6 deficient mice showed an increased bacterial load compared to the wild-type mice and failure of PMN infiltration into the central cornea.[168] In human contact lens wearers, single nucleotide polymorphisms in the promoter region of IL-6 have been found to carry increased risks of developing microbial keratitis and severe microbial keratitis; it was suggested in this study that these polymorphisms may lead to the production of less IL-6 in response to keratitis and increased inflammation.[171]

IL-10 has an immunoregulatory role in modulating excessive inflammation and immune response in infection. IL-10 is produced by monocytes, keratinocytes, cytotoxic T-cells, B-lymphocytes, mast cells, and eosinophils.[172,173] Although human PMNs have been reported to produce IL-10,[174] these data are controversial, as they have not been reproduced in other studies.[175] Levels of IL-10 tend to become elevated late in the course of an infection.[176] IL-10 has been shown to inhibit production of pro-inflammatory cytokines, such as IL-1β, IL-6, IL-8, IL-12 and TNF-α, by mononuclear phagocytes, as well as IFN-γ and TNF-α by NK cells.[172] However, in a mouse study of pseudomonas keratitis, IL-10 knockout mice had a significantly lower corneal bacterial load than wild-type mice on day 7 of infection. The number of PMNs and levels of cytokines IFN-γ, TNF-α and MIP-2 were also lower in the IL-10 knockout mice.[176] In addition, a reduced bacterial burden and smaller inflammatory foci have been detected in the spleen and liver of IL-10 deficient mice that were infected with Listeria monocytogenes.[177] Interestingly, in an in-vitro experiment of this study, when IL-l0 deficient peritoneal exudate cells and spleen cells were stimulated with heat-killed Listeria they produced an intense pro-inflammatory cytokine response for IL-12, IFN-γ, TNF-α, IL-1α, and IL-6.

GM-CSF stimulates a broad range of leukocytes, including PMNs, macrophages, monocytes and eosinophils, and is a powerful chemotactic agent for human PMNs.[178] Its production has been found significantly increased in murine corneas infected with pseudomonas.[179] Expression of GM-CSF increased in cultured corneal fibroblasts from patients with prior corneal infection, once stimulated with LPS derived from *Pseudomonas aeruginosa*.[180] In herpes virus

infection, GM-CSF was expressed in corneal epithelial cells and infiltrating inflammatory cells in corneal buttons of patients with herpetic keratitis. In the same study GM-CSF was found to delay PMN apoptosis.[181] Extended PMN survival may contribute to tissue damage with the sustained release of proteases and reactive oxidants.[118]

Cytokine IL-2 was initially described as a T-cell growth factor. It is predominantly produced by activated T-cells, but also NK and dendritic cells.[182] It is considered a central cytokine in the regulation of T-cell responses, but also of immune cells of the innate system, including NK cells, monocytes or macrophages and PMNs.[183] IL-2 has pro-inflammatory properties, although most of the evidence is from in-vitro work. It can induce healthy human PMNs to increase mRNA specific for TNF-α and release TNF-α.[156] Human PMNs express surface receptors for IL-2 and have been shown in-vitro to respond to IL-2 with increased antimicrobial activity against *Candida albicans*.[184] IL-2 production was also stimulated when whole blood of patients with tuberculosis was stimulated with *Mycobacterium tuberculosis* antigens.[185]

Finally, pro-inflammatory cytokine IL-18 may also have a role in BK. In a murine study involving a gene knockout model, IL-18 contributed to resistance against pseudomonas keratitis through the induction of IFN-γ.[186] More recently, IL-18 has been found to be produced by infection mediated inflammasome activation and involved in pyroptosis, although there are no studies on BK. Pyroptosis is an inflammasome mediated cell death that is a key defence mechanism against microbial infection, via halting intracellular bacterial replication and also exposing the bacteria to phagocytes.[187]

Although animal infection models support the role of the cytokines discussed above, there is limited evidence that they are clinically relevant or present in human BK.

1.5 Imaging of the cornea and ocular surface

Imaging of the cornea and the ocular surface has become a rapidly advancing field of ophthalmology. In recent years, anterior segment imaging devices have improved understanding of keratoconus treatment,[188-190] the visual outcomes of endothelial keratoplasty [191-193] and the cornea-keratoprosthesis interface following Boston keratoprosthesis.[194,195] They provide qualitative information, but also a range of quantitative data, such as corneal thickness, surface topography, corneal volume and corneal densitometry.[196]

In this section the newer imaging modalities, Pentacam-Scheimpflug (Pentacam, Oculus Inc, Lynnwood, WA, USA) and anterior segment optical coherence tomography are presented, in addition to the more established Orbscan scanning-slit topography (Orbscan IIz, Bausch & Lomb Surgical Inc, San Dimas, CA, USA) and in-vivo confocal microscopy. Their imaging capabilities and clinical applications are discussed in relation to corneal infection and inflammation.

1.5.1 Orbscan scanning-slit topography

Orbscan scanning-slit topography is a non-contact optical system, the imaging properties of which are based on the principle of measuring the dimensions of a slit-scanning beam that is projected on the cornea. The Orbscan II and newer versions also have a Placido disc attachment that provides curvature measurements directly. The latest Orbscan IIz scans the entire surface of the cornea and acquires over 9000 data points in 1.5 seconds.[196]

The Orbscan assesses and maps the curvature of the anterior and posterior corneal surfaces, anterior lens surface and anterior iris surface. It provides maps that describe the elevation of the anterior and posterior corneal surfaces in relation to a best-fit model, the keratometric power of the anterior corneal surface and the corneal thickness (figure 2). However, mapping of the internal ocular surfaces is not as precise as that of the anterior surface because, in addition to hardware and operator acquisition tolerances, it is affected by the precision of the anterior surface maps.[197] Orbscan imaging capabilities and precision are considerably compromised in the presence of a poor tear film

and poor ocular surface, as curvature reconstruction of the anterior corneal surface relies on software processing to detect the edges of the reflected ring mires of the Placido disk.[197] This is usually manifested as areas of dropout on Placido based topography and an increase in surface irregularity measured by the corneal topography surface regularity index.[198]

The Orbscan has played a pivotal and crucial role in the assessment of keratorefractive surgery candidates and patients since its introduction in 1995.[197,199,200] Refractive surgery has been its principal application, as it requires a healthy ocular surface and transparent non-pathological cornea. In a comparison with optical coherence tomography, the Orbscan was found to have limited scanning potential in patients with corneal scarring and surface irregularity due to Salzmann's nodular degeneration.[201] Most likely a reflection of these limitations, there has been no description of Orbscan scanning-slit imaging in corneal infection or inflammation.

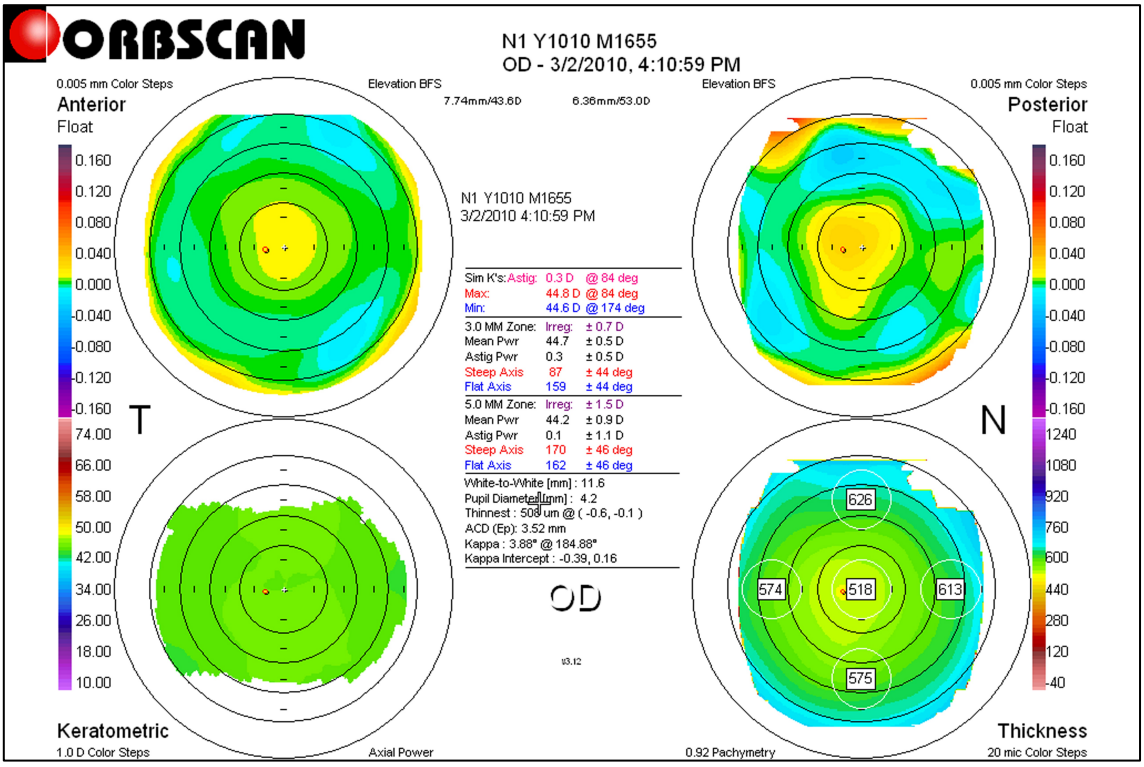

Figure 2. Orbscan 'Quad map' of normal cornea. This image illustrates the 'Quad' map set-up on a healthy right (OD) cornea. The four maps, in clockwise order, are anterior elevation (float), posterior elevation (float), thickness and keratometric.

1.5.2 Pentacam-Scheimpflug

Pentacam-Scheimpflug imaging is a non-contact optical system that uses the Scheimpflug principle to obtain images of the anterior segment. The Scheimpflug principle describes the optical properties involved in the photography of objects when the plane of image is not parallel to the film of the camera or the lens plane. It requires that the plane containing the slit beam and the image plane intersect at one point, with the corresponding angles equal.[202] A second device that uses the Scheimpflug imaging principle, the GALILEI™ Dual Scheimpflug Analyzer (Ziemer Group, Port, Switzerland) has recently become available.

The Pentacam by Oculus Inc has a rotating Scheimpflug camera that takes 50 cross-sectional slit images of the anterior segment of the eye in less than 2

seconds.[203] The upgraded version, the Pentacam HR, has a higher resolution camera that obtains up to 100 high-resolution slit images.[196] A second camera captures eye movements and makes appropriate corrections. The light source is a UV-free blue light emitting diode with a wavelength of 475 nm. Software is then used to construct a three-dimensional image. It analyses data from up to 138000 measuring points to compute maps of corneal thickness and topography of the anterior and posterior corneal surfaces, including elevation and keratometry. In addition to refractive software for analysis of the cornea, it offers a tomographic overview of all captured Scheimpflug images (figure 3) and an analysis of corneal transparency by optical densitometry. It also provides data on anterior chamber depth, lens opacification and lens thickness.[196,204]

Corneal densitometry, as a measure of optical transparency of the cornea, has been applied to the objective assessment of corneal infection. It has been found elevated in patients with microbial keratitis compared to healthy controls. The increased corneal densitometry most likely reflects the increased light scatter and reduced transparency of the cornea in the presence of infection.[204] As discussed above (section 1.4.1), microbial keratitis manifests clinically as an accumulation of inflammatory cells and oedema in the corneal stroma that disrupt the regular arrangement of collagen fibres, causing increased light scatter.

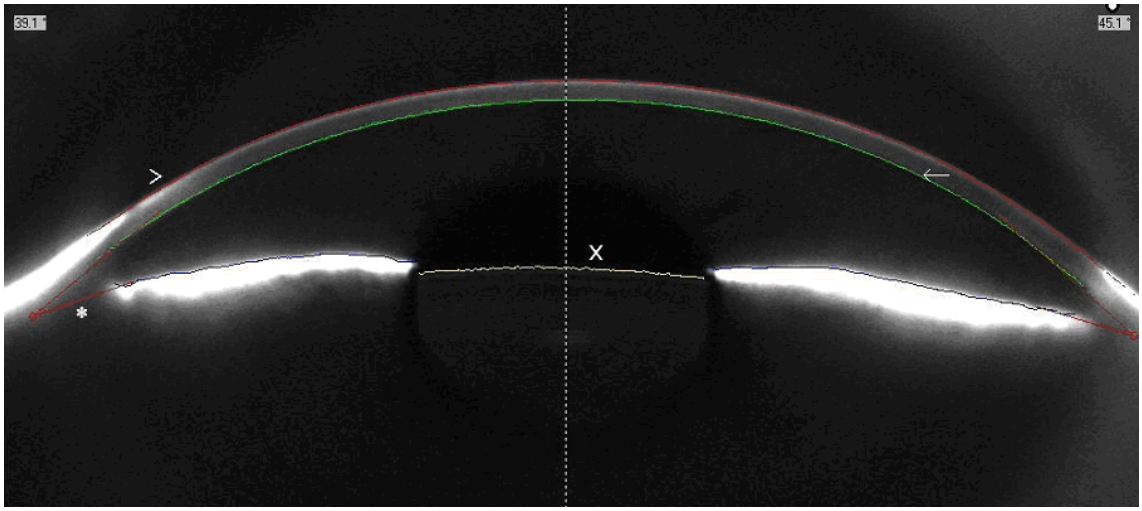

Figure 3. Anterior chamber Pentacam-Scheimpflug image. The arrowhead (>) shows the anterior surface of the cornea, as delineated by software. The arrow (←) points to the posterior surface of the cornea, as delineated by software. The x shows the anterior lens surface. The asterisk (*) shows that direct anterior chamber angle visualisation is not possible.

1.5.3 In-vivo confocal microscopy

In-vivo confocal microscopy (IVCM) is a contact imaging modality that provides en face images of the corneal cells at different depths of the cornea. The images have a higher resolution than with conventional light microscopy.[205,206] The most commonly used confocal microscope system is the Heidelberg Retinal Tomograph with the Rostock Corneal Module (HRT-RCM, Heidelberg Engineering, GmBH, Dossenheim, Germany); it provides images with better resolution and contrast than other confocal systems.[206] This is a laser scanning confocal microscope that operates by scanning a 670 nm laser beam in a raster pattern, in which an area is scanned from side to side in lines from top to bottom, typically covering an area of 400 µm by 400 µm. It has a 63X objective lens and produces images with a transverse optical resolution of 2 µm and an axial optical resolution of 4 µm.[205,207]

The IVCM produces images of high resolution and magnification, allowing identification of structures and individual cells within the cornea, as demonstrated in figure 4. It has detected a key role for the corneal superficial

nerve plexus in dry eye, with increased tortuosity of the nerves being demonstrated.[208] It can identify dendritic cells in the corneal epithelium, as dendritic Langerhans cells and leukocytes have been found increased in the cornea of dry eye patients.[209] It has also been used to study herpetic keratitis, showing a decrease in the numerical density of superficial epithelial cells that corresponded to the reduction in corneal sensation.[210]

IVCM may have an invaluable role in the diagnosis of fungal and acanthamoebal keratitis. The Acanthamoeba protozoon can either be in an active trophozoite form or as a quiescent cyst. The trophozoites are typically 25-40 μm in diameter, whereas the cysts are smaller, 15-28 μm in diameter; both structures being within the resolving power of IVCM. Single-observer studies have demonstrated a sensitivity of 90.9–100% and a specificity of 77.3–100% in the diagnosis of acanthamoebal keratitis.[211-212] However, when the observer experience is limited, the sensitivity and specificity can be as poor as 27.9% and 42.1% respectively.[213] The difference between these studies may also be compounded by the fact that in the latter study the observers were masked to the clinical diagnosis, whereas in the former studies the researchers did not explicitly comment on masking. IVCM has an analogous diagnostic application in fungal keratitis, as fungi tend to have large and long bodies; filamentous fungi tend to be 200-400 μm long and yeasts, such as *Candida albicans*, 10-40 μm long.[214,215] Similar to *Acanthamoeba* keratitis, an experienced examiner and observer are required to maximize its diagnostic potential.[213]

IVCM does not have a diagnostic role in BK, as bacteria are much smaller organisms than fungi and *Acanthamoeba*. It has, however, been used to study the condition. The density of epithelial dendritic cells was shown to be elevated and the density of the sub-basal nerve plexus decreased in BK compared to controls.[216] Even as a research tool, IVCM has severe imaging limitations in the presence of corneal opacity or oedema, as is often the case in BK, due to loss of contrast between cellular structures and extracellular tissue. These manifested in a study, where the authors stated that ‘when a corneal ulcer was present with an epithelial defect or severe ulceration in eyes with BK, the ulcer and periphery of the ulcer were scanned. If the images of the ulcer

were not suitable due to severe edema or opacity, the periphery of the ulcer was chosen for the analysis'.[217]

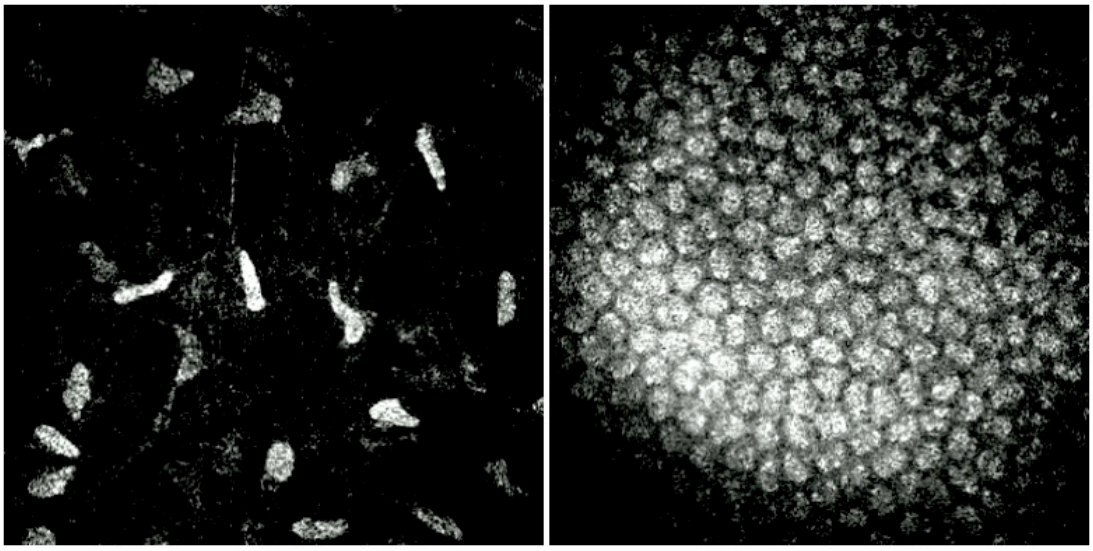

Figure 4. In vivo confocal microscopy of the cornea. The image on the left shows healthy keratocytes of a rabbit cornea, the image on the right healthy endothelial cells.

In addition to the cornea, the conjunctiva has also been investigated with IVCM, especially following glaucoma drainage surgery.[218,219] Microcysts, typically 10 to 150 µm in size, can be identified in the conjunctiva and the arrangement of the subepithelial connective tissue assessed and graded for density. Well functioning trabeculectomy blebs have been shown to have a conjunctival epithelium that is rich in microcysts and a subepithelial tissue that is loosely arranged and includes a high number of optically clear spaces. A dense subepithelial tissue is characteristic of non-functioning blebs.[219]

IVCM can also image the presence of immune cells in the conjunctiva. In meibomian gland dysfunction, IVCM has found that patients who are refractory to treatment have a higher density of infiltrating immune cells in the conjunctival epithelium and subepithelial stromal tissue compared to treatment-responsive meibomian gland dysfunction patients and healthy subjects.[220]

Limitations with IVCM confine its use to specialised units with an interest in ophthalmic imaging. The field of imaging is small, 400 µm by 400 µm for the HRT-RCM. This requires very careful and thorough imaging along the x, y and z axes in order not to miss the relevant diagnostic features. In addition, a significant degree of patient cooperation is required for optimum imaging quality. The contact examination via applanation can cause compression and distortion of tissues, altering morphological characteristics of the superficial layers.[205] Finally, all these factors necessitate a skilled technician for IVCM imaging and also an experienced interpreter of the images.[214]

1.5.4 Optical coherence tomography

Optical coherence tomography (OCT) is a non-contact imaging modality. In ophthalmology, this technology was initially applied to the retinal OCT; the first OCT became commercially available in 1995 by Carl Zeis Meditec (Carl Zeiss Meditec Inc, Dublin, CA, USA). Anterior segment OCT (AS-OCT) evolved from the retinal OCT and the dedicated AS-OCT devices, such as the Visante OCT, use a longer wavelength (1310 nm) than the retinal OCT (820 nm).[221,222] This allows for greater penetration through tissues that highly scatter light, such as the sclera and the limbus, providing visualisation of the irido-corneal angle.[221] The ocular media absorb about 90% of the 1310 nm light before it reaches the retina. As a result, AS-OCT can use higher power than corresponding retinal Time-Domain OCT (TD-OCT), eliminating motion artefacts.[222] The latest retinal OCT devices, predominantly using Fourier-Domain OCT (FD-OCT) technology, may also incorporate an anterior segment module; however, they use the shorter wavelength light that is optimised for retinal imaging. AS-OCT provides cross-sectional images of anterior segment structures, including the cornea, iris, angle and anterior lens (figure 5).[221] Pachymetry maps can also be plotted.

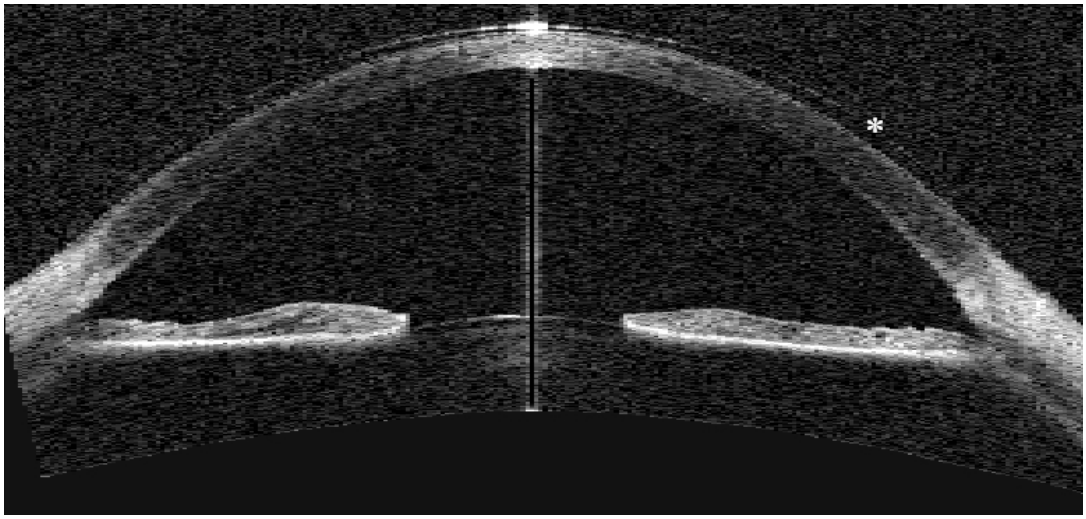

Figure 5. Visante OCT cross-sectional image of the anterior segment. The cornea, limbus, anterior sclera, iris and anterior lens are imaged in cross-section. Direct irido-corneal angle visualisation is possible, with details of the angle morphology visible. The asterisk (*) shows the presence of a contact lens.

1.5.4.1 Principles of Optical Coherence Tomography

In OCT imaging, light from a low-coherence light source is emitted and split via a Michelson type interferometer into a reference beam and a probing or measurement beam (figure 6). The probing beam is reflected from the tissue being scanned with different time delays that correspond to the structure of the tissue. The reference beam light is reflected from a moving reference mirror. The multiple backscattered waves from the tissue and the backscattered waves from the mirror are combined to produce a low time-coherence interferometry depth-scan, similar to the A-scan of ultrasound, which is based on the photodetector signal at the interferometer exit. In order to measure the time delays from different structures of the scanned tissue, the position of the reference mirror changes so that the time delay of the reference beam is adjusted accordingly; this is a feature of TD-OCT. A series of laterally adjacent depth-scans are combined to synthesise the cross-sectional OCT images. In OCT, the depth and lateral or transverse data acquisition are decoupled; the depth-scan is performed by the reference mirror and the lateral

scan by laterally moving focus of the probing beam that is illuminating the sample.[223,224]

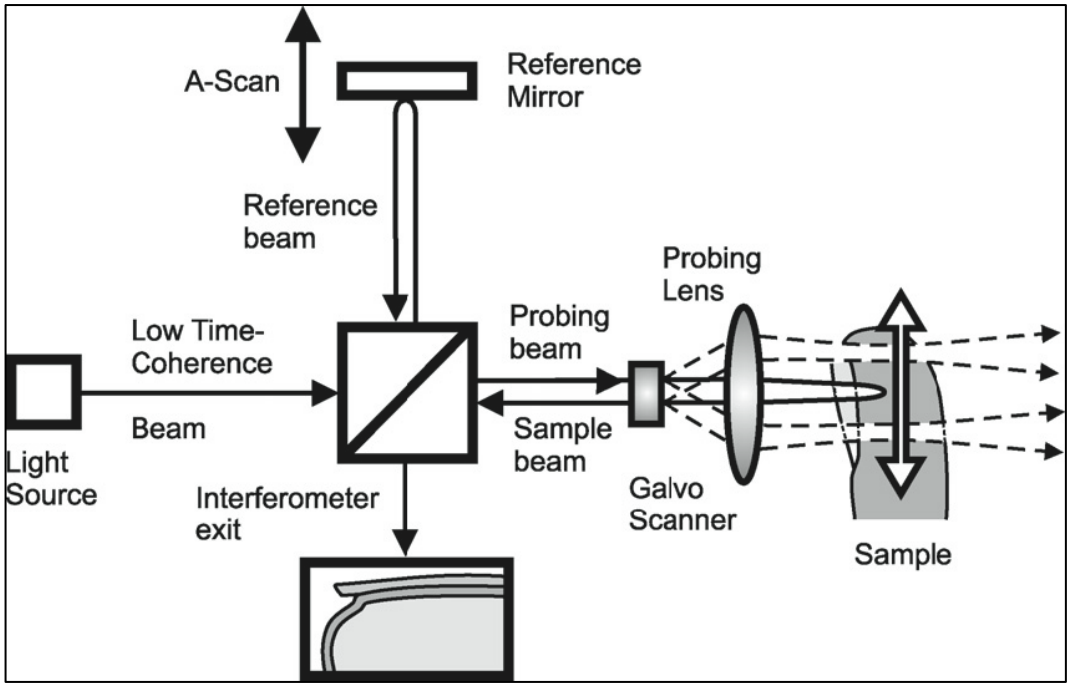

Figure 6. Principles of Optical Coherence Tomography Imaging. The low coherence light beam is split by a Michelson type interferometer into a reference beam and a probing beam. The backscattered beams, i.e. the reference and sample beams, are combined to produce a low time-coherence interferometry depth-scan that is based on the photodetector signal at the interferometer exit. (image from Fercher AF.[224])

In FD-OCT, the detector arm of the Michelson interferometer uses a spectrometer instead of a single detector. The spectrometer measures spectral modulations and the spectral pattern that is produced by interference between the sample and reference backscattered reflections. A depth scan (A-scan) is then generated based on Fourier transformation of the spectral interferogram. In FD-OCT, no physical movement of the reference mirror is required, enabling FD-OCT to be much faster than TD-OCT.[225]

FD-OCT is primarily used by retinal OCT devices. However, numerous manufacturers have recently modified the software and hardware of their devices to image the anterior segment. The faster scan rate of FD-OCT devices improves image quality by achieving higher resolution and reduction of motion artefact. Currently, FD-OCT uses shorter wavelength light than dedicated AS-OCT devices, potentially limiting penetration through opaque structures.[226,227] This is illustrated in figure 7, which shows that visualisation of the iris root is less detailed with FD-OCT than TD-OCT. An example of an FD-OCT device that provides AS-OCT scans is the Topcon 3D-OCT 2000 (Topcon Medical Systems Inc, Paramus, NJ, USA). Resolution is much better than TD-OCT; according to the manufacturer, it has an axial resolution of 5-6 µm and a transverse resolution of 20 µm.

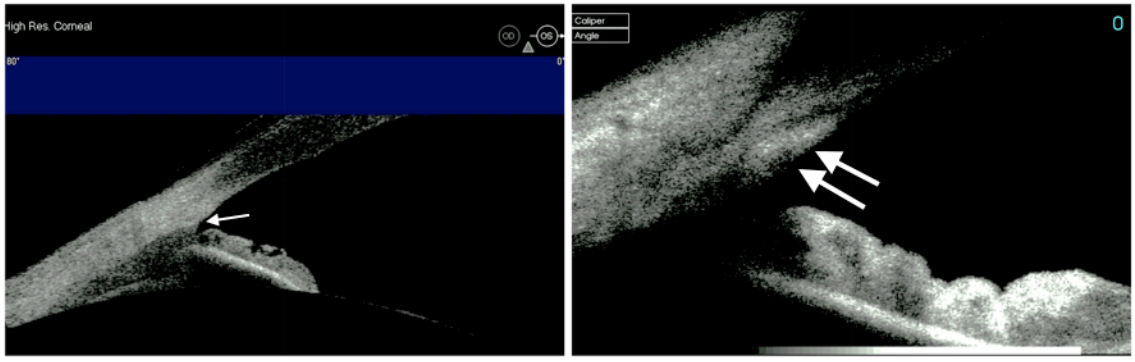

Figure 7. Time domain and Fourier domain AS-OCT imaging of the irido-corneal angle. The image on the left is a time domain AS-OCT scan of the angle; the image on the right, the corresponding Fourier domain scan of the same patient. The Fourier domain image provides higher resolution and magnification with clearer visualisation of the trabecular meshwork (double arrow). The root of the iris and the scleral spur (arrow) are visualised better with time domain OCT, demonstrating its better penetration through tissues that scatter light, such as the limbus.

Two dedicated AS-OCT devices are currently commercially available, the Visante OCT and the SL-OCT. Numerous retinal OCT devices with an anterior segment module are available, such as the Topcon 3D OCT 2000 and the

RTVue-100 (Optovue Inc, Freemont, CA, USA). The Visante OCT and the RTVue-100 were used for the research of this thesis; therefore, their imaging capabilities are presented in detail.

1.5.4.2 Visante OCT

The Visante OCT provides anterior segment scans, as illustrated in figure 5, with 256 A-scans per image, and high-resolution scans of the cornea (figure 8) or other anterior segment structures with 512 A-scans per image. Pachymetry maps are plotted at a rate of up to 2048 A-scans per second. It has an optical axial resolution of up to 18 µm and optical transverse resolution of up to 60 µm. Integrated software, automated and manual, provide a range of biometric information, such as corneal thickness, anterior chamber depth and width, and irido-corneal angle parameters.[196]

The Visante OCT, as explained above, can scan through the opaque cornea and image intracameral structures that would not normally be visualised with slit-lamp biomicroscopy. It has been used to assess the anterior segment in secondary glaucoma with corneal opacity after penetrating keratoplasty, and visualise the patency and position of aqueous shunt devices in the presence of poor corneal transparency.[228,229] AS-OCT has shown excellent imaging capabilities in analysing clear corneal incisions after cataract surgery and the corneal architecture after lamellar corneal transplantation.[10,230] It has also enabled visualisation of the placement and measurement of the depth of intrastromal rings after implantation for astigmatism reduction in keratoconus.[11]

Long wavelength AS-OCT measurements of central corneal thickness, using a prototype of the Visante OCT, showed good correlation with the gold standard ultrasound pachymetry. In a study of 42 healthy eyes, the correlation coefficient was 0.97 and the mean corneal thickness with AS-OCT was less than with ultrasound (546.9 vs. 553.3 µm, $p<0.001$). AS-OCT also showed excellent repeatability; within a central 7 mm zone the repeatability of corneal thickness, expressed as the standard deviation of repeated measurements, was 2 µm.[231]

Although the Visante OCT has primarily been designed to image the cornea and anterior chamber structures, it has also been applied to studying the conjunctiva and Tenon's layer. Subconjunctival fluid collections, suprascleral cystic fluid spaces and the fluid route under the scleral flap have been visualised on AS-OCT images of trabeculectomy blebs.[232] AS-OCT has also been used to image the effect of suture lysis on the morphology of trabeculectomy blebs; in a small study of 7 patients, an increase in total bleb height with increased bleb wall thickness and separation of the scleral flap from the underlying sclera was observed.[233]

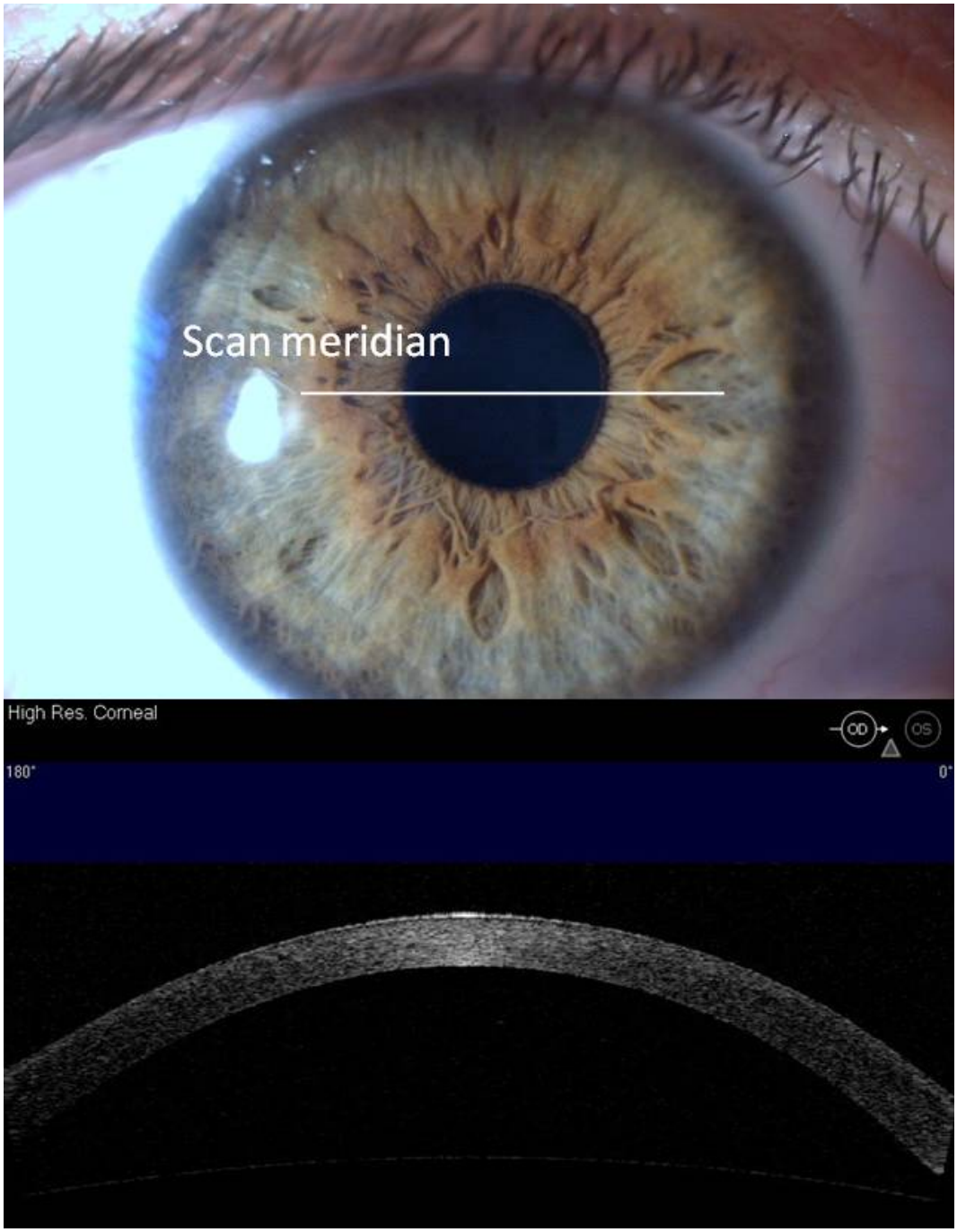

Figure 8. Visante OCT high-resolution image of the healthy cornea. The cross-sectional scan through the cornea shows that the epithelium and endothelium appear hyper-reflective relative to the ground glass appearance of the stroma.

1.5.4.3 RTVue-100

The RTVue-100 by Optovue Inc was the first commercially available FD-OCT device to receive FDA approval. It provides AS-OCT scans, in addition to retinal OCT images, and uses a wavelength of 840 nm. Due to its faster FD-OCT technology it scans at a rate of 26000 A-scans per second, its highest quality images consisting of 4096 A-scans per frame. Images have an axial resolution of up to 5 μm and a transverse resolution up to 15 μm. In addition to cross-sectional images of the anterior segment and pachymetry maps, its high resolution and scan rate allow mapping of the epithelial thickness.[234] Although FD-OCT penetration through opaque structures may be poorer than long-wavelength AS-OCT,[226,227] it does provide higher resolution scans of the healthy cornea (figure 9).

FD-OCT has been used to map the epithelial thickness in normal and keratoconic corneas; keratoconus patients had a thinner epithelium in the inferior cornea compared to controls and a greater asymmetry in epithelial thickness between the superior and inferior cornea.[235] FD-OCT has the imaging capability to detect abnormalities of the basement membrane in corneal epithelial basement membrane dystrophy; it has a specificity of 100% and a sensitivity of 98% in identifying features of the condition, such as thickening, undulation and protrusion of the basement membrane in the epithelium.[236]

FD-OCT has been found to have excellent imaging and pachymetry capabilities in corneas with stromal opacities, such as in Reis-Buckler and granular dystrophies, and post-trauma scars. Corneal hyper-reflective areas that corresponded to the stromal opacities were identified on the scans and the presence of opacities did not affect imaging of the posterior border of the cornea and, therefore, pachymetry.[237]

FD-OCT has also been applied to imaging microbial keratitis. In a 2012 study, 20 patients with microbial keratitis were imaged with the RTVue-100. Morphological characteristics, such as hyper-reflective stromal lesions, hyper-reflective material over lost epithelium, hyper-reflective lesions attached to the endothelium, localized stromal thinning, Descemetocoele and stromal cystic spaces were identified. Although the authors stated that the borders of these

characteristics could be visualised, no attempt was made to quantify these features or other parameters of infection.[238]

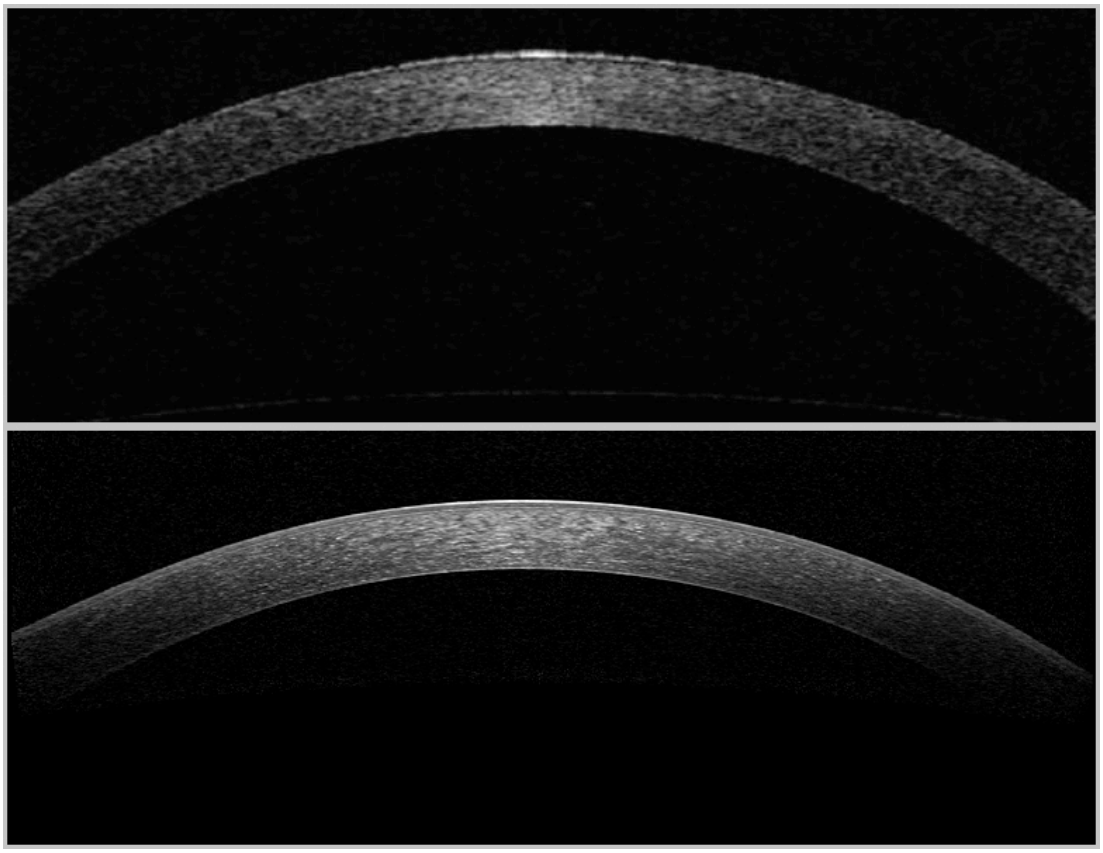

Figure 9. Time domain and Fourier domain AS-OCT imaging of the cornea. The top image is a time domain AS-OCT scan of the cornea, demonstrating the hyper-reflective epithelial and endothelial surfaces. The lower image is a Fourier domain AS-OCT scan of the same patient that demonstrates its superior imaging resolution of the healthy cornea.

The peer-reviewed literature on the Visante OCT that was available at the onset of this research in 2007, as summarised above, suggested that the imaging capabilities of long-wavelength AS-OCT were the most appropriate and promising for investigating the inflamed ocular surface and especially bacterial corneal infection. Its ability to scan through the opaque cornea with high-resolution images,[228,229] combined with the novelty of the imaging modality and non-contact examination were crucial factors in the decision to study ocular

surface inflammation with the Visante OCT. In 2009, a manuscript that compared TD-OCT and FD-OCT for anterior segment imaging highlighted the deficiency of FD-OCT in penetrating the opaque limbus and cornea,[239] a feature that is often present in corneal infection. During the course of this research degree, an opportunity to investigate BK with FD-OCT became available at the Singapore Eye Research Institute in Singapore.

1.6 Aims and objectives of research

The aim of this research thesis is to evaluate the imaging capabilities, quantification capabilities, and clinical and research application of AS-OCT in ocular surface inflammation and corneal infection.

More specifically, the three objectives are:

1) To ascertain the imaging capabilities of AS-OCT and identify AS-OCT quantification parameters in inflammation and infection of the ocular surface (chapter 3). Three studies are conducted to achieve objective one:
   a) In the first study (3.1), I analyse AS-OCT images of patients with corneal infection for morphological qualitative features and quantitative parameters than can be used to characterize the condition.
   b) In the second study (3.2), I assess the imaging capabilities of AS-OCT in PUK by analysing AS-OCT images for qualitative and quantitative morphological features that may characterise active and quiescent PUK.
2) To assess the quantification capability of AS-OCT in BK, by evaluating the identified parameters in a large cohort of patients (chapter 4). Three studies are conducted to achieve objective two:
   a) In the first study (4.1), I assess the capability of AS-OCT to quantify morphology-based parameters in BK and ascertain the intra-observer and inter-observer repeatability of the AS-OCT measurements.
   b) In the second study (4.2), I compare AS-OCT repeatability and reproducibility in BK to repeatability and reproducibility in the healthy cornea and the post-endothelial keratoplasty cornea.
   c) In the third study (4.3), I evaluate the correlation of identified AS-OCT morphological parameters of inflammation in BK with slit-lamp morphological and functional parameters of infection.
3) To apply AS-OCT quantification of corneal inflammation to improving the prevention, diagnosis, monitoring, and treatment of BK (chapters 5 and 6). Five studies are conducted to achieve this objective:
   a) In the first study (5.1), I ascertain the diagnostic value of AS-OCT in identifying Gram-ve infection in patients who present with BK.
   b) In the second study (5.2), I measure the temporal change of corneal morphological parameters of inflammation in treated BK patients and

propose AS-OCT criteria that will assist the objective assessment of the treatment response in BK.

c) In the third and fourth studies (5.3 & 5.4), I validate morphology-based AS-OCT quantification of inflammation with molecular and cellular markers of inflammation in tears of BK patients.

d) In the fifth study (6.1), I investigate whether FD-OCT imaging can quantify the difference in corneal inflammatory response between two groups of rabbits with experimental BK, one group receiving prophylactic antibiotics, the other not.

2. Methods

The first half of this thesis (chapters 3 and 4) explores the application of AS-OCT to imaging and quantifying the inflammatory response in ocular surface inflammation, with a particular focus on the cornea. AS-OCT scanning protocols that provide standardised and repeatable assessment are developed and presented in this chapter 2.

In the second half of this thesis (chapters 5 and 6), AS-OCT imaging and laboratory investigations are used to study corneal infection in humans and in a rabbit model of keratoprosthesis (Kpro) associated infection. They are applied to the study of prevention, diagnosis, monitoring and treatment of bacterial keratitis (BK). Techniques, such as cytokine and chemokine analysis, cytospin microscopy, immunohistochemistry and liquid chromatography mass spectrometry are used and described in this chapter 2.

2.1 Ethical approval

2.1.1 Human studies

Patients presenting to the Eye Unit of University Hospital Southampton NHS Foundation Trust were invited to take part in the research investigations of this thesis. All patients had a level of care that was appropriate for the condition and their acceptance or refusal to participate did not affect the quality of the provided treatment. Local NHS Research Ethics Committee (REC reference 08/H0502/7) and patient informed consent were obtained. The research adhered to the tenets of the Declaration of Helsinki.[240]

2.1.2 Animal studies

Thirty-one New Zealand White rabbits, aged 1 to 2 months and weighing 2 to 2.5 kg, were used for an animal study of Kpro associated infection. The study adhered to the Statement for Use of Animals in Ophthalmic Vision and Research by the Association for Research in Vision and Ophthalmology. The

protocol was approved by the Institutional Animal Care and Use Committee and Institutional Biosafety Committee at Singapore Eye Research Institute.

Trained staff of SingHealth Academia in Singapore transported the animals from the animal housing room to the procedure room in special rabbit transport cages. All sedated rabbits were carried by hand. The rabbits were not visible to the public during transport, as the facility was only accessible by authorised personnel. In addition, the rabbit transport cages were fully enclosed with small openings, sufficient for the rabbits to breathe comfortably.

Surgery and investigations were carried out under sedation with intramuscular xylazine hydrochloride and ketamine hydrochloride. Immediately following surgery, frequent and careful observation of the rabbits was carried out. The animals were kept warm and returned to the cage when able to walk. Breathing and gum colour were monitored. The surgical site was monitored frequently for bleeding, infections or wound dehiscence.

Humane endpoint criteria were set; at any given time during the research study, animals that suffered from severe or chronic pain and distress that could not be relieved with therapeutic intervention, would be painlessly euthanized. Euthanasia was carried out at the end of the investigations with an overdose of pentobarbitone.

2.2 Anterior Segment Optical Coherence Tomography

2.2.1 AS-OCT imaging protocol for the healthy cornea

The Visante OCT by Carl Zeiss Meditec was used for scans. Healthy participants had a four-quadrant high-resolution AS-OCT scan of both corneas, at the 0°, 45°, 90° and 135° meridians. This scanning protocol would allow the construction of reference pachymetry maps that are not based on automated corneal thickness (CT) measurements, but on manual measurements. This is important for two reasons. Firstly, manual CT measurements are required for the inflamed or infected cornea, due to the limited capability of the automated software of the Visante OCT to measure the pathological cornea. Secondly, it is known that automated CT measurements are smaller than manual measurements.[241]

The four-quadrant scanning mode divided each cornea into 8 pie segments. Each segment was then divided into a central 4mm area, a mid-peripheral area defined by the 4mm zone and an outer 8mm zone, and a peripheral area extending from the 8mm zone to the limbus. The CT was measured in the centre of each area with calliper tools of the Visante OCT software (version 1.1.2), as illustrated in figure 10. The mean CT of each area for all participants was calculated and mapped for the right and left eyes.

The AS-OCT images were also analysed for qualitative morphological features. Specifically, they were examined for the presence of:

a. Hypo-reflectivity of the corneal stroma relative to the endothelium and epithelium

b. Homogeneity of reflectivity of the corneal stroma.

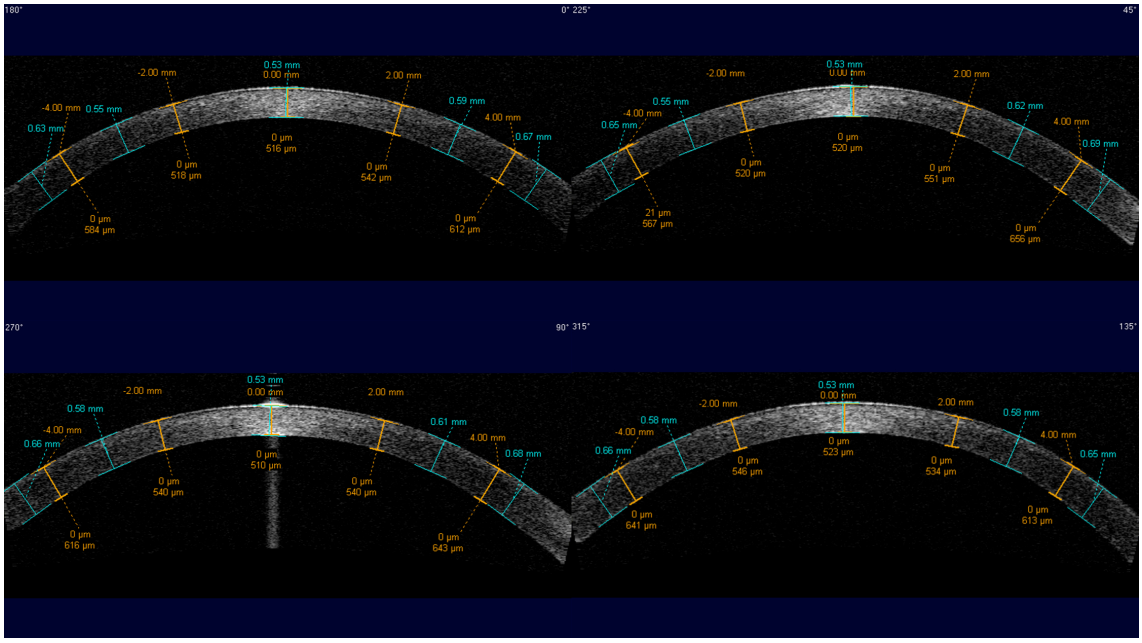

Figure 10. Four-quadrant AS-OCT scans of the healthy cornea. The flap tool was used to identify a central 4 mm area, a mid-peripheral area defined by the 4 mm zone and an outer 8 mm zone, and a peripheral area extending from the 8 mm zone to the limbus. The corneal thickness was measured in the centre of each area on all four scans with calliper tools.

2.2.2 AS-OCT imaging protocol in human corneal infection

Patients with corneal infection underwent Visante OCT imaging at presentation and follow-up appointments. A standardised protocol was set up in order to image the same corneal area and infiltration at all examination visits.

At all visits, a high-resolution AS-OCT scan was carried out through the infiltration with the scanning beam running through the axis that crossed the centre of the infiltration. The imaging protocol is illustrated in figure 11.

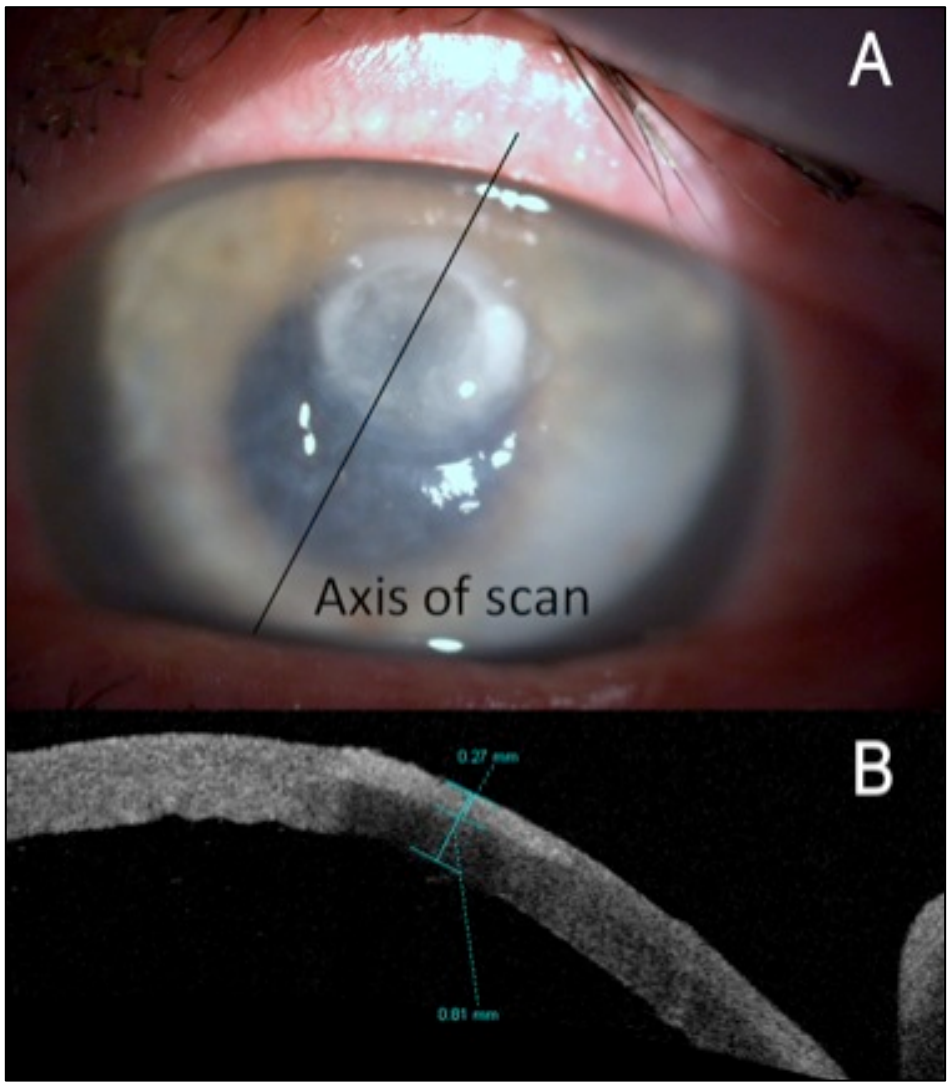

Figure 11. AS-OCT imaging protocol in corneal infection. A. Photo of corneal ulcer due to bacterial keratitis; the black line illustrates the AS-OCT scanning beam running through the centre of the infiltrate at a defined axis. B. The AS-OCT image illustrates the measurement of morphological parameters.

The images were analysed for the presence of morphological features that were not observed in images of healthy participants. In addition, the calliper tools of the Visante OCT software (version 1.1.2) were used to explore the quantification potential of identified morphological features.

2.2.3 AS-OCT imaging protocol in peripheral ulcerative keratitis

Patients with peripheral ulcerative keratitis (PUK) had AS-OCT imaging with the Visante OCT at presentation and follow-up examinations. High-resolution AS-OCT scans were carried out at presentation through a defined axis, which depended on the ulcer location. At follow-up examinations, the AS-OCT scans were repeated through the same defined axis (figure 12).

The AS-OCT images were compared to images of healthy controls and analysed for the presence of morphological features that were characteristic of the condition. The software callipers of the device (software version 1.1.2) were used for quantification. In addition, the images were exported into the GNU Image Manipulation Program (GIMP version 2.8.8) and the quantification potential investigated.

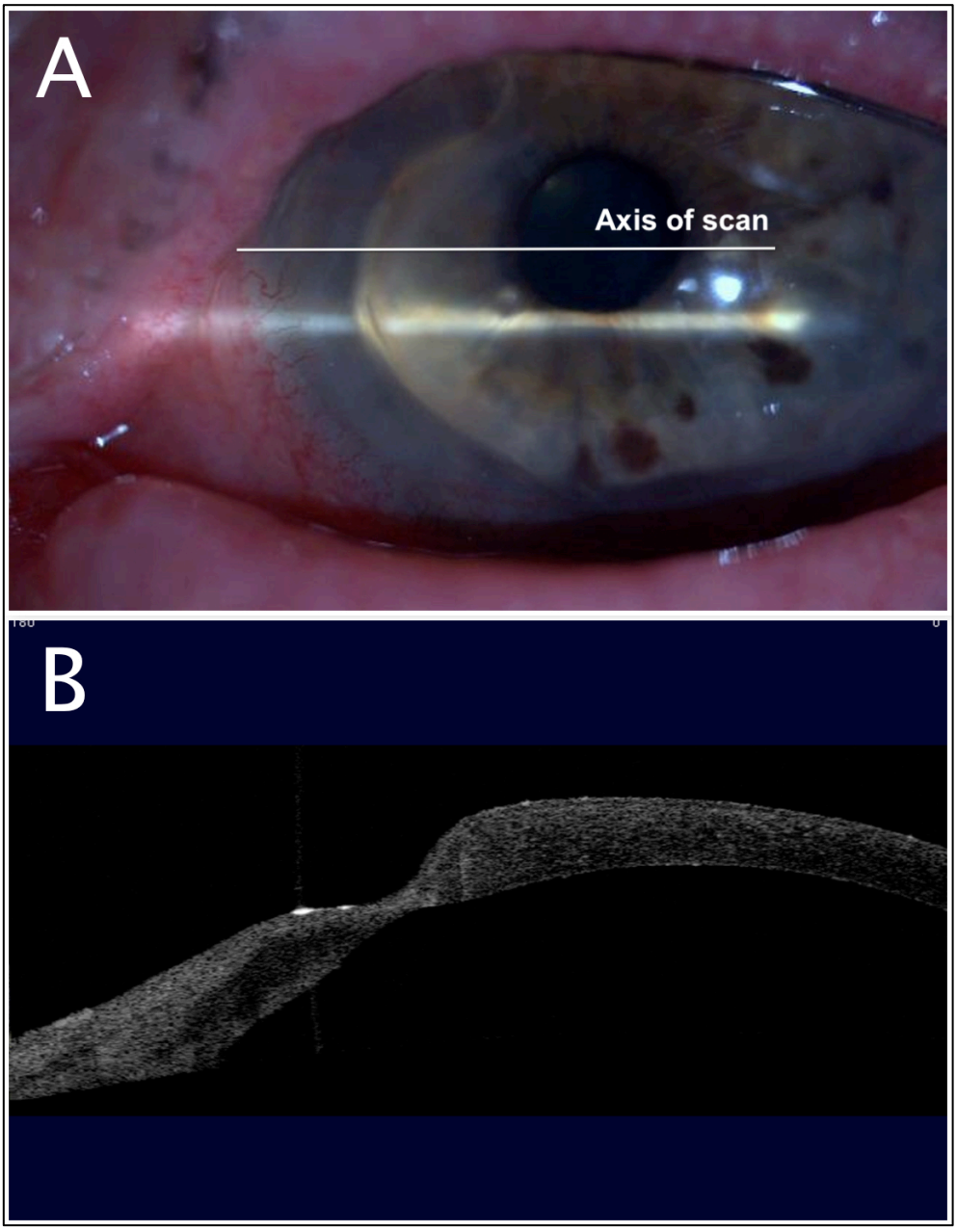

Figure 12. AS-OCT imaging protocol in peripheral ulcerative keratitis. A. Photo at presentation showed peripheral corneal thinning with a 'contact lens cornea' appearance. The white line illustrates the AS-OCT scanning beam running through the ulcerated area at a defined axis. At all examinations the AS-OCT scan was repeated with the scanning beam running through the affected area at the defined axis. B. The AS-OCT image of this case shows a cross-section of the pathological cornea.

2.2.4 AS-OCT imaging protocol in Descemets stripping endothelial keratoplasty

Patients who had Descemets stripping endothelial keratoplasty (DSEK) had high-resolution AS-OCT scans at the 180^{o} meridian with the Visante OCT (figure 13). The scan that was best centred on the graft was chosen for analysis. Measurements of corneal and graft thickness were made with manual placement of the flap tool arms in the centre of the cornea.

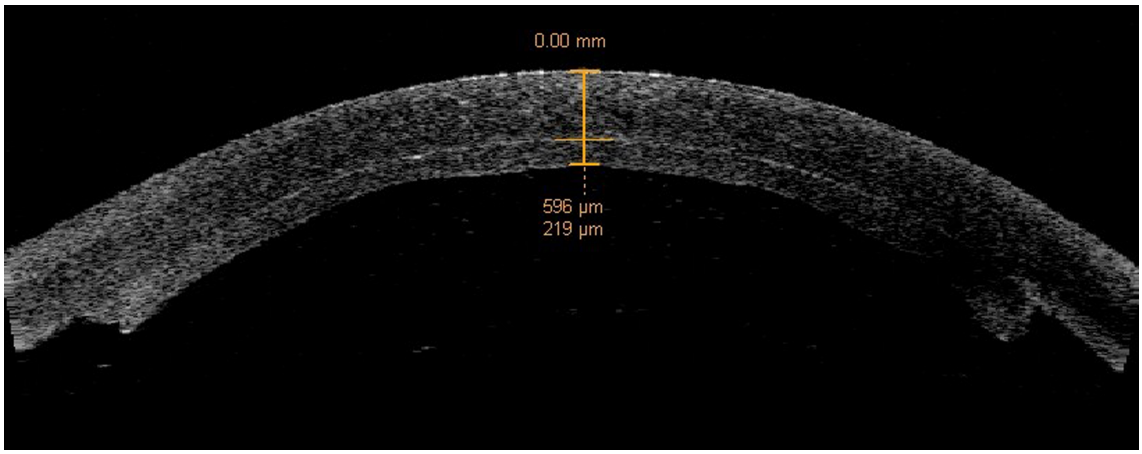

Figure 13. AS-OCT imaging in Descemets stripping endothelial keratoplasty. The endothelial graft is attached to the inner surface of the host cornea. The graft-host cornea interface, the epithelium and endothelium appear hyper-reflective relative to the stroma, facilitating manual placement of the arms of the flap measurement tool.

2.2.5 AS-OCT imaging in animal model of keratoprosthesis infection

AS-OCT scans in a rabbit model of keratoprosthesis associated BK (section 2.5) were carried out with the FD-OCT RTVue by Optovue, immediately before and following bacterial inoculation. The cornea anterior module (CAM) lens was fitted to the device for corneal scans. The AS-OCT scans were carried out at all examinations through the centre of a titanium keratoprosthesis implant using the 'cross line scan' mode (figure 14). The CT was measured in 5 locations along the cross-sectional image of the titanium plate, as detailed in chapter 6.

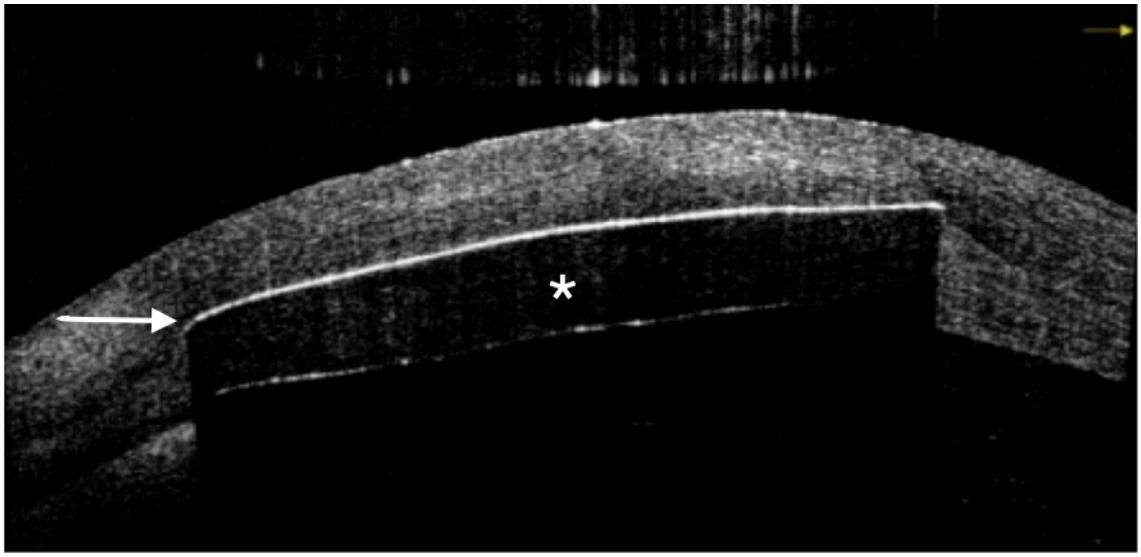

Figure 14. AS-OCT imaging in animal model of keratoprosthesis associated infection. The mid-stromal hyper-reflective line (arrow) represents the titanium keratoprosthesis implant. A dark shadow is present below the implant (*) due to lack of penetration of AS-OCT signal through the implant.

2.3 Tear chemokine and cytokine analysis

Tear samples were collected by carrying out a conjunctival lavage of the affected eye using sterile normal saline without topical anaesthetic drops. The conjunctival fluid was spun down in a centrifuge (2000 rpm/0.4G for 10 minutes at 4 ^{o}C) to produce a cell pellet and a supernatant. The supernantant was stored at -80 ^{o}C for analysis at a later date.

The cell pellet was resuspended with 300 µL phosphate-buffered saline (PBS) solution and 4 cytospin slides were prepared. The cytospin slides were stained by the May Grunwald Giemsa method for differential cell counting. In more detail, they were stained with the May Grunwald solution (Sigma Aldrich, Germany) for 5 min. They were then washed with water and stained with Giemsa (Sigma Aldrich, Germany) for 15 minutes. The slides were then washed with water and left to dry.

Differential cell counting was carried out with light microscopy (X40 magnification) on 400 cells. The cytospin slides were also examined with oil immersion light microscopy (X100 magnification) in order to assess the health of identified cells.

The frozen supernatant of tear sample collections was thawed and analyzed for levels of the following cytokines and chemokines: IL-2, IL-8, IL-12p70, IL-1β, GM-CSF, IFN-γ, IL-6, IL-10, and TNF-α. The pro-inflammatory multiplex assay kit by Meso Scale Discovery (MSD) (Gaithersburg, MD, USA), which is based on the electrochemiluminescence principle, was used for quantification of cytokine and chemokine levels.

2.3.1 Principles of MSD electrochemiluminescence assay

The 96-well MSD plate has been pre-coated with capture antibody for the above 9 cytokines and chemokines on spatially distinct spots at the base of each well. After addition of the tear sample and a solution that contains the detection antibodies that are labeled with an electrochemiluminescent compound, MSD SULFO-TAG™ label, the target protein molecules in the tear sample are captured by the immobilized antibodies on the working electrode

surface. Recruitment of the labeled detection antibodies by the target molecules completes the sandwich (figure 15). An MSD reader buffer is also required in order to provide the appropriate chemical environment for electrochemiluminescence. Once the plate is placed in the reading MSD SECTOR™ instrument, a voltage is applied to the plate electrodes causing the labels that are bound to the electrode surface to emit light. The MSD SECTOR™ instrument then measures the intensity of emitted light, providing a quantitative measure of IL-2, IL-8, IL-12p70, IL-1β, GM-CSF, IFN-γ, IL-6, IL-10, and TNF-α that are present in the sample.

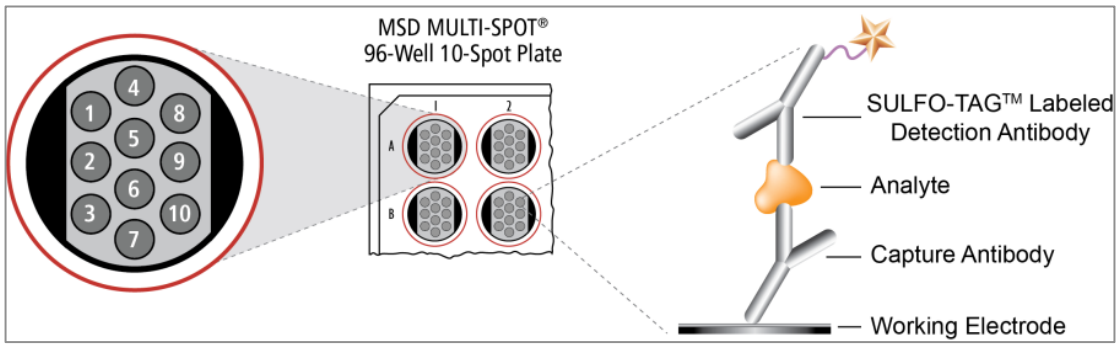

Figure 15. Spot diagram showing placement of the capture antibody. A sandwich is formed between the capture antibody and the SULFO-TAG™ labeled detection antibody.

2.3.2 Protocol of MSD electrochemiluminescence assay

2.3.2.1 Reagents

1. SULFO-TAG Detection Antibody Blend (50X)
2. Human Proinflammatory Calibrator Blend
3. Diluent 2
4. Diluent 3
5. Read Buffer T (4X)

6. Phosphate buffered saline plus 0.05% Tween-20 (PBS-T)

2.3.2.2 Preparation of calibrator and control solutions

A diluted stock Calibrator was prepared by diluting the stock Calibrator 100-fold in diluent 2. MSD recommends the preparation of an 8-point standard curve consisting of at least 2 replicates of each point. For the assay, MSD recommends 4-fold serial dilution steps and diluent 2 alone for the 8th point. To prepare this 8-point standard curve for up to 4 replicates, the diluted stock Calibrator was prepared by transferring 10 µL of the Human Proinflammatory Calibrator Blend to 990 µL of diluent 2. The highest Calibrator point was prepared by transferring 50 µL of the Human Proinflammatory diluted stock Calibrator to 150 µL diluent 2. Then, 4-fold serial dilutions were repeated 6 additional times to generate 7 Calibrators. The recommended 8th Standard was Diluent 2 (i.e. zero Calibrator).

2.3.2.3 Preparation of Detection Antibody Solution

The Detection Antibody Blend was provided at 50X stock solution. The final concentration required was 1X; in order to prepare this, a 60 µL aliquot of the stock Detection Antibody Blend was diluted into 2.94 mL of diluent 3.

2.3.2.4 Preparation of Read Buffer

The Read Buffer was diluted 2-fold in deionized water to make a final concentration of 2X Read Buffer T; 10 mL of 4X Read Buffer T was added to 10 mL of deionized water.

2.3.2.5 Assay Protocol

1. Addition of diluent 2. Into each well, 25 µL of diluent 2 was dispensed. The plate was sealed with an adhesive plate seal and incubated for 30 minutes with vigorous shaking (500 rpm) at room temperature.
2. Addition of Sample or Calibrator. Into separate wells, 25 µL of sample or Calibrator was dispensed. The plate was sealed with an adhesive plate seal

and incubated for 2 hours with vigorous shaking (500 rpm) at room temperature.

3. Wash and addition of the Detection Antibody Solution. The plate was washed 3 times with PBS-T. Into each well, 25 µL of the 1X Detection Antibody Solution was dispensed. The plate was sealed with an adhesive plate seal and incubated for 2 hours with vigorous shaking (500 rpm) at room temperature.
4. Wash and reading of plate. The plate was washed 3 times with PBS-T. Into each well, 150 µL of 2X Read Buffer T was added. The plate was then analyzed and read on the SECTOR Imager.

2.3.2.6 Sensitivity of assay

The values below represent the manufacturer quoted average lower limit of detection (LLOD):

LLOD (pg/mL)	IL-2 0.35	IL-8 0.09	IL-12p70 1.4	IL-1β 0.36	GM-CSF 0.20
	IFN-γ 0.53	IL-6 0.27	IL-10 0.21	TNF-α 0.5	

2.4 Animal model of keratoprosthesis associated bacterial keratitis

New Zealand White rabbits were used for the study of keratoprosthesis associated bacterial infection. This infection model was previously developed at the Singapore Eye Research Institute by the research teams of Associate Professor Jod Mehta, Professor Roger Beuerman and Professor Donald Tan.[42] The similarities of the rabbit cornea to the human cornea were described in the introduction chapter (section 1.2.4). Titanium was chosen by the Singapore team as a substrate material for the Kpro device, as their previous work had shown that titanium oxide had excellent properties regarding corneal fibroblast adhesion and integration, and in reducing bacterial adhesion when compared with hydroxyapatite, aluminum, and yttria-stabilized zirconium substrates.[242] In addition, they found that this material could be successfully coated with an anti-microbial peptide and, thus, be used in Kpro devices with the potential to reduce the risk of post-operative infection.[42] A titanium back-plate is now used for the Boston type 1 Kpro.[243]

Anaesthesia of the rabbits was carried out using an intramuscular injection of ketamine hydrochloride (35 mg/kg; Parnell Laboratories, Alexandria, Australia) and xylazine hydrochloride (5 mg/kg; Troy Laboratories, Smithfield, Australia). The right eye was chosen for surgery and implantation of the titanium implant. A 7 mm diameter and 75% deep corneal stromal pocket was created using the Visumax™ femtosecond laser (Carl Zeiss Meditec, Jena, Germany). A 5 mm wide arcuate incision was made to 75% depth by a guarded diamond blade (Storz, Bausch and Lomb, USA), the pocket opened up with a Seibel spatula (Rhein Medical Inc., Petersburg, FL) and the 4 mm diameter titanium film implanted into the pocket. The arcuate access incision was sutured with three 10/0 nylon sutures.

At 7-12 days post-implantation, bacterial inoculation of the right eye with *Staphylococcus aureus* (*S. aureus*) was carried out. A 25 µl bacterial solution of *S. aureus* (ATCC29213, $2X10^4$ CFU/ml) was inoculated with a 29 G needle into the corneal pocket above the titanium film. The animals were sacrificed at predetermined time-points, as detailed in chapter 6. Euthanasia was carried out with intravenous pentobarbitone (85 mg/kg) in anaesthetized rabbits.

2.5 Slit-lamp photography grading

Slit-lamp photographs (figure 16) were taken with an anterior segment slit-lamp camera (Zoom Slit Lamp NS-2D, Righton, Tokyo, Japan) before and after bacterial inoculation. They were then graded in a masked manner, using a well-established grading scale for BK in animal studies.[244] Scores of 0,1,2,3 or 4 were given for each of 4 parameters: conjunctival injection, conjunctival chemosis, corneal oedema and corneal infiltration. The parameter scores were added-up to a total slit-lamp photography (SLP) score ranging from 0 to 16.

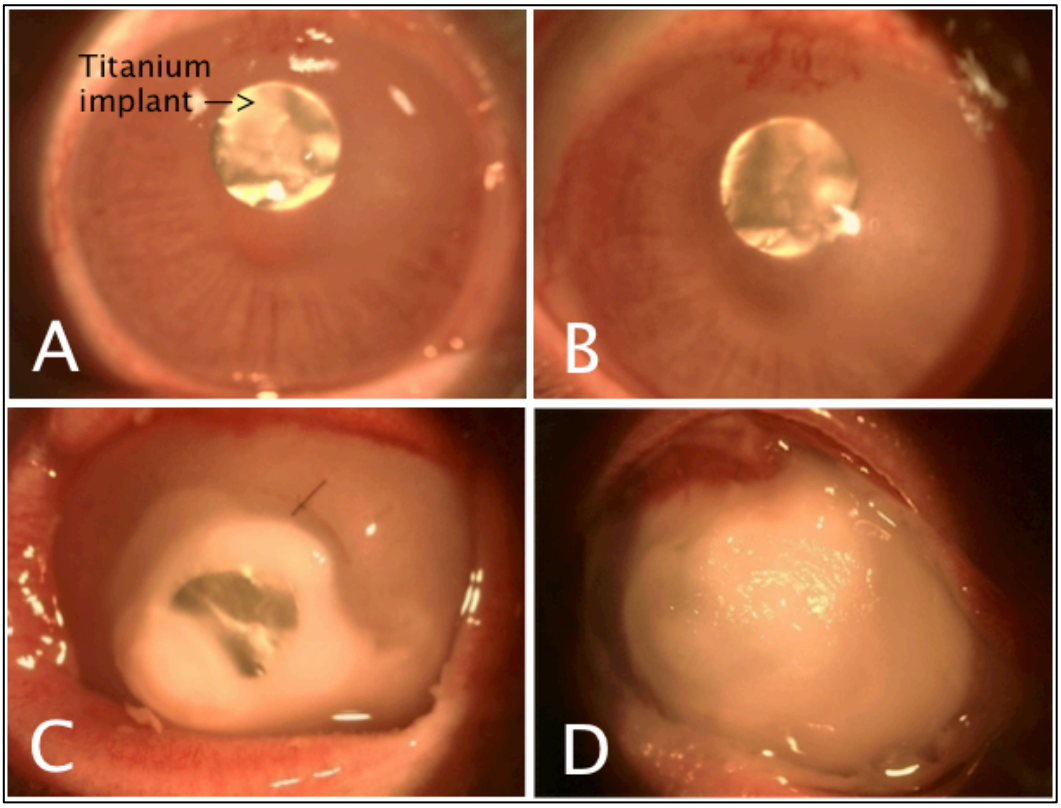

Figure 16. Slit-lamp photography grading of severity of corneal infection. A. Less than 25% of the cornea is affected by oedema (score 1) and infiltration (score 1). B. Between 25 and 50% of the cornea is affected by oedema (score 2) and infiltration (score 2). C. Between 50 and 75% of the cornea is affected by infiltration (score 3) and 100% by oedema (score 4). D. More than 75% of the cornea is affected by oedema (score 4) and infiltration (score 4).

2.6 Quantification of viable bacteria

Following bacterial inoculation, the rabbits were euthanized at predetermined time-points and the corneas removed by trephination. They were individually homogenized in PBS using plastic pestles followed by fine homogenization with bead beating using sterile glass beads (2 mm). The homogenate then underwent serial dilution plating using Tryptic Soy Agar (TSA) plates (Beckman, USA). The plates were incubated at 35 ^{o}C for 48 hours. The numbers of colonies were counted and the results expressed as log10 number of CFU/ cornea.

2.7 Histology and immunohistochemistry

Excised corneas of rabbits that were euthanized at predetermined time-points were fixed in 4% paraformaldehyde followed by serial dehydration with an increasing concentration of ethanol. After dehydration, tissue blocks were embedded into paraffin and cut at 5 µm thickness using a microtome. The sections were stained with haematoxylin (Sigma Aldrich, Germany) and eosin (Sigma Aldrich, Germany) and then viewed under a light microscope.

Tissue blocks were also embedded in optimum cutting temperature (OCT) cryo-compound (Leica Microsystems, Nussloch, Germany) for immunohistochemistry studies. Frozen tissue blocks were stored at -80 ^{o}C until sectioning. Serial sagittal corneal 10 µm sections were cut using a cryostat (Microm HM550; Microm, Walldorf, Germany). Sections were placed on polylysine-coated glass slides and air dried for 15 minutes.

For haematoxylin and eosin (H&E) staining, tissue sections were immersed in H&E solutions for 10–20 seconds before cleaning with pure xylene. For immunohistochemistry, tissue sections were post-fixed with 4% paraformaldehyde for 15 minutes, washed with PBS and blocked with 10% normal goat serum in 1X PBS and 0.15% Triton X-100 for 1 hour. The sections were incubated with rat monoclonal antibody against CD11b (Abcam, SanFrancisco CA) diluted 1:100 at 4 ^{o}C overnight. After washing with 1X PBS, the sections were incubated with goat anti-rat Alexa Fluor 488 conjugated secondary antibody (Invitrogen, Carlsbad, CA) at room temperature for 1 hour. Slides were then mounted with UltraCruz Mounting Medium containing 4′, 6-diamidino-2-phenylindole (DAPI; Santa Cruz Biotechnology, Santa Cruz, CA). For negative controls, non-immune serum was used in place of the specific primary antibody. Sections were observed and imaged with a fluorescence microscope (Carl Zeiss).

Microscopic qualitative assessment was carried out on H&E stained sections. Five random corneal sections from each rabbit were examined for the ratio of CD11b positive/non-CD11b positive cells, CD11b being a marker of granulocytes, such as neutrophils, and monocytes.[245]

2.8 Liquid Chromatography - Mass Spectrometry

Vancomycin pharmacokinetics were investigated in eyes of New Zealand White rabbits. The eyes had instillation of vancomycin 1.4% drops five times a day for variable time intervals before aqueous humour and corneal samples were collected. Aqueous humour was collected under anaesthesia of the rabbits with intramuscular ketamine hydrochloride and xylazine hydrochloride. The corneas were removed by trephination after euthanasia under anaesthesia. Quantification of corneal and aqueous vancomycin was carried out by Liquid Chromatography – Mass Spectrometry (LC-MS).

Vancomycin standards (Vancomycin hydrochloride, Hospira, Lake Forest, Illinois, USA) were prepared by dissolution of a single dose vial and serial dilution with water (Ultrapure water, Millipore purification unit). Aqueous humour samples of 120-150 µL were extracted from the original collections with three equivalents of methanol (Merck, Darmstadt, Germany). The samples were shaken for 5 min at 1200 rpm (20 ^{o}C) and centrifuged for 10 min at 16,000 g (4 ^{o}C). The supernatants were transferred to fresh tubes and dried in a vacuum concentrator. The corneas were cut and ground with a pestle while frozen. They were next homogenized on ice with 300 µL of 3:1 methanol/water with 0.1% formic acid (Sigma Aldrich, St. Louis, MO, USA) for 1 min. The homogenates were then spun down briefly on a capsule centrifuge and supernatants transferred to fresh tubes. The residues were homogenized and spun down a second time. The extracts were combined and centrifuged for 10 min at 16,000 g (4 ^{o}C). The supernatants were transferred to fresh tubes and dried in a vacuum concentrator. All samples were then reconstituted in water (Ultrapure water, Millipore purification unit) and centrifuged for 5 min at 16,000 G (10 ^{o}C) before transferring to autosampler vials for LC-MS analysis.

Chromatographic separation was performed on a Waters 2695 Separations Module (Milford, MA, USA) with a Thermo Scientific Hypersil Gold C18 column (Whaltham, MA, USA) (2.1 × 50 mm, 3 µm). The mobile phase was A: 0.1% formic acid in water and B: 0.1% formic acid in acetonitrile. The gradient profile was 2% B at 0 min, 25% B at 6 min, 90% B from 6.5 to 8.5 min and 2% B from 9 to 13 min. The flow rate was 0.3 ml/min. The autosampler and column heater

temperatures were maintained at 10 and 30 ^{o}C, respectively. Detection was performed by an AB Sciex API 2000 triple quadrupole mass spectrometer (Concord, Canada) with an electrospray ionization source operating in the positive ionization mode. The ion source voltage was set to 5 kV. Vancomycin was detected by monitoring the transition 725.5/144.0 with collision energy of 25 V.

Calculation of the corneal vancomycin concentration was based on the amount of vancomycin detected in the corneal sample by LC-MS, the gross weight of the corneal sample and the assumptions that 1 ml of water weighs 1 gram and that the water content of the cornea was 78%.[246,247] The following formula was used:

corneal vancomycin concentration = amount vancomycin in corneal sample/weight corneal sample X 0.78.

2.9 Statistics

Data were examined for normal distribution with Shapiro-Wilk or Kolmogorov-Smirnov statistics, distribution plots and histograms. Data with a normal distribution were examined with parametric tests, data with a skewed distribution with non-parametric tests. Details of specific tests and comparisons are provided in the individual studies and chapters.

Analysis was carried out with the Statistical Package for Social Sciences (IBM SPSS Statistics for Macintosh, Versions 19.0 to 21.0, Armonk, NY: IBM Corp). A P-value less than 0.05 was considered statistically significant, unless specified differently in the individual study.

3. Imaging Capabilities of Anterior Segment Optical Coherence Tomography in Inflammation

3.1 Anterior Segment Optical Coherence Tomography imaging in corneal infection

3.1.1 Introduction

Microbial keratitis is a potentially serious corneal infection that can lead to severe visual loss.[248] In bacterial keratitis (BK), the most common microbial keratitis, up to 40% of patients develop final vision poorer than at presentation,[17] and 23.3% experience loss of two or more Snellen lines of visual acuity (VA) compared to the fellow eye.[79] It is often associated with contact lens wear, trauma and ocular surface disease.[7,17,77-80] Diagnosis of the condition is usually based on a typical history and clinical slit-lamp features of a corneal epithelial defect associated with stromal infiltration.

Assessment of corneal infection is difficult and relies greatly on the experience of the examining clinician, especially regarding the depth and extent of pathology. Evaluation of the response to treatment is subjective and is traditionally carried out by serial measurement of the epithelial defect dimensions on the slit-lamp,[7] and less commonly with the aid of serial anterior segment photography. Improvement in patient symptoms is also considered an indication of resolving infection. In animal studies that require quantification of corneal infection, a semi-quantitative grading system is used that is based on assessment of slit-lamp features.[8,9] Similar to clinical examination of patients, assessment of these features is greatly subjective. Objective assessment and quantification of microbial keratitis, or any corneal inflammatory condition, would assist the initial examination at patient presentation and also the monitoring of the response to treatment.

AS-OCT produces high-resolution cross-sectional images of the cornea, making it a promising device for imaging corneal anatomy and pathology.[10,11,228] It has

been used to analyze the architecture of clear corneal incisions following cataract surgery and to assess the depth of intrastromal corneal rings in keratoconic eyes.[10,11] It has also shown promising properties in visualising the anterior segment in the presence of severe corneal opacity.[228] The imaging capabilities displayed in these studies suggest that AS-OCT may provide images that will allow objective assessment and quantification in microbial keratitis. Due to the non-contact nature of examination and ease of scanning,[196] it may be the ideal imaging modality for evaluating and monitoring the condition.

3.1.2 Hypothesis

I hypothesise that AS-OCT imaging of the cornea in microbial keratitis will provide morphological and quantitative information that can be applied to the objective examination of the condition and also to the monitoring of the condition with serial scans. The hypothesis is explored in this study by scanning patients who presented to the emergency corneal service at University Hospital Southampton NHS Foundation Trust with suspected microbial keratitis.

3.1.3 Materials and methods

3.1.3.1 Patient recruitment

Seven patients who presented over a 4-month period with a suspected microbial corneal ulcer and were interested in participating in the study were recruited. Corneal infection was diagnosed, as per previous studies, in the presence of a typical history and an epithelial ulceration with underlying stromal infiltration associated with signs of inflammation.[7,84,146] Due to the pilot nature of this study only patients with corneal infiltration on clinical examination were included. Patients with a history and clinical findings suggestive of a viral keratitis or hypersensitivity type corneal ulceration were not recruited. The infection was considered resolved when the epithelial defect and signs of inflammation resolved completely. All patients underwent treatment based on slit-lamp examination and clinical findings; treatment was not altered by AS-OCT findings.

Local NHS Research Ethics Committee and patient informed consent were obtained. The research adhered to the tenets of the Declaration of Helsinki (section 2.1.1).

3.1.3.2 Examination and imaging

Patients underwent imaging with the Visante AS-OCT and clinical sit-lamp examination. Imaging and examination were carried out at presentation and subsequently at two follow-up appointments. A standardised imaging protocol was set up and used for each patient in order to image the same area of the cornea and infiltration at all examinations; this is detailed in the methods chapter (section 2.2.2).

The AS-OCT scans were examined for the presence of morphological features of microbial keratitis. In addition, the calliper tools of the Visante OCT software (version 1.1.2) were used to explore the potential to quantify the identified morphological features.

3.1.4 Results

The AS-OCT images showed the presence of a hyper-reflective area in the anterior corneal stroma. This hyper-reflective area corresponded in location to the corneal infiltrate. At presentation, it was detected in 6 of the 7 cases. The thickness of this hyper-reflective area could be measured with the software callipers in these 6 cases; as the hyper-reflective area corresponded to the clinical corneal infiltrate, this AS-OCT morphological parameter was termed infiltrate thickness (IT). IT was measured in the centre of the hyper-reflective area by placing one calliper arm on the most anterior hyper-reflective corneal surface, whether stromal or epithelial, and the second arm on the posterior border of the hyper-reflective area. IT could not be measured in 1 case, as the endothelium could not be distinguished from an attached endothelial plaque.

Hyper-reflective particles in the anterior chamber of the eye were identified in two images (cases) at presentation. Two cases also showed the presence of a hyper-reflective plaque or mass just posterior or attached to the endothelium.

The corneal thickness (CT) could be measured in the centre of the hyper-reflective area by placing one calliper arm on the most anterior hyper-reflective

corneal surface, whether stromal or epithelial, and the second arm on the hyper-reflective layer of the endothelium. Measurement of CT was possible in 6 of the 7 images at presentation. In 1 image this was not possible, as the endothelium could not be distinguished from an attached endothelial plaque. This is the same case in which IT could not be measured.

The imaging capabilities and quantification potential of AS-OCT are described in more detail in the individual case reports that follow. Overall, serial measurements of quantitative parameters were possible in all cases. CT and IT were measured serially in six cases. In the one case (case 6) in which this was not possible, the width of the inflammatory plaque was measured on serial examination. The AS-OCT findings are summarised in table 1.

3.1.4.1 Case 1

A 29-year-old male contact lens wearer presented with a painful left eye. Slit-lamp examination showed mild conjunctival injection and a small epithelial defect associated with stromal infiltration (figure 17A). An AS-OCT scan through the infiltrate centre at the 43-degree axis showed a superficial stromal hyper-reflective area corresponding to the clinical infiltrate (figure 17B). CT in the infiltrated area measured 800 µm; IT was 190 µm. Intensive topical ofloxacin was commenced. Two days later, conjunctival injection was reduced and the epithelial defect had clinically resolved. Microbiology cultures were negative. On AS-OCT scan, CT and IT were both reduced to 690 and 120 µm respectively (figure 17C). Twelve days later, the infiltrate had clinically resolved with development of a corneal scar. The AS-OCT CT in the affected area was 650 µm; the hyper-reflective area corresponding to the scar was thin and linear (figure 17D).

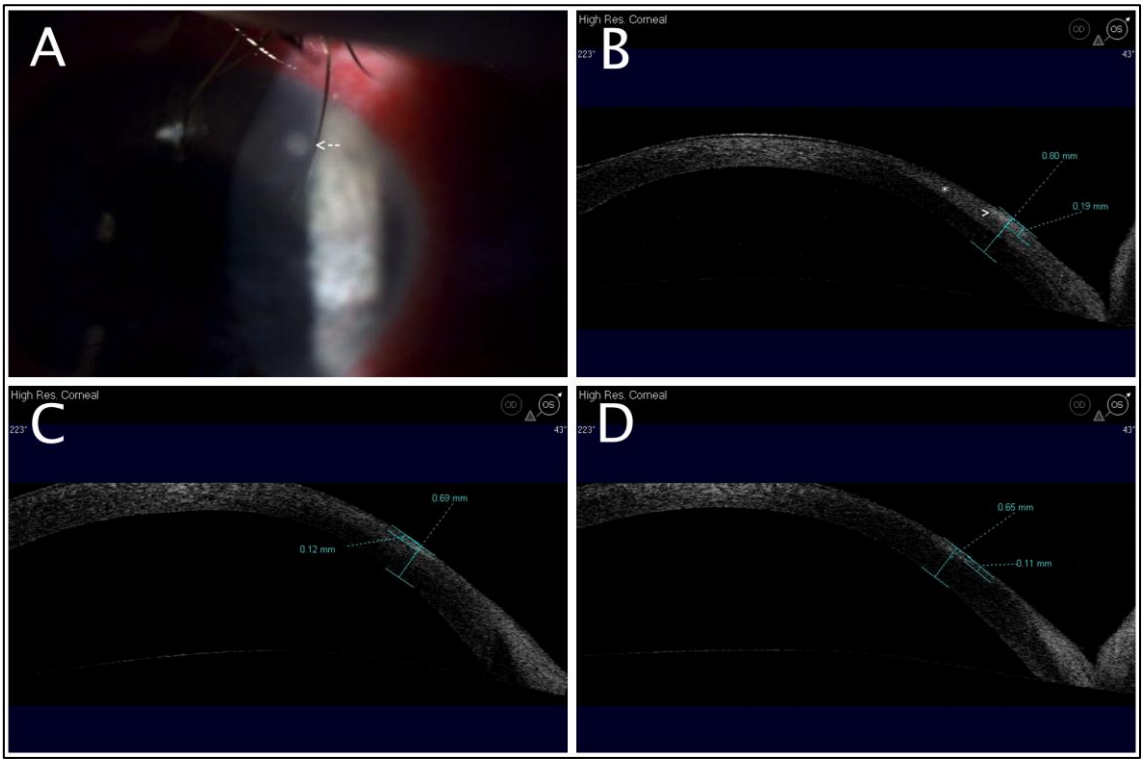

Figure 17: Case 1. Contact lens associated keratitis and serial AS-OCT scans at 43-degree axis. A. Anterior segment photo at presentation shows small corneal infiltrate (<--). B. AS-OCT through the infiltrate at presentation shows a superficial stromal hyper-reflective area (>); a less well-defined hyper-reflective area in the anterior stroma (*) may represent oedema. C. AS-OCT 2 days after presentation shows reduction of infiltrate and corneal thickness. D. AS-OCT through the scar 2 weeks after presentation shows further reduction of corneal thickness and the presence of a flat hyper-reflective area corresponding to the scar.

3.1.4.2 Case 2

A 63-year-old female contact lens wearer presented with a painful right eye. Slit-lamp examination showed conjunctival injection associated with an inferior epithelial defect and stromal infiltration (figure 18A). An AS-OCT scan at the 95-degree axis through the infiltrate centre showed a superficial hyper-reflective area with IT measuring 130 µm; CT in the infiltrated area measured 670 µm (figure 18B). Intensive topical ofloxacin 0.3% was commenced. Four

days later the epithelial defect had clinically resolved with the presence of an irregular and slightly raised epithelial surface. Microbiology cultures were negative. On repeat AS-OCT, an intact epithelium was present over the hyper-reflective infiltrate; IT and CT had increased to 280 and 750 µm respectively (figure 18C). Inclusion of the raised epithelium in the thickness measurements may have accounted for this. Topical ofloxacin 6 times a day was continued. Clinical examination 10 days later showed a quiet eye with no epithelial defect and the development of scar tissue in the infiltrated area. AS-OCT CT had decreased, measuring 590 µm; the hyper-reflective area was thinner (120 µm) and had a flat appearance (figure 18D).

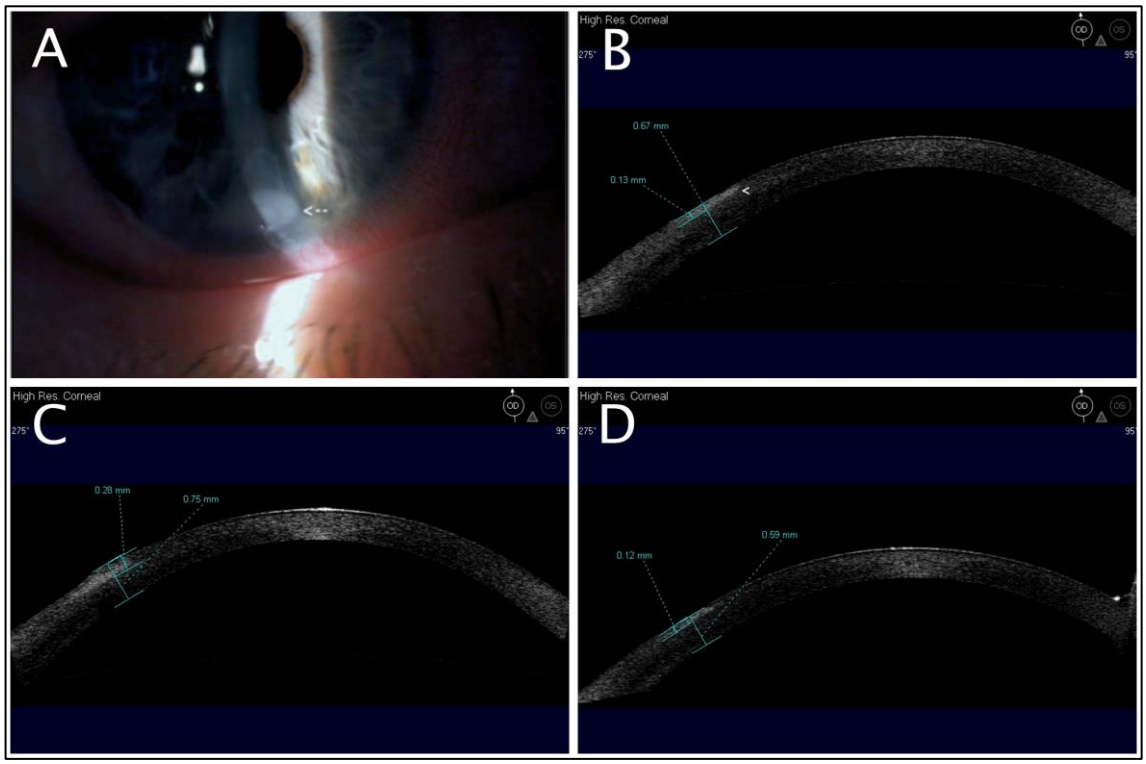

Figure 18: Case 2. Contact lens associated keratitis and serial AS-OCT scans at 95-degree axis. A. Anterior segment photo at presentation shows an inferior corneal infiltrate (<--). B. AS-OCT at presentation shows an epithelial defect and a superficial anterior stromal hyper-reflective area at the location of the infiltrate (<). C. AS-OCT 4 days after presentation shows resolution of the epithelial defect and a raised epithelial surface. D. AS-OCT 2 weeks after

presentation shows reduction of corneal thickness; the hyper-reflective area corresponding to the scar is flat and well defined.

3.1.4.3 Case 3

A 35-year old lady with a history of recurrent corneal erosion syndrome presented with a painful right eye. Slit-lamp examination showed a large corneal epithelial defect associated with 3 small superficial stromal infiltrates (figure 19A). High-resolution AS-OCT imaging through the inferior infiltrate at the 60-degree meridian showed that IT was 370 µm thick and CT 910 µm (figure 19B). Intensive topical ofloxacin 0.3% and cefuroxime 5% were commenced, with a good response. *Staphylococcus aureus* was grown on culture. Ten days after presentation, the epithelial defect had healed and the infiltrates were clinically resolving. Repeat AS-OCT showed that IT was reduced, measuring 240 µm, as was CT that measured 630 µm (figure 19C). One week later, the infiltrates had clinically resolved and scar tissue had developed. The AS-OCT CT was further reduced and the hyper-reflective area that corresponded to the scar tissue was imaged to a depth of 250 µm (figure 19D).

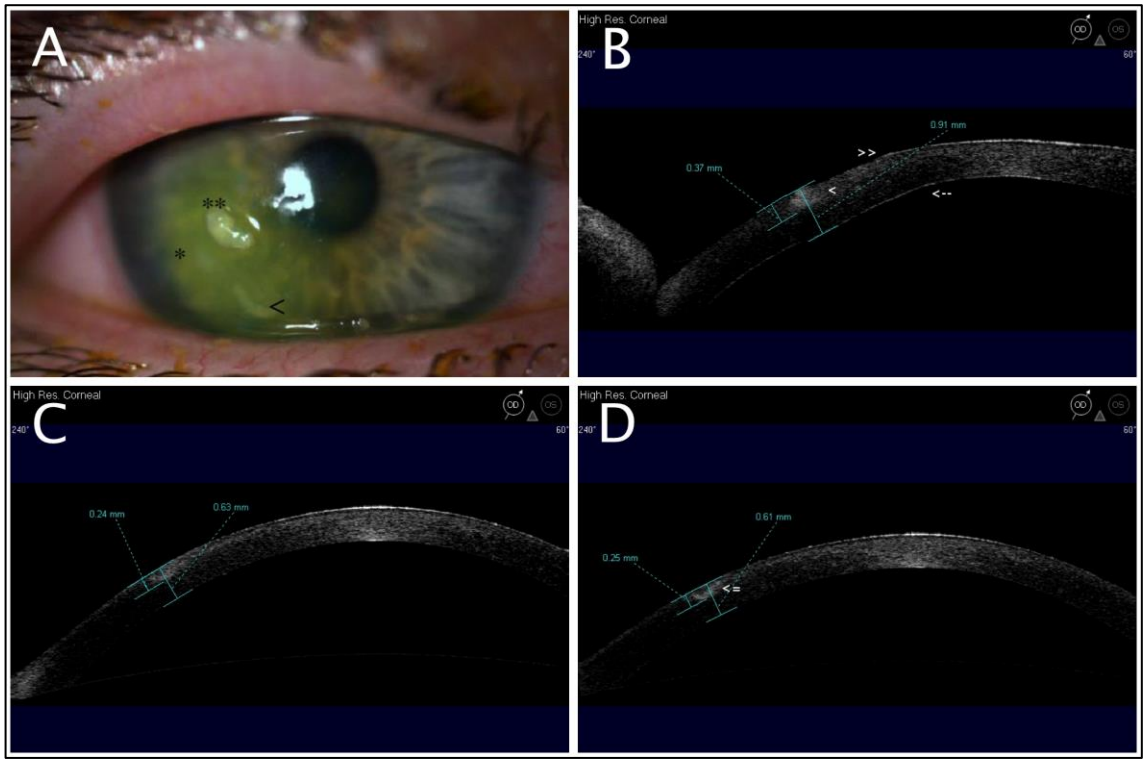

Figure 19: Case 3. Bacterial keratitis in recurrent corneal erosion syndrome imaged with serial AS-OCT scans at 60-degree meridian. A. Anterior segment photo at presentation shows corneal infiltrates (□ and <) and mucus (□□). B. AS-OCT through the lower infiltrate (<) at presentation shows a hyper-reflective area that corresponds to the corneal infiltration (<) and loss of epithelial continuity (>>). The lower border of the epithelial defect cannot be seen due to the underlying hyper-reflective stromal infiltration. A change in convexity of the posterior corneal surface (<--) can be observed, most likely due to the presence of stromal oedema. C. AS-OCT 10 days on treatment shows reduction of infiltrate and corneal thickness; an intact epithelial surface is now present. D. AS-OCT through the scar after 17 days of treatment shows further reduction of corneal thickness; the hyper-reflective area corresponding to the scar is thinner with a well-defined and flatter appearance (<=).

3.1.4.4 Case 4

A 57-year-old male contact lens wearer presented with a two-day history of painful right eye. Slit-lamp examination showed moderate conjunctival injection with an epithelial defect and stromal infiltration associated with a

hypopyon (figure 20A). On the AS-OCT scan through the infiltrate centre at the 90-degree axis, IT measured 530 µm; CT in the infiltrated area measured 1180 µm (figure 20B). Intensive topical cefuroxime 5% and ofloxacin 0.3% were commenced. Two days later, the epithelial defect size and hypopyon height were smaller on slit-lamp examination. *Pseudomonas aeruginosa* was grown on culture. One week after presentation, the epithelial defect had decreased in size, the hypopyon had resolved and the infiltrate was clinically less dense. Repeat AS-OCT showed that both IT and CT were reduced, measuring 490 and 920 µm respectively. Topical ofloxacin 6 times a day was continued and a week later the epithelial defect had clinically resolved. AS-OCT IT and CT were further reduced, measuring 360 and 670 µm respectively (figure 20C). Topical ofloxacin was continued four times a day. On clinical examination 6 weeks later, the eye was quiet with the development of scar tissue in the infiltrated area. AS-OCT through the scar showed that CT had decreased further, measuring 450 µm (figure 20D). The hyper-reflective area corresponding to the scar was flatter and IT was 170 µm.

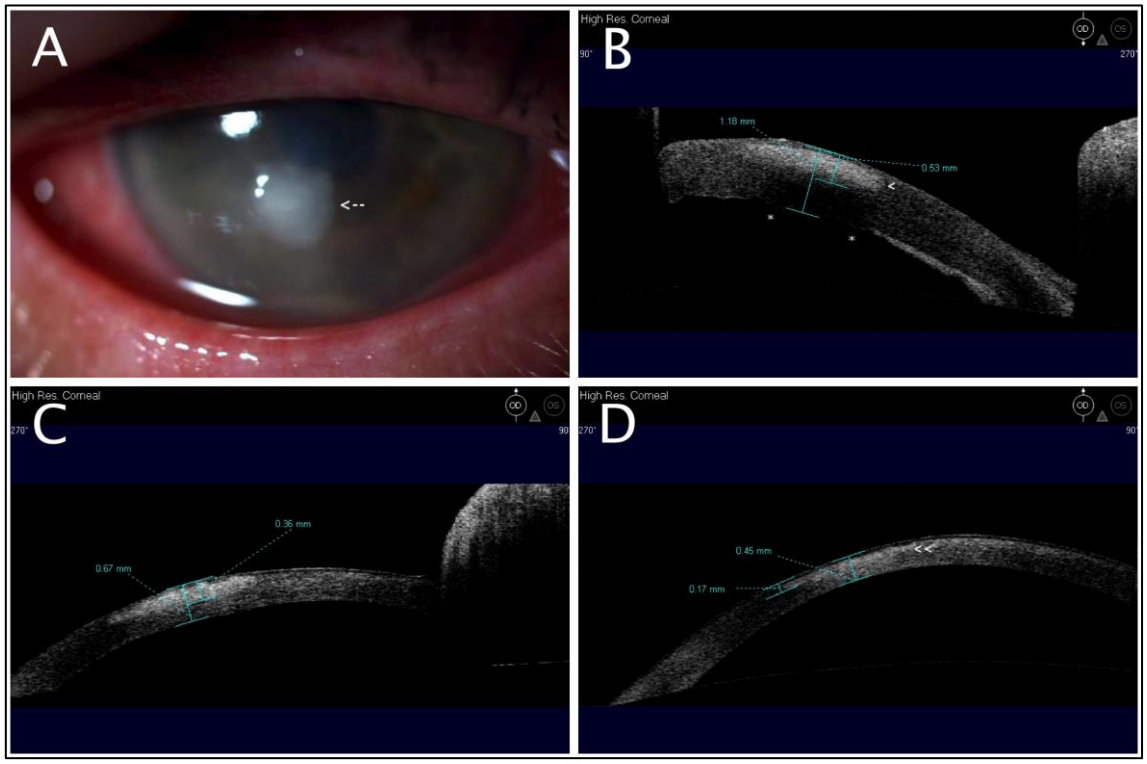

Figure 20: Case 4. Pseudomonas keratitis imaged serially with AS-OCT scans at 90-degree axis. A. Anterior segment photo at presentation shows a dense corneal infiltrate (<--). B. AS-OCT at presentation shows a thick hyper-reflective area in the anterior stroma (<), corresponding to the clinical infiltration. Descemets folds (*) are also present due to associated corneal oedema. C. AS-OCT 2 weeks after presentation shows reduction of infiltrate and corneal thickness with a smoother endothelial surface. D. AS-OCT through the scar 8 weeks after presentation shows further reduction of corneal thickness and a flatter anterior stromal hyper-reflective area corresponding to the scar (<<).

3.1.4.5 Case 5

A 60-year-old female contact lens wearer presented with a two to three day history of increasing pain and redness of right eye. Slit-lamp examination showed moderate conjunctival injection and a large epithelial defect associated with stromal infiltration (figure 21A). Anterior chamber inflammation was present with a hypopyon. AS-OCT through the infiltrate centre at the 180-degree axis showed a thick hyper-reflective area in the anterior stroma (figure 21B). CT in the infiltrated area measured 1560 µm and IT 590 µm. Corneal scrapes were carried out and intensive topical ofloxacin 0.3% and cefuroxime 5% commenced. Examination 2 days later showed a reduction in hypopyon height and epithelial defect size. AS-OCT CT and IT had decreased to 900 and 390 µm respectively (figure 21C). *Pseudomonas aeruginosa* was cultured. Clinical improvement continued and 4 days later AS-OCT CT in the infiltrated area measured 820 µm. A week later, the corneal ulcer had clinically resolved with the development of scar tissue; AS-OCT CT through the scar was 540 µm (figure 21D).

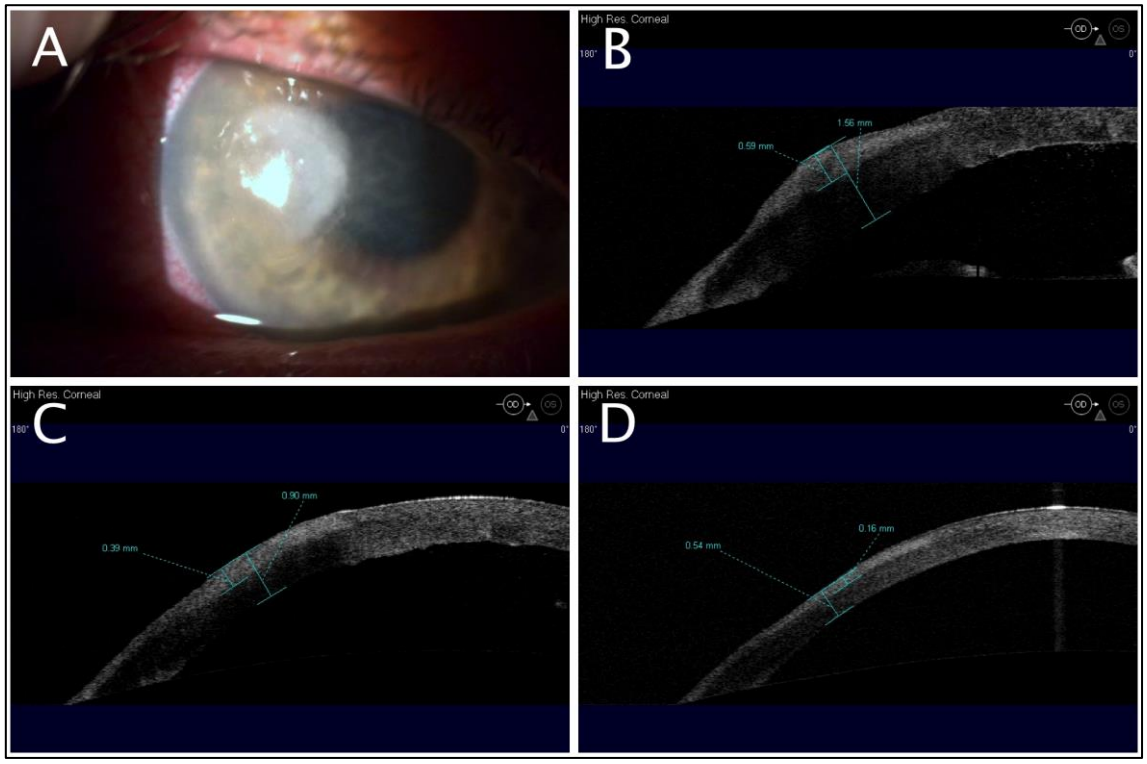

Figure 21: Case 5. Pseudomonas keratitis imaged serially with AS-OCT scans at 180-degree axis. A. Anterior segment photo at presentation shows a dense corneal infiltrate (<--). B. AS-OCT at presentation shows a thick anterior stromal hyper-reflective area (<) with marked thickening of the cornea; folds in Descemets membrane are present and hyper-reflective anterior chamber particles are visible (*), most likely representing inflammatory cells. C. AS-OCT 2 days after presentation shows reduction in infiltrate and cornea thickness; anterior chamber hyper-reflective particles are still present (*). D. AS-OCT through the scar 2 weeks after presentation shows further reduction in corneal thickness and a thinner anterior stromal hyper-reflective area (<<) corresponding to the scar.

3.1.4.6 Case 6

A 72-year old patient presented with a three to four week history of discomfort and decreasing vision in the left eye. He had a history of trichiasis and lagophthalmos. Slit-lamp examination showed conjunctival injection and a corneal epithelial defect associated with corneal thinning and deep stromal infiltration (figure 22A). Posterior synechiae and anterior chamber

inflammation were present. AS-OCT imaging through the centre of the ulceration at the 110-degree axis (figure 22B) showed loss of stromal tissue. A large hyper-reflective mass or plaque was attached to the endothelium, measuring 3.64 mm in width. CT could not be measured in the thinned area, as the endothelium could not be distinguished from the plaque. Corneal scrapes were carried out and intensive topical ofloxacin 0.3% and cefuroxime 5% commenced. Over the next 3 days conjunctival injection diminished but there was no clinically detectable change in the epithelial defect or corneal infiltration. However, repeat AS-OCT (figure 22C) showed that the retro-endothelial plaque was smaller, measuring 3.09 mm wide. Diphtheroid bacteria were grown on culture. The frequency of antibiotics was reduced and during the following week the size of the epithelial defect and infiltration clinically diminished. Ten days post-presentation the risk of perforation was raised, as the cornea appeared very thin clinically. AS-OCT (figure 22D) showed that the plaque had resolved completely. CT in the ulcerated area, which could now be assessed, measured 190 µm, providing reassurance that perforation was not imminent.

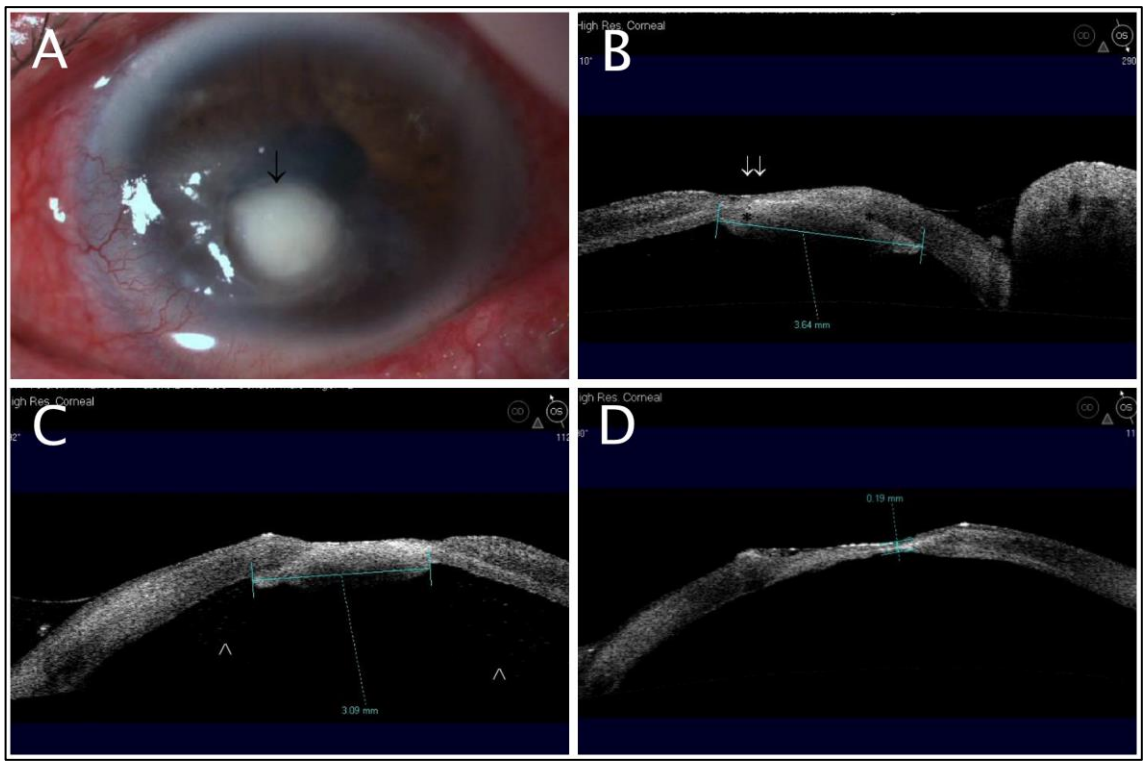

Figure 22: Case 6. Bacterial keratitis in a patient with trichiasis and lagophthalmos, scanned serially with AS-OCT images at 110-degree axis. A. Anterior segment photo at presentation shows corneal infiltrate (↓). B. AS-OCT through the infiltrate centre at presentation shows sloping ulcer edges with loss of stromal tissue and a hyper-reflective plaque attached to the endothelium (∗). C. AS-OCT three days on treatment shows reduction of the plaque width, suggesting that this is an inflammatory plaque. Individual hyper-reflective particles (∧), most likely inflammatory cells, can be seen in the anterior chamber. D. AS-OCT ten days on treatment shows resolution of the plaque; corneal thickness can now be measured.

3.1.4.7 Case 7

A 61-year-old male contact lens wearer was reviewed with a 3-week history of a poorly responding corneal ulcer in the right eye. Slit-lamp examination showed marked conjunctival injection and a central epithelial defect associated with stromal infiltration (figure 23A). Anterior chamber inflammation with a hypopyon was present. AS-OCT through the centre of the infiltrate at the 180-degree axis showed a hyper-reflective anterior stromal area (figure 23B). CT in the infiltrated area was 800 µm, IT 370 µm. Corneal scrapes were carried out and intensive topical ofloxacin 0.3% and cefuroxime 5% commenced. Two days later, coagulase negative *Staphylococcus* was cultured and topical dexamethasone 0.1% 2 hourly commenced. Four days after presentation, the condition remained unchanged on slit-lamp examination; AS-OCT CT was unchanged, but the stromal hyper-reflective area was thicker, with IT measuring 480 µm (figure 23C). Repeat AS-OCT 3 days later showed that the hyper-reflective area was even thicker. In addition, CT had decreased, measuring 630 µm, and morphological evidence of posterior surface ectasia was present (figure 23D). Fungal aetiology was highly suspected now and lamellar corneal biopsy was carried out; *Fusarium* species fungus was subsequently cultured. Despite systemic and topical antifungal treatment, corneal thinning with a descemetocoele developed (figure 23E). The patient subsequently underwent penetrating keratoplasty.

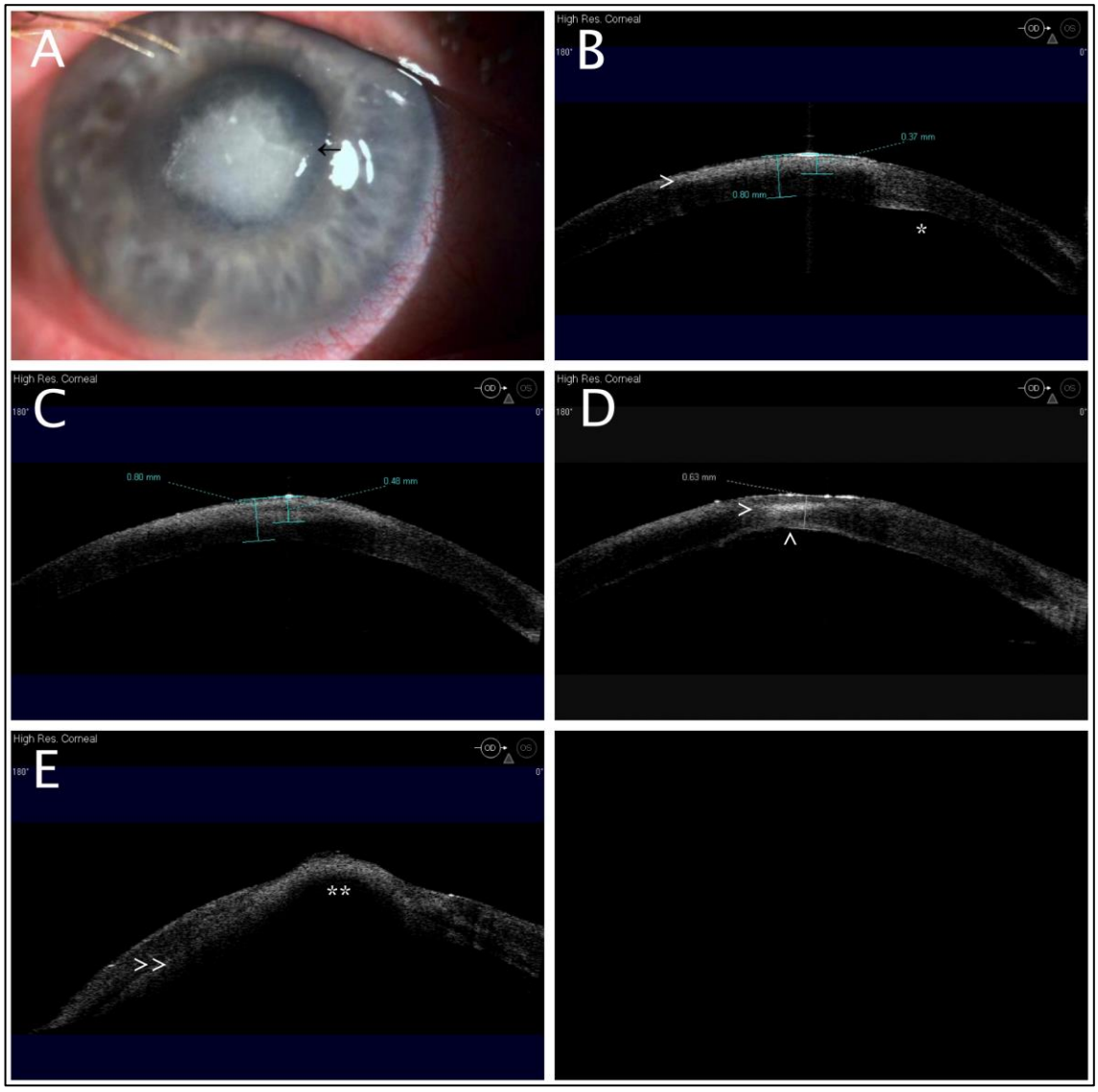

Figure 23: Case 7. Fungal keratitis imaged with serial AS-OCT images at 180-degree axis. A. Anterior segment photo at presentation shows a dense corneal infiltrate (←). B. AS-OCT through the clinical infiltrate at presentation shows an anterior stromal hyper-reflective area (>) and posterior bowing of the endothelial surface (*). C. AS-OCT 4 days after presentation shows an increase in the hyper-reflective infiltrate thickness. D. AS-OCT 7 days after presentation shows a further increase in infiltrate thickness (>) and reduction in corneal thickness. Evidence of ectasia is now present (^). E. AS-OCT 2 weeks after presentation shows corneal thinning with descemetocoele formation (**); a plaque can be seen attached to endothelial surface (>>).

Case	AS-OCT features	Presentation AS-OCT IT	Presentation AS-OCT CT	Final AS-OCT IT	Final AS-OCT CT
1	Infiltrate, scar	190 µm	800 µm	110 µm	650 µm
2	Infiltrate, scar	130 µm	670 µm	120 µm	590 µm
3	Infiltrate, scar	370 µm	910 µm	250 µm	610 µm
4	Infiltrate, Descemets folds, retro-endothelial mass, scar	530 µm	1180 µm	170 µm	450 µm
5	Infiltrate, Descemets folds, AC cells, scar	590 µm	1560 µm	160 µm	540 µm
6	Retro-endothelial plaque, AC cells	3640 µm (a)	NP	0 µm (a)	190 µm
7	Infiltrate, descemeto coele	370 µm	800 µm	630 µm	630 µm

a: inflammatory plaque width (infiltrate thickness could not be measured); NP: measurement of corneal thickness was not possible at presentation; IT: infiltrate thickness; CT: corneal thickness at infiltrated area; AC: anterior chamber

Table 1. Summary of AS-OCT characteristics in microbial keratitis.

3.1.5 Discussion

In this study, the imaging capabilities of AS-OCT in microbial keratitis have been demonstrated and its quantification potential explored. Two quantitative parameters, CT and IT, which could be applied to the objective assessment of the condition, were identified. Corneal oedema and immune cell infiltration are both features of corneal infection.[5,6,249,250] As a result, CT and IT are parameters with clinical relevance to the condition and, thus, promising quantification parameters. Qualitative features, such as anterior chamber cells and a retro-endothelial plaque, were also observed on AS-OCT images. Serial standardized examination with a consistent imaging protocol allowed comparison of these parameters, providing objective monitoring of the disease course and response to treatment. Six cases responded well to standard topical antibiotic treatment, one required penetrating keratoplasty.

The CT at the infiltrated area could be measured on high-resolution corneal scans with the use of software calliper tools. The epithelium and endothelium were imaged as hyper-reflective layers compared to the stroma, facilitating placement of the callipers. In one case (case 6), CT measurement was not possible. This was a bacterial infection in which the endothelium could not be distinguished from a hyper-reflective plaque that was attached to the endothelium.

AS-OCT images through the infiltration showed the presence of a hyper-reflective area in the anterior stroma that corresponded in location to the clinical infiltration. As a result, the thickness of this hyper-reflective area was termed IT. IT could be measured with calliper tools and this was possible in all cases except for the patient that presented with advanced thinning and the retro-endothelial mass (case 6). In the late phase of BK, when the infection and inflammation had resolved, scar tissue was present clinically in the area of infiltration. Measurement of IT in this phase most likely represented the thickness of scar tissue.

An AS-OCT imaging protocol, in which the scanning beam ran through the centre of the infiltrate at a defined axis at all examinations for each patient, was designed and used; this enabled the same area of the infiltrate to be scanned on serial examinations. CT and IT could, therefore, be measured

during the course of the infection with serial scans. Serial CT and IT measurements were possible in 6 of the 7 cases. As explained above, it was not possible to measure CT and IT in case 6. In this small series of cases with microbial keratitis, resolution of infection and corneal inflammation appeared to be associated with a reduction in both CT and IT.

Case 7, however, demonstrated that reduction in CT could also occur with progression of infection. Interestingly, a progressive increase in IT was observed in this case, suggesting that an increase in IT could be indicative of infection progression. As the infection continued to deteriorate, a descemetocoele developed. Experimental evidence from animal studies shows that infiltration with polymorphonuclear neutrophils, the predominant immune cell in BK, starts superficially in the anterior stroma and progresses deeper into the stroma, leading to stromal necrosis and descemetocoele formation.[5,249] In the other 5 cases in which IT measurement was possible, infection resolution was associated with a reduction in IT. These small changes in CT and IT, whether an increase or a decrease, would most likely be detected earlier with AS-OCT imaging rather than clinical observation.

AS-OCT imaging also detected qualitative information that may be useful in the assessment of microbial keratitis. Hyper-reflective floating anterior chamber particles were observed in images of early microbial keratitis; their location and size suggested that they were most likely inflammatory cells. Similarly, hyper-reflective particles appeared as aggregates on the endothelial surface forming keratic precipitates. Case 6 illustrated that retro-corneal pathology, such as an endothelial plaque, could also be imaged and measured. Measurement of the width of this plaque on serial scans allowed objective assessment of the disease course, despite the fact that CT or IT could not be measured. The progressive reduction in its size, combined with the clinical examination, suggested that this plaque was inflammatory in origin. AS-OCT imaging could also identify Descemets folds (cases 4 and 5) as “ruffles” in the normally smooth endothelial surface. This is another parameter that may be useful for objective assessment of the condition and treatment response. Although they can be detected clinically, it would be difficult to objectively document their extent and change at follow-up visits.

AS-OCT imaging capabilities in inflammation

A limitation of this study was the lack of correlation of the AS-OCT findings with histo-pathological examination. This was not possible, as the study was conducted on humans. The images, however, were analysed in the clinical context of the individual cases.

The value of AS-OCT in imaging and studying corneal and anterior segment pathology is constantly being explored. At the time of conducting this study no research had been published on the use of AS-OCT in imaging corneal infection. In 2012, a study reported on the use of FD-OCT on microbial keratitis, as discussed in section 1.5.4.3. Morphological characteristics, such as hyper-reflective stromal lesions and localized stromal thinning, were identified on the images. However, no attempt was made to quantify these parameters of infection.[238]

Ultrasound is considered the gold standard in the measurement of CT.[251-253] However, it does not have a described role in the assessment or quantification of corneal infection. It generally has good repeatability in normal corneas,[251,254] but in the pathological keratoconic cornea ultrasound pachymetry has been shown to have poorer reproducibility and repeatability than the newer Pentacam-Scheimpflug imaging.[252] It is not known whether ultrasound CT measurements would be repeatable and reproducible in the very pathological infected cornea.

Densitometry of the cornea, measured with Pentacam-Scheimpflug imaging, has shown good potential as an imaging parameter that could be used to monitor BK. A study that investigated BK with serial Pentacam-Scheimpflug scans found a reduction in corneal transparency between presentation and 4-6 weeks after resolution of the infection, but this study did not examine the early treatment phase.[204]

Finally, in-vivo confocal microscopy has a limited role in the assessment of corneal infection, as discussed in section 1.5.3.

3.1.6 Conclusion

The results of this pilot study suggested that the imaging properties of long-wavelength AS-OCT could facilitate objective assessment and quantification of corneal infection. Two corneal parameters, CT and IT, could be measured on

serial examination and a range of qualitative parameters imaged. Further studies with larger patient cohorts are required to investigate the imaging and quantification capabilities of AS-OCT and the clinical application of the identified parameters.

3.2 Characterisation of active and quiescent peripheral ulcerative keratitis with Anterior Segment Optical Coherence Tomography

3.2.1 Introduction

Peripheral ulcerative keratitis (PUK) is a destructive inflammatory process of the peripheral cornea, limbus and sclera, as discussed in section 1.3.2. It is associated with significant ocular morbidity, as it has a high risk of concomitant scleritis, corneal perforation and requirement for emergency tectonic surgery.[255,256]

Diagnosis is based on slit-lamp features of peripheral crescent-shaped corneal ulceration, corneal thinning and stromal inflammation, in conjunction with a relevant medical history.[256] Assessment at presentation and of the treatment response is carried out with slit-lamp biomicroscopy, an examination modality that requires experience and most importantly does not quantify the extent of corneal-limbal thinning, a cardinal feature of PUK.

Study 3.1 identified that AS-OCT could be applied to the measurement of corneal thickness (CT) in the pathological cornea, specifically in microbial keratitis. Measurement of CT in the ulcerated area of PUK at presentation could provide an indication of disease activity and the risk of perforation. Serial CT measurements could also assist objective assessment of the treatment response, allowing prompt escalation of immunosuppression when deterioration is detected.

3.2.2 Hypothesis

The aim of this study is to explore the imaging capabilities of AS-OCT in PUK. I hypothesise that AS-OCT imaging will provide qualitative and quantitative morphological features that may characterise active and quiescent PUK.

3.2.3 Materials and methods

Patients who presented to University Hospital Southampton NHS Foundation trust with active PUK over a 12-month period and were interested in taking part

in the study were recruited. Each patient had clinical examination with slit-lamp biomicroscopy, systemic health investigations and treatment based on clinical findings. AS-OCT scanning with the Visante OCT was carried out at presentation and follow-up through a specified axis for each case, as per a standardised imaging protocol (section 2.2.3).

AS-OCT images were analysed for minimum CT at the ulcer base using the Visante OCT software calliper tools. Images were also exported into the GNU Image Manipulation Program (GIMP version 2.8.8) and the gradient of the two ulcer walls, relative to the anterior corneal surface, was measured with angle measurement software. The gradient of the steepest ulcer wall was recorded. In view of its non-linear shape, the gradient of the top 1/3 - 1/2 of the ulcer wall was measured.

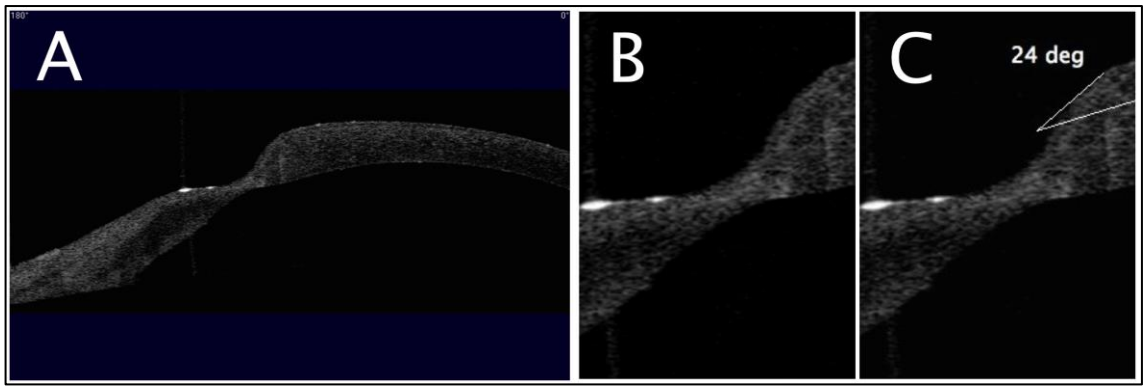

Figure 24. Peripheral ulcerative keratitis gradient measurement protocol with AS-OCT. A. The AS-OCT scan through the ulcerated area of the cornea. B & C. High magnification view was used for placement of the calliper arms. The gradient of the steepest ulcer wall, at its top 1/3 - 1/2, was measured relative to the anterior corneal surface.

3.2.4 Results

Six patients (eyes) were recruited for this study (table 2). The imaging capabilities of AS-OCT and the qualitative and quantitative morphological features of active and quiescent PUK are presented in the case reports.

3.2.4.1 Case 1

An 80-year-old female with rheumatoid arthritis (RA) presented with active PUK in the left eye (figure 25A). AS-OCT showed the ulcerated cornea in cross-section; the gradient of the ulcer walls was steep and the ulcer base was thin. The gradient of the steepest ulcer wall was 24° and minimum CT at the ulcer base was 260 µm (figure 25B). Clinically, she responded well to intravenous methylprednisolone and infliximab. Three days later, minimum CT and ulcer wall gradient had decreased to 190 µm and 20° respectively (figure 25C). Two days later, CT had stabilised but the ulcer wall gradient was even less steep, measuring 15° (figure 25D).

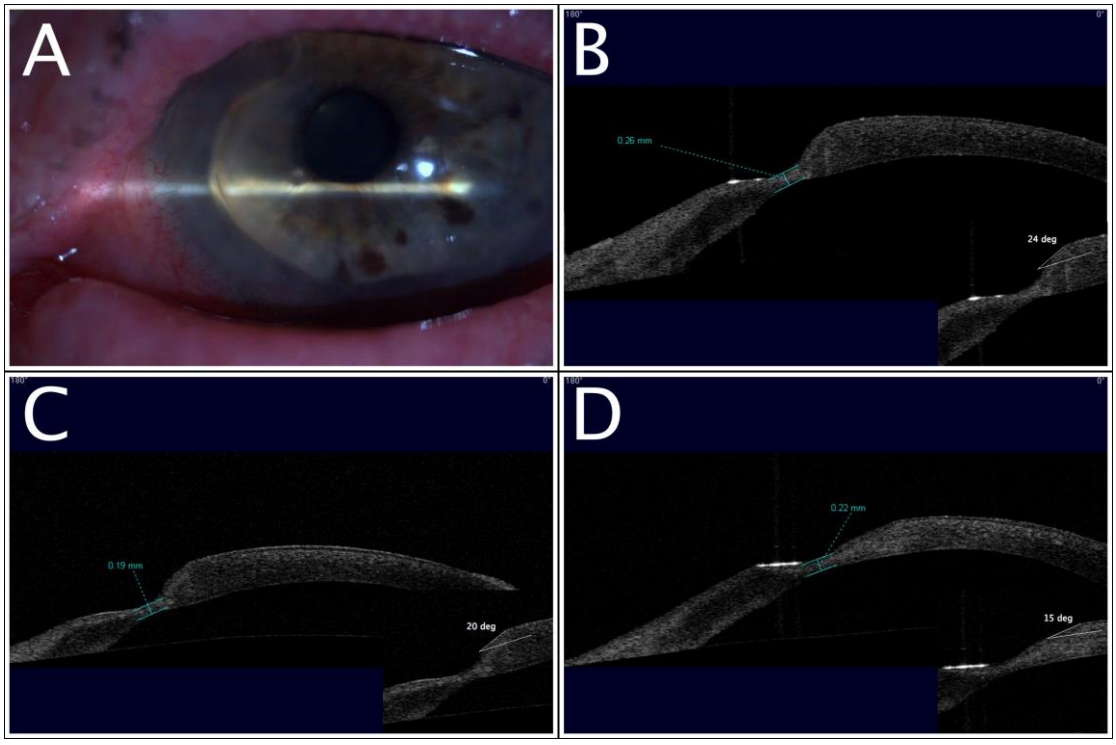

Figure 25: Case 1. Serial AS-OCT scans through the peripheral ulcerative keratitis in association with rheumatoid arthritis. A. Photo at presentation shows peripheral corneal thinning with a 'contact lens cornea' appearance. B. At the acute presentation, the gradient of the ulcer walls was steep, the steepest measuring 24°. The cornea at the ulcer base was thin and minimum corneal thickness (CT) measured 260 µm; the adjacent cornea appeared thickened, most likely due to oedema. C. Three days later, following successful

immunosuppression, the ulcer wall gradient was less steep, measuring 20°; minimum CT had also decreased to 190 µm. D. Two days later, minimum CT had stabilised and the ulcer wall gradient appeared less steep, measuring 15°, most likely due to reduction in oedema.

3.2.4.2 Case 2

A 57-year-old male with Wegener's granulomatosis presented with active PUK in the right eye (figure 26A). On AS-OCT, minimum CT at the ulcer base was 630 µm and the gradient of the steepest ulcer wall 22°. Clinically, the inflammation resolved following treatment with intravenous methylprednisolone, oral prednisone and oral methotrexate (figure 26B). One week later, minimum CT in the affected area was reduced, measuring 560 µm; the ulcer was less steep, with a gradient of 14° (figure 26C). Three months later, AS-OCT showed stable CT and a smooth anterior corneal surface with no ulcer (figure 26D).

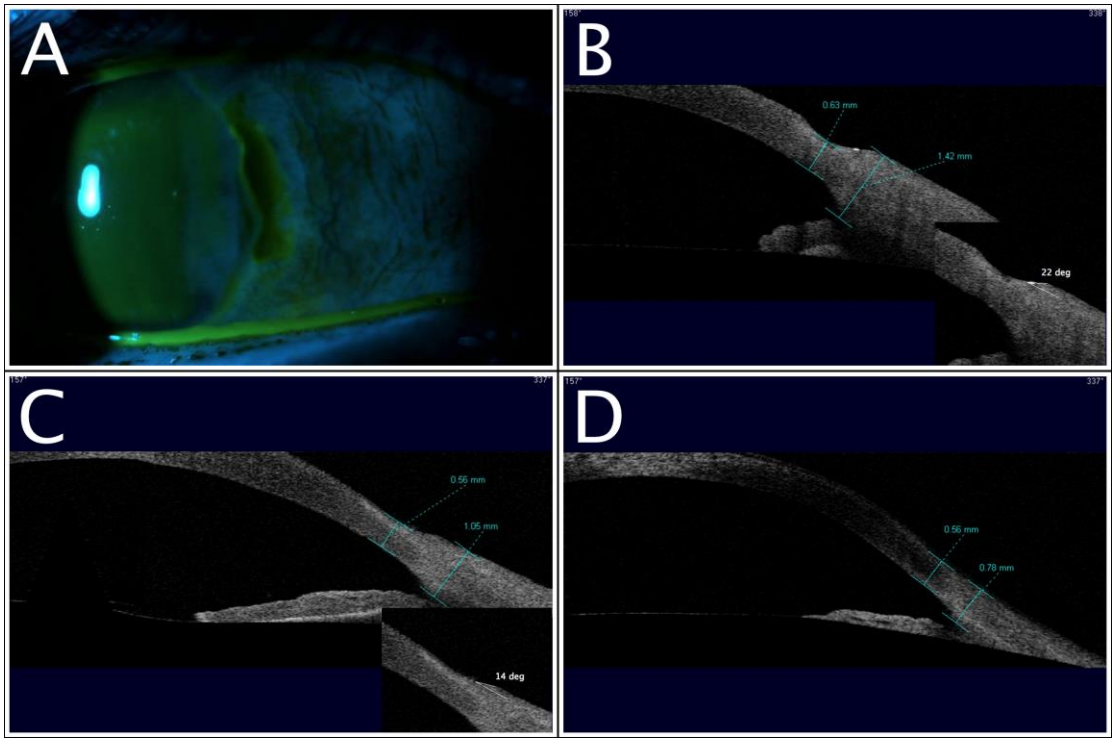

Figure 26: Case 2. Serial AS-OCT scans through the nasal cornea in Wegener's granulomatosis. A. Photo of right eye at presentation showed

peripheral corneal thinning. B. At presentation, the active ulcer had steep walls, the gradient of the steepest wall measuring 22°. Minimum corneal thickness (CT) at the ulcer base measured 630 µm and the adjacent limbus 1420 µm in thickness. C. One week later, when the inflammation had clinically resolved, the gradient of the ulcer wall was less steep, measuring 14°. Minimum CT at the ulcer base was reduced, measuring 560 µm, and the limbal thickness had also decreased to 1050 µm, most likely due to reduction in oedema. D. Three months later, CT had stabilised and the limbal thickness had decreased further to 780 µm. The walls of the ulcer had become flat and did not form a gradient relative to the anterior corneal surface.

3.2.4.3 Case 3

A 73-year old RA patient presented with active PUK in the right eye (figure 27A), despite on-going treatment with oral prednisolone and methotrexate. On the AS-OCT, minimum CT at the ulcer base measured 580 µm. The ulcer walls had a relatively steep gradient, with the steepest measuring 21°. The endothelium appeared irregular with the presence of Descemet's folds (figure 27B). Clinical remission was achieved with three intravenous methylprednisolone infusions and an increase of the methotrexate dose. Two months later, the PUK remained inactive; on AS-OCT, the ulcer walls had become flat and did not form a gradient relative to the anterior cornea (figure 27C). The CT, both central and peripheral, had decreased and the endothelial folds had resolved, most likely due to resolution of corneal oedema. Repeat AS-OCT, 8 months later, confirmed clinical quiescence with similar qualitative and quantitative imaging findings (figure 27D).

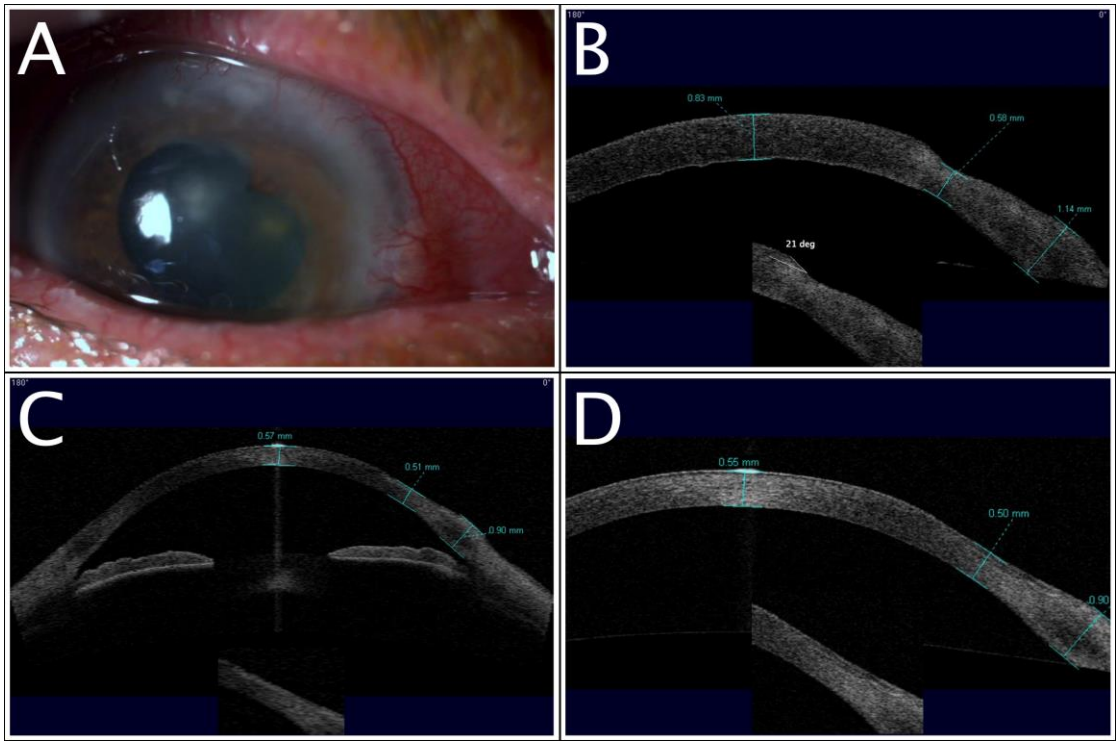

Figure 27: Case 3. Serial AS-OCT scans through peripheral ulcerative keratitis in rheumatoid arthritis. A. Photo at presentation showing active nasal peripheral ulcerative keratitis. B. At presentation, the acute ulcer had walls with a steep gradient, the steepest measuring 21°; minimum corneal thickness (CT) at the ulcer base was 580 µm. The endothelial surface and Descemet's membrane were irregular due to diffuse corneal oedema. C. Following clinical remission, AS-OCT two months from presentation, showed that the CT had decreased at the ulcer base, centrally and peripherally; the Descemet's folds had cleared, suggesting resolution of oedema, and no ulcer was detected. D. Repeat AS-OCT, eight months later, confirmed clinical stability with CT and ulcer characteristics remaining unchanged.

3.2.4.4 Case 4

A 65-year-old female with RA presented with nasal PUK in the right eye (figure 28A). AS-OCT showed peripheral corneal thinning; minimum CT measured 300 µm at the ulcer base and the steepest ulcer wall gradient 18° (figure 28B). Despite an increase in methotrexate dose, 4 days later the eye remained inflamed. Repeat AS-OCT showed minimum CT had decreased to 250 µm and

the ulcer wall gradient was steeper, measuring 44° (figure 28C). In view of the deterioration, the patient had emergency corneal Tisseel glue application and a rituximab intravenous infusion that stabilized the condition. AS-OCT 1 week later showed evidence of posterior surface ectasia; CT measured 300 µm, most likely reflecting the bulking effect of Tisseel (figure 28D).

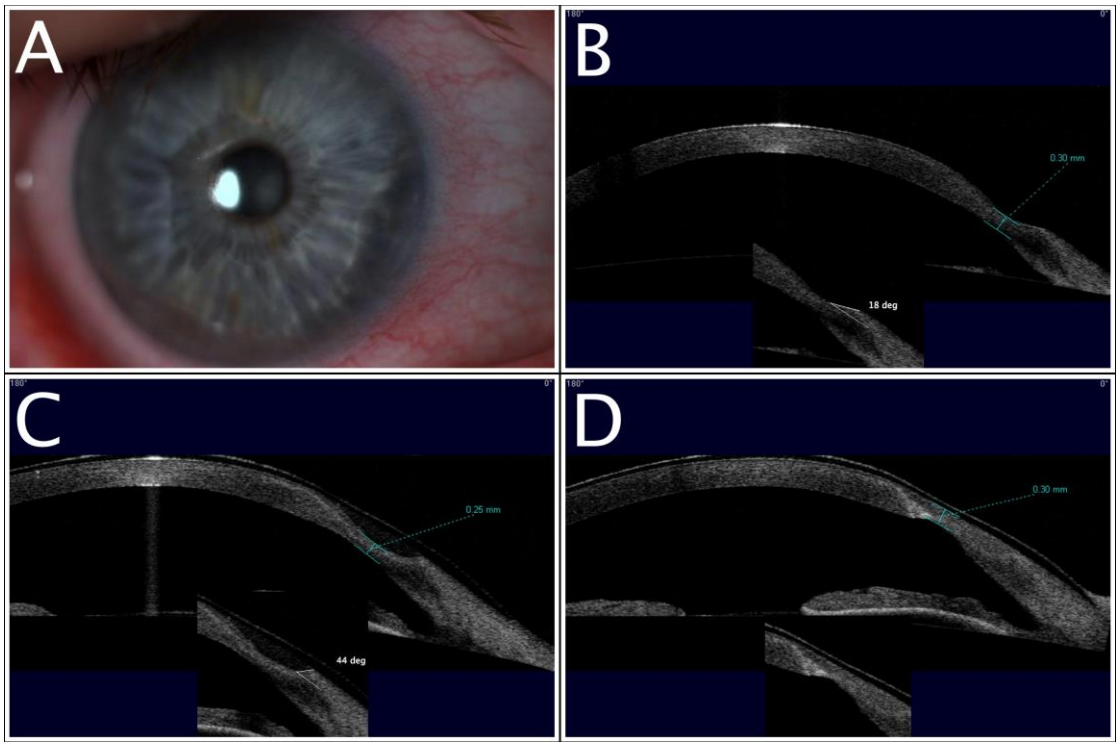

Figure 28: Case 4. Serial AS-OCT scans through progressive peripheral ulcerative keratitis. A. Colour photo of right eye at presentation showing conjunctival injection and nasal corneal thinning. B. The active ulcer at presentation had relatively steep walls, with the steepest wall having a gradient of 18°; minimum corneal thickness (CT) at the ulcer base measured 300 µm. C. Four days later, the gradient of the steepest ulcer wall had increased to 44° and the minimum CT had decreased to 250 µm, suggesting that the corneal inflammation and melting were ongoing. D. One week later, following stabilisation with a rituximab infusion and emergency Tisseel glue application, the posterior corneal surface showed localised ectasia but CT had increased to 300 µm, most likely due to the adhesive and bulking properties of Tisseel.

3.2.4.5 Case 5

An 84-year old patient presented with active PUK due to Wegener's granulomatosis. AS-OCT showed advanced corneal thinning with posterior surface ectasia; the ulcer wall gradients were very steep, the steepest measuring 87° (figure 29A). Due to the risk of perforation, he underwent cyanoacrylate glue application with a drape disc (figure 29B) and had intravenous methylprednisolone, followed by oral prednisolone and methotrexate. This stabilised the cornea and penetrating keratoplasty was subsequently carried out.

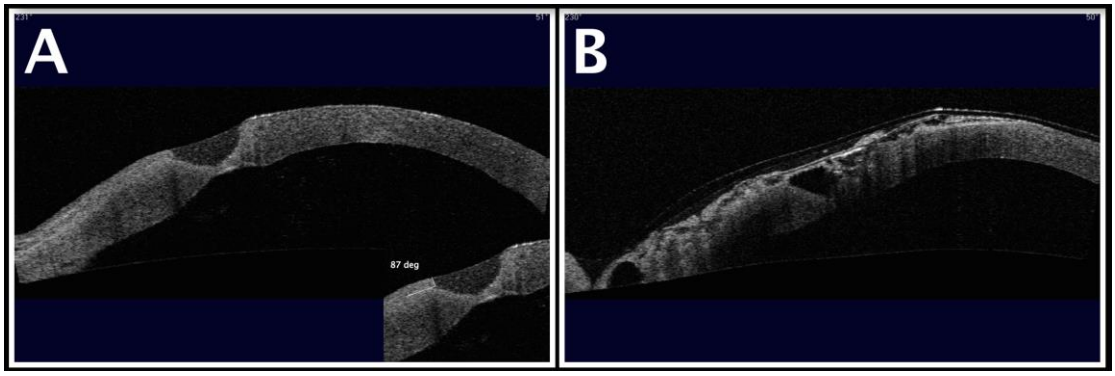

Figure 29: Case 5. AS-OCT scans through peripheral ulcerative keratitis with perforation risk. A. The active ulcer had steep wall gradients, the steepest measuring 87°. Advanced corneal thinning was present at the ulcer base with evidence of posterior surface ectasia; minimum corneal thickness measured 210 µm. B. Following application of cyanoacrylate glue with a drape disc, the corneal surface appeared irregular and hyper-reflective. Details of the corneal stroma were limited by the shadows caused by the glue and drape, but there was no evidence of perforation and the anterior chamber appeared well formed.

3.2.4.6 Case 6

A 70-year-old patient presented with perforation of the right eye due to active PUK in association with RA (figure 30A). AS-OCT showed that the iris was plugging the base of the ulcer. The ulcer walls had a steep gradient, the

steepest measuring 45° (figure 30B). The patient was treated with intravenous methylprednisolone and emergency penetrating keratoplasty.

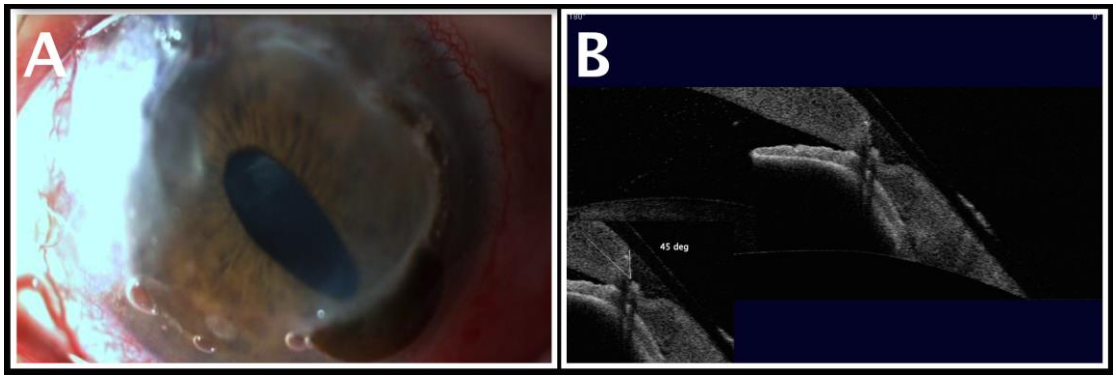

Figure 30: Case 6. AS-OCT scan through perforated peripheral ulcerative keratitis. A. Colour photo of right eye at presentation. B. The active ulcer at the perforation site had steep walls, with the steepest gradient measuring 45°. Iris was plugging the base of the ulcer.

Case	Diagnosis	Minimum CT of active PUK	Maximum ulcer wall gradient of active PUK	Treatment	Minimum CT at follow-up scan/s	Maximum ulcer wall gradient at follow-up scan/s
1	RA	260 µm	24°	IV methylprednisolone and infliximab	190 µm / 220 µm	20° / 15°
2	Wegener's	630 µm	22°	IV methylprednisolone, PO prednisolone, PO methotrexate	560 µm / 560 µm	14° / 0°
3	RA	580 µm	21°	IV methylprednisolone, PO methotrexate	510 µm / 500 µm	0° / 0°
4	RA	250 µm	44°	IV rituximab, glue	300 µm	0°
5	Wegener's	210 µm	87°	IV methylprednisolone, PO prednisolone, PO methotrexate, glue	NA	NA
6	RA	Perforation	45°	IV methylprednisolone, PKP	NA	NA

CT: corneal thickness, PUK: peripheral ulcerative keratitis, RA: rheumatoid arthritis, Wegener's: Wegener's granulomatosis, PKP: penetrating keratoplasty IV: intravenous, PO: oral, NA: not available

Table 2. AS-OCT quantitative morphological features of active and quiescent peripheral ulcerative keratitis.

3.2.5 Discussion

This study has shown a unique role for AS-OCT in evaluating morphological qualitative and quantitative parameters in PUK. Measurement of CT at the ulcer base and quantification of the ulcer wall gradient allowed assessment and documentation of the condition at presentation. Serial examination provided monitoring of the inflammatory process and the response to treatment.

In active PUK, the ulcer base was thin and the gradient of the ulcer walls steep. The adjacent cornea was thickened, most likely due to oedema (cases 1,2,3,5). The minimum CT at the ulcer base could be measured, thus providing an estimation of the severity of the condition and the risk of perforation. Measurement of CT and morphological assessment of the ulcer profile on serial examination aided monitoring of the inflammatory activity. As the PUK responded to treatment, the ulcer edges became smoother and the ulcer walls less steep (cases 1-3). The minimum CT stabilised over time, although, a further small CT reduction was observed after initiation of treatment; in cases 1 and 2, minimum CT decreased by 70 μm within the first week of treatment, before stabilisation was achieved. A global normalisation of corneal morphology suggests that reduction in oedema throughout the cornea contributed considerably to the early reduction in CT and limbal thickness. Final minimum CT in the cases that responded well to treatment ranged between 40-80 μm below the minimum CT at presentation.

In progressive PUK, as illustrated by case 4, the ulcer edge became sharper, the walls developed a steeper gradient and the minimum CT decreased, possibly a reflection of on-going active inflammation and melting. Sharp ulcer edges and steep ulcer wall gradients were also observed in the two cases with perforation and impending perforation (cases 5,6). Active ulcers were, therefore, characterised by a sharp edge and steep wall, whereas quiescent or responding ulcers by a smooth edge and gradually sloping wall. All six cases had active ulcers at presentation and the wall gradients ranged from 21 to 87°. In all three cases with risk of perforation or actual perforation (cases 4-6), the gradient was greater than 44°. Although no firm conclusions can be reached from this small case series, a wall gradient greater than 44° may be indicative of high-risk PUK.

AS-OCT imaging has the advantage of combining quantitative information with morphological qualitative evaluation. Slit-lamp biomicroscopy is the gold-standard examination modality that provides qualitative and semi-quantitative information. However, slit-lamp measurement of CT is not possible and assessment of morphological features is subjective, dependant on examiner experience, and may not detect small changes at follow-up examinations. The supplementary information provided by AS-OCT imaging may overcome these limitations in the examination of PUK patients.

Newer OCT devices, primarily retinal devices with anterior segment modules, such as the Spectralis (Carl Zeiss Meditec, Dublin, CA, USA) and the Topcon 3D OCT-2000, provide much more rapid imaging with better resolution due to the use of Fourier domain technology (section 1.5.4.1). With rapid high-density raster scans they can image an area of the cornea, enabling three-dimensional visualisation of the affected area. This may prove advantageous compared to the B-scan images that were possible with the Visante OCT in my study, potentially overcoming limitations in scanning the same location of the affected cornea at follow-up examinations.

Slit-image based imaging modalities, such as Pentacam-Scheimpflug and Orbscan scanning-slit topography, have a lower image resolution than AS-OCT and are unlikely to produce the detail of OCT based devices; in addition, they are more prone to light scatter that could limit accurate quantification of CT.[201] Measuring corneal light scattering by densitometry with Pentacam-Scheimpflug imaging, however, may potentially have a role in the examination of PUK, as densitometry readings have been found to correlate with corneal inflammation in corneal infection.[204]

3.2.6 Conclusions

Measurement of CT at the ulcer base provided objective evaluation of disease severity and risk of perforation. Evaluation of the ulcer wall gradient on serial examination could be used for assessment of ulcer activity, as active ulcers had a steeper wall gradient than remitting or quiescent PUK. This study has illustrated how AS-OCT can aid the clinical examination of patients with PUK.

4. Quantification capabilities of Anterior Segment Optical Coherence Tomography in bacterial keratitis

4.1 Capability of AS-OCT to detect and measure parameters of inflammation in corneal infection

4.1.1 Introduction

The study in section 3.1, where the capability of AS-OCT to identify morphological parameters of corneal infection was investigated, found that clear visualisation of the corneal infiltration and measurements of corneal thickness (CT) and infiltrate thickness (IT) were possible in 6 of the 7 cases of microbial keratitis. These findings suggest that AS-OCT is a promising imaging modality for the quantification of corneal inflammation in microbial keratitis. However, measurements were not achieved in all cases, indicating a possible limitation in its quantification potential.

Following publication of the study in section 3.1,[257] Soliman et al presented the morphological features that could be identified in microbial keratitis with FD-OCT.[238] Hyper-reflective stromal lesions and stromal cystic spaces were the main imaging findings. This study was descriptive and did not attempt to quantify or measure any of the identified parameters. The development of in-vivo quantification methods for corneal infection and inflammation is important. It would provide objective assessment of the condition at presentation and potentially objective monitoring of the treatment response, and in addition facilitate clinical research.

Encouraged by the findings of chapter 3, and considering the potential limitations identified in section 3.1 and the glaucoma AS-OCT studies, a larger study into the imaging and quantification capabilities of AS-OCT in corneal infection was carried out.

4.1.2 Hypothesis

I hypothesise that AS-OCT measurements of CT and IT can be applied to the quantification of corneal inflammation in patients who present with bacterial keratitis (BK). The first aim of this study is to explore the capability of AS-OCT to quantify CT and IT in BK. The second aim is to investigate the intra-observer repeatability and inter-observer reproducibility of the CT and IT measurements in BK, and identify the parameter with the highest repeatability.

4.1.3 Materials and methods

4.1.3.1 Patient recruitment

Patients presenting with a clinical diagnosis of BK were prospectively recruited to the study. Inclusion criterion was the clinical diagnosis of BK, defined by the presence of a typical history and an epithelial ulceration with underlying stromal infiltration associated with signs of inflammation.[7,84] Patients with previous corneal infection, antibacterial treatment already commenced, advanced ulceration with risk of corneal perforation at presentation, symptoms greater than 14 days were excluded. Known neurotrophic and blind eyes were also excluded as they often show an atypical immune response, due to the fact that the immune and nervous system pathways in the cornea are intertwined.[258] Patients with a history and clinical findings suggestive of a viral keratitis or hypersensitivity type corneal ulceration were not recruited. Patients in whom the diagnosis was subsequently revised to non-bacterial infection, once microbiology results were available, were excluded. Infection was considered resolved when the epithelial defect and signs of inflammation resolved completely.

Local NHS Research Ethics Committee and patient informed consent were obtained. The research adhered to the tenets of the Declaration of Helsinki (section 2.1.1).

4.1.3.2 Patient examination

At presentation and resolution of the infection, patients had clinical examination and assessment of logMAR visual acuity (logMAR VA). Slit-lamp measurements of the epithelial defect (ED) and infiltrate diameter (ID) were

carried out along the longest axis and its perpendicular axis. The cornea was also imaged with Visante OCT AS-OCT. All patients underwent treatment based on clinical findings and requirements. Standard antibacterial treatment was intensive guttae ofloxacin 0.3% and guttae cefuroxime 5% to the affected eye.

4.1.3.3 AS-OCT imaging and measurement protocol

A standardized AS-OCT scanning protocol was used, as presented in section 2.2.2. High-resolution scans, at least 3, were carried out and the best scan was saved and used for analysis.

The CT and IT were measured by examiner 1 with calliper tools of the Visante OCT software, as described in study 3.1. The CT was assessed at presentation, termed CT1, and at resolution of the infection, termed CT2. In addition, a new parameter termed infiltrate width (IW), defined as the distance between the transverse borders of the hyper-reflective area of infiltration, was measured by placement of the calliper arms on the borders.

The measurements of CT, IT and IW were repeated by examiner 1 with a time interval of at least 1 month, in order to assess the intra-observer repeatability. They were also repeated by a second examiner, examiner 2, for assessment of the inter-observer reproducibility.

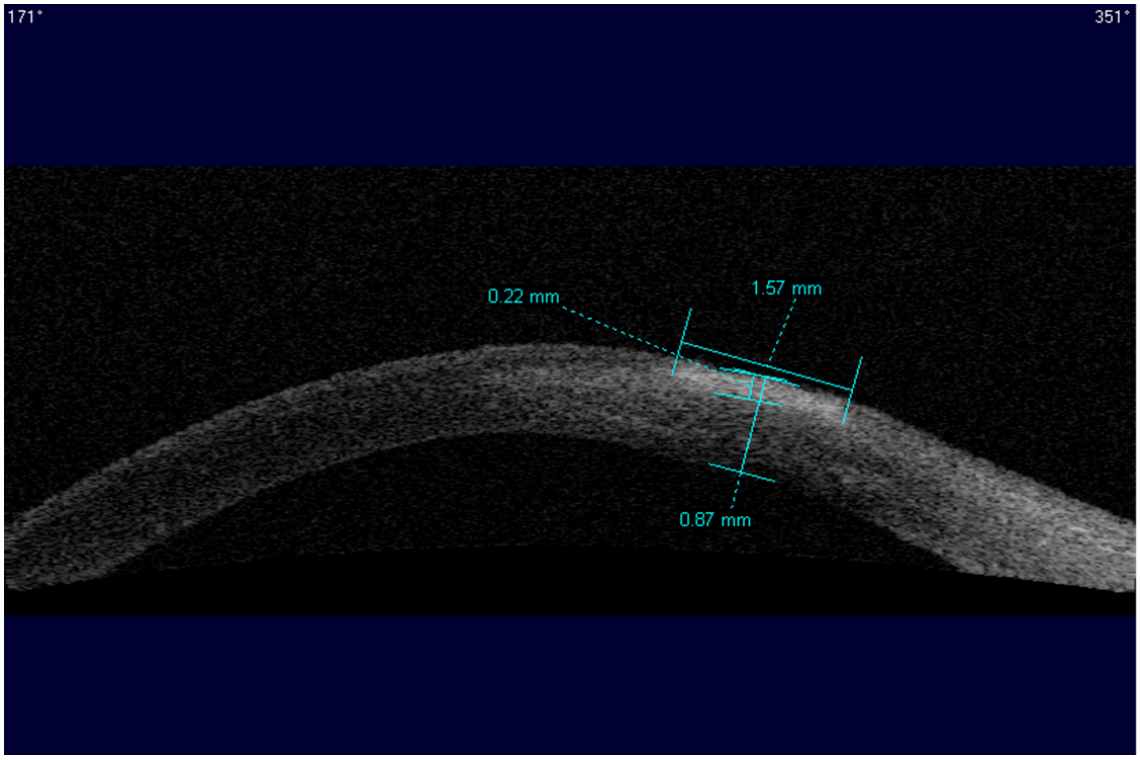

Figure 31. AS-OCT measurement protocol in bacterial keratitis. The infiltrate thickness (IT) and infiltrate width (IW) were measured with placement of the callipers at the axial and transverse borders of the hyper-reflective infiltrate. Corneal thickness (CT) was measured at the infiltrate centre with calliper placement on the axial borders of the cornea.

4.1.3.4 Statistical analysis

The number of cases in which CT, IT and IW could be measured at presentation was calculated and expressed as a percentage of total cases. The cases in which IT could be measured were compared to cases in which IT could not be measured for CT, ID, ED and logMAR VA, aiming to identify factors that may affect the capability to measure AS-OCT parameters in BK. VA of counting fingers at 30 cm, hand motion at 30 cm and perception of light were given scores of 2, 3 and 4 respectively.

Mean CT, IT and IW were calculated for each assessment and compared between the two assessments of examiner 1 (intra-observer difference) and between the assessments of examiner 1 and 2 (inter-observer difference). Intra-observer and inter-observer precision, coefficient of variation (CV) and

intra-class correlation coefficient (ICC) were calculated. Precision was calculated as 1.96 x the standard deviation (SD) of the absolute difference (Sw) between the two measurements. The CV was calculated as the Sw between the two measurements divided by the overall mean.[241] A sample size n≥30 cases (eyes) was aimed for, as when n>30 the sampling distribution of the mean is very closely approximated by the normal distribution with a small standard error.[259]

Data on CT, IT and IW measurements were examined with the Shapiro-Wilk test and normal distribution plots. A normal distribution was detected; therefore, parametric tests were used for statistical analysis. Statistical analysis was carried out with the Statistical Package for Social Sciences (IBM SPSS Statistics for Macintosh, Version 19.0. Armonk, NY: IBM Corp).

4.1.4 Results

Forty five patients (eyes) with clinical BK, 21 male and 24 female, were recruited. Mean [SD] age was 47 [20.6] years. Twenty three right and 22 left eyes had BK (table 3).

A. Bacteriology	
Pseudomonas aeruginosa	18
Coliforms species	1
Chryseobacterium	1
Coagulase negative *Staphylococcus* [a]	7
Diphtheroids species	2
Staphylococcus aureus [a]	3
Streptococcus pneumoniae	1
Bacillus species [a]	1
Enterococcus species [a]	1
Gram -ve on microscopy	1
Microbiology negative	11
B. Risk factor	
Contact lens wear	30
RCES	4
Trauma	1
Surgery	1
Eczema	1
AKC	1
Lagophthalmos	2
Trichiasis	1
Rosacea	1
Corneal suture	1
Not identified	2

[a] polymicrobial Gram positive cases, RCES: recurrent corneal erosion syndrome, AKC: atopic keratoconjunctivitis

Table 3. Bacteriology (A) and risk factors (B).

4.1.4.1 Quantification capability

The CT1 could be measured by examiner 1 in 44 (97.8%) of the 45 AS-OCT images, IT in 34 (75.6%) and IW in 28 (62.2%). A clinical infiltrate on slit-lamp examination was present in 37 (82.2%) of the 45 cases. When these 37 cases were analysed, CT1 could be measured in 37 cases (100%), IT in 27 cases (73.0%) and IW in 21 cases (56.8%). No significant difference in CT1, ED, ID and logMAR VA was found between cases in which IT could and could not be measured (964.7 [247.2] vs. 901.8 [134.7] µm, p=0.427; 2.16 [1.45] vs. 1.92 [1.47] mm, p=0.639; 2.24 [1.47] vs. 1.80 [0.87] mm, p=0.379; 1.16 [1.20] vs. 1.46 [1.25], p=0.494].

On repeat assessment by examiner 1, CT1 could be measured in 44 (97.8%) of 45 images, IT in 31 (83.8%) of 37 images and IW in 27 (73%) of 37 AS-OCT images. The agreement between the two assessments in the capability to measure CT1, IT and IW was 100, 84.4 and 82.2%, respectively.

Examiner 2 measured CT1 in 45 (100%) of 45 images, IT in 33 (89.2%) of 37 images and IW in 24 (64.9%) of 37 AS-OCT images. The agreement between the first assessment of examiner 1 and that of examiner 2 in the capability to measure CT1, IT and IW was 97.8, 84.4 and 77.8%, respectively.

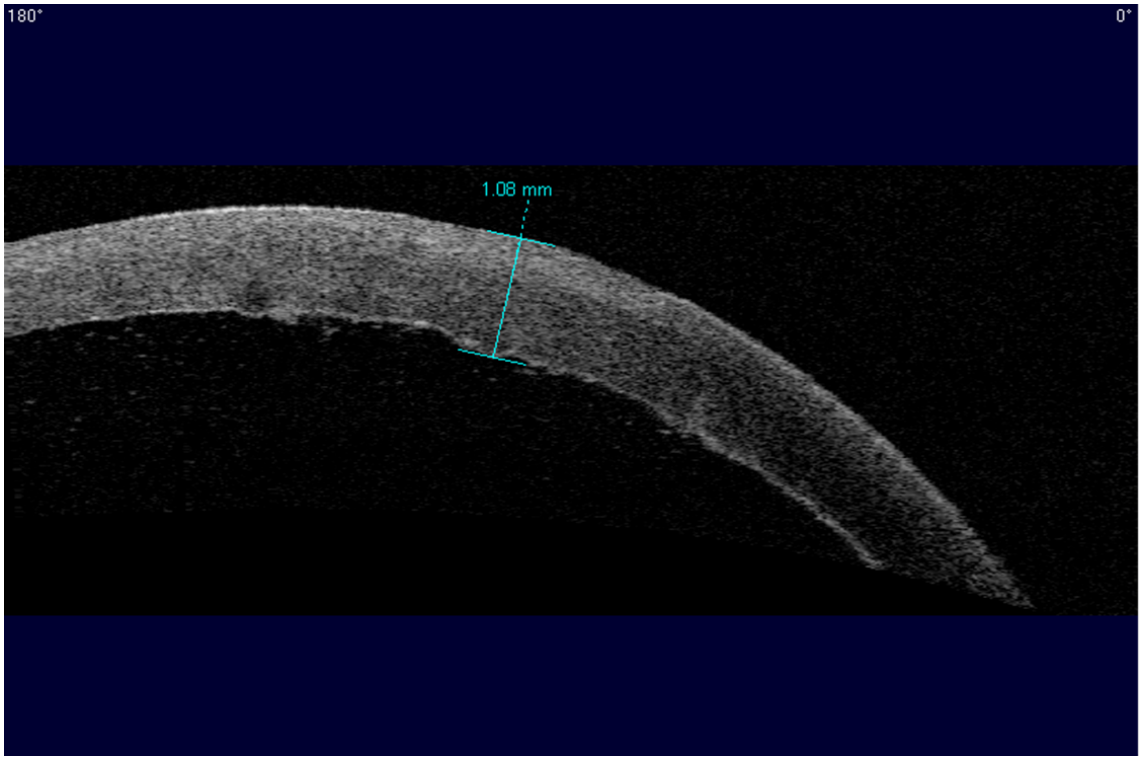

Figure 32. AS-OCT scan of *Pseudomonas* keratitis at presentation. The scan is characterised by the absence of a well-defined hyper-reflective corneal infiltrate. Corneal thickness in the affected area was 1080 µm. The endothelial surface was irregular due to the presence of stromal oedema.

4.1.4.2 Repeatability of quantification parameters

4.1.4.2.1 Corneal thickness

Repeat mean [SD] CT1 was 929.3 [228.7] µm, significantly less than the first set of measurements of 949.3 [225.2] µm (p=0.040). The intra-examiner mean [Sw] difference was -20 [63.3] µm or 2.13% of the mean CT1 and the precision 124.1 µm. Overall mean CT1 of the two measurement sets was 939.3 µm and the CV 6.73%. The ICC was 0.958 (95% CI: 0.923-0.977).

Repeat mean [SD] CT2 was 504.0 [137.1] µm, compared to 502.7 [130.2] µm at the first assessment (p=0.779). Intra-examiner mean [Sw] difference was 1.3 [28.4] µm or 0.26% of the mean CT2 and precision 55.7 µm. Overall mean CT2

of both measurement sets was 503.4 µm and the CV 5.64%. Finally, the ICC was 0.978 [95% CI: 0.955-0.990].

4.1.4.2.2 Infiltrate thickness

Repeat mean [SD] IT was 412.4 [176.8] µm, not significantly different to the first measurement set of 437.2 [192.8] µm (p=0.128). Intra-examiner mean [Sw] difference was -24.8 [85.2] µm and precision 167.0 µm. The overall mean value of IT was 424.8 µm and CV 20.1%. The ICC was 0.889 [95% CI: 0.778-0.946].

4.1.4.2.3 Infiltrate width

Repeat mean [SD] IW was 2055.2 [1245.4] µm, not significantly different to 1900.0 [1122.7] µm of the first measurement (p=0.14). The intra-examiner mean [Sw] difference was -155.2 [486.0] µm and precision 952.6 µm. The overall mean IW was 1977.6 µm and CV 24.6%. The ICC was 0.912 [95% CI: 0.803-0.961].

4.1.4.3 Reproducibility of quantification parameters

4.1.4.3.1 Corneal thickness

The mean [SD] CT1 of examiner 2 was not significantly different to the first measurement set of examiner 1 (935.8 [206.1] vs. 949.3 [225.2] µm, p=0.250). The inter-examiner mean [Sw] difference for CT1 was -13.6 [78.0] µm or 1.44% of the mean CT1 and precision 152.9 µm. The overall mean value of CT1 was 942.6 µm and CV 8.27%. The ICC was 0.934 [95% CI: 0.884-0.963].

The mean [SD] CT2 of examiner 2 was not significantly different to the first measurement set of examiner 1 (511.3 [120.8] vs. 502.7 [130.2] µm, p=0.085). Inter-examiner mean [Sw] difference for CT2 was 8.7 [26.6] µm or 1.72% of mean CT2 and precision 52.1 µm. The overall mean CT2 was 507.7 µm and CV 5.24%. The ICC was 0.976 [95% CI: 0.949-0.989].

4.1.4.3.2 Infiltrate thickness

The mean [SD] IT of examiner 2 was significantly different to the first measurement set of examiner 1 (448.7 [185.3] vs. 401.0 [142.9] µm, p=0.038). Inter-examiner mean [Sw] difference was -47.7 [119.9] µm and precision 235.0 µm. The overall mean value of IT was 424.9 µm and CV 28.2%. The ICC was 0.714 [95% CI: 0.471-0.855].

4.1.4.3.3 Infiltrate width

The mean [SD] IW of examiner 2 was borderline significantly different to the first measurement set of examiner 1 (1997.1 [1206.9] vs. 1731.9 [994.9] µm, p=0.054). Inter-examiner mean [Sw] difference was -265.2 [593.8] µm and precision 1163.8 µm. The overall mean IW was 1864.5 µm and CV 31.8%. The ICC was 0.838 [95% CI: 0.626-0.932].

The repeatability and reproducibility results of the AS-OCT parameters in BK are summarised in table 4.

	Repeatability			Reproducibility		
AS-OCT parameter	*Mean [Sw] difference (µm)*	*CV (%)*	*ICC*	*Mean [Sw] difference (µm)*	*CV (%)*	*ICC*
CT1	-20 [63.3]	6.73	0.958	-13.6 [78.0]	8.27	0.934
CT2	1.3 [28.4]	5.64	0.978	8.7 [26.6]	5.24	0.976
IT	24.8 [85.2]	20.1	0.889	-47.7 [119.9]	28.2	0.714
IW	-155.2 [486.0]	24.6	0.912	-265.2 [593.8]	31.8	0.838

CT1: corneal thickness at presentation, CT2: corneal thickness at resolution, IT: infiltrate thickness, IW: infiltrate width, Sw: precision, CV: coefficient of variation, ICC: intra-class coefficient

Table 4. Repeatability and reproducibility of AS-OCT parameters in bacterial keratitis.

4.1.5 Discussion

This study investigated the capability of AS-OCT to quantify morphology-based parameters of the acute corneal inflammatory response in BK. The CT could be measured in 97.8 to 100%, IT in 73 to 89.2% and IW in 56.8 to 73% of cases. At presentation, CT showed the highest repeatability and reproducibility of the 3 AS-OCT parameters with a CV of 6.73% and 8.27% respectively.

The AS-OCT parameters could not be measured in all cases, but CT was the most commonly measured parameter. In 1 case of the 45, an inflammatory endothelial plaque did not permit visualisation of the endothelial surface. The capability to measure infiltrate parameters was poorer than for CT, due to difficulty in identifying the transverse and axial borders of the infiltrate on the AS-OCT images. The poorest performance for IW is consistent with the poorer transverse resolution of optical coherence tomography compared to axial resolution; for the Visante OCT, Carl Zeiss Meditec quotes an axial resolution of 18 µm and a transverse resolution as 60 µm.[196]

The resolution quoted by the manufacturer reflects the resolving power of the device in the healthy cornea. The greater capability, repeatability and reproducibility for CT, compared to IT, reflect the better performance of AS-OCT in imaging the axial borders of the cornea than the axial borders of the infiltrate. The change in refractive index that occurs at the interfaces of the epithelium with air and endothelium with aqueous produces a signal peak on each A-scan, resulting in the hyper-reflective epithelial and endothelial layers that can be readily imaged,[260] and thus facilitating CT measurement. The dense arrangement of epithelial and endothelial cells causes greater backscatter of light than the corneal stroma, most likely from the cell nuclei, also contributing to the hyper-reflective appearance of epithelium and endothelium.

The optically dense nature of the stromal infiltrate causes increased backscatter of light compared to healthy stroma, resulting in the hyper-reflectve AS-OCT appearance of the infiltrate. It also reduces penetration of light, thus causing AS-OCT signal attenuation with increasing depth. This could limit the resolving power and compromise identification of the posterior border of the infiltrate. Other factors that may contribute to the difficulty in identifying the posterior infiltrate border include absorption of the AS-OCT signal by the optically dense infiltrate and the fact that some infiltrates may not have well defined borders, with the inflammatory infiltrate blending into the non-affected stroma.

Studies on OCT imaging of coronary atheromatous plaques have shown that the signal becomes too attenuated for reliable analysis beyond 1.5–2 mm thickness. In addition, dense and thick fibrosis or calcifications exert an attenuation effect, hindering analysis of deep wall structures.[261] A similar effect has been observed in OCT imaging of laryngeal carcinoma, where the markedly increased thickness and hyper-cellularity of the epithelial layer produced increased optical backscatter and absorption of the OCT signal, which eliminated light penetration to the deeper structures. As a result, the basement membrane could not be delineated and deeper structures could not be imaged.[262] Imaging of oesophageal carcinoma has analogous limitations with poor visualisation of the mucosal and submucosal architecture, due to insufficient OCT light penetration through thick lesions or scattering from hyper-cellular tissues.[263]

Limitations have also been identified with AS-OCT imaging of the irido-corneal angle. Sakata and colleagues, in a large study involving 502 participants, showed that the scleral spur could be imaged and identified in only 72% of AS-OCT images. The authors attributed the low detection of the scleral spur to technical difficulties in imaging certain quadrants, anatomical variation between eyes, but also to the low lateral or transverse resolution of the Visante OCT.[264] Tan et al also found a similar scleral spur detection rate, as it could be identified in 76% of the 1932 AS-OCT images that were analysed.[265] In this BK study, the CT could be measured in 97.8 to 100%, IT in 73 to 89.2% and IW in 56.8 to 73% of cases.

Repeat measurement of the 3 AS-OCT parameters that were investigated showed that CT had the highest repeatability and reproducibility. At presentation, CT repeatability precision was 124.1 µm, the CV 6.73% and the ICC 0.958. Reproducibility was slightly worse; the reproducibility precision was 152.9 µm, CV 8.27% and ICC 0.934. In comparison, the repeatability precision for IT was 167 µm, CV 20.1% and ICC 0.889; the reproducibility precision for IT was 119.9 µm, CV 28.2% and ICC 0.714. The better results for CT reflect the better capability of AS-OCT in imaging the anterior and posterior surfaces of the cornea compared to the axial borders of the infiltrate, as discussed above.

Repeatability and reproducibility were also investigated after resolution of the infection. Compared to CT measurements at presentation, the repeatability was improved with a precision of 55.7 µm, CV of 5.64% and ICC of 0.978. Similarly, reproducibility was also improved; precision was 52.1 µm, CV 5.24% and ICC 0.976. The improvement compared to presentation suggests that corneal inflammation tends to affect precision adversely. The most likely explanation is that signal attenuation with increasing depth through the inflammed and oedematous stroma may limit visualisation of the endothelium and thus placement of the calipers. In addition, the hyper-reflective infiltrate, almost invariably located in the anterior stroma, does not have a well-defined and homogeneous anterior hyper-reflective layer, such as the epithelium of the healthy cornea, to facilitate caliper placement.

Quantification capabilities of AS-OCT in bacterial keratitis

In this study, the repeatability and reproducibility in measuring the corneal parameters on the scans were investigated. The repeatability and reproducibility of acquiring the AS-OCT scans and, thus, of imaging the same axis of the cornea and lesion were not. This represents a limitation in the methodology design, but also the difficulties in organising such a study. Patients with corneal infection present at random times, and as a result availability of the same second examiner at all times would very difficult, if not impossible.

The repeatability of CT has not previously been investigated in the pathological cornea. Poorer OCT repeatability results, however, have been observed in imaging retinal pathology compared to healthy retina. A FD-OCT study measured retinal thickness of the central foveola in diabetic macular oedema and healthy controls.[266] The repeatability precision was 18.2 μm in the presence of oedema and 5.9 μm for healthy retina. The reproducibility precision was 41.4 μm for the oedematous retina and 9.6 μm for the healthy retina.

The precision of LASIK flap thickness measurements has been evaluated. In an AS-OCT study, the mean intra-observer difference in flap measurements was 2.9%, whereas the mean inter-observer difference ranged from 4.62% to 7.0%.[267] A second LASIK study found that the mean inter-observer difference in central and peripheral flap thickness measurements was 8.05% and 3.87% respectively.[268] Repeatability and reproducibility for BK compare favourably to flap measurements. The intra-observer and inter-observer differences at presentation were 2.13% and 1.44% of the mean CT; at resolution of infection, the respective figures were 0.26% and 1.72% of the mean CT. In the healthy cornea, the repeatability and reproducibility, as expected, have been found to be much better than in BK. Li H et al found that for central CT the repeatability CV was 1.2% and the ICC 0.96.[241] In the same study, the reproducibility CV was 1.3% and ICC 0.96. In comparison, for BK the repeatability CV for presentation CT was 6.73% and ICC 0.958; the reproducibility CV was 8.27% and ICC 0.934.

Measurement of CT with FD-OCT may provide better repeatability and reproducibility in corneal infection than TD-OCT, although there are no data to support this. In a study that investigated LASIK flap thickness with both TD-

OCT and FD-OCT, the FD-OCT device showed better reproducibility.[268] In a retinal OCT study investigating retinal nerve fibre layer thickness in glaucoma, the FD-OCT device also demonstrated lower measurement variability with a repeatability CV of 6.4% compared to 12.8% for the TD-OCT.[269] Imaging corneal infection with Fourier-Domain AS-OCT is an area with huge potential that requires investigation.

4.1.6 Conclusions

This study has found that AS-OCT imaging can provide in-vivo morphology based quantification of the acute corneal inflammatory response in BK. Of the 3 presentation AS-OCT parameters that were examined, CT performed the best; it could be quantified in nearly all, 97.8 to 100%, of the AS-OCT scans and showed the highest repeatability and reproducibility. The IT was the second best parameter, as it could be quantified in 73 to 89.2% of AS-OCT scans, but repeatability and reproducibility were poorer.

4.2 Repeatability and reproducibility of AS-OCT corneal thickness measurements in the non-inflamed cornea

4.2.1 Introduction

In the above study (4.1), CT performed better than IT and IW as a quantification parameter of inflammation in corneal infection and showed the best potential. However, repeatability and reproducibility of presentation CT were modest with a CV of 6.73% and 8.27% respectively. After resolution of infection, the repeatability and reproducibility improved slightly but remained modest; CV was 5.64% and 5.24% respectively. In the healthy cornea, however, the repeatability and reproducibility of automated measurements for central CT have been found to be much better; Li H et al reported an intra-observer CV of 1.2% and inter-observer CV of 1.3%.[241] Even better figures have been quoted; a study by Mohamed et al, investigating AS-OCT automated pachymetry maps found that the intra-observer and inter-observer CV for central CT was 0.3% and 0.5% respectively.[260]

The pachymetry map study by Mohamed et al also presented two further interesting findings. It found a poorer performance of AS-OCT for the peripheral than the central cornea; the repeatability and reproducibility were worse for CT measurements in the 5-7 and 7-10 mm zones compared to the central 0-2 mm zone.[260] Poorer repeatability and reproducibility in measuring peripheral CT has also been documented with the Orbscan scanning-slit and Pentacam-Scheimpflug devices.[270] The second interesting finding of the study by Mohamed et al was that for corneas with keratoconus, an ectatic condition that is not associated with any significant corneal opacification or clinical inflammation, the precision of CT measurements was good, although worse than for healthy corneas. The intra-observer and inter-observer CV, using automated measurements, ranged from 0.5 to 0.8% and 0.9 to 1.2% respectively.[260]

Studies investigating AS-OCT imaging and its repeatability have been carried out on healthy or relatively healthy corneas and, therefore, almost invariably use automated software for measurement of CT.[241,260,271] Anterior and posterior corneal boundaries are identified in the computer algorithm by signal peaks at

the air–tear film interface and cornea–aqueous interface on each AS-OCT A-scan. Automated scan processing allows correction for image distortion due to refractive index transition at the air–cornea interface.[260] Corneal infection, however, is a very pathological condition of the cornea with considerable deformity and transparency loss; as a result, the algorithms used by the device software cannot delineate successfully the anterior and posterior boundaries of the cornea. Measurement of CT, therefore, requires manual placement of callipers on the anterior and posterior corneal boundaries.

It is not known whether the poorer repeatability in corneal infection compared to published literature on the healthy cornea, represents a limitation of the imaging capabilities of AS-OCT in infection or a limitation of the measurement skills of the examiners. It is essential, therefore, to investigate the repeatability and reproducibility of CT measurements in a less pathological condition.

In the second study of this chapter, the repeatability and reproducibility of AS-OCT CT measurements in two locations of the healthy cornea are investigated; due to the variable position of ulcers in BK, a central and a mid-peripheral corneal location are investigated. Secondly, repeatability and reproducibility of CT measurements following Descemets stripping endothelial keratoplasty (DSEK) are investigated, as the post-endothelial keratoplasty cornea does not show clinical evidence of inflammation but does represent a pathological cornea.

4.2.2 Hypothesis

I hypothesize that repeatability and reproducibility of AS-OCT CT measurements in the non-inflamed cornea are better than in BK. The aims are to investigate the repeatability and reproducibility of CT measurements, firstly in the healthy cornea and secondly in the post-DSEK cornea, and then compare the outcomes to those in BK.

4.2.3 Materials and methods

4.2.3.1 Patient recruitment

Twenty healthy volunteers with no prior ocular history and a normal slit-lamp examination were recruited from staff at University Hospital Southampton NHS

Foundation Trust. Thirty-five patients with a minimum of 3 months following DSEK were also recruited from the corneal service.

Local NHS Research Ethics Committee and participant informed consent were obtained. The research adhered to the tenets of the Declaration of Helsinki (section 2.1.1).

4.2.3.2 Scanning methods

Anterior segment imaging was carried out with the Visante OCT. Healthy participants had a four-quadrant high-resolution AS-OCT scan of both corneas. DSEK patients had a high-resolution AS-OCT scan at the 180° meridian. The scanning protocols are illustrated in sections 2.2.1 and 2.2.5, respectively.

4.2.3.3 Image, repeatability and reproducibility analysis

4.2.3.3.1 Healthy controls

The four-quadrant radial scans at 0°, 45°, 90° and 135° divided each cornea into 8 pie segments. Each of the 8 segments was divided concentrically into a central 4mm area, a mid-peripheral area defined by the 4mm zone and an outer 8mm zone, and a peripheral area extending from the 8mm zone to the limbus. The CT in the centre of each area was measured manually with calliper tools of the device software (version 1.1.2). The mean CT of each area for all participants was calculated and mapped for the right and left eyes. Mean CT values in the central, mid-peripheral and outer zones were compared with analysis of variance (ANOVA).

The CT measurements on the 180° meridian scan were repeated manually with calliper tools one month after the first set of measurements by examiner 1, in order to investigate the intra-examiner repeatability. Two locations of the cornea were chosen for repeat measurements; the central cornea and a mid-peripheral area at a +3 mm distance point from the central cornea. This +3 mm point was located using the software flap tool (figure 33). The flap tool was also used to obtain automated CT measurements at these two points. The CT measurements on the 180° meridian scan were also repeated at the same two locations by examiner 2, in order to investigate the inter-examiner reproducibility.

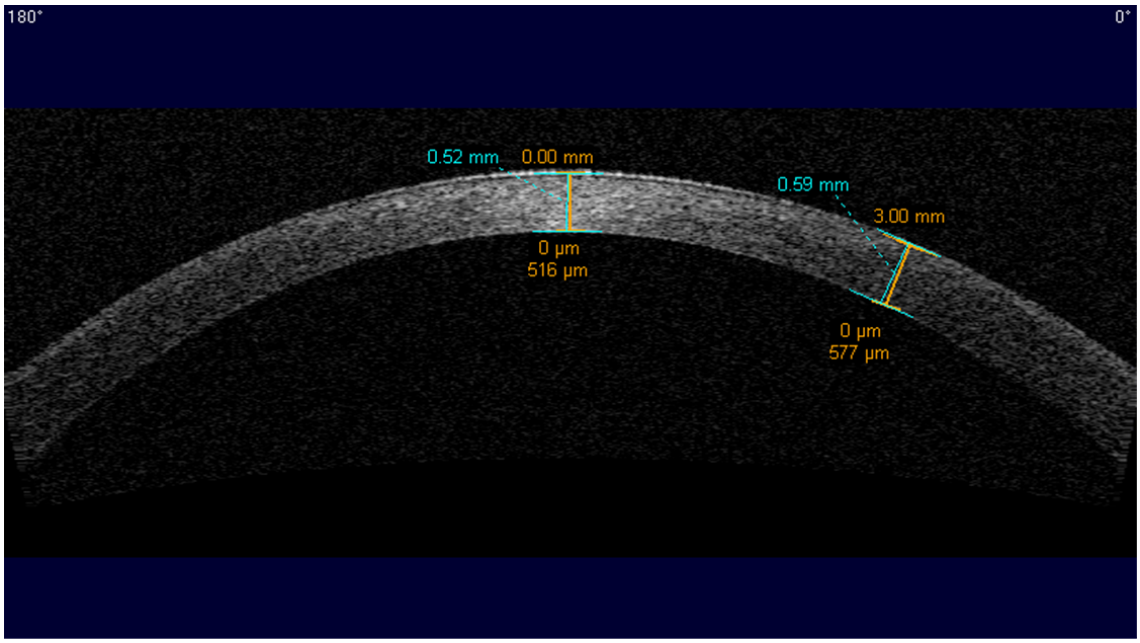

Figure 33. AS-OCT measurement of central and mid-peripheral corneal thickness in the healthy cornea. Measurements were repeated in two locations, centrally and 3 mm peripheral to the centre.

Data on CT measurements were examined with the Shapiro-Wilk test and normal distribution plots. A normal distribution was detected and, therefore, parametric tests were used for statistical analysis. Agreement between the automated and first set of manual measurements of examiner 1 was analysed with the paired t-test, Pearson correlation coefficient and Bland-Altman plots. Repeatability and reproducibility in obtaining CT measurements were analysed and reported with the use of repeatability and reproducibility indices, as detailed in section 4.1.3.4.

The images were also analysed for qualitative morphological information. Specifically, they were examined for the presence of:

1. Hypo-reflectivity of the corneal stroma relative to the endothelium and epithelium.

2. Homogeneity of reflectivity of the corneal stroma.

4.2.3.3.2 Descemets stripping endothelial keratoplasty

Similar to the analysis in healthy corneas, manual central CT measurements on the 180° meridian scan were repeated by examiner 1, at least one month after the first set of measurements. The CT measurements on the 180° meridian scan were also repeated at the same central location by examiner 2. Graft thickness (GT) of the DSEK was also measured centrally by both examiners 1 and 2, as illustrated in figure 34. Measurements were made with manual placement of the flap tool arms. Repeatability and reproducibility indices for CT and GT measurements were calculated, as per section 4.1.3.4.

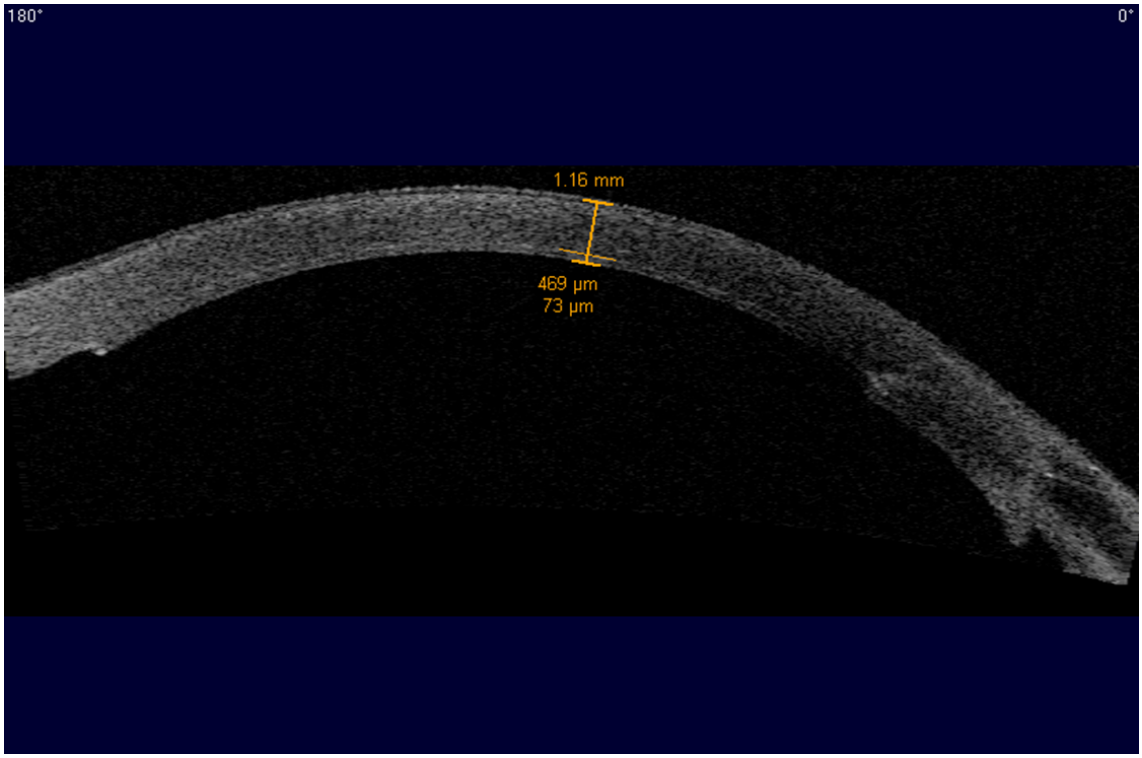

Figure 34. AS-OCT measurement of corneal and graft thickness following Descemets stripping endothelial keratoplasty. Graft thickness was 73 µm and thickness of the cornea above the graft 469 µm.

Statistical analysis for both healthy and DSEK corneas was carried out with the Statistical Package for Social Sciences (IBM SPSS Statistics for Windows, Version 19.0. Armonk, NY: IBM Corp). A sample size n≥30 cases (eyes) was aimed for,

as when n>30 the sampling distribution of the mean is very closely approximated by the normal distribution with a small standard error.[259]

4.2.4 Results

4.2.4.1 Healthy corneas

Five male and 15 females, had an AS-OCT scan of both corneas. Mean [SD] age was 42.7 [10.7] years (range 27-59).

4.2.4.1.1 Qualitative morphological observations

All AS-OCT corneal images showed the presence of two hyper-reflective layers that corresponded in location to the epithelium and endothelium (figure 33). Both layers were smooth and appeared to have a prolate profile that is characteristic of the normal cornea. The corneal stroma had a ground glass appearance and was hypo-reflective relative to the epithelium and endothelium.

4.2.4.1.2 Corneal thickness maps

The first set of CT measurements was used to plot the CT maps. Mean [SD] manual central CT was 552 [36.4] µm for the right eye and 547.5 [33.1] µm for the left eye. The cornea was thicker in the mid-peripheral and outer zones (table 5). Mean CT in the centre of each zone and the plotted CT maps are shown in figure 35.

Region of cornea	Central zone CT	Mid-peripheral zone CT	Outer zone CT	P-value
		Right eye		
Nasal	552	623.5	701.5	<0.001
Superior-nasal	552	635	716	<0.001
Superior	552	629	712	<0.001
Superior-temporal	552	604	684	<0.001
Temporal	552	575	640	<0.001
Inferior-temporal	552	574	644.5	<0.001
Inferior	552	595.5	669.5	<0.001
Inferior-nasal	552	609.5	697	<0.001
		Left eye		
Nasal	547.5	615	694.5	<0.001
Superior-nasal	547.5	634.5	705.5	<0.001
Superior	547.5	631	713.5	<0.001
Superior-temporal	547.5	606	683	<0.001
Temporal	547.5	579	640.5	<0.001
Inferior-temporal	547.5	584	652	<0.001
Inferior	547.5	598	672	<0.001
Inferior-nasal	547.5	609	694	<0.001

CT: corneal thickness in µm

Table 5. Corneal thickness in central, mid-peripheral and outer zones. There is a statistically significant increase in thickness from the centre of the cornea to the periphery in all regions.

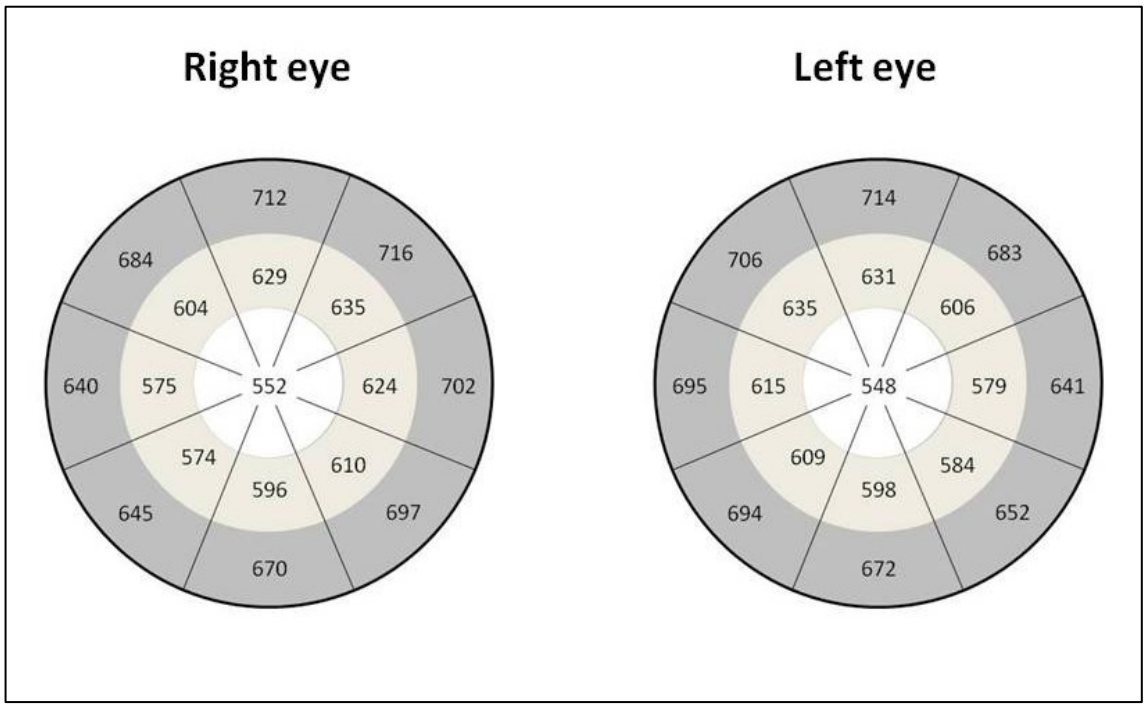

Figure 35. Corneal thickness maps of healthy control subjects. The cornea was divided into 8 pie segments and each pie segment into a central, mid-peripheral and outer area. Corneal thickness was measured in the centre of each area and the mean corneal thickness of all patients plotted.

4.2.4.1.3 Agreement of manual and automated corneal thickness measurements

Mean [SD] manual central CT of right and left eyes by examiner 1 was 549.8 [34.4] µm compared to automated central CT of 540.2 [35.3] µm ($p<0.001$). Automated readings were on average 9.6 [7.2] µm lower and 95% limits of agreement were between -24 and 4.8 µm. There was a strong correlation between manual and automated measurements ($r=0.979$, $p<0.001$).

Mean [SD] manual CT by examiner 1 at the 3mm point was 601.3 [43.4] µm compared to automated CT at the same point of 588.6 [46.0] µm ($p<0.001$). Automated readings were on average 12.7 [13] µm lower than manual and 95%

limits of agreement were between -38.7 and 13.3 µm. There was a strong correlation between manual and automated measurements (r=0.959, p<0.001).

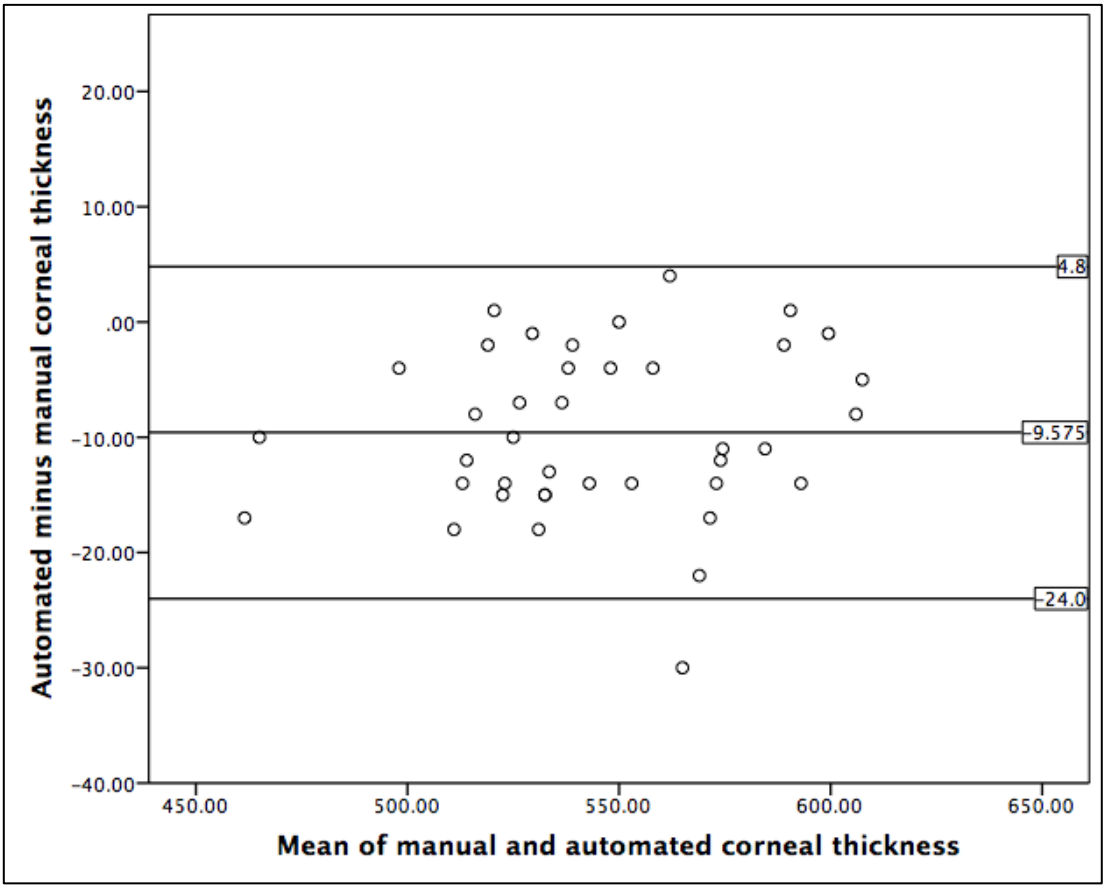

Figure 36. Bland-Altman plot comparing manual and automated central corneal thickness measurements. Automated readings were on average 9.575 µm lower than manual measurements and the 95% limits of agreement were between -24 and 4.8 µm. The horizontal lines represent the mean and 95% limits of agreement.

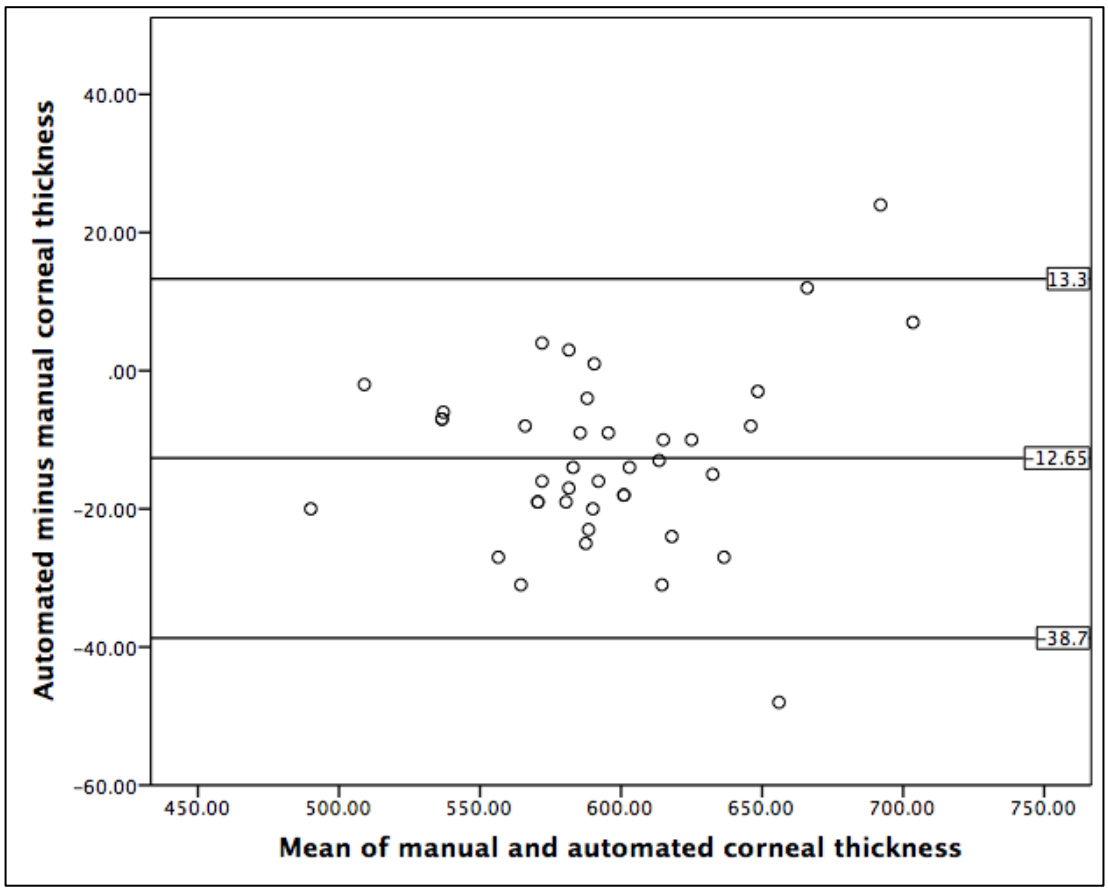

Figure 37. Bland-Altman plot comparing manual and automated corneal thickness measurements at 3 mm from centre. Automated readings were on average 12.65 µm lower than manual measurements and the 95% limits of agreement were between -38.7 and 13.3 µm. The horizontal lines represent the mean and 95% limits of agreement.

4.2.4.1.4 Repeatability of corneal thickness measurements

Repeat mean [SD] central CT of right and left eyes by examiner 1 was 545.5 [34.8] µm, significantly lower than the first measurement set of 549.8 [34.4] µm (p=0.002). The mean [Sw] difference was 4.3 [8.1] µm and the precision 15.9 µm. Overall mean of the two measurements was 547.6 µm and the CV of the two measurement sets 1.48%. The ICC was 0.966 (95% CI 0.917-0.984).

Repeat mean [SD] CT at the 3mm point by examiner 1 was 594.8 [42.8] µm, significantly lower than the first measurement set of 601.3 [43.4] µm

(p=0.001). The mean [Sw] difference was 6.5 [11.9] µm and the precision 23.3 µm. Overall mean of the two measurement sets was 598 µm and CV of the two measurement sets 1.99%. The ICC was 0.952 (95% CI 0.880-0.978).

4.2.4.1.5 Reproducibility of corneal thickness measurements

Mean [SD] central CT of right and left eyes by examiner 2 was 544.8 [34.8] µm, significantly lower than the first measurement set of examiner 1 (544.8 [34.8] vs. 549.8 [34.4] µm, p=0.002). The mean [Sw] difference was 5.0 [9.6] µm and the precision 18.8 µm. Overall mean of the two measurement sets was 547.3 µm and the CV 1.75%. The ICC was 0.952 (95% CI 0.886-0.978).

Mean [SD] CT at the 3 mm point by examiner 2 was 593.5 [49.1] µm, significantly lower than the first measurement set of examiner 1 (593.5 [49.1] vs. 601.3 [43.4] µm, p=0.025). The mean [Sw] difference was 7.8 [21.1] µm and the precision 41.4 µm. Overall mean of the two measurement sets was 597.4 µm and the CV 3.53%. The ICC was 0.887 (95% CI 0.785-0.940).

4.2.4.2 Descemets stripping endothelial keratoplasty

Thirty-five patients (16 right eye; 19 left eye), 17 male and 18 female, were recruited for the DSEK study; mean [SD] age was 73.3 [11.9] years. Indications for surgery were pseudophakic bullous keratopathy (n=12), Fuchs endothelial dystrophy (n=10), failed DSEK (n=2) and posterior polymorphous dystrophy (n=1).

4.2.4.2.1 Repeatability and reproducibility of corneal thickness

Repeat mean [SD] central CT by examiner 1 was 635.3 [94.4] µm, not significantly different to the first measurement set of 634.2 [91.8] µm (p=0.507). The mean [Sw] difference was 1.1 [9.6] µm and the precision 18.8 µm. The repeatability CV was 1.51%. The ICC was 0.997 (95% CI 0.995-0.999).

Mean [SD] central CT by examiner 2 was 626.2 [88.3] µm, not significantly different to the first measurement set of examiner 1 (p=0.209). The mean [Sw] difference was -8 [36.9] µm, the precision 72.3 µm and the reproducibility CV 5.8%. The ICC was 0.955 [95% CI: 0.912-0.977].

4.2.4.2.2 Repeatability and reproducibility of graft thickness

Mean [SD] central GT by examiner 1 was 151.2 [65.5] µm, not significantly different to the second measurement set of 150.2 [66.6] µm (p=0.566). The mean difference was -1.0 [10.2] µm, precision 20.0 µm, CV 6.77% and ICC 0.988 [95% CI: 0.977-0.994].

Mean [SD] central GT by examiner 2 was 144.3 [64.8] µm; the difference to the first measurements of examiner 1 was of borderline significance (p=0.063). The inter-examiner difference was -6.9 [21.4] µm, precision 41.9 µm, CV 14.5% and ICC 0.942 [95% CI: 0.886-0.971].

4.2.5 Discussion

AS-OCT provided high-resolution images of the healthy cornea in cross-section, which allowed visualisation of the epithelium and endothelium as hyper-reflective layers. The healthy corneal stroma was relatively hypo-reflective and had a homogenous ground glass appearance. However, the imaging resolution of the Visante OCT was not sufficient to resolve Bowman's layer from the epithelium, nor Descemets membrane from the endothelium. Newer OCT devices that use Fourier domain technology provide higher resolution imaging with clear visualisation of the epithelium and distinction from the underlying Bowman's layer.[235,272]

Pachymetry maps of healthy corneas were plotted from four-quadrant high-resolution scans, despite the Visante OCT providing automated pachymetry maps. Manual CT measurements were used to plot the maps, as manual measurements with software callipers are often required for the pathological cornea, such as in BK that will be investigated in this research thesis. The maps confirmed that the peripheral cornea was thicker than the central cornea. This

variation in CT was observed as early as the 1960s,[273,274] and subsequently confirmed with more modern techniques.[275,276]

The comparison of manual to automated CT measurements showed that the manual measurements in the healthy cornea were of good quality. Central and peripheral CT measurements were significantly larger than the corresponding automated measurements by 9.6 µm and 12.7 µm respectively. However, there was a strong correlation between manual and automated measurements, both centrally (r=0.979) and peripherally (r=0.959). It is well documented that the Visante OCT automated software tends to read lower CT measurements than those carried out manually. A study of normal eyes, by Li H et al, found that automated Visante OCT central CT measurements were smaller than manual measurements by 23.1 µm.[241] Rio-Cristobal A et al also showed a similar discrepancy; central CT was at least 30 µm smaller with automated measurements.[277]

Manual AS-OCT CT measurements in the healthy cornea showed good repeatability and reproducibility, and were consistent with published literature; they were better than measurements in BK (study 4.1). The repeatability CV was 1.48% for central and 1.99% for peripheral CT; the ICC 0.966 and 0.952 respectively. The difference in central CT between examiners 1 and 2 was 5.0 µm or 0.91% of the average measurement; the Sw of their difference was 9.6 µm for central and 21.1 µm for peripheral measurements. The reproducibility CV was 1.75% for central and 3.53% for peripheral measurements; the ICC 0.952 and 0.887 respectively. In the study by Li H et al, the repeatability CV for central CT was 1.2% and the ICC 0.96; the reproducibility CV was 1.3% and the ICC 0.96.[241] Kim et al found that the mean difference in central CT between two examiners was 6.9 µm or 1.4% of the average measurement.[271] The study by Rio-Cristobal A et al examined the reproducibility in central CT measurements between 3 examiners and found that the Sw of the inter-examiner difference ranged from 9 to 15 µm.[277]

Repeatability and reproducibility were both worse for peripheral than central CT measurements. This has previously been shown in an AS-OCT study that

examined repeatability and reproducibility of automated CT measurements on pachymetry maps; the coefficients of repeatability, reproducibility and variation were greater for peripheral than central measurements.[260] The poorer repeatability in peripheral corneal measurements may not be exclusive to AS-OCT imaging. A study using Orbscan scanning-slit topography and Pentacam-Scheimpflug imaging also found that CT measurements of the inferior and inferior-nasal cornea had a poorer ICC than those of the central cornea.[270] It may be that the imaging capabilities of these devices and the algorithms used to capture and analyse data are optimised for the central area of the cornea.

The repeatability and reproducibility in measuring CT following DSEK surgery were overall better than in BK. The repeatability and reproducibility CV for central CT following DSEK were 1.51% and 5.8% respectively, compared to 6.73% and 8.27% in acute BK, and 5.64% and 5.24% in resolved BK. The repeatability CV following DSEK was as good as in the healthy cornea (1.48%); however, the reproducibility CV was not (5.8% vs. 1.75%). This suggests that the repeatability of AS-OCT CT may depend on the extent of corneal pathology, being poorest in BK and equivalent in healthy cornea and following DSEK. Clear identification of the epithelium and endothelium in the healthy cornea and following DSEK may facilitate placement of callipers and precision. For the same reason, reproducibility in CT was also better following DSEK and in the healthy cornea than in acute BK. Therefore, it can be summated that the poorer indices in BK reflect a poorer imaging capability of the Visante OCT in this condition, rather than a limitation of examiner skills.

Repeatability and reproducibility CV for central GT, 6.77% and 14.5% respectively, were much poorer than for CT following DSEK, 1.51% and 5.8% respectively. This suggests that, when assessing endothelial keratoplasty with serial AS-OCT scans, CT may be prefereable to GT as an indicator of graft function. The poorer performance for GT most likely reflects limitations in the imaging resolution of the Visante OCT and the difficulty in identifying the interface between the host cornea and the endothelial keratoplasty. As discussed in section 4.1.5, a study that investigated LASIK flap thickness with both TD-OCT and FD-OCT found that the FD-OCT device had better reproducibility, reflecting its better performance in identifying the flap interface.[268]

4.2.6 Conclusions

AS-OCT imaged the healthy cornea in cross-section, the epithelium and endothelium appearing hyper-reflective relative to a ground-glass stroma. The repeatability and reproducibility of CT measurements in the healthy cornea were consistent with the published literature and better than following DSEK. DSEK repeatability and reproducibility indices were better than in BK. In conclusion, repeatability and reproducibility were better in the non-inflamed cornea.

4.3 Correlation of AS-OCT parameters with function

4.3.1 Introduction

The above studies (4.2 and 4.3) have shown that AS-OCT imaging can provide morphology-based quantification of the acute corneal inflammatory response in BK, with measurements of CT and IT. Measurement of the final CT after resolution of infection could potentially facilitate quantification of the extent of the associated corneal damage.

Studies that investigate the effect of a treatment often use visual acuity (VA) as an outcome measure, as it is the most common test of quality of vision in clinical practise. Although VA is a gold standard measure that cannot be minimised in importance, it is invariably confounded in studies by ocular comorbidity such as macular pathology, optic nerve damage and cataract. The lack of sensitivity of VA may be one of the reasons the large Steroids for Corneal Ulcers Trials (SCUT) found that corticosteroid drops did not have an overall beneficial effect on best spectacle-corrected VA, but did improve best spectacle-corrected VA for patients with ulcers that covered the central 4mm pupil area.[278] Although VA remains the standard measure of reporting outcomes in BK, it is not known whether it is sensitive enough to detect mild to moderate damage in BK, especially for paracentral or peripheral ulcers. The use a corneal parameter to quantify the extent of acute pathology and corneal damage in BK may have better sensitivity in investigating the effect of treatment.

Ophthalmologists specialising in the fields of glaucoma and retinal pathology often use OCT based morphological parameters, such as retinal nerve fibre layer (RNFL) thickness and macular volume, to document the extent of pathology and evaluate the effect of treatment. Objective quantification is of great interest to clinicians and also investigators conducting clinical trials. In glaucoma patients, OCT measured peripapillary RNFL thickness and optic nerve head parameters has been shown to have moderate to good correlation with automated visual field perimetry.[279-282] In diabetic macular oedema, photoreceptor outer segment thickness, retinal thickness and retinal volume measured with OCT have been found to be important associations and

predictors of VA and function.[283] Similarly, macular retinal thickness in central retinal vein occlusion has been found to correlate well with VA and macular sensitivity, assessed with microperimetry.[284]

A correlation of structure with function would validate the use of morphology-based AS-OCT corneal parameters in BK. These could potentially be used as a research outcome measure in clinical studies, but also in clinical practise to document and monitor the treatment effect. In this study, I investigate the correlation of AS-OCT morphology based parameters, CT and IT, with slit-lamp based parameters that are indicative of severity of infection, specifically with epithelial defect (ED) and infiltrate diameter (ID), and also evaluate their correlation with function, i.e. VA.

4.3.2 Hypothesis

I hypothesise that AS-OCT CT and IT correlate well with ED, ID and logMAR VA.

4.3.3 Materials and methods

The 45 patients (eyes) with clinical BK who were recruited in study 4.1 were used in this study. Slit-lamp examination, Visante OCT imaging (figure 38) and logMAR VA assessment were carried out, as detailed in study 4.1.

CT at presentation (CT1), CT at resolution of infection (CT2) and IT at presentation were examined for correlation with ED, ID and logMAR VA at presentation and logMAR VA at resolution of infection (final logMAR VA). The infection was considered resolved when the epithelial defect and signs of inflammation resolved completely (section 4.1.3).

Data normality was assessed by Shapiro-Wilk statistics and histograms. CT and IT showed a normal distribution, but ED, ID and logMAR VA a skewed distribution. The Spearman rank test was thus used for correlation analysis; values of correlation coefficient r between 0.00-0.19, 0.20-0.39, 0.40-0.59, 0.60-0.79 and 0.80-1.0 were considered very weak, weak, moderate, strong and very strong respectively.[285,286] Statistical analysis was carried out with the Statistical Package for Social Sciences (IBM SPSS Statistics for Windows, Version 21.0. Armonk, NY: IBM Corp); $p<0.05$ was considered statistically significant.

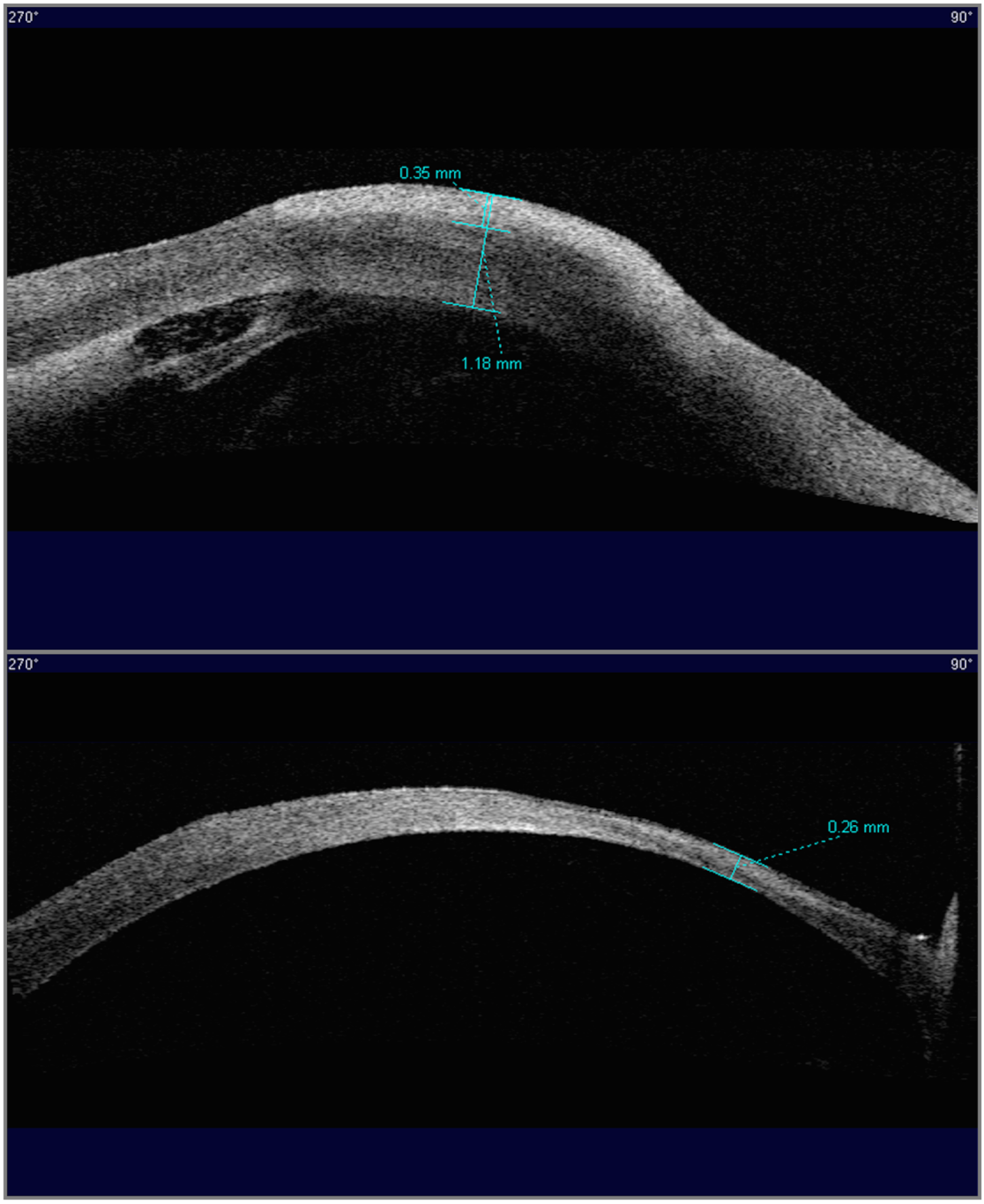

Figure 38. AS-OCT scans of *Pseudomonas* keratitis at presentation and resolution. A. Presentation corneal thickness (CT1) at the infiltration measured 1180 µm and infiltrate thickness 350 µm; intense anterior chamber inflammation was observed. B. Final corneal thickness (CT2) measured 260 µm; severe tissue loss in association with the infection was observed.

4.3.4 Results

Demographics of the 45 patients and bacteriology of the cases were summarised in section 4.1.4.

Mean [SD] logMAR VA at presentation was 1.21 [1.22]. Mean [SD] final logMAR VA was significantly better than at presentation (0.33 [0.71] vs. 1.21 [1.22], p<0.001). At presentation, the mean [SD] ED was 2.2 [1.5] mm and the mean [SD] ID 2.1 [1.3] mm.

Mean [SD] IT at presentation was 414.7 [186.7] µm. It correlated with CT1 (r=0.597, p<0.001), ED (r=0.328, p<0.001) and logMAR VA (r=0.703, p<0.001) at presentation. It also correlated with CT2 (r=-0.575, p=0.003). It did not correlate with ID (r=0.328, p=0.083) and final logMAR VA (r=0.258, p=0.161).

Mean [SD] CT1 at presentation was 966.7 [223] µm. It correlated with logMAR VA (r=0.560, p<0.001), IT (r=0.597, p<0.001), ED (r=0.528, p<0.001) and ID (r=0.647, p<0.001) at presentation. It also correlated with CT2 (r=-0.606, p<0.001), but not final logMAR VA (r=0.057, p=0.723).

Mean [SD] CT2, at resolution of infection, was significantly less than at presentation (509 [124.1] vs. 966.7 [223] µm, p<0.001). It correlated with CT1 (r=-0.606, p<0.001), IT (r=-0.575, p=0.003), ED (r=-0.578, p=0.001), ID (-0.570, p=0.003), and logMAR VA (r=-0.669, p<0.001) at presentation. It also correlated with final logMAR VA (r=-0.474, p=0.009).

The correlation analysis is summarised in table 6.

Parameter	CT1		IT		CT2	
	r	*P-value*	*r*	*P-value*	*r*	*P-value*
Presentation logMAR VA	0.560	<0.001	0.703	<0.001	-0.669	<0.001
Presentation ED	0.528	<0.001	0.328	<0.001	-0.578	0.001
Presentation ID	0.647	<0.001	0.328	0.083	-0.570	0.003
Final logMAR VA	0.057	0.723	0.258	0.161	-0.474	0.009

r: Spearman correlation coefficient, VA: visual acuity, ED: epithelial defect, ID: infiltrate diameter, CT1: corneal thickness at presentation, CT2: corneal thickness at resolution, IT: infiltrate thickness

Table 6. Correlation of AS-OCT parameters with clinical parameters of bacterial keratitis.

4.3.5 Discussion

This study detected a moderate to strong correlation between structural AS-OCT morphological parameters of corneal inflammation and function. A larger CT at presentation correlated moderately with poorer presentation vision, and a larger presentation IT strongly with presentation vision. In addition, a smaller final CT once infection had resolved correlated moderately with poorer final vision. These findings support the use of AS-OCT as an imaging modality in clinical practice, but also as a research tool investigating inflammation and tissue damage in corneal infection.

The AS-OCT morphological parameters also correlated with the clinical severity of infection and inflammation. At presentation, CT showed a moderate and strong correlation with the ED and ID respectively; correlations for IT were weaker. Interestingly, final CT once infection had resolved showed a strong negative correlation with presentation logMAR VA and a moderate negative correlation with presentation ED and ID. In addition, a strong negative correlation was found between presentation CT and final CT. These findings provided in-vivo evidence that greater severity of infection and inflammation at

presentation was associated with a lesser final CT. A greater infiltration with polymorphonuclear neutrophils, the predominant immune cells in BK, may contribute to greater stromal destruction with the release of superoxide anions, hydrogen peroxide and lysosomal enzymes.[28]

It is known from clinical experience that large corneal ulcers at presentation are associated with a poor prognosis and the need for penetrating keratoplasty.[16] However, this AS-OCT study has shown that AS-OCT may provide the opportunity to study corneal inflammation, tissue loss and the outcome in BK more accurately than with the use of clinical measures, such as VA, slit-lamp measured infiltrate or scar size and rate of perforation, as currently used in clinical studies, including the SCUT.[278]

4.3.6 Conclusions

A moderate to strong correlation was found in BK between the morphology-based AS-OCT corneal parameters, CT and IT, and function but also clinical parameters of severity of infection. The findings validate the use of AS-OCT CT and IT in clinical practise, to document the condition and monitor the treatment response in BK, and also as an outcome measure in clinical research studies.

5. Morphological and cytokine quantification of the inflammatory response in bacterial keratitis

5.1 Differential inflammatory response in Gram-negative and Gram-positive bacterial keratitis quantified with Anterior Segment Optical Coherence Tomography

5.1.1 Introduction

Bacterial keratitis (BK) is diagnosed clinically with a typical history and slit-lamp biomicroscopy findings. However, as detailed in section 1.4.4, diagnosis of the causative pathogen based on slit-lamp characteristics is at best of modest predictive value.[76] Corneal scrapes for microbiology cultures, the 'gold standard' for pathogen identification, only achieve growth in 63.8 to 71.2% of cases.[17,77,81] They involve the use of a sharp needle or spatula to obtain culture material from the infection site and, although safe in the vast majority of cases, the procedure can cause discomfort or phobia to the patient, precipitating a vasovagal syncope. As a late presentation of BK is associated with poor outcome,[16,17] a rapid diagnosis and initiation of appropriate treatment are very important, especially for highly virulent pathogens.

The imaging and quantification capabilities of AS-OCT in corneal infection, as presented in chapters 3 and 4, suggest that AS-OCT may have the potential to differentiate between the acute corneal inflammatory response of Gram-ve and Gram+ve BK. Thus, AS-OCT could provide safe office based, immediate, non-contact and non-invasive diagnostic information.

5.1.2 Hypothesis

I hypothesize that AS-OCT morphology based quantification can differentiate between the acute corneal inflammatory response of Gram-ve and Gram+ve BK. The primary aim of this study is to investigate the diagnostic value of AS-OCT CT and IT in identifying Gram-ve BK. The secondary aim is to quantify the differential acute corneal inflammatory response of Gram-ve and Gram+ve BK.

5.1.3 Materials and methods

5.1.3.1 Recruitment of patients and healthy controls

The patients recruited for the study in section 4.1 were used. In brief, patients with new-onset, previously untreated BK were recruited. Subsequent non-bacterial growth was an exclusion criterion (sections 4.1.3.1). The infection was considered resolved when signs of inflammation and the epithelial defect resolved completely. The volunteers with healthy corneas who were recruited for the study in section 4.2 were used as controls (section 4.2.3.1).

Local NHS Research Ethics Committee and patient informed consent were obtained. The research adhered to the tenets of the Declaration of Helsinki (section 2.1.1).

5.1.3.2 Examination and scanning protocol

5.1.3.2.1 Bacterial keratitis patients

Clinical slit-lamp examination and Visante AS-OCT imaging were carried out at presentation and after resolution of the infection. Data on patient demographics, risk factor for infection, duration of symptoms, logMAR VA, slit-lamp corneal epithelial defect (ED), slit-lamp corneal infiltration diameter (ID) and aetiological pathogen were collected (section 4.1.3.2). The standardized AS-OCT scanning protocol was used and image analysis with measurements of IT and CT was carried out, as previously described in section 2.2.2 and study 3.1.

Microbiology tests at presentation included Gram and calcofluor white slide microscopy and culture on blood agar, chocolate agar, Sabourauds, non-nutrient agar coated with *E. Coli* and broth medium. All patients were treated with intensive guttae ofloxacin 0.3% and cefuroxime 5% to the affected eye, after corneal scrapes had been carried out. Topical steroid drops were used after day 3, once a positive bacterial growth had been identified. Cases were categorized into Gram-ve, Gram+ve and microbiology negative, the latter being cases that did not have bacteria identified on microscopy or culture.

5.1.3.2.2 Healthy control participants

Control subjects had a four-quadrant high resolution AS-OCT scan of both corneas, at 0^{o}, 45^{o}, 90^{o} and 135^{o}, dividing each cornea into 8 pie segments. Each segment was divided into central, mid-peripheral and outer zones, based on the definitions in section 4.2.3.3.1; manual CT measurements were carried out and CT maps plotted.

A parameter of corneal inflammation termed corneal tissue swelling (CTS) was defined as the difference between the patient's CT at presentation and the mean control CT, obtained from the area of the plotted CT maps corresponding to the location and eye laterality of the patient's corneal ulcer. A parameter of corneal tissue loss after resolution of infection, termed corneal tissue loss (CTL), was defined as the difference between the patient's final CT after resolution of infection and the mean control CT, also obtained from the area of the CT maps corresponding to the location and laterality of the ulcer. The corneal infiltration was also classified as central, mid-peripheral or outer zone, based on the above zone definitions and the location of the centre of the infiltrate.

5.1.3.3 Statistical analysis

Mean values of IT, CT, CTS and CTL were calculated and compared between Gram-ve, Gram+ve and microbiology negative groups. The correlation between parameters was investigated. The sensitivity, specificity, positive predictive value (PPV) and negative predictive value (NPV) of increased CT and IT as diagnostic indicators of Gram-ve infection were examined.

Normality distribution of data was assessed by Shapiro-Wilk statistics, distribution plots and histograms. IT, CT and CTS showed a normal distribution, CTL a skewed distribution. ANOVA, post-hoc Dunnett and paired t-tests were used for normally distributed data. The Kruskal Wallis, Mann-Whitney U and Wilcoxon signed-rank tests were used for non-normal data. The Spearman rank test was used to analyze correlation between parameters. A P-value less than 0.05 was considered statistically significant.

Analysis was carried out with the Statistical Package for Social Sciences (IBM SPSS Statistics for Windows, Version 19.0. Armonk, NY: IBM Corp).

5.1.4 Results

5.1.4.1 Control participants

The data of 20 healthy volunteers was used to manually plot CT maps (figure 35).

5.1.4.2 Bacterial keratitis group

Forty-five patients (eyes) with clinical BK were included in the study (section 4.1.4). Mean [SD] age was 47 [20.6] years. Mean [SD] duration of symptoms before presentation was 3.3 [2.8] days. The infiltration was located in the central zone in 14 cases, the mid-peripheral zone in 25 cases and the outer zone in 6 cases.

Bacteriology showed 21 Gram-ve, 13 Gram+ve and 11 negative cases. Age and duration of symptoms were not significantly different in the three groups (p=0.927 and 0.228, respectively). Contact lens wear was the most common risk factor (30 cases), followed by recurrent corneal erosion syndrome (4 cases). Bacteriology and risk factors are detailed in table 3 (section 4.1.4). Mean [SD] follow up duration at the final AS-OCT scan was 28.6 [28.4] days; there was no significant difference between Gram-ve, Gram+ve and microbiology negative groups (39.5 [31.7] vs. 17.9 [12.6] vs. 22.2 [26.8] days, p=0.146).

5.1.4.2.1 Infiltrate thickness

The mean [SD] IT at presentation was 414.7 [186.7] µm. Mean [SD] IT was significantly different between Gram-ve, Gram+ve and microbiology negative groups (560.8 [182.4] vs. 304.4 [75.0] vs. 301.3 [104.7] µm, p=0.001). This difference was significant between Gram-ve and Gram+ve BK (p=0.001), Gram-ve and microbiology negative BK (p=0.002), but not between Gram+ve and microbiology negative BK (p=1.0).

In the Gram-ve group, 13 (72.2%) cases had IT ≥ 450 µm and 16 (88.9%) cases had IT ≥ 400 µm. In the Gram+ve group, only 1 (11.1%) case had IT ≥ 450 µm and only 1 (11.1%) case had IT ≥ 400 µm. The differences between Gram-ve and Gram+ve groups were significant for both 450 and 400 µm criteria (p=0.003 and p<0.001 respectively). The sensitivity, specificity, PPV and NPV of IT ≥ 400 µm as a diagnostic indicator of Gram-ve infection were 88.9%, 83.3%, 84.2% and 88.2% respectively. The sensitivity, specificity, PPV and NPV of IT ≥ 450 µm were 72.2%, 88.9%, 86.7% and 76.2% respectively.

5.1.4.2.2 Corneal thickness

Mean [SD] CT at presentation was 966.7 [223] µm. There was a significant difference between Gram-ve, Gram+ve and microbiology negative BK (1147.1 [152.2] vs. 840 [104.2] vs. 782.7 [69.7] µm, p<0.001). This difference was significant between Gram-ve and Gram+ve BK (p<0.001) and between Gram-ve and microbiology negative BK (p<0.001). Differences between the groups are summarized in table 7 and illustrated in figure 39.

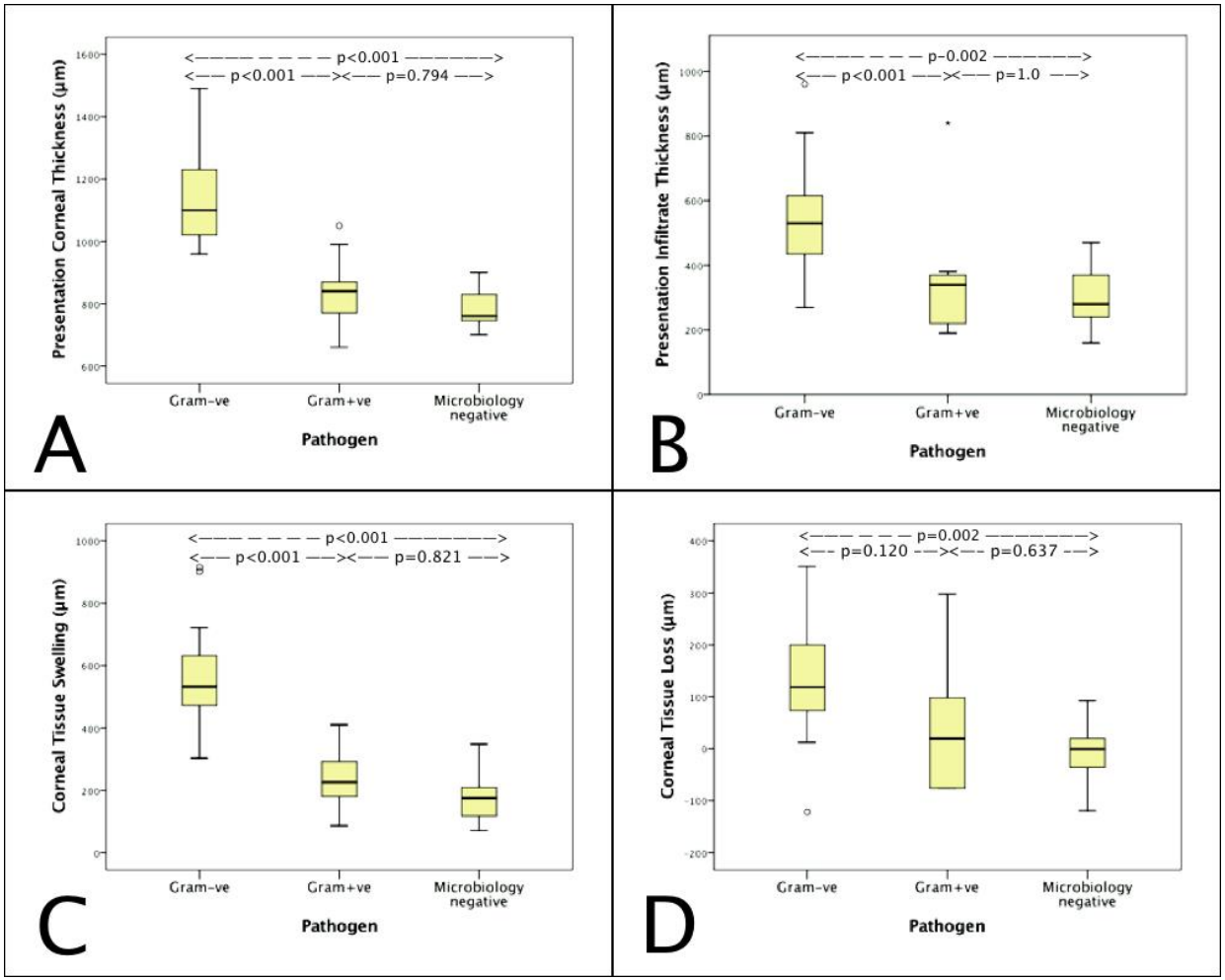
Presentation Corneal Thickness (µm)
<——— p<0.001 ———>
<— p<0.001 —><— p=0.794 —>
Gram-ve
Gram+ve
Microbiology negative
Pathogen
A
Presentation Infiltrate Thickness (µm)
<——— p=0.002 ———>
<— p<0.001 —><— p=1.0 —>
Gram-ve
Gram+ve
Microbiology negative
Pathogen
B
Corneal Tissue Swelling (µm)
<——— p<0.001 ———>
<— p<0.001 —><— p=0.821 —>
Gram-ve
Gram+ve
Microbiology negative
Pathogen
C
Corneal Tissue Loss (µm)
<——— p=0.002 ———>
<— p=0.120 —><— p=0.637 —>
Gram-ve
Gram+ve
Microbiology negative
Pathogen
D

Figure 39. Comparison of AS-OCT quantification parameters between Gram-ve, Gram+ve and microbiology negative bacterial keratitis. A. There was a significant difference in presentation corneal thickness between Gram-ve and Gram+ve groups, and between Gram-ve and microbiology negative groups, but not between Gram+ve and microbiology negative groups. B. There was a significant difference in presentation infiltrate thickness between Gram-ve and Gram+ve BK, and Gram-ve and microbiology negative BK, but not between Gram+ve and microbiology negative BK (p=1.0). C. There was a significant difference in corneal tissue swelling between Gram-ve and Gram+ve groups, and Gram-ve and microbiology negative groups, but not between Gram+ve and microbiology negative groups. D. There was a borderline significant difference in corneal tissue loss between Gram-ve and Gram+ve BK (p=0.12), a significant difference between Gram-ve and microbiology negative BK, and no significant difference between Gram+ve and microbiology negative BK.

In the Gram-ve group, 18 (85.7%) cases had a presentation CT ≥ 1000 µm, whereas in the Gram+ve group only 1 (7.7%) case had CT ≥ 1000 µm ($p<0.001$). In the Gram-ve group, all 21 (100%) cases had a presentation CT ≥ 950 µm compared to 2 cases (15.4%) in the Gram+ve group ($p<0.001$). The sensitivity, specificity, PPV and NPV of presentation CT ≥ 1000 µm as a diagnostic indicator of Gram-ve infection were 85.7%, 95.8%, 94.7% and 84.6% respectively. The sensitivity, specificity, PPV and NPV of presentation CT ≥ 950 µm were 100%, 91.7%, 91.3% and 100% respectively. Using a criterion of presentation CT ≥ 950 µm or IT ≥ 400 µm would have a sensitivity, specificity, PPV and NPV of 100%, 79.2%, 80.8% and 100%. A criterion of presentation CT ≥ 950 µm or IT ≥ 450 µm would have a respective sensitivity, specificity, PPV and NPV of 100%, 83.3%, 84% and 100% as a diagnostic indicator of Gram-ve infection. The diagnostic criteria for Gram-ve BK are summarized in table 8.

Mean [SD] final CT was significantly less than presentation CT (509 [124.1] vs. 966.7 [223] µm, $p<0.001$). There was a significant difference in final CT between Gram-ve, Gram+ve and microbiology negative BK (445 [94.9] vs. 531.7 [157] vs. 607.8 [76.8] µm, $p=0.003$). This difference was significant between Gram-ve and microbiology negative BK ($p=0.002$), but not between Gram-ve and Gram+ve BK ($p=0.17$). Representative AS-OCT scans of Gram-ve and Gram+ve BK, illustrating the presentation CT and final CT are shown in figure 40.

Parameter	Gram-ve vs. Gram+ve vs. microbiology -ve	P-value	Post-hoc P-value Gram-ve vs. Gram+ve
Presentation VA -logMAR (mean [SD])	1.78 [1.28] vs. 0.90 [1.0] vs. 0.53 [0.95]	0.002	0.014
Presentation ED -mm (mean [SD])	2.7 [1.5] vs. 2.0 [1.2] vs. 0.9 [0.5]	<0.001	0.138
Presentation ID -mm (mean [SD])	2.7 [1.4] vs. 1.5 [0.7] vs. 1.1 [0.6]	0.001	0.002
Presentation IT -µm (mean [SD])	560.8 [182.4] vs. 304.4 [75.0] vs. 301.3 [104.7]	0.001	0.001
Presentation CT -µm (mean [SD])	1147.1 [152.2] vs. 840 [104.2] vs. 782.7 [69.7]	<0.001	<0.001
CTS -µm (mean [SD])	562.3 [159.5] vs. 240 [100.5] vs. 181.4 [81.9]	<0.001	<0.001
Final VA -logMAR (mean [SD])	0.22 [0.45] vs. 0.69 [1.11] vs. 0.07 [0.16]	0.12	NA
Final CT -µm (mean [SD])	445 [94.9] vs. 531.7 [157] vs. 607.8 [76.8]	0.003	0.17
Corneal Tissue Loss -µm (mean [SD])	131.7 [112.5] vs. 44.4 [158.6] vs. -6.8 [60.2]	0.011	0.12
VA: visual acuity, ED: epithelial defect, ID: infiltrate diameter, IT: infiltrate thickness, CT: corneal thickness, CTS: corneal tissue swelling			

Table 7. Comparison of clinical and AS-OCT parameters between Gram-ve, Gram+ve and microbiology negative keratitis.

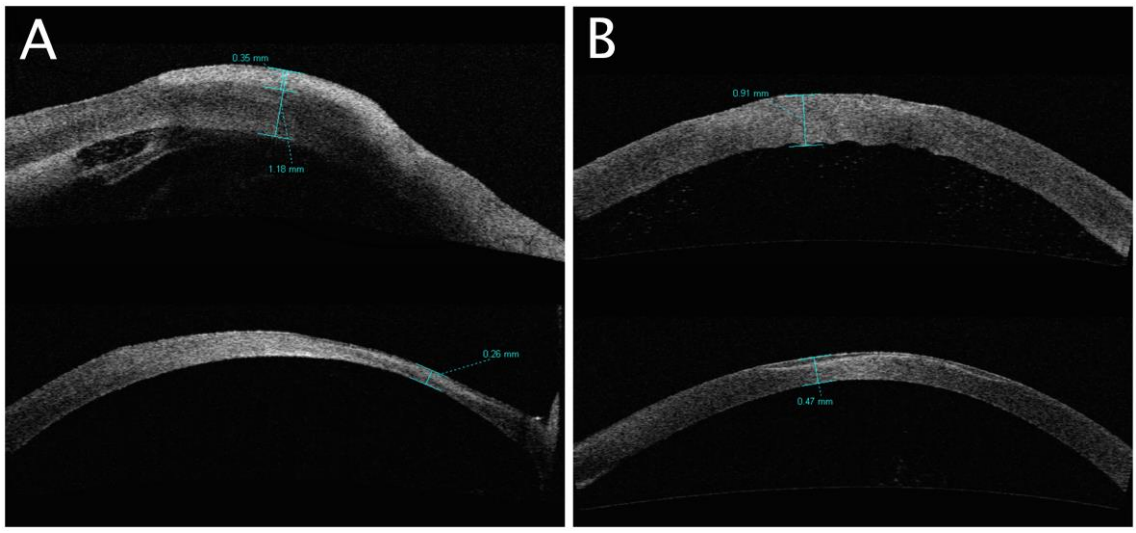

Figure 40. Representative AS-OCT scans of Gram-ve and Gram+ve bacterial keratitis. A. At presentation of Gram-ve bacterial keratitis (top image), the cornea was oedematous and a highly hyper-reflective infiltration was present; corneal thickness was 1180 µm. At resolution of infection (lower image), the scan illustrates the extent of corneal tissue loss; corneal thickness was 260 µm. B. At presentation of Gram+ve keratitis (top image), the cornea was not as oedematous as in Gram-ve keratitis; corneal thickness measured 910 µm. At resolution of infection, corneal thickness measured 470 µm and an anterior stromal scar was visualized.

5.1.4.2.3 Corneal tissue swelling

Mean [SD] CTS at presentation was 376.1 [217.6] µm. There was a significant difference between Gram-ve, Gram+ve and microbiology negative BK (562.3 [159.5] vs. 240 [100.5] vs. 181.4 [81.9] µm, $p<0.001$). This difference was significant between Gram-ve and Gram+ve BK ($p<0.001$); the ratio of Gram-ve to Gram+ve CTS was 2.3. The difference between Gram-ve and microbiology negative BK was also significant ($p<0.001$) and the ratio was 3.1.

Mean [SD] CTS at presentation was borderline significantly different between central, mid-peripheral and outer zone corneal infiltrates (485.3 [200.1] vs. 335.4 [222.5] vs. 290.8 [156.9] µm, $p=0.067$). Presentation

CTS correlated with IT (r=0.662, p<0.001), CTL (r=0.547, p=0.002) and final CT (r=-0.610, p<0.001).

5.1.4.2.4 Corneal tissue loss

Mean [SD] CTL was 75.1 [120.5] µm. There was a significant CTL difference between Gram-ve, Gram+ve and microbiology negative BK (131.7 [112.5] vs. 44.4 [158.6] vs. -6.8 [60.2] µm, p=0.011). The difference was significant between Gram-ve and microbiology negative BK (p=0.002), borderline significant between Gram-ve and Gram+ve BK (p=0.12) and not significant between Gram+ve and microbiology negative BK (p=0.637). CTL correlated with IT (r=0.432, p=0.031), CT (r=0.578, p=0.001) and CTS (r=0.547, p=0.002) at presentation. The correlation analyses are summarized in table 9.

AS-OCT parameter	IT ≥ 400	IT ≥ 450	CT ≥ 1000	CT ≥ 950	CT ≥950 or IT ≥400	CT ≥950 or IT ≥450
Sensitivity	88.9%	72.2%	85.7%	100%	100%	100%
Specificity	83.3%	88.9%	95.8%	91.7%	79.2%	83.3%
PPV	84.2%	86.7%	94.7%	91.3%	80.8%	84%
NPV	88.2%	76.2%	84.6%	100%	100%	100%

IT: infiltrate thickness in µm, CT: corneal thickness in µm, PPV: positive predictive value, NPV: negative predictive value

Table 8. AS-OCT criteria for diagnosis of Gram-ve bacterial keratitis. Sensitivity, specificity, positive and negative predictive values of AS-OCT corneal thickness and infiltrate thickness for the diagnosis of Gram-ve bacterial keratitis.

Parameter	CTS		CTL	
	r	*P-value*	*r*	*P-value*
Presentation logMAR VA	0.610	<0.001	0.603	0.001
Presentation epithelial defect	0.553	<0.001	0.520	0.004
Presentation infiltrate diameter	0.693	<0.001	0.423	0.040
Presentation infiltrate thickness	0.662	<0.001	0.432	0.031
Presentation corneal thickness	NA		0.578	0.001
CTS	NA		0.547	0.002
Final corneal thickness	0.610	<0.001	NA	
Final logMAR VA	0.090	0.577	0.448	0.017
CTL	0.547	0.002	NA	

CTS: corneal tissue swelling, CTL: corneal tissue loss, r: Spearman correlation coefficient, VA: visual acuity, NA: not applicable

Table 9. Correlation analysis for Corneal Tissue Swelling and Corneal Tissue Loss.

5.1.5 Discussion

This study quantified the differential acute corneal inflammatory response and associated tissue damage in Gram-ve, Gram+ve and microbiology -ve BK. A presentation CT ≥ 950 µm or IT ≥ 400 µm was associated with Gram-ve BK. Gram-ve bacteria induced greater corneal swelling than Gram+ve bacteria by a factor of 2.3. AS-OCT also enabled quantification of the tissue damage in BK by calculating the CTL after resolution of infection and it was found that the greatest CTL was observed in Gram-ve BK.

A presentation CT in excess of 950 µm was highly indicative of Gram-ve BK, as all cases in the Gram-ve group presented with CT ≥ 950 µm. A presentation CT ≥ 950 µm had 100% sensitivity, 91.7% specificity, 94.7%

PPV and 84.6 NPV as a diagnostic indicator of Gram-ve BK. However, BK is a dynamic condition and late presentation or poor treatment response may be associated with tissue necrosis and, thus, a reduced CT. Animal studies have found an increase in corneal inflammatory cell infiltration with progression of infection.[28] A diagnostic criterion that also uses IT in combination with CT may, therefore, be more applicable to BK. A criterion of CT ≥ 950 µm or IT ≥ 450 µm had 100% sensitivity, 83.3% specificity, 84% PPV and 100% NPV as a diagnostic indicator of Gram-ve BK. In a study that used clinical slit-lamp examination features, the sensitivity, specificity, PPV and NPV for prediction of *Pseudomonas* keratitis were 75%, 90%, 65% and 94% respectively.[81] Of note, the vast majority (86%) of assessments in this study were carried out by corneal specialists. The diagnostic potential of AS-OCT with the use of morphology-based quantification is, therefore, at least comparable to the opinion of clinicians with an expertise in corneal pathology.

Small case series have also presented the application of AS-OCT in imaging *Acanthamoeba* and fungal keratitis. In a study of 4 eyes with *Acanthamoeba* keratitis, radial keratoneuritis that characterizes the condition could be imaged as highly reflective bands or lines in the corneal stroma; however, *Acanthamoeba* cysts or trophozoites could not be visualized because of the limited resolution capacity of optical coherence tomography.[112] In cases reports of fungal keratitis, the corneal thickness could be measured and the hyper-reflective areas corresponding to the infiltrate could be imaged.[287,288] These findings were very similar to the *Fusarium* keratitis case that was described in chapter 3 (section 3.1.4.7.) Larger studies are required to investigate the diagnostic potential of AS-OCT in non-bacterial infections.

I found that presentation CT and IT were significantly larger in Gram-ve infection. The CTS in Gram-ve BK was greater than in Gram+ve BK by a factor of 2.3. Until the advent of AS-OCT it has not been possible to accurately quantify this difference in-vivo. These findings are consistent with the clinical experience that Gram-ve pathogens, and specifically *Pseudomonas*, are associated with large corneal infiltrates, as measured with the slit-lamp.[81] Bourcier et al have also shown that Gram-ve bacteria

cause corneal infiltration of greater surface area and severe anterior chamber inflammation.[17] However, no attempt has been made to further analyse and quantify the corneal differences between bacterial groups. The different bacterial virulence factors and activation of different pattern recognition receptors of corneal resident cells with corresponding intra-cellular pathways may account for the more intense inflammatory response observed in Gram-ve infection.[124,180,289]

The imaging capabilities of AS-OCT have enabled the in-vivo quantification of the corneal tissue damage that is caused by bacterial infection. The mean CTL after full re-epithelialisation was 75.1 μm and the greatest tissue loss was observed in Gram-ve BK. Interestingly, a larger tissue loss correlated moderately with greater CTS at presentation. These findings provide evidence for the detrimental effect that corneal inflammation may have on the outcome of patients with BK. Also in support, as presented in the structure-function association study (section 4.3), final CT once infection had resolved showed a strong negative correlation with presentation logMAR VA and a moderate negative correlation with presentation ED and ID. This may be explained by the fact that polymorphonuclear neutrophils (PMNs), the predominant corneal infiltrating cells in BK, release superoxide anions, hydrogen peroxide and lysosomal enzymes, resulting in stromal destruction.[28,290,291] This novel application of AS-OCT may provide more sensitive outcome measures in research that involves investigating corneal tissue damage, such as the potential benefit of steroid drops or other immune-modulatory agents.

This study focused on quantifying the difference in acute corneal inflammatory response between Gram-ve and Gram+ve BK in treatment naive patients who presented with relatively early BK. The mean duration of symptoms at presentation was 3.3 days and the mean infiltrate width 2.1 mm. Due to its novelty, the study was conducted on early corneal ulcers in order to avoid confounding factors that may be present in late cases, such as polymicrobial infection, prior inadequate treatment and corneal melting. In addition, small to moderate ulcers are the cases from which clinicians may be tempted not to obtain microbiology scrapes, as all advanced corneal ulcerations would necessitate microbiology scrapes.

A limitation of this study is that the diagnostic evaluation of AS-OCT IT and CT as indicators of Gram-ve infection was based on 45 patients living exclusively on the South coast of the United Kingdom. The most commonly identified bacteria were *Pseudomonas* and *Staphylococcus* species, a finding that is consistent with data from other Western studies in the United States, Australia, Canada and the United Kingdom.[76,77,79,85,86] There is, however, a wide geographic variation in the spectrum of bacteria involved in BK.[83] In South India, for example, the most common bacterium is *Streptococcus pneumoniae*.[84] The findings, therefore, need to be interpreted within this context and may be applicable to settings with a similar cohort of patients.

5.1.6 Conclusions

This study found that AS-OCT CT and IT can be used as diagnostic indicators in BK, as a criterion of presentation CT ≥ 950 µm or IT ≥ 450 µm was indicative of Gram-ve aetiology. In Gram-ve BK, the corneal tissue swelling was greater than Gram+ve BK by a factor of 2.3. Finally, AS-OCT could quantify the extent of tissue loss following resolution of infection. Tissue loss correlated positively with greater inflammation at presentation and was greatest in Gram-ve infection.

5.2 Serial quantification of the corneal inflammatory response in treated bacterial keratitis with Anterior Segment Optical Coherence Tomography

5.2.1 Introduction

In clinical practice, BK is routinely assessed with slit-lamp biomicroscopy, an imaging modality that is primarily limited by the physical properties of light. Objective assessment of the treatment response with slit-lamp examination is difficult, especially during the early phase of treatment. It relies on the semi-quantification of clinical features, such as corneal oedema, infiltrate density and conjunctival injection. Closure of the epithelial defect is also a sign of improvement.[7] Subjective features, such as improvement of patient symptoms, are often used as indicators of resolving infection. Repeat serial slit-lamp photography at presentation and follow-up examinations could potentially aid assessment of the treatment response, but there is no relevant published literature and photography is sensitive to illumination.

Assessment of the treatment response, especially in the early stages, is important in the management of BK, as improvement is a strong indication of appropriate antimicrobial treatment. Initial diagnosis and initiation of antimicrobial treatment are largely empirical, until microbiology results become available; even then, culture growth is only achieved in 63.8-71.2% of cases (section 1.4.4).[17,77,81]

In section 3.1, it was shown that serial standardised AS-OCT examination with measurement of corneal morphological parameters of infection and inflammation has the potential to provide objective monitoring of the disease course. The moderate to strong correlation these parameters, especially CT and IT, had with function, and their good repeatability and reproducibility, as presented in chapter 4, reinforce this potential.

5.2.2 Hypothesis

In this study, I hypothesize that AS-OCT can quantify with serial scans the corneal inflammatory response in resolving BK. The primary aim is to quantify this corneal inflammatory response in treated BK, by measuring the temporal change of corneal morphological parameters of inflammation. The secondary aim is to define criteria that will assist the objective assessment of the treatment response in BK.

5.2.3 Materials and methods

5.2.3.1 Recruitment of patients

Patients presenting with new-onset untreated clinical BK at University Hospital Southampton NHS Foundation Trust were recruited, as detailed in section 4.1.3.1. Local NHS Research Ethics Committee and patient informed consent were obtained. The research adhered to the tenets of the Declaration of Helsinki (section 2.1.1).

5.2.3.2 Examination and scanning protocol

AS-OCT imaging with the Visante OCT and clinical examination were carried out at presentation (day 0) and subsequently on days 3, 7 and 14 of treatment. Clinical examination included assessment of logMAR VA and slit-lamp measurements of ED and ID (section 4.1.3.2). Data on patient demographics, risk factor for infection and aetiological pathogen were collected.

Standard antibacterial treatment was intensive guttae ofloxacin 0.3% and guttae cefuroxime 5% to the affected eye. Antibiotics were instilled at an hourly frequency for 48 hours, then reduced to two hourly for a further 48 hours. The frequency was then reduced to six hourly until the infection had clinically resolved and the corneal surface re-epithelialized. Topical steroid drops were initiated after examination and AS-OCT imaging on day 3.

A standardized AS-OCT scanning protocol, as described in section 2.3.2, was used at each visit (figure 41). The scanning beam was positioned through the centre of the infiltrate at a defined axis. At repeat scans, the

scanning beam was positioned through the infiltrate centre at the same defined axis. CT, IT and IW were measured with calliper tools of the Visante OCT software (section 4.1.3.3).

5.2.3.3 Statistical analysis

The treatment response in BK was quantified with serial measurements of AS-OCT parameters, the ED overlying the infiltration and logMAR VA. VA of counting fingers at 30 cm, hand motion at 30 cm and perception of light were given scores of 2, 3 and 4 respectively. Mean values for CT, IT, IW, ED and logMAR VA were calculated and compared between days 0, 3, 7 and 14 of treatment.

For AS-OCT parameters that showed statistically significant change, the daily rate of change was calculated for the early (day 0 to 3), middle (day 3 to 7) and late (day 7 to 14) phases of treatment. Daily rate of change of each parameter was calculated for each eye according to the formula:

[X day B - X day A] / X day A / time interval in days,

where X is the parameter value and A and B is the first and last day of the treatment phase respectively. Mean values of daily rate of change were compared.

Shapiro-Wilk statistics, distribution plots and histograms were used to assess the normality distribution of data. All parameters showed a normal distribution. Mean CT, IT, IW, ED and IW were compared over time for a statistically significant difference with one-way ANOVA. Bonferonni post-hoc tests were carried out to examine the differences at the various time points. Daily rates of change for CT, IT and IW were compared using the paired t-test. P values less than 0.05 were considered statistically significant. Analysis was carried out with the Statistical Package for Social Sciences (Version 15.0; SPSS Inc, Chicago, IL).

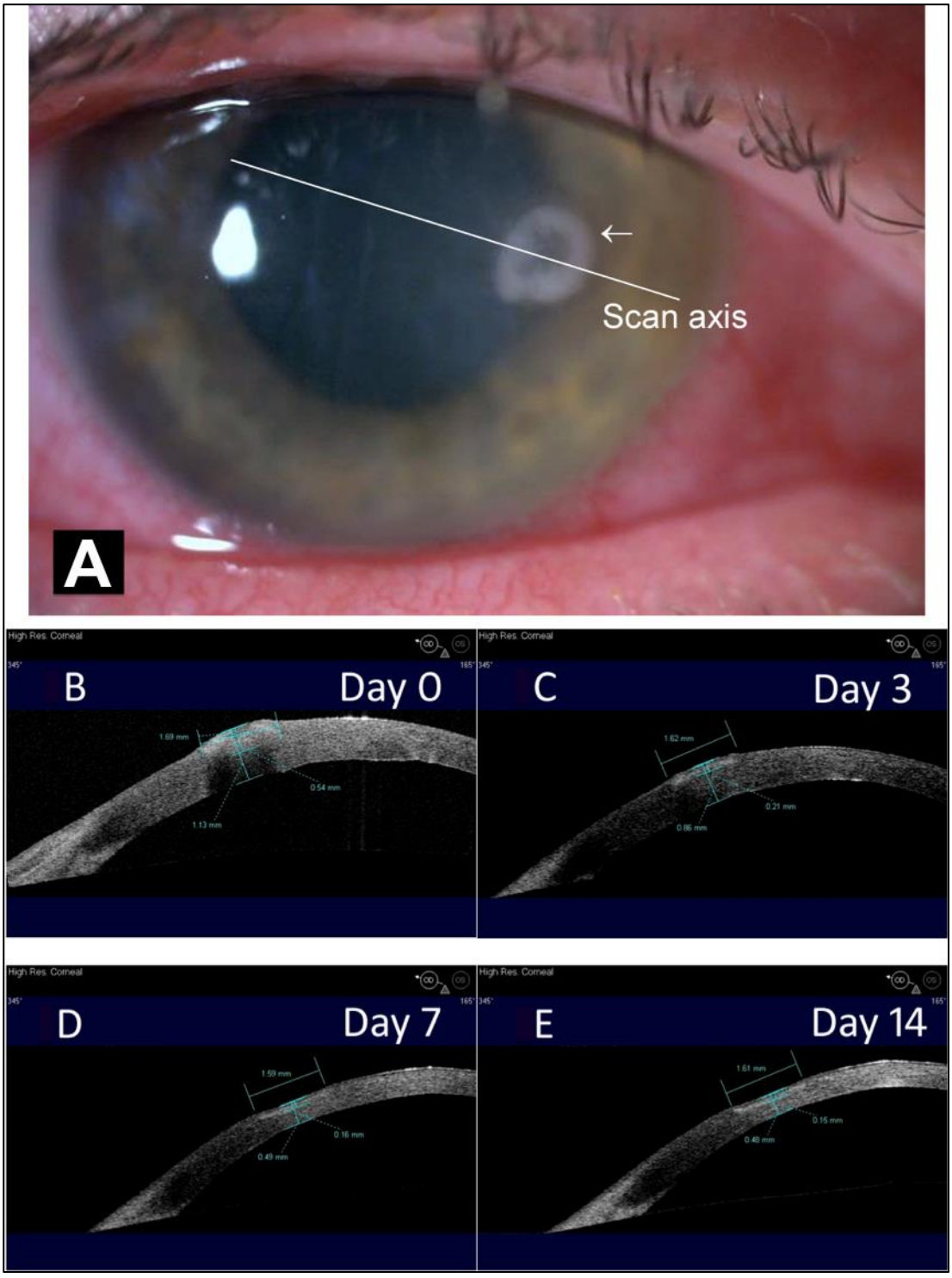

Figure 41. Serial AS-OCT imaging of treated bacterial keratitis. A. A corneal ulcer with inflammatory infiltration (←) due to *Pseudomonas aeruginosa*. B. High-resolution AS-OCT image through the center of the infiltrated area at the 165° axis at presentation. Corneal thickness, infiltrate thickness and infiltrate width measured 1130, 540 and 1690 µm respectively. C, D and E. A reduction in corneal and infiltrate thickness

was observed on days 3, 7 and 14 respectively. Infiltrate width does not change considerably.

5.2.4 Results

Twenty seven patients (27 eyes) with a clinical diagnosis of BK were recruited. One patient who was subsequently diagnosed with fungal keratitis was excluded. In the remaining 26 BK patients the infection resolved. Patient and BK characteristics are summarized in table 10.

The CT in the infiltrated area was largest on day 0 with a mean [SD] value of 905 [206] µm; CT measurements were possible in all 26 (100%) eyes. It decreased significantly over the 14-day period ($p<0.001$). Multiple test analysis with Bonferroni correction showed a significant reduction, compared to presentation, on days 3, 7 and 14; mean [SD] CT decreased significantly to 753 [161] µm ($p<0.001$), 678 [178] µm ($p<0.001$) and 584 [146] µm ($p<0.001$) respectively. A significant reduction was detected between days 3 and 14 ($p<0.001$), a borderline reduction between days 3 and 7 ($p=0.081$), and no significant change between days 7 and 14 ($p=0.330$). Compared to presentation, CT was reduced in 92.3% of cases on day 3, 96.2% on day 7 and 100% on day 14. The temporal change in CT is illustrated in figure 42.

The IT was also largest on day 0 with a mean [SD] value of 388 [184] µm; IT measurements could be carried out in 21 (80.8%) cases. The IT decreased significantly over the 14-day period ($p<0.001$). Multiple test analysis with Bonferroni correction showed a significant reduction, compared to presentation, on days 3, 7 and 14; mean [SD] IT decreased to 320 [163] µm ($p=0.001$), 296 [135] µm ($p=0.004$) and 207 [87] µm ($p<0.001$) respectively. A significant difference was present between days 3 and 14 ($p=0.006$), a borderline difference between days 7 and 14 ($p=0.104$), and no difference between days 3 and 7 ($p=1.0$). Compared to presentation, IT was reduced in 100% of cases on day 3, in 94.7% on day 7 and in 100% on day 14. The temporal change in IT is illustrated in figure 42.

Mean [SD] IW on day 0 was 1530 [1048] µm; IW measurements were possible in 13 (50%) eyes. IW did not change significantly during treatment (p=0.378) with mean [SD] values of 1498 [855] µm (p=0.591), 1547 [956] µm (p=0.878) and 1680 [1014] µm (p=0.308) on days 3, 7 and 14 respectively (figure 42).

CT decreased most rapidly in the early phase of treatment with a mean [SD] daily rate of 4.49 [3.78] %. The mean [SD] daily rate of CT reduction in the middle phase was 2.69 [3.62] % (4.49 vs. 2.69, p=0.21); in the late phase, the rate decreased to 1.33 [2.29] % (4.49 vs. 1.33, p=0.006).

IT also decreased most rapidly in the early treatment phase with a mean [SD] daily rate of 5.41 [5.13] %. In the middle phase, the mean [SD] daily rate of IT reduction was slower at 1.19 [6.80] % (5.41 vs. 1.19, p=0.042), but accelerated again in the late phase to 3.38 [3.08] % (5.41 vs. 3.38, p=0.70).

The mean daily rates of CT and IT reduction were not significantly different in the early (4.49% vs. 5.41%, p=0.49) and middle phases of treatment (2.69 vs. 1.19, p=0.40). In the late phase, however, IT decreased at a significantly faster rate than CT (3.38% vs. 1.33%, p=0.003) (table 11).

The mean [SD] ED overlying the infiltrated area was 2.2 [1.5] mm at presentation (before scrapes), and 3.2 [1.2] mm after corneal scrapes. It decreased significantly over the 14 days (p<0.001). Multiple tests with Bonferroni correction showed a significant reduction, compared to post-scape measurements, on days 3, 7 and 14; the ED decreased significantly to 1.7 [1.4] mm (p<0.001), 1.0 [1.1] mm (p<0.001) and 0.3 [0.8] mm (p<0.001) respectively. A significant difference was detected between days 3 and 14 (p=0.001), but not between days 3 and 7 (p=0.464), and days 7 and 14 (p=0.235). Compared to the post-scrape ED, the ED was reduced in 88.2% of cases on day 3, in 100% on day 7 and in 100% on day 14.

LogMAR VA decreased significantly over the 14 days (p<0.001). At presentation, the mean [SD] logMAR VA was 1.29 [1.26]. Multiple test analysis with Bonferroni correction showed a significant reduction, compared to presentation, only on day 14; on days 3, 7 and 14, it was

1.29 [1.19] (p=1), 0.57 [0.65] (p=0.072) and 0.26 [0.31] (p=0.002) respectively. A significant difference was detected between days 3 and 14 (p=0.002), a borderline difference between days 3 and 7 (p=0.088), and no significant difference between days 7 and 14 (p=1). Compared to presentation, logMAR VA was improved in 59.1% of cases on day 3, in 66.7% on day 7 and in 83.3% on day 14.

Patients	
Number	26
Sex: male/female	13/13
Age: mean, range (years)	48.4, 21-80
Eyes	
Number	26
Laterality: left/right	8/18
Risk factor	
Contact lens wear	20
Recurrent corneal erosion syndrome	2
Lagophthalmos	2
Atopy with dry eye	1
Corneal surgery - limbal relaxing incisions	1
Microbiology	
Pseudomonas aeruginosa	9
Diphtheroids	1
Coagulase –ve *staphylococcus*	1
Staphylococcus aureus	1
Negative	8
Not performed	6

Table 10. Patient characteristics, risk factors and microbiology of bacterial keratitis.

Rate of change (% per day)	Days 0-3	Days 3-7	Days 7-14
Mean daily CT decrease [SD]	4.49 [3.78]	2.69 [3.62]	1.33 [2.29]
Mean daily IT decrease [SD]	5.41 [5.13]	1.19 [6.80]	3.38 [3.08]
P-value	0.49	0.40	0.003

CT: corneal thickness, IT: infiltrate thickness

Table 11. Rate of change of corneal thickness and infiltrate thickness in resolving bacterial keratitis.

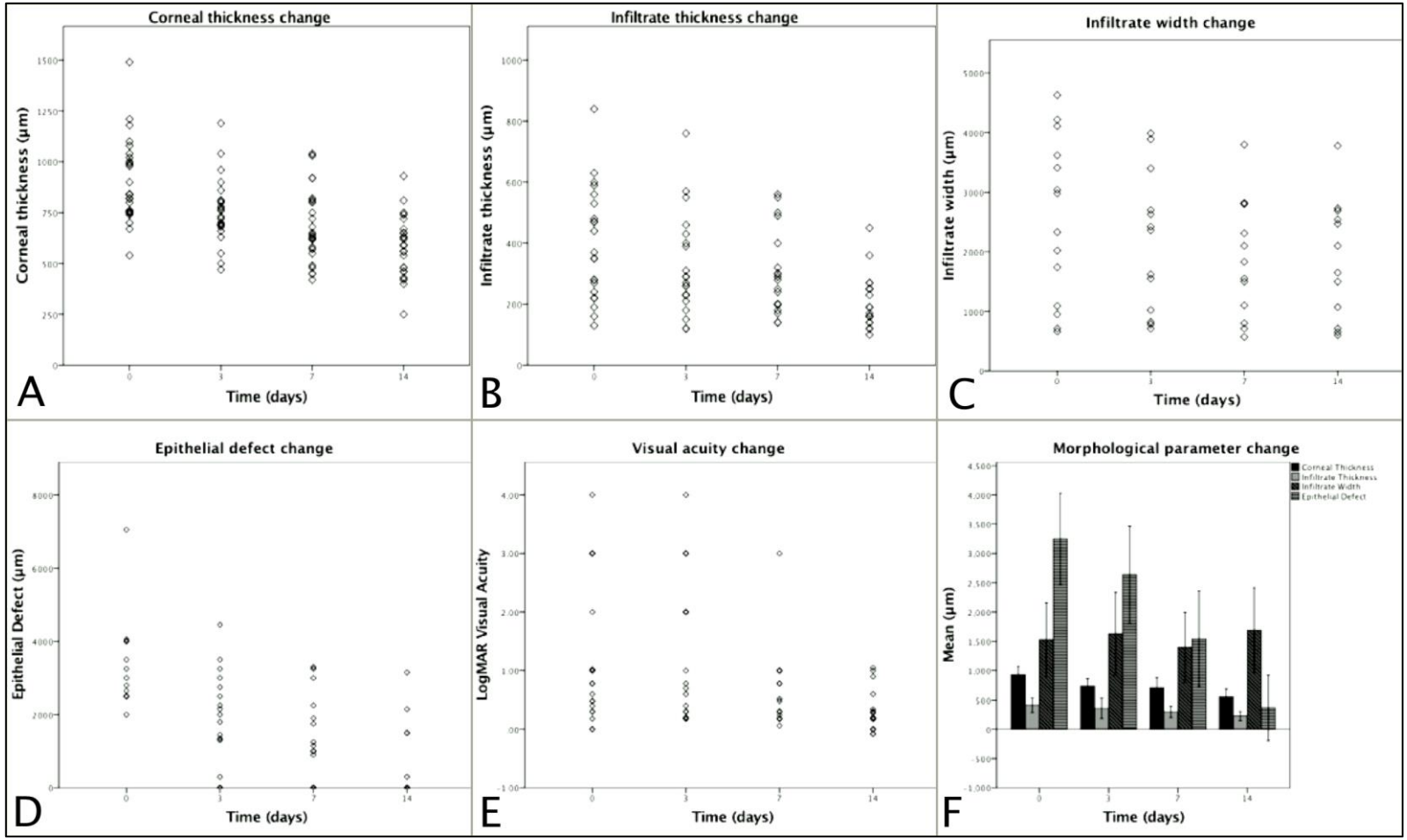

Figure 42. Corneal thickness, infiltrate thickness, infiltrate width, epithelial defect and visual acuity change during treatment of bacterial keratitis. A. Corneal thickness decreased significantly between presentation and day 3 ($p<0.001$), a

borderline reduction was present between days 3 and 7 (p=0.081) and no significant change between days 7 and 14 (p=0.330). B. Infiltrate thickness decreased significantly between presentation and day 3 (p=0.001), no reduction was present between days 3 and 7 (p=1.0) and a borderline reduction was detected between days 7 and 14 (p=0.104). C. The infiltrate width did not change significantly during treatment (p=0.378). D. The epithelial defect decreased significantly between presentation and day 3 (p<0.001), but not between days 3 and 7 (p=0.464), and days 7 and 14 (p=0.235). E. LogMAR Visual Acuity showed a significant reduction compared to presentation only on day 14 (p<0.001). F. Summary of change in morphological parameters during treatment of bacterial keratitis (error bars represent 95% confidence intervals).

5.2.5 Discussion

This study has shown that AS-OCT can be applied to the in-vivo quantification of the course of an acute corneal inflammatory condition and be used to monitor the condition, providing serial measurements of CT, IT and IW in BK. Both CT and IT decreased significantly within 3 days of starting antibiotic treatment. In contrast, IW did not decrease. Serial AS-OCT morphology based quantification of the inflammatory response provided objective evidence that successful treatment resulted in an early reduction in corneal oedema and the inflammatory response.

The mean CT and IT decreased significantly within the first 3 treatment days and continued to decrease throughout the 14-day period. In the early and middle phases of resolving BK, IT and CT decreased at similar rates, indicating that a similar process may be taking place in the infiltrated and deeper non-infiltrated cornea. Reduction in corneal oedema is the most likely explanation for the changes in the early and middle phases. In the late phase, however, the reduction in CT decelerated compared to the earlier phases and IT decreased at a significantly faster rate than CT. This suggests a different biological process to the earlier phases. Resolution of inflammatory cells and other components of the stromal infiltrate may be taking place in this late phase.

Compared to presentation, CT was reduced in 92.3% and IT in 100% of cases on day 3. This quantification information can be used to define the expected response in successfully treated BK. Failure to visualise a reduction in CT and IT by day 3 could be used as an indicator of poor treatment response and a sign of an atypical or resistant pathogen. Reiterative scans and measurements of CT and IT can, therefore, be used for objective and quantitative assessment of the treatment response in BK. Although slit-lamp biomicroscopy is an essential examination modality, it is very unlikely the mean CT reduction of 152 µm that was measured with AS-OCT in the early treatment phase could be detected with the slit-lamp, especially on different examination days. A study using Pentacam-Scheimpflug found a reduction in corneal densitometry between presentation and 4-6 weeks after resolution of infection, but this study did

not investigate the early treatment phase.[204] In my PhD studies, I investigated corneal reflectivity on AS-OCT images as a measure of corneal transparency by using the mean grey value of reflectivity with Image J (http://imagej.nih.gov/ij/; provided in the public domain by the National Institutes of Health, Bethesda, MD, USA).[292] Grey values did not correlate with clinical severity, CT or IT; mean values may have been confounded by the presence of a weak AS-OCT signal deep to dense corneal infiltration (figure 41B) and also a strong specular reflection at the centre of AS-OCT scans (figure 33).

The CT and IT decreased throughout the treatment period. It is known that the degree of corneal oedema in BK is proportional to the extent of PMN infiltration in the corneal stroma.[293] Thus, successful treatment of the condition may result in reduction of PMN infiltration that would produce a reduction in both IT and CT. The unchanged IW throughout treatment may be explained by the fact that, as the inflammatory components are gradually replaced with collagen and scar tissue, the measured width of the infiltrate would not change, as co-existing scar tissue and inflammatory infiltration both appear hyper-reflective on AS-OCT.

An interesting finding was that the VA did not improve significantly until day 14, although there was an improvement of borderline statistical significance by day 7. Morphology based quantification of the healing response with AS-OCT suggests that morphological improvement in BK occurs before the functional improvement. The improvement in the slit-lamp measured ED by day 3 also supports an earlier improvement for morphology than function. It can be postulated that, although a reduction in corneal oedema was observed as early as day 3, an improvement in optical transparency of the cornea lagged this rapid improvement in oedema. This has also been observed following endothelial keratoplasty; although post-operative corneal thickness does not decrease beyond the first month, VA continues to improve up to at least 6 months or longer.[193,294] In BK, other factors, such as the presence and persistence of intraocular inflammation, may have also contributed to the slower improvement in vision.

5.2.6 Conclusions

In summary, serial AS-OCT imaging has quantified in-vivo the acute corneal inflammatory response in resolving BK, demonstrating its capabilities as a modality that can quantify the course of an inflammatory condition. Resolving infection was characterized by an early reduction in corneal oedema by day 3, followed by a later reduction in infiltration thickness. On day 3 of treatment, CT was reduced in 92.3% and IT in 100% of cases, suggesting that failure to observe such an improvement in clinical practice by day 3 should prompt reconsideration of the diagnosis and treatment.

5.3 Corneal inflammatory response in bacterial keratitis quantified with tear cytokine and cytospin analysis

5.3.1 Introduction

In-vivo imaging in the previous studies (5.1 and 5.2) has shown that acute phase corneal inflammation, defined by AS-OCT morphological parameters, was greater in Gram-ve than Gram+ve BK and that it decreased significantly by day 3 of treatment. Corneal tissue loss in BK correlated with the extent of AS-OCT corneal inflammation at presentation and, in addition, greater tissue loss was associated with poorer vision. It would, therefore, be reasonable to assume that reducing the inflammation at presentation could have a favourable outcome on vision. This is the basis for the use of corticosteroid anti-inflammatory drops during the treatment of BK. The largest study to date, the Steroids for Corneal Ulcers Trials (SCUT), found that corticosteroid drops significantly improved the visual outcomes for patients with ulcers that covered the central 4mm pupil area, although overall in the trial, corticosteroids did not have a beneficial effect on the vision.[278]

It is not known whether the AS-OCT morphology based parameters of corneal inflammation truly represent inflammation. In section 5.1, AS-OCT CT and IT correlated well with function and slit-lamp based quantification parameters of corneal inflammation. Due to the human nature of this research work, it was not possible to directly correlate AS-OCT morphology with histopathological markers of inflammation. Therefore, in this study, molecular and cellular markers of inflammation in the tears of patients with BK are used to validate the two key AS-OCT findings, that Gram-ve BK is associated with greater levels of inflammation than Gram-ve BK, and that inflammation in BK decreases significantly by day 3 of treatment.

Current knowledge on the molecular and cellular phenotype in human BK is limited and greatly based on animal studies, as summarised in section

1.4.5. Although animals provide important insight into the human condition, differences in corneal anatomy and physiology may result in immune-pathology and immune-phenotype differences. In addition, the inbred nature of animals used in studies is not representative of humans,[295] and the relevance of animal-based findings on the inflammatory factors involved in human BK is not clear. Understanding cytokine production, the profile of involved immune cells and the associated tissue necrosis would greatly improve the translation of targeted molecular therapies and limit cornea damage and blindness in BK.[117]

5.3.2 Hypothesis

I hypothesise that molecular and cellular markers of inflammation are greater in Gram-ve than Gram+ve BK, and that by the third day of treatment the levels of these inflammatory markers have decreased significantly.

Primary aim of this study is to validate the morphology based AS-OCT findings of the previous studies (5.1 and 5.2) with molecular and cellular markers of inflammation. Secondary aim is to characterise and quantify the human immune response in BK.

5.3.3 Materials and methods

5.3.3.1 Recruitment of bacterial keratitis patients and controls

Patients presenting over a 12-month period to University Hospital Southampton NHS Foundation Trust with untreated, new onset clinical BK were prospectively recruited. The inclusion and exclusion criteria were as per study 4.1 (section 4.1.3.1). All patients had a level of care that is appropriate for patients with suspected BK, including VA assessment, slit-lamp examination, scraping of the ulcer for microbiology analysis and treatment as per departmental protocol (section 5.2.3.2). Steroid drops were commenced after the day 3 examination.

In addition to clinical investigations, recruited BK patients had tear sample collection at presentation (day 0) and days 3, 7 and 14 of treatment.

Healthy volunteers with no prior ocular history and a normal slit-lamp examination were also recruited as controls and had tear sample collection.

Local NHS Research Ethics Committee and patient informed consent were obtained. The research adhered to the tenets of the Declaration of Helsinki (section 2.1.1).

5.3.3.2 Tear sample collection

Tear samples were collected by carrying out a conjunctival lavage of the affected eye without the use of topical anaesthetic drops. Fifty microliters (50μL) of sterile normal saline at room temperature were infused into the lower conjunctival sac by gently pulling down the lower eyelid and with an insulin syringe that did not have a needle attached. After an interval of approximately two seconds, the conjunctival lavage fluid was aspirated back into the same syringe without the syringe touching the conjuntiva. The conjunctival lavage was repeated and the two syringes were sealed and transferred on ice to the laboratory.

5.3.3.3 Tear analysis

The conjunctival lavage fluid was processed using a modification of a protocol that has been used by the department of Clinical and Experimental Sciences at the Univesity of Southampton for examination of bronchial alveolar lavage fluid.[296] The conjunctival fluid from the two syringes was pooled and spun down in a centrifuge (2000 rpm or 0.4G for 10 minutes at 4 ^{o}C). The supernantant was stored at -80 ^{o}C for analysis at a later date. The cell pellet was resuspended with 300 μL phosphate-buffered saline solution and 4 cytospin slides were prepared. The cytospin slides were stained by the May Grunwald Giemsa method for differential counting (section 2.3).

5.3.3.3.1 Cytospin examination

Differential cell counting was carried out with light microscopy (X40 magnification) on 400 cells. The cytospin slides were also examined with oil immersion light microscopy (X100 magnification) in order to assess the

health of PMNs in the tears and their state of apoptosis. Apoptotic PMNs were defined as those cells that exhibited cell shrinkage, nuclear condensation, nuclear fragmentation and plasma membrane ruffling, features known to be characteristic of apoptotic cells and widely used for their identification.[297,298]

Four hundred PMNs were classified into 3 groups. Group 1 were healthy PMNs with no apoptosis and evidence of at least 1 chromatin bridge. Group 2 were PMNs showing evidence of apoptosis with the presence of no chromatin bridges or a fully condensed nucleus (loss of cytoplasm). Group 3 were dead PMNs with evidence of lysis (rupture of the plasma membrane).

5.3.3.3.2 Tear cytokine and chemokine analysis

The frozen tear supernatant collections were thawed and analyzed for levels of: IL-2, IL-8, IL-12p70, IL-1β, GM-CSF, IFN-γ, IL-6, IL-10, and TNF-α. The pro-inflammatory multiplex assay kit by Meso Scale Discovery (Gaithersburg, MD, USA) that employs the electrochemiluminescence principle was used (section 2.3). A multiplex kit was necessary, due to the small volumes of conjunctival lavage fluid. This pro-inflammatory kit was chosen, as all its 9 cytokines have been described to have a role in BK (section 1.4.5).

5.3.3.4 Statistical analysis

Mean cell counts per slide were compared between groups (t-test). Cytokine data were examined for normality distribution with Shapiro-Wilk statistics and distribution plots. A non-normal distribution was found; mean and median values were compared between groups (Mann-Whitney U test & Friedman's Two-Way Analysis of Variance). The Statistical Package for Social Sciences (IBM SPSS Statistics for Windows, Version 21.0. Armonk, NY: IBM Corp) was used.

5.3.4 Results

Thirteen patients were recruited. Seven cases were Gram-ve and six Gram+ve. Aetiological pathogens were *Pseudomonas aeruginosa* in 6

cases, *Staphylococcus aureus* in 3, coagulase negative *Staphylococcus* in 2, coliform bacteria in 1 and *Streptococcus pneumoniae* in 1. Mean patient age was 56.7 years.

5.3.4.1 Cytospins

Five Gram-ve and 4 Gram+ve BK cases had differential cell counting at presentation and day 3 of treatment; 4 cases of the 13 presented out of hours and did not have cytospin slides prepared. Overall, 4 cases, all Gram-ve, had cells identified on the cytospins and 5 did not. PMNs were by far the most common cells, ranging from 96.5 to 99.25% of the total of cells. The remaining cells were macrophages and epithelial cells (table 12). No PMNs were detected on day 3 cytospins.

In the Gram-ve group (n=5), mean [SD] PMN count was 314.4 [175.8] (78.6%), whereas no PMNs were detected in the Gram+ve group (n=4). The difference in PMN counts between the two groups was statistically significant (p=0.016).

Case	Neutrophils	Macrophages	Epithelial cells
		Cell counts (%)	
		Gram negative	
1	396 (99)	2 (0.5)	2 (0.5)
2	393 (98.25)	2 (0.5)	4 (1)
3	386 (96.5)	1 (0.25)	13 (3.25)
4	397 (99.25)	3 (0.75)	0
5	0	0	0
		Gram positive	
1,2,3 4	0	0	0

Table 12. Differential cell counting of cytospin slides at presentation of bacterial keratitis. The predominant cell in the tear film was the polymorphonuclear neutrophil.

Four cases, all Gram-ve at presentation, had microscopy for the state of apoptosis of PMNs (table 13). The mean [SD] number (%) of cells in group 1 was 268.8 [74.3] (67.2%), in group 2 it was 92.8 [17.7] (23.2%) and in group 3 it was 38.5 [74.4] (9.6%).

Case	Group 1	Group 2	Group 3
		Cell counts (%)	
1	282 (70.5)	118 (29.5)	0
2	160 (40)	90 (22.5)	150 (37.5)
3	319 (79.75)	77 (19.25)	4 (1)
4	314 (78.5)	86 (21.5)	0

Table 13. Microscopy of neutrophils for state of apoptosis. At presentation of bacterial keratitis the majority of neutrophils in the tears were healthy with no evidence of apoptosis.

5.3.4.2 Cytokines: bacterial keratitis compared to controls

Thirteen cases of culture positive BK (7 Gram-ve and 6 Gram+ve) at presentation were compared to five control cases. All cytokines/chemokines were elevated in the tear samples of BK patients, as summarised in table 14.

Cytokine	Conc in BK (pg/ml) Mean [SD] Median [IQR]	Conc in Cntrl (pg/ml) Mean [SD] Median [IQR]	Conc BK/Cntrl	P-value
IL-1β	50.24 [90.04] 9.85 [60.64]	0.12 [0.19] 0.00 [0.30]	419 NP	**<0.001**
IFN-γ	111.24 [242.68] 25.40 [12.78]	1.35 [1.57] 0.71[3.00]	82 36	**0.001**
GM-CSF	15.39 [26.31] 8.82 [12.78]	0.64 [0.52] 0.57 [0.82]	24 15	**<0.001**
IL-10	17.97 [39.79] 4.70 [8.76]	0.22 [0.30] 0.02 [0.54]	82 235	**0.003**
IL-12p70	17.10 [37.73] 5.77 [12.06]	0.98 [1.05] 0.77 [1.54]	17 7	0.10
IL-2	12.16 [14.75] 7.62 [15.24]	0.36 [0.27] 0.41 [0.82]	34 19	**<0.001**
IL-6	370.15 [431.83] 205.18 [609.04]	0.63 [0.20] 0.58 [1.16]	587 354	**<0.001**
IL-8	1129.03 [1518.37] 358.77 [2197.64]	18.54 [17.98] 15.02 [32.74]	61 24	**0.001**
TNF-α	33.25 [71.44] 9.98 [18.98]	0.84 [0.78] 0.86 [1.72]	40 12	**0.007**

Conc: concentration, BK: bacterial keratitis, IQR: interquartile range, Cntrl: controls, NP: not possible

Table 14. Comparison of cytokine and chemokine levels between bacterial keratitis at presentation and controls.

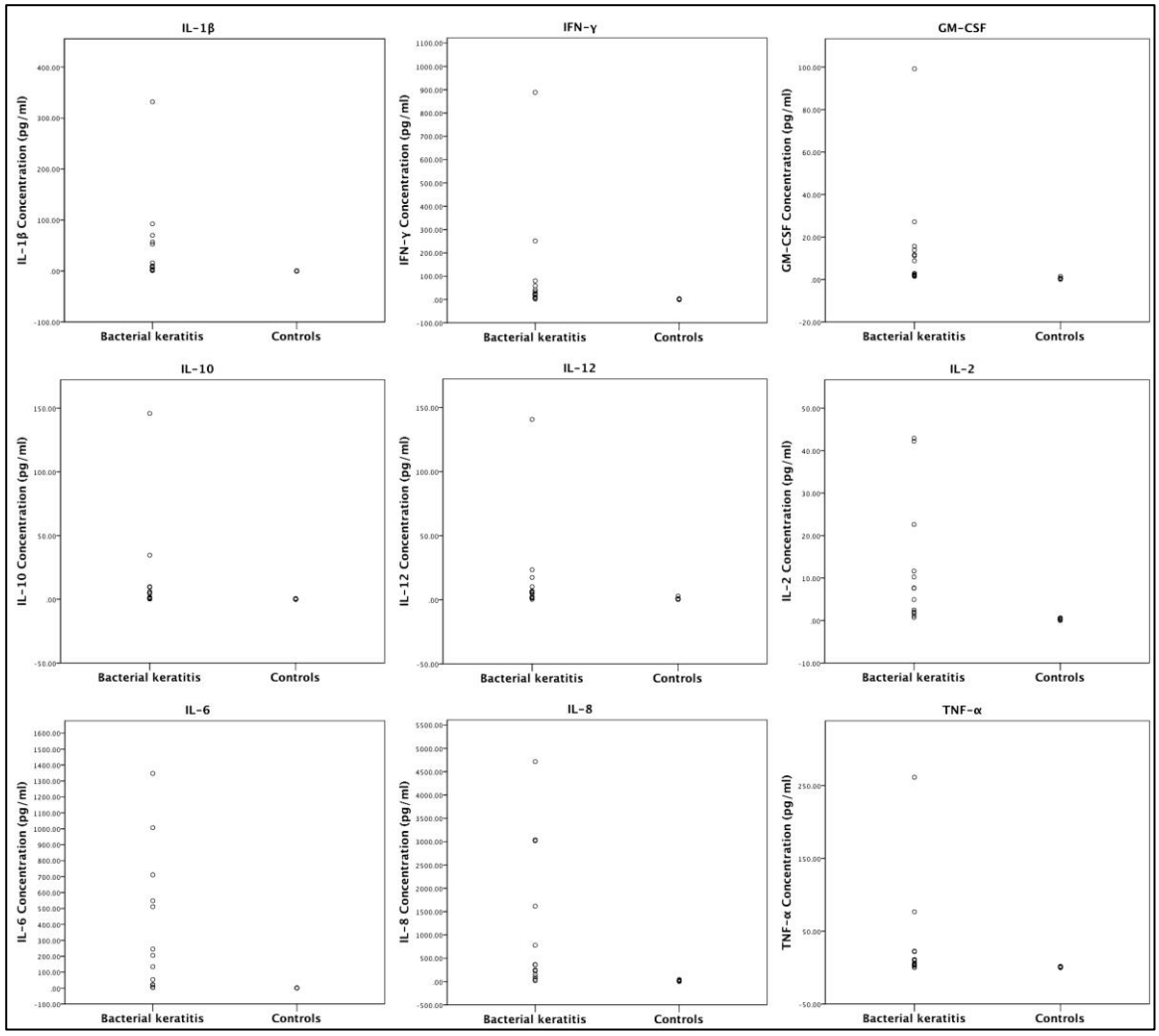

Figure 43. Comparison of cytokine and chemokine levels between bacterial keratitis at presentation and controls. The levels of all cytokines/chemokines were significantly increased compared to controls, except for IL-12p70.

5.3.4.3 Cytokines: Gram negative versus Gram positive bacterial keratitis

Seven Gram-ve cases were compared to six Gram+ve cases at presentation; IL-1β, IL-6 and IL-8 levels were significantly higher in Gram-ve BK (table 15).

Cytokine	Conc Gram-ve (pg/ml) Mean [SD] Median [IQR]	Conc Gram+ve (pg/ml) Mean [SD] Median [IQR]	Conc Gram -ve/+ve	P-value
IL-1β	82.67 [114.69] 52.65 [84.00]	12.40 [21.98] 2.76 [20.3]	6.7 19.1	**0.035**
IFN-γ	58.51 [86.96] 22.03 [47.58]	172.76 [351.90] 29.72 [277.24]	0.3 0.7	1.0
GM-CSF	10.90 [8.63] 11.19 [11.92]	20.64 [38.86] 2.71 [34.66]	0.5 4.1	0.836
IL-10	8.78 [11.75] 4.97 [9.94]	26.52 [58.57] 1.47 [43.62]	0.3 3.4	0.628
IL-12p70	8.80 [8.43] 6.49 [15.74]	26.80 [55.88] 3.42 [41.12]	0.3 1.9	0.836
IL-2	14.53 [13.80] 10.24 [17.66]	9.39 [16.63] 1.92 [15.44]	1.5 5.3	0.138
IL-6	599.62 [454.03] 547.91 [801.66]	102.43 [201.11] 20.46 [163.7]	5.9 26.8	**0.008**
IL-8	1789.48 [1785.28] 778.88 [2682.96]	358.50 [620.71] 120.18 [533.44]	5.0 6.5	**0.014**
TNF-α	18.80 [26.36] 10.94 [18.26]	50.12 [103.83] 8.14 [82.00]	0.4 1.3	0.836

Conc: concentration, BK: bacterial keratitis, Gram-ve: Gram negative, Gram+ve: Gram positive, IQR: interquartile range

Table 15. Comparison of cytokine and chemokine levels between Gram negative and Gram positive bacterial keratitis. The levels of IL-1β, IL-6 and IL-8 were significantly greater in Gram negative bacterial keratitis.

5.3.4.4 Cytokines: time course in bacterial keratitis

Seven BK cases (6 Gram-ve, 1 Gram+ve) had tear sample collection and cytokine analysis at presentation and days 3,7 and 14 of treatment. The change in cytokine levels over time and comparison to controls are detailed in tables 21-28. Figure 44 illustrates the change in cytokine and chemokine levels over time.

Cytokine	Day 0	Day 3	Day 7	Day 14
	Cytokine concentration (pg/ml)			
	Mean [SD] *Median [IQR]* *BK/Cntrl conc*	*Mean [SD]* *Median [IQR]* *BK/Cntrl conc*	*Mean [SD]* *Median [IQR]* *BK/Cntrl conc*	*Mean [SD]* *Median [IQR]* *BK/Cntrl conc*
IL-1β	35.47 [36.08] 15.83 [62.74] 295.6	1.60 [1.03] 1.89 [2.08] 13.3	1.69 [1.35] 1.69 [2.68] 14.1	1.35 [1.44] 0.55 [2.62] 11.3
IFN-γ	26.26 [18.51] 22.03 [30.94] 19.5	24.74 [13.42] 12.04 [23.84] 18.3	8.99 [9.89] 7.62 [12.08] 6.7	9.08 [7.09] 7.92 [10.36] 6.7
GM-CSF	7.37 [5.23] 8.82 [9.76] 11.5	2.35 [1.57] 1.97 [2.94] 3.7	2.39 [1.88] 1.70 [3.84] 3.7	2.08 [1.39] 1.74 [1.94] 3.3
IL-10	4.06 [3.16] 4.70 [4.94] 18.4	0.92 [1.21] 0.42 [2.64] 4.2	1.11 [1.56] 0.31 [1.96] 5.0	0.38 [0.43] 0.24 [0.56] 1.7
IL-12p70	6.62 [7.78] 5.77 [4.96] 6.8	1.60 [1.12] 1.14 [2.02] 1.6	1.29 [1.28] 0.85 [2.16] 1.3	1.44 [1.27] 1.13 [1.00] 1.5
IL-2	11.60 [13.98] 7.62 [9.14] 32.2	1.32 [0.98] 0.99 [1.90] 3.7	1.18 [1.06] 0.89 [0.70] 3.3	1.22 [0.84] 0.87 [0.88] 3.4
IL-6	407.94 [359.38] 244.94 [576.46] 647.5	18.81 [26.51] 8.55 [26.00] 29.9	5.31 [5.14] 3.05 [7.48] 8.4	2.68 [2.90] 1.62 [2.40] 4.3
IL-8	1122.52 [1321.48] 363.46 [2770.90] 60.5	137.13 [77.84] 124.10 [84.76] 7.4	113.07 [141.77] 55.99 [175.50] 6.1	73.91 [77.84] 30.43 [138] 4.0
TNF-α	8.75 [6.71] 6.31 [7.48] 10.4	3.59 [3.04] 2.79 [6.44] 4.3	2.08 [2.12] 1.71 [2.30] 2.5	2.44 [1.70] 1.96 [2.20] 2.9

BK: bacterial keratitis, Cntrl: controls, conc: concentration, IQR: interquartile range

Table 16. Cytokine and chemokine changes during treatment of bacterial keratitis.

Cytokine	Day 0	Day 3	% change	P-value
	Cytokine concentration (pg/ml)			
	Mean [SD] *Median [IQR]*	*Mean [SD]* *Median [IQR]*		
IL-1β	35.47 [36.08] 15.83 [62.74]	1.60 [1.03] 1.89 [2.08]	-95.5 -88.1	**0.028**
IFN-γ	26.26 [18.51] 22.03 [30.94]	24.74 [13.42] 12.04 [23.84]	-5.8 -45.3	0.091
GM-CSF	7.37 [5.23] 8.82 [9.76]	2.35 [1.57] 1.97 [2.94]	-68.1 -77.7	0.063
IL-10	4.06 [3.16] 4.70 [4.94]	0.92 [1.21] 0.42 [2.64]	-77.3 -91.1	0.063
IL-12p70	6.62 [7.78] 5.77 [4.96]	1.60 [1.12] 1.14 [2.02]	-75.8 -80.2	0.063
IL-2	11.60 [13.98] 7.62 [9.14]	1.32 [0.98] 0.99 [1.90]	-88.6 -87.0	**0.028**
IL-6	407.94 [359.38] 244.94 [576.46]	18.81 [26.51] 8.55 [26.00]	-95.4 -96.5	**0.018**
IL-8	1122.52 [1321.48] 363.46 [2770.90]	137.13 [77.84] 124.10 [84.76]	-87.8 -65.9	**0.028**
TNF-α	8.75 [6.71] 6.31 [7.48]	3.59 [3.04] 2.79 [6.44]	-59.0 -55.8	**0.043**
IQR: interquartile range				

Table 17. Cytokine and chemokine change between presentation and day 3 of treatment of bacterial keratitis. A significant reduction was observed for IL-1β, IL-2, IL-6, IL-8 and TNF-α.

Cytokine	Day 3	Day 7	P-value
	Cytokine concentration (pg/ml)		
	Mean [SD] *Median [IQR]*	*Mean [SD]* *Median [IQR]*	
IL-1β	1.60 [1.03] 1.89 [2.08]	1.69 [1.35] 1.69 [2.68]	0.735
IFN-γ	24.74 [13.42] 12.04 [23.84]	8.99 [9.89] 7.62 [12.08]	**0.028**
GM-CSF	2.35 [1.57] 1.97 [2.94]	2.39 [1.88] 1.70 [3.84]	0.237
IL-10	0.92 [1.21] 0.42 [2.64]	1.11 [1.56] 0.31 [1.96]	0.600
IL-12p70	1.60 [1.12] 1.14 [2.02]	1.29 [1.28] 0.85 [2.16]	0.612
IL-2	1.32 [0.98] 0.99 [1.90]	1.18 [1.06] 0.89 [0.70]	0.866
IL-6	18.81 [26.51] 8.55 [26.00]	5.31 [5.14] 3.05 [7.48]	**0.018**
IL-8	137.13 [77.84] 124.10 [84.76]	113.07 [141.77] 55.99 [175.50]	0.237
TNF-α	3.59 [3.04] 2.79 [6.44]	2.08 [2.12] 1.71 [2.30]	0.063
IQR: interquartile range			

Table 18. Cytokine and chemokine change between days 3 and 7 of treatment of bacterial keratitis. A significant reduction was observed for IFN-γ and IL-6.

Cytokine	Day 7	Day 14	P-value
	Cytokine concentration (pg/ml)		
	Mean [SD] *Median [IQR]*	*Mean [SD]* *Median [IQR]*	
IL-1β	1.69 [1.35] 1.69 [2.68]	1.35 [1.44] 0.55 [2.62]	0.499
IFN-γ	8.99 [9.89] 7.62 [12.08]	9.08 [7.09] 7.92 [10.36]	0.735
GM-CSF	2.39 [1.88] 1.70 [3.84]	2.08 [1.39] 1.74 [1.94]	0.499
IL-10	1.11 [1.56] 0.31 [1.96]	0.38 [0.43] 0.24 [0.56]	0.176
IL-12p70	1.29 [1.28] 0.85 [2.16]	1.44 [1.27] 1.13 [1.00]	0.866
IL-2	1.18 [1.06] 0.89 [0.70]	1.22 [0.84] 0.87 [0.88]	0.612
IL-6	5.31 [5.14] 3.05 [7.48]	2.68 [2.90] 1.62 [2.40]	0.310
IL-8	113.07 [141.77] 55.99 [175.50]	73.91 [77.84] 30.43 [138]	0.237
TNF-α	2.08 [2.12] 1.71 [2.30]	2.44 [1.70] 1.96 [2.20]	0.176
IQR: interquartile range			

Table 19. Cytokine and chemokine change between days 7 and 14 of treatment of bacterial keratitis. No significant change was detected between days 7 and 14.

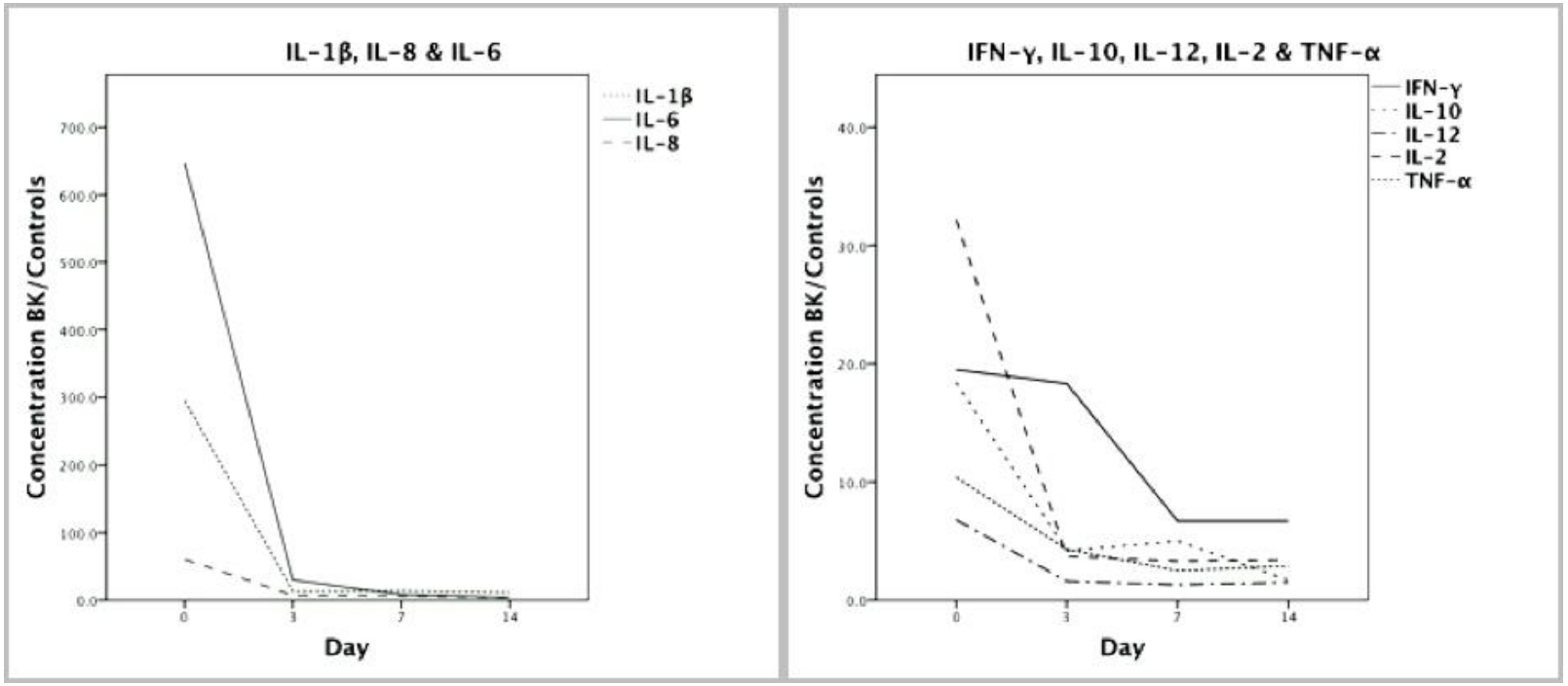

Figure 44. Time course of cytokine and chemokine change in resolving bacterial keratitis. The graphs illustrate the reduction in concentration of cytokines and chemokines by day 3 of treatment (data presented in tables 16-19).

Cytokine	Day 0 BK	Control		P-value
	Cytokine concentration (pg/ml)			
	Mean [SD] *Median [IQR]*	*Mean [SD]* *Median [IQR]*	*Conc* *BK/Control*	
IL-1β	35.47 [36.08] 15.83 [62.74]	0.12 [0.19] 0.00 [0.30]	295.6	**<0.001**
IFN-γ	26.26 [18.51] 22.03 [30.94]	1.35 [1.57] 0.71 [3.00]	19.5 31.0	**0.001**
GM-CSF	7.37 [5.23] 8.82 [9.76]	0.64 [0.52] 0.57 [0.82]	11.5 15.5	**<0.001**
IL-10	4.06 [3.16] 4.70 [4.94]	0.22 [0.30] 0.02 [0.54]	18.5 235	**0.002**
IL-12p70	6.62 [7.78] 5.77 [4.96]	0.98 [1.05] 0.77 [1.54]	6.8 7.5	**0.011**
IL-2	11.60 [13.98] 7.62 [9.14]	0.36 [0.27] 0.41 [0.82]	32.2 18.6	**<0.001**
IL-6	407.94 [359.38] 244.94 [576.46]	0.63 [0.20] 0.58 [1.16]	647.5 422.3	**<0.001**
IL-8	1122.52 [1321.48] 363.46 [2770.90]	18.54 [17.98] 15.02 [32.74]	60.5 24.2	**0.001**
TNF-α	8.75 [6.71] 6.31 [7.48]	0.84 [0.78] 0.86 [1.72]	10.4 7.3	**0.004**
BK: bacterial keratitis, conc: concentration, IQR: interquartile range				

Table 20. Comparison of cytokine and chemokine levels between bacterial keratitis at presentation and controls. In this cohort of patients all cytokines and chemokines were elevated in bacterial keratitis compared to controls.

Cytokine	Day 3 BK	Control	P-value
	Cytokine concentration (pg/ml)		
	Mean [SD] *Median [IQR]*	*Mean [SD]* *Median [IQR]*	
IL-1β	1.60 [1.03] 1.89 [2.08]	0.12 [0.19] 0.00 [0.30]	**0.018**
IFN-γ	24.74 [13.42] 12.04 [23.84]	1.35 [1.57] 0.71 [3.00]	**0.018**
GM-CSF	2.35 [1.57] 1.97 [2.94]	0.64 [0.52] 0.57 [0.82]	**0.018**
IL-10	0.92 [1.21] 0.42 [2.64]	0.22 [0.30] 0.02 [0.54]	0.432
IL-12p70	1.60 [1.12] 1.14 [2.02]	0.98 [1.05] 0.77 [1.54]	0.343
IL-2	1.32 [0.98] 0.99 [1.90]	0.36 [0.27] 0.41 [0.82]	**0.048**
IL-6	18.81 [26.51] 8.55 [26.00]	0.63 [0.20] 0.58 [1.16]	**0.003**
IL-8	137.13 [77.84] 124.10 [84.76]	18.54 [17.98] 15.02 [32.74]	**0.018**
TNF-α	3.59 [3.04] 2.79 [6.44]	0.84 [0.78] 0.86 [1.72]	0.073
BK: bacterial keratitis, IQR: interquartile range			

Table 21. Comparison of cytokine and chemokine levels between bacterial keratitis on day 3 of treatment and controls. Levels of IL-1β, IFN-γ, GM-CSF, IL-2, IL-6 and IL-8 remained elevated in bacterial keratitis patients.

Cytokine	Day 7 BK	Controls	P-value
	Cytokine concentration (pg/ml)		
	Mean [SD] *Median [IQR]*	*Mean [SD]* *Median [IQR}*	
IL-1β	1.69 [1.35] 1.69 [2.68]	0.12 [0.19] 0.00 [0.30]	**0.010**
IFN-γ	8.99 [9.89] 7.62 [12.08]	1.35 [1.57] 0.71 [3.00]	0.149
GM-CSF	2.39 [1.88] 1.70 [3.84]	0.64 [0.52] 0.57 [0.82]	**0.048**
IL-10	1.11 [1.56] 0.31 [1.96]	0.22 [0.30] 0.02 [0.54]	0.268
IL-12p70	1.29 [1.28] 0.85 [2.16]	0.98 [1.05] 0.77 [1.54]	0.639
IL-2	1.18 [1.06] 0.89 [0.70]	0.36 [0.27] 0.41 [0.82]	**0.030**
IL-6	5.31 [5.14] 3.05 [7.48]	0.63 [0.20] 0.58 [1.16]	**0.010**
IL-8	113.07 [141.77] 55.99 [175.50]	18.54 [17.98] 15.02 [32.74]	**0.048**
TNF-α	2.08 [2.12] 1.71 [2.30]	0.84 [0.78] 0.86 [1.72]	0.268
BK: bacterial keratitis, IQR: interquartile range			

Table 22. Comparison of cytokine and chemokine levels between bacterial keratitis on day 7 of treatment and controls. Levels of IL-1β, GM-CSF, IL-2, IL-6 and IL-8 remained elevated in bacterial keratitis patients.

Cytokine	Day 14 BK	Controls	P-value
	Cytokine concentration (pg/ml)		
	Mean [SD] *Median [IQR]*	*Mean [SD]* *Median [IQR]*	
IL-1β	1.35 [1.44] 0.55 [2.62]	0.12 [0.19] 0.00 [0.30]	**0.010**
IFN-γ	9.08 [7.09] 7.92 [10.36]	1.35 [1.57] 0.71 [3.00]	**0.030**
GM-CSF	2.08 [1.39] 1.74 [1.94]	0.64 [0.52] 0.57 [0.82]	**0.030**
IL-10	0.38 [0.43] 0.24 [0.56]	0.22 [0.30] 0.02 [0.54]	0.530
IL-12p70	1.44 [1.27] 1.13 [1.00]	0.98 [1.05] 0.77 [1.54]	0.343
IL-2	1.22 [0.84] 0.87 [0.88]	0.36 [0.27] 0.41 [0.82]	**0.030**
IL-6	2.68 [2.90] 1.62 [2.40]	0.63 [0.20] 0.58 [1.16]	**0.010**
IL-8	73.91 [77.84] 30.43 [138]	18.54 [17.98] 15.02 [32.74]	0.149
TNF-α	2.44 [1.70] 1.96 [2.20]	0.84 [0.78] 0.86 [1.72]	**0.048**

BK: bacterial keratitis, IQR: interquartile range

Table 23. Comparison of cytokine and chemokine levels between bacterial keratitis on day 14 of treatment and controls. Levels of IL-1β, IFN-γ, GM-CSF, IL-2, IL-6 and TNF-α remained elevated in bacterial keratitis patients.

5.3.5 Discussion

In this study, quantification of the tear inflammatory markers validated the AS-OCT findings that the acute corneal inflammatory response was greater in Gram-ve than Gram+ve BK, and that it decreased significantly by day 3 of treatment. Levels of the cardinal cytokines of inflammation, IL-1β, IL-8 and IL-6, and the numbers of PMNs were greater in Gram-ve than Gram+ve BK. A significant reduction in the levels of IL-1β, IL-2, IL-6, IL-8 and TNF-α was also observed between presentation and day 3 of treatment.

Mean levels of pro-inflammatory cytokines, IL-1β, IL-6 and IL-8, were greater in Gram-ve than Gram+ve BK by a factor of 6.7, 5.9 and 5.0 respectively. In study 5.1, morphological quantification with AS-OCT showed that corneal tissue swelling (CTS) was greater in Gram-ve BK by a factor of 2.3. The greater levels of IL-1 and IL-8 that are present in Gram-ve BK, most likely produced from epithelial cells, fibrobalsts and PMNs,[153,154] may in turn result in greater PMN recruitement and infiltration, more corneal oedema and thus greater corneal inflammation in Gram-ve BK. In a guinea pig corneal infection study that used radiolabelled PMNs, the degree of corneal oedema was shown to be proportional to the extent of PMN ingress to the corneal stroma.[293]

The molecular and cellular markers of acute inflammation decreased by day 3 of treatment. Not only was there a significant reduction in IL-1β, IL-2, IL-6, IL-8 and TNF-α levels, but also no PMNs were present in the tears on day 3, most likely reflecting the reduction in pro-inflammatory cytokine and chemokine levels. This is consistent with the AS-OCT morphological finding that CT and IT decreased by day 3 of treatment. Morphological, cellular and molecular quantification of inflammation, all showed a reduction in inflammation by day 3 of successfully treated BK. This validation of the AS-OCT findings strongly supports the use of AS-OCT corneal parameters as markers of acute inflammation and the application of AS-OCT to monitoring the treatment response in BK.

Inflammatory response in bacterial keratitis

This study has provided novel insight into the timing of the use of anti-inflammatory agents. In clinical practice, corticosteroid anti-inflammatory drops are introduced to the treatment regimen once there is evidence of improvement and the cornea is considered sterile. Traditionally, corticosteroids drops are started 5-7 days after initiation of antibiotic treatment.[79,299] In the Steroids for Corneal Ulcers Trials (SCUT), steroid drops were started after at least 48 hours of antibiotic treatment.[278] However, the molecular tear analysis of this study has shown that, even without the use of corticosteroid drops, by day 3 of treatment there has already been a great reduction in inflammatory mediators, ranging from 59% for TNF-α to 95.5% for IL-1β mean concentrations, with only small change thereafter. This suggests that the critical period for immunomodulation and introduction of anti-inflammatory agents, with the aim of reducing the associated tissue damage, may be earlier than currently practised. A subgroup analysis in the SCUT study did find that patients who received steroid drops within 2-3 days of starting antibiotic treatment had approximately 1 line better spectacle corrected VA at 3 months compared to patients who received placebo. There was no significant effect of steroid drop initiation on day 4 or later compared to placebo.[300]

The SCUT study did not find the use of g. prednisolone phosphate 1%, applied initially four times a day and then with a reducing regimen, to be of overall benefit. Potential reasons for the lack of efficacy may include a relatively low frequency of drop instillation, non-specific immune-modulatory function of corticosteroid drops and a delay in initiating steroid treatment. However, the finer details of the study show that large central ulcers did benefit; in ulcers completely covering the central 4-mm pupil, corticosteroid treated patients had significantly better spectacle corrected VA by 0.20 logMAR (approximately 2 lines) compared with placebo at 3 months.[278]

The optimum time for starting steroid drops or other immune-modulatory treatment requires further research. Induction of an immune response, particularly the recruitment of PMNs, is essential not only for resolution of BK, but also to prevent systemic spread of the infection. In studies with

induced neutropaenia, either with intravenous cyclophosphamide or whole body X-irradiation, animals with pseudomonas keratitis progressed to septicaemia and death, even though the corneal damage was less than in non-neutropaenic animals.[120,121] In addition, the use of topical steroids can precipitate a deterioration of fungal, *Acanthamoeba* or herpetic keratitis, either in cases of incorrect diagnosis or cases with polymicrobial infection.[299,301]

All 9 cytokines and chemokines that were examined were significantly elevated at presentation compared to controls; IL-1β, IFN-γ, IL-10, IL-6 and IL-8 showed the greatest ratio of BK to control concentration, especially IL-1β and IL−6. Cytokine IL-1β, a potent pro-inflammatory cytokine that influences PMN influx in tissues, is produced by resident corneal cells and immune cells, such as mononuclear cells, macrophages and PMNs.[146,148-150] It is expressed by all layers of the cornea,[152] and has previously been detected in the tear fluid of patients with corneal infection and inflammation.[151] A plausible hypothesis is that once corneal integrity is compromised by trauma or contact lens related injury, corneal epithelial cells respond to the presence of pathogens with the expression and secretion of pro-inflammatory cytokines. This is supported by the fact that TLR 2 and TLR 4 are expressed in the human cornea, and that they are found localized in the wing and basal cell layers of corneal epithelium, but not in the apical layer.[154] Only when the epithelial barrier is breached and pathogens interact with TLR 2 and TLR 4 of the deeper epithelial layers does this result in activation of intracellular pro-inflammatory pathways. In addition, the TLRs may reside in the cells, responding with translocation to the cell surface only in the presence of an inflammatory stimulus.[302]

IL-8 was the cytokine/chemokine with the highest absolute concentration in the tears of BK patients. IL-8 is most likely a mediator of the pro-inflammatory effect of IL-1β, as IL-1β may exert its pro-inflammatory effect through the induction of chemokines that attract PMNs.[154] Karthikeyan et al have suggested that, as PMNs are the predominant cells involved in corneal ulcers, they may be the source of most of the pro-inflammatory cytokines, including IL-8; mononuclear cells and corneal

epithelial cells are also likely to contribute.[303] I suggest that activated keratocytes and fibroblasts that migrate to the injury site may also be an important source of IL-8, as it has been shown that IL-8 is secreted by cultured human corneal fibroblasts in response to activation of the TLR pathways.[180,304]

High concentrations of IFN-γ, which also persisted on day 3, were detected. Reduction in its levels lagged the reduction of the other cytokines, with no significant decrease between presentation and day 3. This is a pro-inflammatory cytokine that promotes bacterial clearance by stimulating the bactericidal activity of phagocytic cells.[305] Although produced by PMNs in response to bacterial infection,[158,159] the high levels of IFN-γ on day 3, when no PMNs were present in tears, suggest that corneal resident cells, such as activated keratocytes, fibroblasts and dendritic cells, may contribute greatly to IFN-γ production. Previous work has shown that IFN-γ can be produced by macrophages, antigen presenting cells, and corneal fibroblasts.[145,180]

The highest concentration in tears of BK patients relative to controls was detected for IL-6. IL-6 has been described as having both pro-inflammatory and anti-inflammatory actions.[28,166-168] Its role in BK is not clear. In a murine study of *Pseudomonas* keratitis, corneal PMN recruitment was dependent on IL-6 production. The IL-6 deficient mice showed an increased bacterial load compared to the wild-type mice and failure of PMN infiltration into the central cornea; interestingly, they also had lower levels of MIP-2 (murine homologue of IL-8) than wild-type mice.[168] A study of *Staphylococcus aureus* keratitis, carried out by the same research group, found slightly contrasting results despite using the same IL-6 gene knockout mice. The knockout mice had greater levels of bacteria and greater levels of PMNs in the cornea; they also had greater levels of MIP-2 and IL-1 compared to wild-type mice.[306] The greater levels of MIP-2 and IL-1 that were present in the IL-6 deficient mice of the second study are consistent with the greater numbers of PMNs, but not with the greater levels of bacteria. The authors postulated that, in the absence of

IL-6, PMNs may have been unable to kill the bacteria and that IL-6 may play a role in the activation of PMNs during staphylococcal infection. Of further interest is the fact that, in the absence of IL-6, there was a decrease of MIP-2 in pseudomonas infection but an increase of MIP-2 in staphylococcal infection compared to wild-type. A possible explanation for the different levels of MIP-2 could be that, in the absence of IL-6, *Pseudomonas* and *Staphylococcus* activate different intracellular pathways leading to different cytokine expression.

TNF-α, a pro-inflammatory cytokine similar to IL-1β, was found elevated. TNF-α stimulates IL-8 release from PMNs, epithelial cells and keratocytes, and it may do so with greater efficacy than IL-1β.[152] This may explain the ten fold lower ratio of BK to control concentration for TNF-α compared to IL-1β. In addition to acting on PMNs, TNF-α is an important product of PMNs; its production may be mediated by other pro-inflammatory molecules, such as IL-2 and IL-8.[156] In BK, the main sources of TNF-α would appear to be the recruited PMNs, the corneal epithelium and keratocytes.[157,180]

The cytokines IL-10, IL-12, IL-2 and GM-CSF were also elevated in BK patients. GM-CSF is a powerful chemotactic agent for human PMNs.[178] In the human condition, it may be produced by epithelial and fibroblast cells, as GM-CSF expression has been detected in human cultured corneal fibroblasts and epithelial cells from patients with prior bacterial and herpetic infection, respectively.[180,181] The role of IL-10 in corneal infection is not well understood.[176] Overall, it modulates excessive inflammation and the immune response by inhibiting production of pro-inflammatory cytokines by mononuclear phagocytes.[172]

Similarly, the roles of IL-2 and IL-12 are not clear. IL-2 is considered to have pro-inflammatory properties, although most of the evidence is from in-vitro studies. It has been shown to induce healthy PMNs to increase mRNA expression for TNF-α and release TNF-α in their supernatant.[156] IL-12 is a multifunctional cytokine that may modulate infection by

stimulating the production of immune-regulatory cytokines and enhancing the proliferation and cytotoxicity of natural killer and T cells.[162,163]

The PMN was by far the most common cell in the tears of patients with BK. In keeping with the larger morphological AS-OCT parameters and greater pro-inflammatory cytokine and chemokine concentrations in Gram-ve BK, this immune cell was detected in large numbers in Gram-ve infection and absent in Gram+ve BK. It can be postulated that differential activation of the TLR 4 and 2 pathways, the principal TLR pathways involved in bacterial infection, by Gram-ve and Gram+ve bacteria respectively, may be responsible for the greater levels of IL-1β and subsequently of chemokines IL-8 and IL-6 that result in a greater PMN recruitment in Gram-ve BK.

The PMNs are the predominant immune cells to initiate defence mechanisms in BK.[118,303] As discussed in section 1.4.5, other cells such as macrophages, dendritic cells and Langerhans cells, all corneal resident cells, may play a role in the response to bacterial infection.[28] Morphology based characterisation of the cells on cytospin slides identified only the occasional macrophage in the tear film, less than 1% of total cell count in frequency. The macrophage is a professional phagocyte of the innate immunity and an antigen-presenting cell of the acquired immunity that not only phagocytoses bacteria, but also phagocytoses and removes apoptotic PMNs that are involved in bacterial clearance.[29]

5.3.6 Conclusions

This study has validated the AS-OCT findings presented in sections 5.1 and 5.2, strongly supporting the use of AS-OCT morphological parameters, CT and IT, as markers of acute inflammation in BK. In agreement with AS-OCT quantification, the molecular markers of inflammation, IL1-β, IL-6 and IL-8, and the cellular markers of inflammation, PMNs, were significantly greater in Gram-ve than Gram+ve BK and their levels decreased significantly by day 3 of treatment. This improvement in morphological, molecular and cellular markers of

inflammation strongly suggests that the first 3 days of treatment after presentation may be the optimum window for immune modulation with the aim of reducing collateral corneal tissue damage in BK.

5.4 Correlation of Anterior Segment Optical Coherence Tomography quantification and pro-inflammatory tear cytokine levels

5.4.1 Introduction

In the previous section (5.3), the analysis of tear inflammatory cytokines validated the AS-OCT morphology based quantification of acute corneal inflammation in BK. Although this provided strong evidence that AS-OCT parameters can be used as markers of acute inflammation, it did not prove a direct association between AS-OCT parameters and inflammation.

In this study, therefore, the association between AS-OCT parameters and tear pro-inflammatory cytokine levels is investigated.

5.4.2 Hypothesis

I hypothesise that AS-OCT parameters of acute corneal inflammation are associated with tear pro-inflammatory cytokine levels.

5.4.3 Materials and methods

5.4.3.1 Patient recruitment

The data of the 13 patients from the study in section 5.3 were used. Patients with clinical BK were recruited and treated as previously described in sections 4.1.3.1 and 5.3.3.1. Three patients with corneal perforation were excluded, as ocular hypotony can alter corneal morphology and confound results. Tear sample collection and AS-OCT imaging were carried out at presentation (day 0) and follow-up examinations on days 3, 7 and 14.

5.4.3.2 Tear sample collection and analysis

Tear samples were collected by conjunctival lavage, as described in section 5.3.3.2. Cytokine and chemokine analysis were carried out with the pro-inflammatory multiplex assay kit by Meso Scale Discovery, as detailed in section 2.3.

5.4.3.3 AS-OCT Imaging

AS-OCT scans were carried out with the Visante OCT and CT measured, as described in section 5.2.3.2.

5.4.3.4 Statistical analysis

AS-OCT CT and cytokine data were examined with Shapiro-Wilk statistics and showed a non-normal distribution. The CT of AS-OCT images was examined for association with pro-inflammatory cytokine concentrations with the Spearman correlation coefficient; values of the correlation coefficient r between 0.00-0.19, 0.20-0.39, 0.40-0.59, 0.60-0.79 and 0.80-1.0 were considered very weak, weak, moderate, strong and very strong respectively.[285,286] The change of CT and cytokine concentrations during treatment was analysed with Friedman's two analysis of variance. Differences between Gram-ve and Gram+ve groups were compared with the Mann-Whitney U test.

The cytokines IL-1β, IL-6 and IL-8 were selected for analysis, as these are the cardinal cytokines in inflammation.[28,152,154] In addition, they were found to be significantly elevated in human BK (study 5.3).

5.4.4 Results

Ten culture positive BK patients (eyes) were included in this study; 5 were Gram-ve and 5 Gram+ve. Microbiology cultures showed 4 cases of *Pseudomonas aeruginosa*, 1 of coliform bacteria, 2 of coagulase negative *Staphylococcus*, 2 of *Staphylococcus aureus* and 1 of *Streptococcus pneumoniae*. Mean [SD] patient age was 48.4 [23.3] years.

5.4.4.1 Correlation of AS-OCT CT and tear cytokine levels

Presentation CT showed a significant strong correlation with the concentration of IL-6 (r=0.697, p=0.025) (n=10). Strong and moderate correlations, but of borderline statistical significance, were also present with the concentrations of IL-8 (r=0.612, p=0.06) and IL-1β (r=0.491, p=0.15), respectively. Presentation IT could only be measured in 6 of the 10 cases and, thus, was not examined further for correlations.

When presentation and follow-up examination points were analysed collectively for association between CT and cytokine concentrations (n=28), a significant strong correlation was found for IL-6 ($r=0.635$, $p<0.001$) and a significant moderate correlation for IL-8 and IL-1β ($r=0.430$, $p=0.022$ and $r=0.386$, $p=0.042$ respectively).

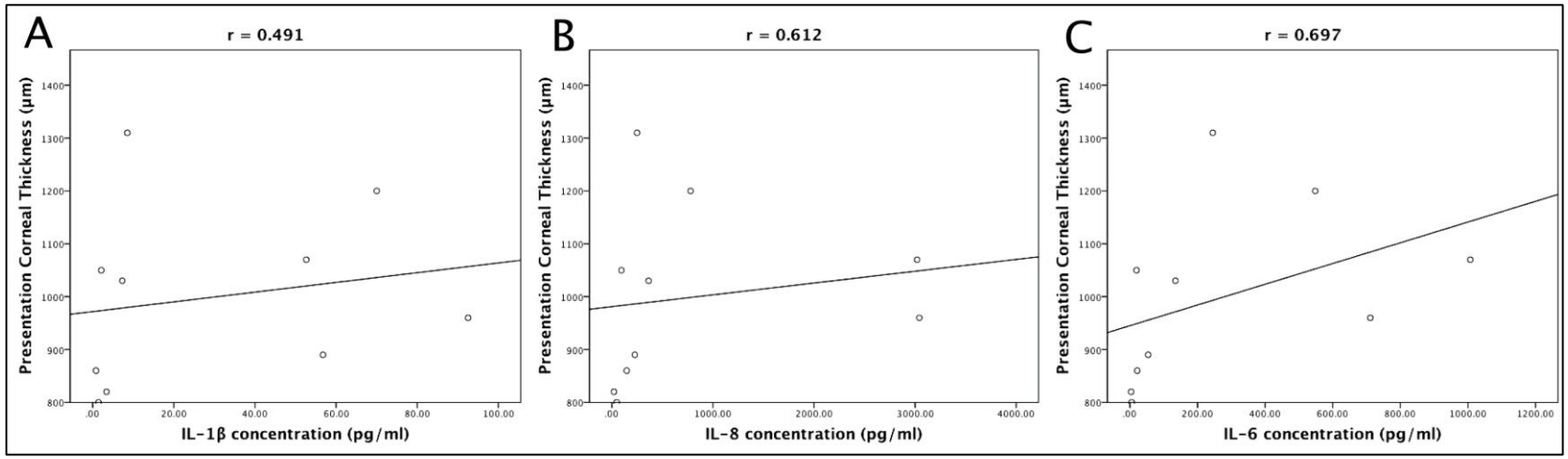

Figure 45. Correlation of pro-inflammatory cytokines with corneal thickness at presentation. Presentation corneal thickness showed a moderate correlation with IL1-β levels (r=0.491) and strong correlations with IL-8 (r=0.612) and IL-6 (r=0.697) levels.

5.4.4.2 AS-OCT CT and cytokines: Gram negative versus Gram positive bacterial keratitis

The 5 Gram-ve and 5 Gram+ve cases were compared for CT and concentrations of IL-1β, IL-6 and IL-8 at presentation. All parameters were significantly greater in Gram-ve BK, as shown in table 24 and figure 46.

Parameter	Gram-ve BK Mean (SD) Median (IQR)	Gram+ve BK Mean (SD) Median (IQR)	P-value
Corneal thickness (μm)	1114.0 (140.1) 1070.0 (260.0)	884.0 (99.1) 860.0 (160.0)	**0.032**
IL-1β Conc (pg/ml)	46.21 (37.71) 52.65 (73.37)	12.91 (24.54) 2.12 (28.95)	**0.038**
IL-6 Conc (pg/ml)	529.07 (352.87) 547.91 (669.19)	20.66 (20.35) 19.37 (33.56)	**0.017**
IL-8 Conc (pg/ml)	1490.27 (1419.76) 778.88 (2724.58)	106.89 (82.37) 94.08 (152.72)	**0.007**

Conc: concentration, BK: bacterial keratitis, Gram-ve: Gram negative, Gram+ve: Gram positive, IQR: interquartile range, SD: standard deviation

Table 24. Comparison of pro-inflammatory cytokines and corneal thickness between Gram negative and Gram positive bacterial keratitis at presentation.

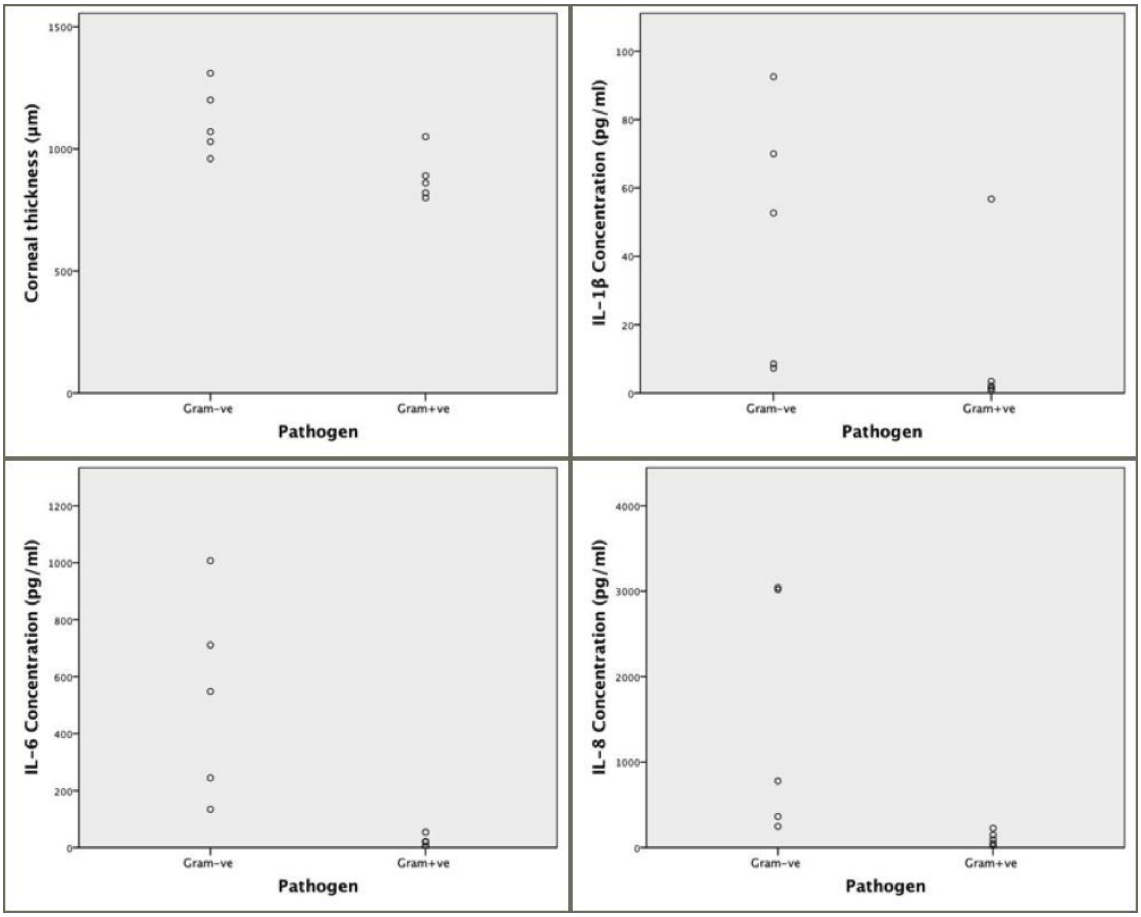

Figure 46. Cytokines levels and corneal thickness comparison in Gram negative and Gram positive bacterial keratitis. At presentation, corneal thickness and IL-1β, IL-6 and IL-8 concentrations were all significantly greater in Gram negative BK.

5.4.4.3 AS-OCT CT and cytokines: time course in bacterial keratitis

Six patients had concurrent AS-OCT imaging and tear analysis carried out at presentation and days 3, 7 and 14 of treatment. The CT and concentrations of IL-6 and IL-8 decreased significantly during treatment ($p=0.01$, $p=0.001$ and $p=0.006$ respectively); the reduction in IL-1β

concentration was of borderline statistical significance (p=0.061), as shown in table 25.

Parameter	Day 0	Day 3	Day 7	Day 14	P-value
	Mean (SD) **Median (IQR)**	**Mean (SD)** **Median (IQR)**	**Mean (SD)** **Median (IQR)**	**Mean (SD)** **Median (IQR)**	
CT (μm)	1061.7 (179.3) 1050.0 (307.5)	740.0 (239.3) 720.0 (420.0)	583.3 (103.1) 600.0 (195.0)	513.3 (81.6) 530 (145.0)	**0.010**
IL-1β Conc	38.74 (38.37) 30.59 (69.88)	1.83 (0.91) 2.07 (1.03)	1.53 (1.40) 1.08 (2.79)	0.94 (1.03) 0.51 (1.04)	0.061
IL-6 Conc	441.73 (381.30) 396.43 (682.8)	21.31 (28.13) 9.24 (37.82)	6.04 (5.22) 5.63 (8.58)	2.58 (3.17) 1.37 (3.03)	**0.001**
IL-8 Conc	1249.82 (1399.81) 571.17 (2826.7)	157.50 (61.55) 139.56 (99.92)	129.51(147.81) 57.16 (204.61)	60.96 (76.58) 28.92 (97.10)	**0.006**

CT: corneal thickness, SD: standard deviation, IQR: interquartile range, Conc: concentration in pg/ml

Table 25. Cytokine and corneal thickness change during treatment of bacterial keratitis.

The reduction in cytokine concentration between presentation and day 3 was significant for IL-1β, IL-6 and IL-8 (p=0.046, p=0.028 and p=0.046 respectively); the reduction in CT was of borderline statistical significance (p=0.068).

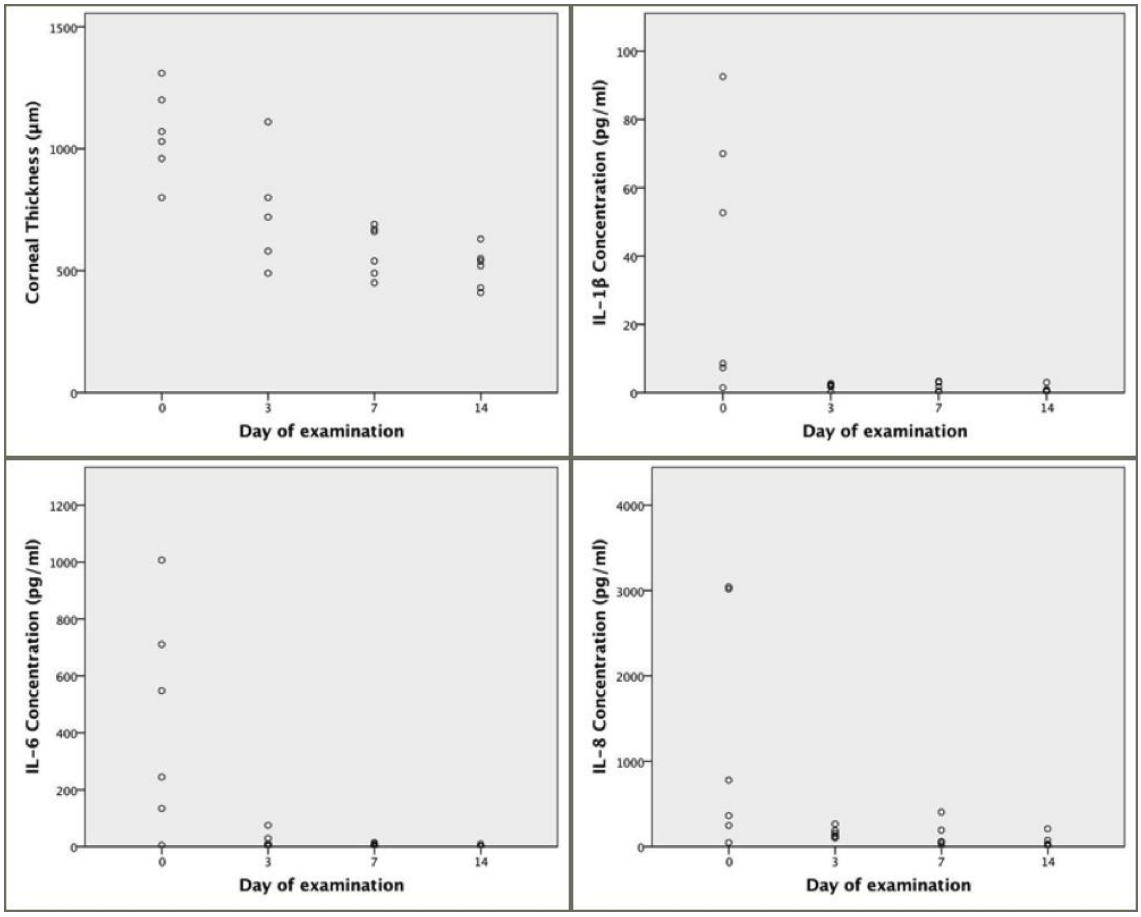

Figure 47. Pro-inflammatory cytokine and corneal thickness reduction during treatment of bacterial keratitis. A significant reduction was detected for corneal thickness, IL-6 and IL-8 concentrations; the reduction in IL-1β concentration was of borderline statistical significnce (p=0.061).

5.4.5 Discussion

In this small study, CT correlated strongly or moderately with the concentration of pro-inflammatory cytokines, IL-1β, IL-6 and IL-8, suggesting a direct association between morphological AS-OCT parameters and tear pro-inflammatory cytokine levels. In addition, when patients were investigated serially over time, both morphological and molecular markers of inflammation showed a corresponding reduction over time, with all parameters decreasing by day 3 of successful treatment.

5.4.6 Conclusions

The association between AS-OCT CT and concentration of pro-inflammatory cytokines has validated the use of AS-OCT not only as an imaging modality in BK, but also for quantification of the acute phase corneal inflammation in BK. AS-OCT morphology based inflammatory parameters, specifically CT, can be used as a surrogate measure and marker of acute inflammation in BK.

6 Vancomycin prophylaxis in a rabbit model of keratoprosthesis associated bacterial keratitis studied with Fourier Domain Optical Coherence Tomography

6.1 Introduction

Corneal disease is a major global cause of blindness; infection, scarring and corneal opacification are responsible for blindness in 1.56 million individuals worldwide.[1,2] However, corneal graft surgery for visual restoration in the presence of ocular surface disease, inflammation or failed previous graft has a relatively poor prognosis.[93,94] Artificial corneas, termed keratoprostheses (Kpro), that have been developed with the aim of reducing immune mediated rejection and failure in these high-risk cases, have also shown poor results with low retention rates, as discussed in the introduction (section 1.4.3).

Infection in keratoprosthesis (Kpro) is a devastating complication that can cause acute deterioration of vision and lead to implant extrusion. The rate of infection in Boston Kpro, the most widely used Kpro device, ranges between 3.2-17% of eyes.[104-107] Prophylactic vancomycin drops that are recommended following Boston Kpro have not been found to reduce bacterial keratitis rates,[106] although they may reduce the rate of bacterial endophthalmitis.[307,308] The quality of clinical evidence from studies on Kpro associated infection is limited, as the studies are retrospective, small, consist of heterogeneous cohorts of patients and ocular morbidity, and often involve a range of microbial pathogens.

Study of the effectiveness of prophylactic antibiotics within the controlled experimental conditions of an animal study may overcome these limitations. Application of AS-OCT to such an animal model would allow in-vivo quantification of the infection and associated corneal inflammation, as per the human condition. This study in chapter 6 has investigated whether regular application of vancomycin drops could prevent the development of *Staphylococcus aureus* (*S. aureus*) keratitis in an established animal model of

Kpro associated microbial keratitis.[42] This model uses an intra-stromal titanium film to simulate the keratoprosthesis (section 2.4), as a titanium back-plate is now used in clinical practice for the Boston type 1 Kpro,[243] and it has been shown that the titanium film can be successfully coated with an anti-microbial peptide, with the potential to reduce the risk of post-operative infection.[42]

6.2 Hypothesis

I hypothesise that prophylactic vancomycin drops can prevent the development of infection in an animal model of Kpro associated bacterial keratitis. This hypothesis is investigated with FD-OCT imaging and the findings validated with slit-lamp photography grading of the infection, immunohistochemistry, quantification of bacteria and liquid chromatography mass spectrometry.

6.3 Materials and methods

Thirty-one New Zealand White rabbits were investigated, 23 for the study of vancomycin prophylaxis versus non-prophylaxis, and 8 for the study of corneal vancomycin pharmacokinetics. The allocation of rabbits is detailed in figure 48.

6.3.1 Vancomycin prophylaxis versus non-prophylaxis study

The right eye of 23 rabbits was chosen for surgery and a titanium film was implanted, as described in chapter 2. Following implantation, they were assigned either to a prophylactic group or a non-prophylactic group. The prophylactic group (13 rabbits) received one drop of vancomycin 1.4% (Singapore General Hospital, SingHealth) to the right eye 5 times a day from titanium film implantation to sacrifice, the non-prophylactic group (10 rabbits) received no drops. All rabbits were inoculated with a 25 µl bacterial solution of *Staphylococcus aureus* ($2X10^4$ CFU/ml) with a 29 G needle into the corneal pocket above the titanium film at 7-12 days post-implantation.

Slit-lamp photography and AS-OCT were carried out before and after bacterial inoculation. The rabbits were sacrificed at conclusion of the imaging investigations at predetermined time-points (figure 48). The corneas of sacrificed rabbits were examined for histology, immunohistochemistry and quantification of viable bacteria. The clinical imaging and laboratory parameters were compared between prophylactic and non-prophylactic groups.

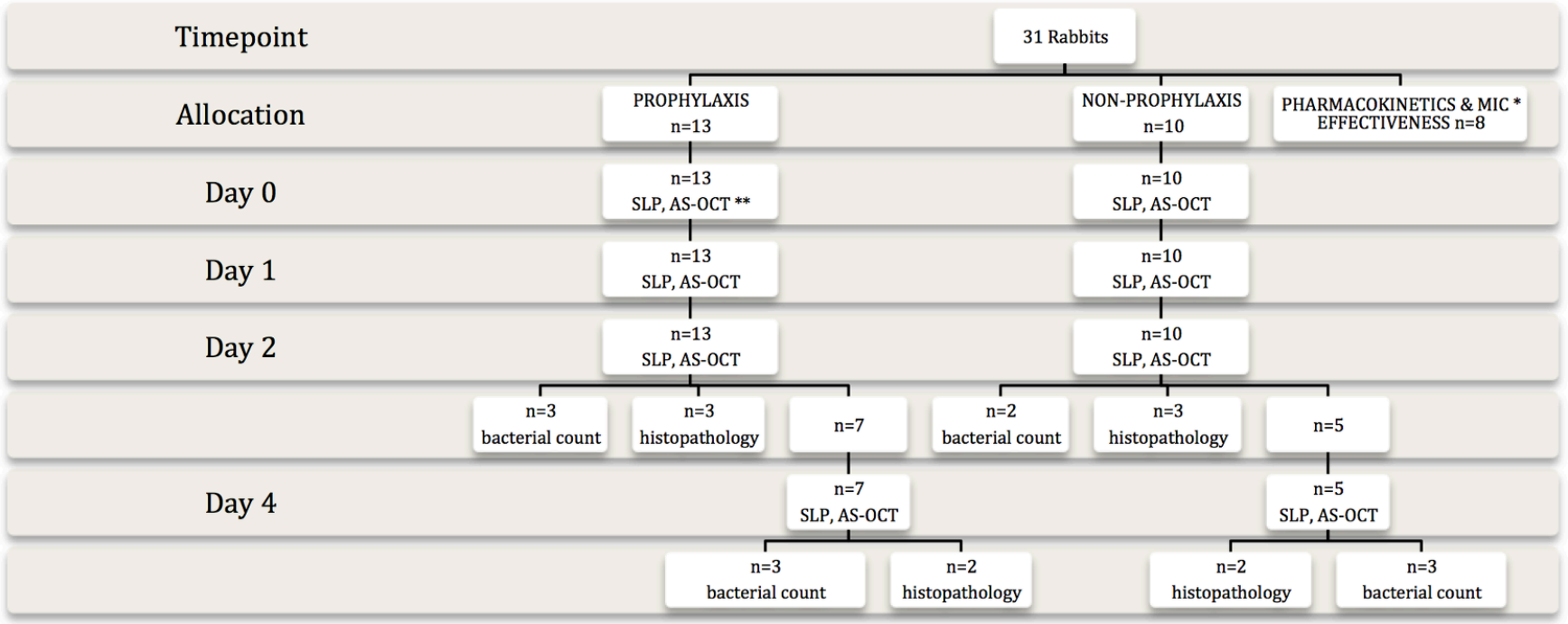

Figure 48. Study design. The flow chart demonstrates rabbit allocation to prophylactic and non-prophylactic groups, follow-up and investigations carried out at each time point. (* MIC: minimum inhibitory concentration, ** SLP: slit-lamp photography, AS-OCT: anterior segment optical coherence tomography)

6.3.1.1 Slit lamp photography and anterior segment optical coherence tomography

Slit-lamp photographs (Zoom Slit Lamp NS-2D, Righton, Tokyo, Japan) and AS-OCT with FD-OCT imaging (RTVue; Optovue, Inc, Fremont, CA) were carried out, as detailed in section 2.5 and 2.2.6 respectively. They were carried out before bacterial inoculation, and on days 1, 2 and 4 after bacterial inoculation.

The slit-lamp photographs were graded, using a scale that was described in section 2.5. The total slit-lamp photography (SLP) score, ranging from 0 to 16, was calculated. Serial slit-lamp photographs in figure 49 illustrate progression of the infection.

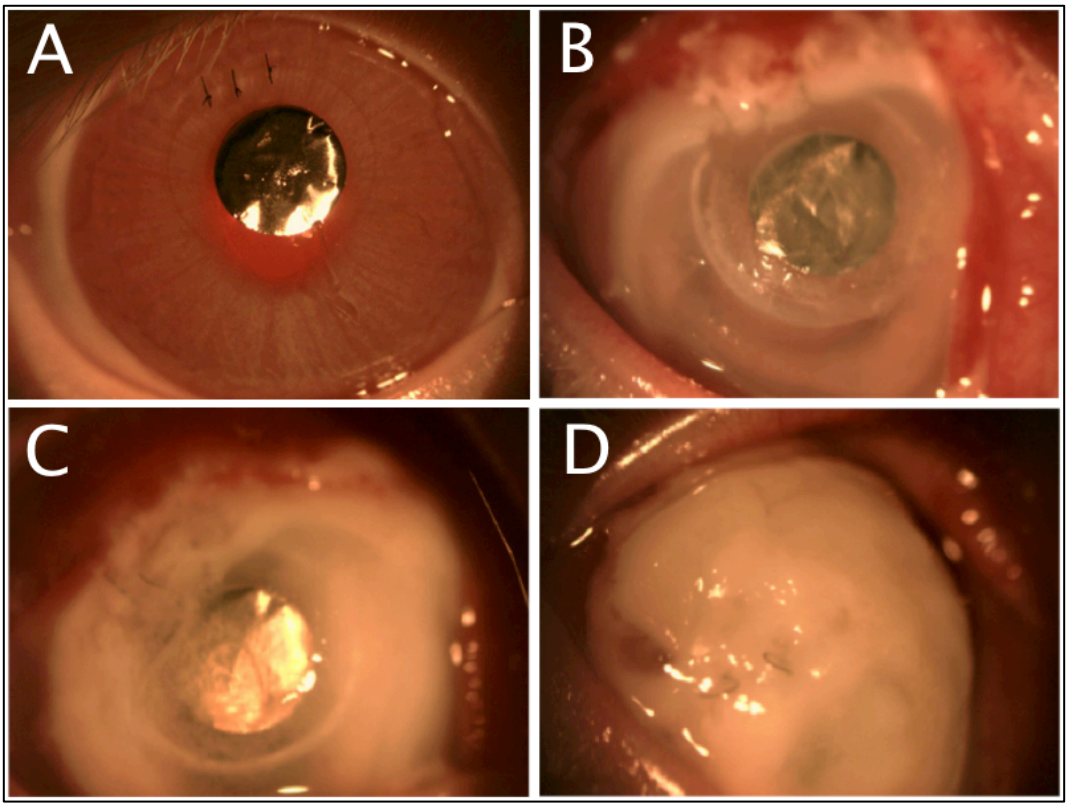

Figure 49. Serial slit-lamp photography. A. A quiet eye with a clear cornea and the titanium keratoprosthesis in-situ before bacterial inoculation. B. On day 1 following inoculation, the conjunctiva is injected and the cornea oedematous with early infiltration. C. On day 2, moderate corneal infiltration has developed. D. On day 4, severe corneal infiltration is present.

Pre-infection and post-infection AS-OCT CT measurements were carried out between the anterior corneal and titanium implant surfaces on AS-OCT scans through the implant centre. Five measurements, all perpendicular to the anterior corneal surface, were carried out and the mean CT for each scan was calculated (figure 50).

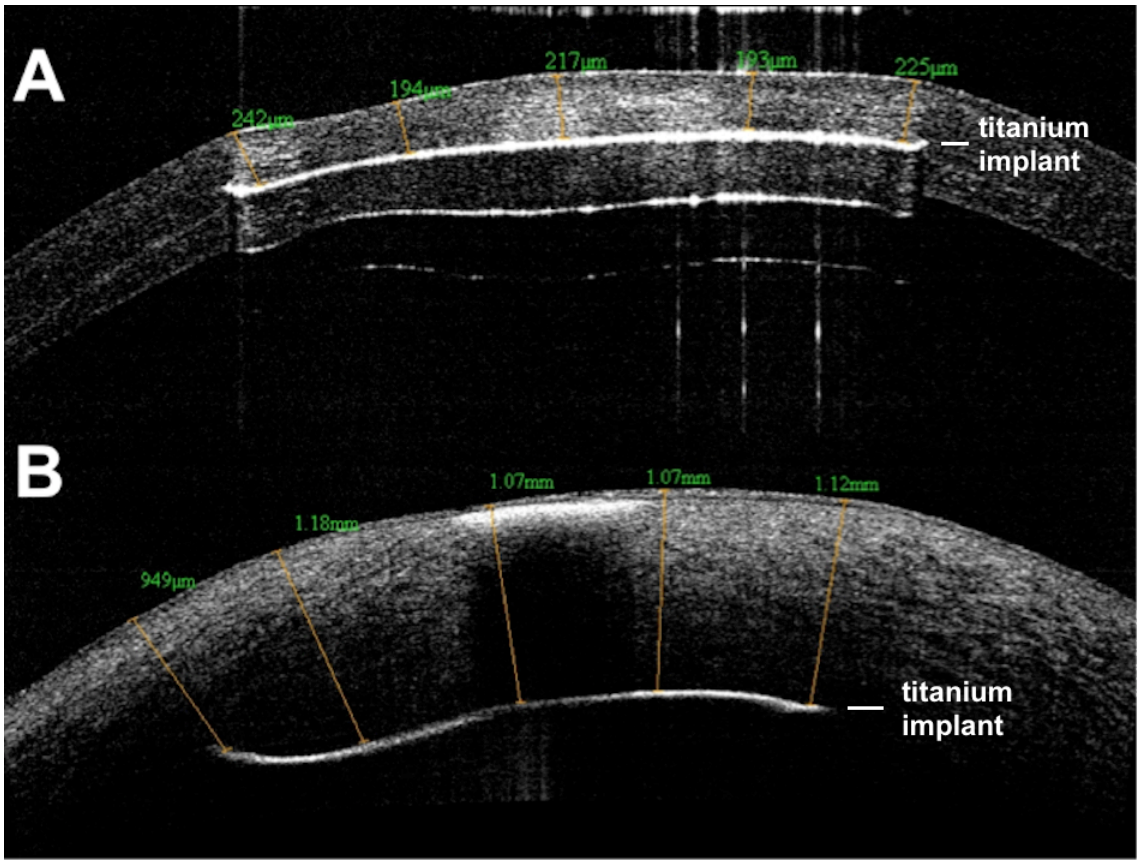

Figure 50. Anterior Segment Optical Coherence Tomography imaging protocol in keratoprosthesis associated infection. Corneal thickness between the implant and the anterior corneal surface was measured at 5 locations before (A) and after (B) bacterial inoculation.

6.3.1.2 Quantification of viable bacteria

On days 2 and 4 post-inoculation, rabbit corneas were removed by trephination and homogenised for culture, as detailed in section 2.6. The numbers of colonies were expressed as log10 number of CFU/cornea and compared between prophylactic and non-prophylactic groups.

6.3.1.3 Histology and immunohistochemistry

Excised corneas of rabbits that were sacrificed on days 2 and 4 were processed for histological and immunohistochemical microscopy (section 2.7). The haematoxylin and eosin (H&E) stained sections were qualitatively compared between prophylactic and non-prophylactic cases. Immunostaining for CD11b +ve cells, expressed as the ratio of CD11b +ve/non-CD11b +ve cells, was quantitatively compared between the two groups.

6.3.2 Corneal vancomycin pharmacokinetics and effectiveness of minimum inhibitory concentration

Eight rabbits were used exclusively to study the corneal pharmacokinetics of vancomycin and the effectiveness of the corneal vancomycin minimum inhibitory concentration (MIC) for *S. aureus*. In addition, the left eye of 6 rabbits from the above vancomycin prophylaxis versus non-prophylaxis study had vancomycin 1.4% drop instillation 5 times a day and was used for vancomycin quantification. Quantification of vancomycin was carried out by Liquid Chromatography–Mass Spectrometry (LC-MS).

Two rabbits with a titanium film implant had corneal and aqueous vancomycin quantification of the right eye after 10 days of instillation of one drop of vancomycin 1.4% 5 times a day.

The left eye of 6 rabbits was used for corneal and aqueous vancomycin quantification; 3 rabbits had one drop of vancomycin 1.4% instilled 5 times a day for 2 days before sacrifice and 3 rabbits for 16 days.

Three rabbits had bilateral corneal and aqueous vancomycin quantification following 4 days of vancomycin 1.4% drop instillation 5 times a day. Prior to starting the antibiotic regimen, the cornea of the right eye had complete

epithelial debridement following application of 20% alcohol for 60 seconds, whereas the epithelium of the left cornea was not debrided.

Three rabbits with a titanium film implant to the right eye had bacterial inoculation (25 µl *S. aureus* solution, $2X10^4$ CFU/ml), as described above, in order to investigate the effectiveness of vancomycin prophylaxis once corneal vancomycin MIC-90 for *S. aureus* (2.0 µg/ml) had been achieved. Inoculation was carried out after 16 days of vancomycin 1.4% drop instillation 5 times a day, as corneal vancomycin quantification at the different time intervals showed that the MIC-90 was achieved by day 16 of antibiotic use. Following bacterial inoculation, development of infection was assessed with SLP grading and FD-OCT imaging.

6.3.3 Statistical analysis

Normality distribution of data was assessed by Shapiro-Wilk statistics and histograms. Mean or median values were compared between the prophylactic and non-prophylactic groups. The CT values were compared with the t-test and ANOVA, the total SLP scores with the Kruskal-Wallis and Mann-Whitney U-tests. Bacterial counts and vancomycin concentrations were compared with the t-test. The Statistical Package for Social Science (IBM SPSS Statistics for Macintosh, Version 19.0. Armonk, NY: IBM Corp), was used; statistical significance was considered $p<0.05$.

6.4 Results

6.4.1 Slit-lamp photography

Overall, the median total SLP score increased from 4.0 (Inter-quartile range [IQR] 1,12) on day 1 to 12 (IQR 5,14.5) on day 2 and 16 (10,16) on day 4 (p=0.004).

On day 1, the median total SLP score was greater in the non-prophylactic group compared to the prophylactic group (p=0.049). On days 2 and 4, the scores were not significantly different between non-prophylactic and prophylactic groups (p=0.456 and p=0.527 respectively). The SLP scores are detailed in table 26.

Parameter	Day	SLP score [median (IQR)]		P value
		Prophylactic	*Non-prophylactic*	
Conjunctival injection	**1**	0 (0, 3)	3 (0, 3.25)	0.166
Conjunctival chemosis		0 (0, 3)	3 (0.75, 3.25)	0.148
Corneal infiltration		0 (0, 1)	1.5 (0, 3)	0.232
Corneal oedema		1 (0, 3)	3 (1, 3.25)	0.115
Total		1 (0, 10.5)	11 (1, 13)	0.049
Conjunctival injection	**2**	2.5 (1, 3)	3 (1, 4)	0.539
Conjunctival chemosis		2.5 (1, 3)	3 (1, 4)	0.497
Corneal infiltration		2.5 (1, 3.75)	3 (1, 4)	0.418
Corneal oedema		3 (1.25, 4)	3.5 (2, 4)	0.628
Total		10.5 (4.25, 13.75)	12.5 (5.75, 16)	0.456
Conjunctival injection	**4**	4 (2, 4)	4 (2.5, 4)	0.648
Conjunctival chemosis		4 (2, 4)	4 (2.5, 4)	0.648
Corneal infiltration		3 (2, 4)	4 (1.75, 4)	0.527
Corneal oedema		4 (3, 4)	4 (2.5, 4)	0.788
Total		15 (10, 16)	16 (9.25, 16)	0.527

Table 26. Slit-lamp photography score comparison between prophylactic and non-prophylactic groups. (SLP: slit-lamp photography)

6.4.2 Anterior segment optical coherence tomography

Pre-inoculation CT (mean ± standard error of mean [SEM]) was not significantly different between non-prophylactic and prophylactic groups (229.9±9.1 vs.

219.3±12.9 µm, p=0.533). On day 1 post-inoculation, CT in the non-prophylactic group was significantly greater than in the prophylactic group (486.9±61.2 vs. 327.4±37.1 µm, p=0.029). On day 2 post-inoculation, CT was also greater in the non-prophylactic group (646.2±52.6 vs. 404.7±36.2 µm, p=0.001). On day 4, however, there was no significant difference between the non-prophylactic and prophylactic groups (683.8±61.2 vs. 765.7±146.9 µm, p=0.645). The CT comparison between the two groups is illustrated in figure 51.

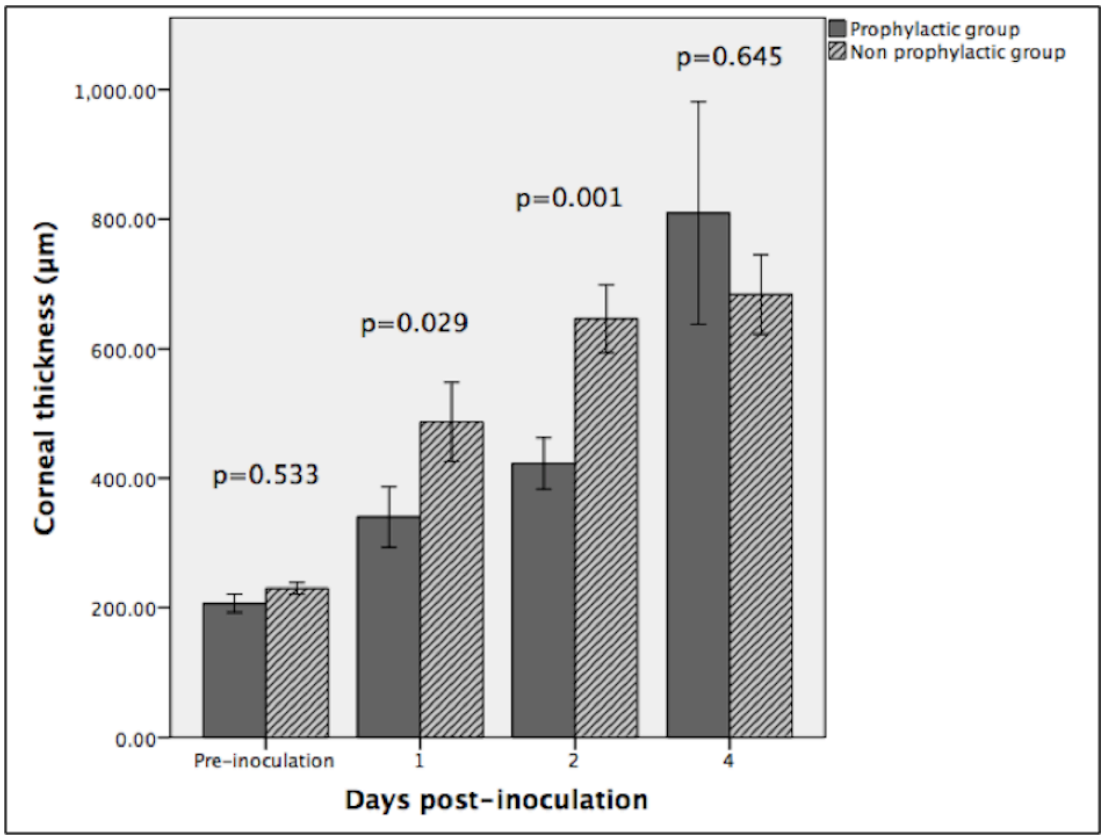

Figure 51. Corneal thickness comparison between prophylactic and non-prophylactic groups. (error bars represent ± 1 standard error of mean)

In the non-prophylactic group, CT increased from 229.9±9.1 µm pre-inoculation to 486.9±61.2, 646.2±52.6 and 683.8±61.2 µm on days 1, 2 and 4

respectively (p<0.001). Bonferroni post-hoc tests showed that the difference was significant between pre-inoculation and day 1 CT (p=0.003), but not between day 1 and day 2 CT (p=0.128) or between day 2 and 4 (p=1).

In the prophylactic group, CT increased from 219.3±12.9 µm pre-inoculation to 327.4±37.1, 400.4.7±36.2 and 765.7±146.9 µm on days 1, 2 and 4 respectively (p<0.001). Bonferroni post-hoc tests showed that, compared to before inoculation, the average CT was not significantly different on day 1 (p=0.590) but became significantly different on day 2 (p=0.050). Average CT was not significantly different between days 1 and 2 (p=1.0) but was between days 2 and 4 (p<0.001).

6.4.3 Bacterial quantification

Log10 mean (±SEM) bacterial counts were not significantly different between non-prophylactic and prophylactic cases on day 2 (4.6±1.0 vs. 5.6±0.4 CFU/cornea, p=0.474) and day 4 (5.7±0.2 vs. 5.4±0.5 CFU/cornea, p=0.574). This is illustrated in figure 52.

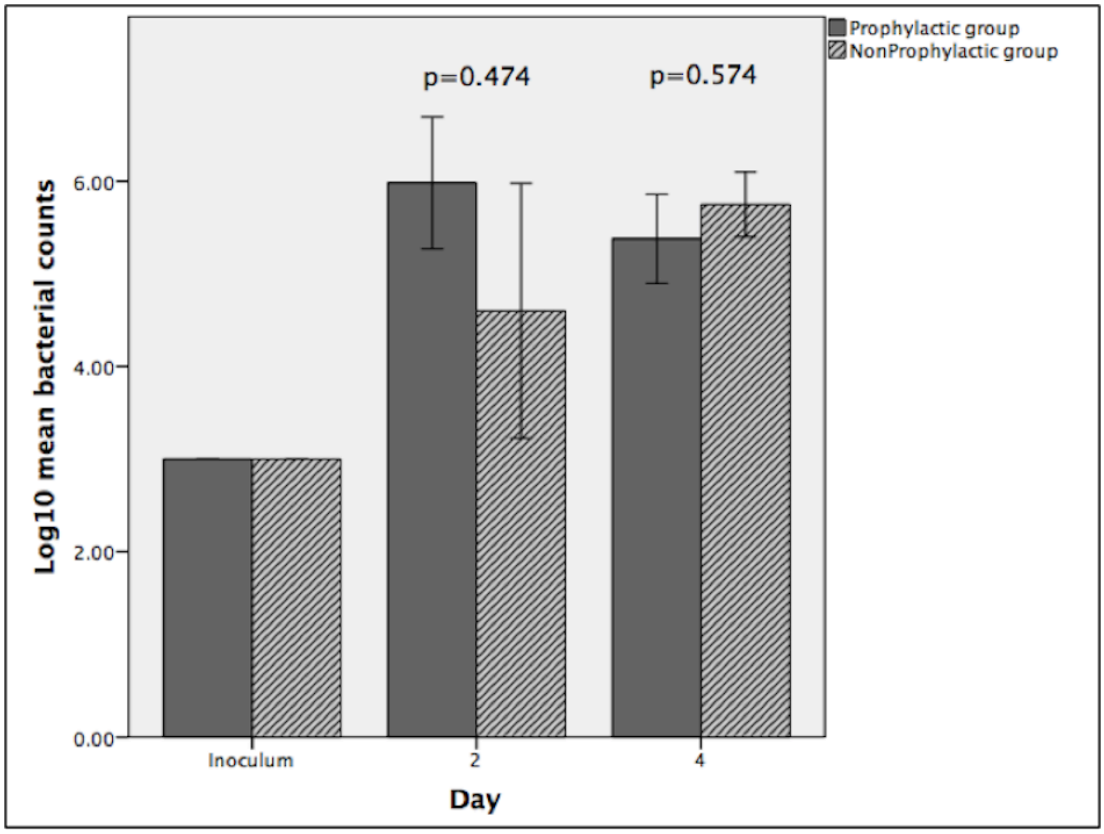

Figure 52. Comparison of bacterial counts between the prophylactic and non-prophylactic group. (error bars represent ± 1 standard error of mean)

6.4.4 Histology and immunohistochemistry

The corneal stroma of rabbits that were euthanized on day 2 was thickened in both groups, with greater thickness present in the non-prophylactic group (figure 53). The epithelial and endothelial surfaces appeared irregular and the stroma less densely populated by keratocytes compared to the healthy cornea. Numerous polymorphonuclear neutrophil (PMN) cells were present throughout the corneal stroma in both infection groups. The corneas of rabbits that were sacrificed on day 4 showed similar microscopic features, but the stromal thickening and oedema appeared to be approximately equal in prophylactic and non-prophylactic cases.

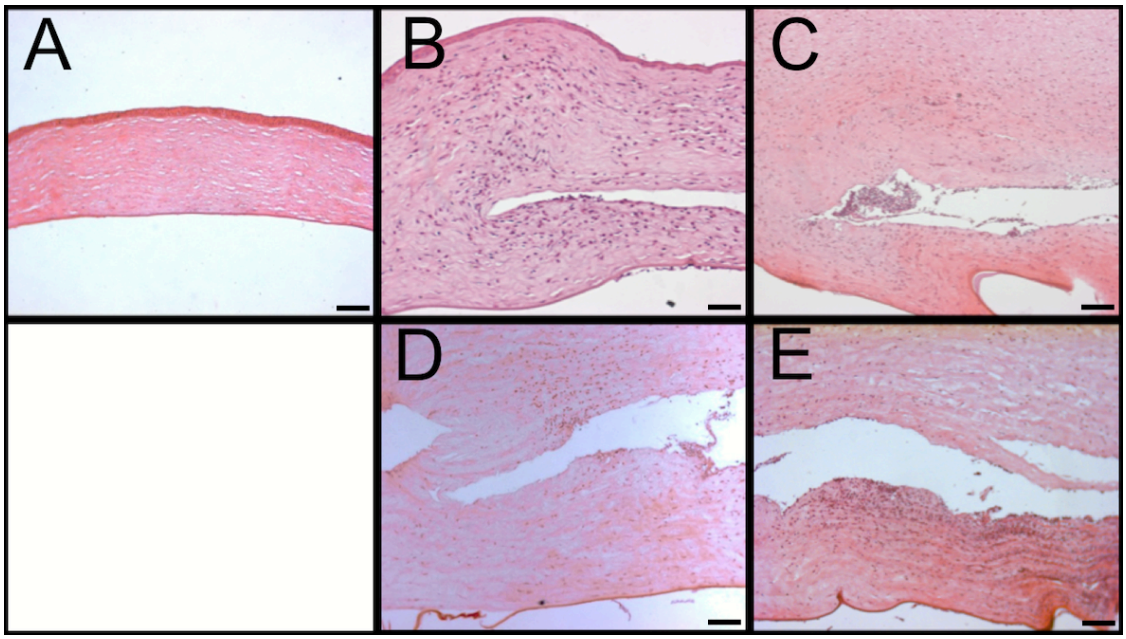

Figure 53. Haematoxylin and eosin stained corneal sections, comparing vancomycin prophylaxis to non-prophylaxis cases. A. Healthy cornea. B (day 2, prophylaxis). Rich infiltration of neutrophils was present throughout the stroma. The epithelial and endothelial surfaces were irregular due to stromal oedema. C (day 2, non-prophylaxis). The stroma appeared more oedematous than in image B. Rich neutrophilic infiltration was also present, mostly in the pocket, but the neutrophils appeared to be less densely arranged in the stroma than in image B, most likely reflecting the presence of more oedema. D (day 4, prophylaxis). The stroma was more oedematous than in image B and the

Descemets membrane was detached, reflecting greater levels of infection. The neutrophilic infiltration was not as dense as in image B, most likely due to more stromal oedema. E (day 4, non-prophylaxis). The stroma appeared similarly oedematous to that in image D and slightly richer in neutrophilic infiltration. (Scale bar 100 μm)

Immunostaining of day 2 corneal sections showed that the CD11b +ve/non-CD11b +ve cell ratio was greater in the non-prophylactic than in the prophylactic cases (1.45 vs. 0.71) (figure 54). On day 4, the ratio was slightly larger in the non-prophylactic than prophylactic cases, but the difference between the two was small (1.71 vs. 1.30).

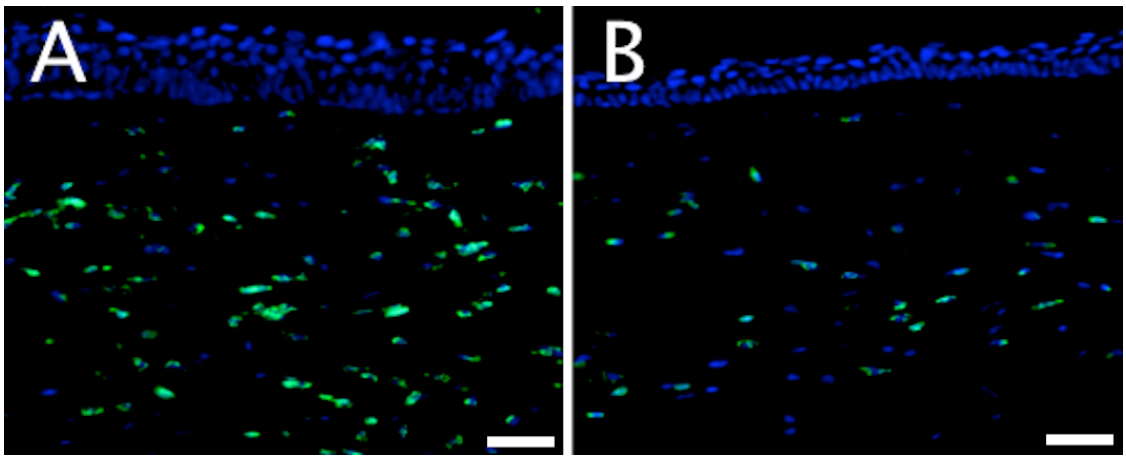

Figure 54. Immunohistochemistry comparison between prophylaxis and non-prophylaxis on day 2 following bacterial inoculation. More CD11b +ve neutrophils (fluorescing green) were present in the non-prophylactic case (A) than the prophylactic case (B). (Scale bar 50 μm)

6.4.5 Vancomycin pharmacokinetics

Corneal vancomycin concentration (mean±SEM) of rabbits that were sacrificed on days 2, 10 and 16 after initiation of vancomycin drops was 0.027±0.008, 0.975±0.215 and 2.835±0.383 μg/ml respectively (p=0.007) (figure 55).

Vancomycin was not detected in the aqueous humour after 2 days of antibiotics; although it was detected in the day 10 and day 16 rabbits, it was below the level of quantification.

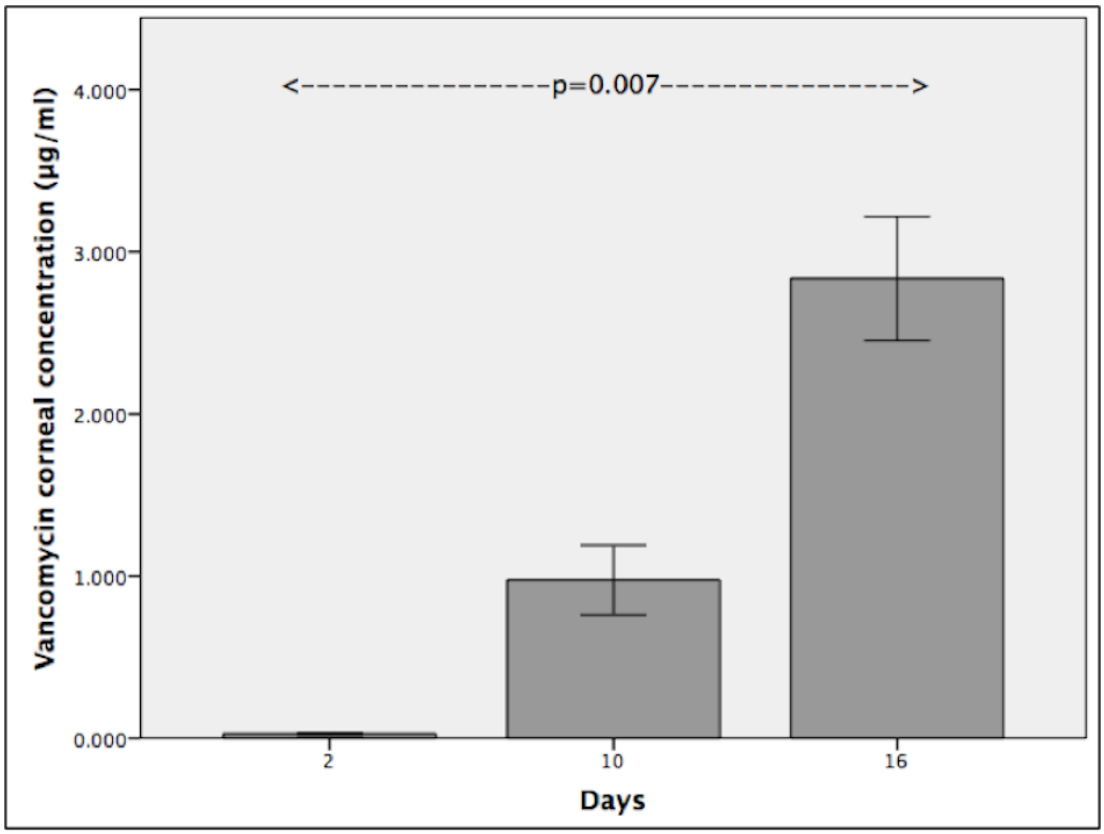

Figure 55. Vancomycin pharmacokinetics. Corneal vancomycin concentration increased with the duration of vancomycin drop administration. (error bars represent ± 1 standard error of mean)

In the experiment that investigated the effect of removing the epithelium on corneal vancomycin concentration, the concentration after 4 days was 1.36±0.45 µg/ml without epithelial removal and 2.57±0.40 µg/ml with epithelial removal (p=0.115). The aqueous humour vancomycin concentration was 0.04±0.005 µg/ml without epithelial removal and 0.43±0.15 µg/ml with epithelial removal (p=0.063).

6.4.6 Effectiveness of minimum inhibitory concentration

In the experiment that investigated the effectiveness of vancomycin prophylaxis once corneal vancomycin MIC-90 for *S. aureus* had been achieved, 2 of the 3 rabbits showed evidence of corneal infection with the development of an injected, sticky eye and a corneal infiltrate by day 2 post-inoculation. In the 3 rabbits, the CT (mean±SEM) increased from 228.8±5.7 μm before inoculation to 336.9±40.9 μm on day 1 and 431.7±47.2 μm on day 2 post-inoculation ($p=0.021$).

6.5 Discussion

In this study, prophylactic vancomycin 1.4% drops, applied five times a day, reduced the severity of *S. aureus* bacterial keratitis for the first 2 days of infection compared to non-prophylaxis. However, they did not provide a sustainable benefit and they did not reduce the corneal bacterial counts. Corneal vancomycin levels remained below MIC for *S. aureus* following 10 continuous days of vancomycin drop instillation, but did reach MIC by day 16. Achieving MIC did not prevent the development of corneal infection.

This study investigated the effectiveness of vancomycin drop prophylaxis, as patients with Boston type-1 Kpro typically receive once or twice daily prophylactic vancomycin 1.4% drops with or without a fluoroquinolone.[107,309] It involved a higher frequency of vancomycin drop use than the typical prophylactic regimens, suggesting that vancomycin drops may only provide a limited prophylactic benefit. Bacterial keratitis can still develop in patients receiving prophylaxis,[107] and the risk of fungal keratitis may even be increased.[309] The recommendation for the use of postoperative prophylactic vancomycin drops stems from the beneficial effect vancomycin drops have been found to have on the rate of endophthalmitis.[307,308] This potential benefit, however, may be confounded by other modifications to the treatment of Boston type-1 patients that were implemented at the same time as vancomycin introduction, such as the use of a bandage contact lens to keep the corneal surface hydrated,[307,308,310] and the redesign of the Kpo back-plate to include holes with the aim of improving nutrition of the corneal graft carrier.[311]

The use of prophylactic vancomycin drops reduced the severity of the early corneal inflammatory response, but the efficacy was lost by day 4 following inoculation. The AS-OCT CT was less in the prophylactic than the non-prophylactic group on days 1 and 2, but was not different between the groups on day 4. The initial efficacy of the prophylactic regimen is also supported by the fact that CT in the prophylactic group on day 1 was not significantly increased compared to pre-inoculation, but day 1 CT was increased in the non-prophylactic group. The SLP scores, verifying the AS-OCT data, also showed an initial prophylactic benefit, as the day 1 total SLP score was 1 in the

prophylactic group compared to 11 in the non-prophylactic, but this was lost by day 2.

Immunohistochemistry and H&E microscopy also detected smaller levels of PMN infiltration in the prophylactic group on day 2, but there did not appear to be a difference on day 4. In addition, the counts of viable bacteria were not reduced by vancomycin prophylaxis on days 2 and 4, providing further evidence that prophylactic drops may not provide a sustainable benefit.

Vancomycin drop instillation did not prevent the development of infection despite MIC levels for *S. aureus* being achieved. In-vivo inhibition of bacteria may require a much higher concentration than the nominal MIC that is based on in-vitro tests, as the protease rich microenvironment of the cornea may degrade the vancomycin. Although there are no data for the cornea, it is known that vancomycin, a glycopeptide antibiotic, shows moderate binding to proteins. It may therefore bind to lectin-like proteins of the stromal extracellular matrix, reducing its bioavailability further.[312] These factors, combined with the slow bactericidal activity of vancomycin,[313] may account for the poor prophylactic effectiveness that was found. In view of this discrepancy between laboratory efficacy and clinical effectiveness for vancomycin, other broad-spectrum antibiotics may need to be investigated as suitable alternatives for prophylaxis.

Study of the corneal vancomycin pharmacokinetics showed that a period of 16 days with a strict drop instillation regimen of five times a day and 100% compliance was required to achieve MIC, unless the epithelium was debrided in which case MIC was achieved within 4 days. This raises the question whether the typical prophylactic use of antibiotic drops once or twice daily,[107,309] would actually achieve MIC for a range of pathogens. Vancomycin is known to have poor penetration into tissues; even after intravenous administration, levels of 0–3.45 μg/ml have been found in the cerebrospinal fluid and 2.8 μg/ml in healthy lung tissue.[312] In the eye, the corneal epithelium may form a tight barrier that does not allow penetration of vancomycin into the stroma. However, in a study on pathological corneas that used vancomycin 3.3% drops intensively (5 drop instillations over 10 hours) very high corneal vancomycin concentration (46.7 μg/g) was achieved;[314] the high levels achieved in this

study may potentially be explained by the high concentration and frequency of the vancomycin drops, and also be confounded by the fact that the study was conducted on pathological pre-transplantation corneas that may have a poor epithelial barrier.

High concentration vancomycin drops, such as 3.3% or 5%, may be more efficacious in reducing the risk of Kpro associated BK. A very frequent drop instillation regimen, such as 2 hourly, may be recommended, but it is unlikely patients would remain compliant with intensive use over the long-term. There is good evidence from glaucoma studies that non-compliance with drops can be as high as 80%.[315] At only 3 months after starting treatment, just over half (55.6%) of patients took greater than 75% of the expected doses, even though once daily dosing was recommended.[316] Future developments, such as sustained drug release systems with liposomes and anti-infective or anti-adhesive biomaterials, may address these limitations.[317,318]

6.6 Conclusions

This animal model study of keratoprosthesis associated corneal infection found that vancomycin drop instillation at a frequency that is higher than prophylactic clinical practice provided a short-term benefit, but did not prevent the development of *S. aureus* keratitis. In addition, even after the vancomycin MIC-90 in the cornea was achieved, this was not sufficient to prevent corneal infection. Investigation of alternative antibiotic agents and of the discrepancy been laboratory efficacy and clinical effectiveness is required to improve our infection prophylaxis strategies in keratoprosthesis surgery.

7 Conclusions

7.1 Summary

Clinical examination of ocular surface inflammation and corneal infection relies greatly on the experience of the examining clinician. Evaluation of the presenting condition and, particularly, assessment of the treatment response are therefore subjective. Quantification of ocular surface inflammation, even with the availability of modern imaging devices, such as in-vivo confocal microscopy, is difficult, time consuming and often requires a specialised technician. Anterior Segment Optical Coherence Tomography (AS-OCT), a novel modality that provides easy, fast and non-contact cross-sectional imaging of the ocular surface, has the potential to objectively assess the extent of inflammation.

The inflammatory response of human bacterial keratitis (BK) is poorly researched, due to lack of suitable in-vivo quantification imaging techniques and inherent limitations in obtaining corneal specimens for study. Improvements in imaging, such as provided by AS-OCT, and laboratory technology may facilitate the in-vivo study of the human condition and improve our understanding of its clinical course and inflammatory response.

This PhD research thesis aimed to evaluate the imaging capabilities, the quantification capabilities, and the application of AS-OCT to ocular surface inflammation and corneal infection.

More specifically, the three objectives were:

1) To ascertain the imaging capabilities of AS-OCT and identify AS-OCT quantification parameters in inflammation of the ocular surface.
2) To assess the quantification capability of AS-OCT in BK.
3) To apply AS-OCT quantification of corneal inflammation to improving the prevention, diagnosis, monitoring, and treatment of BK.

7.1.1 Objective One

The imaging capabilities of AS-OCT were ascertained in 2 conditions that involve inflammation of the ocular surface; microbial keratitis and peripheral ulcerative keratitis (PUK).

In study 3.1, two quantitative parameters, corneal thickness (CT) and infiltrate thickness (IT), which could be applied to the objective assessment of BK, were identified. Qualitative features, such as anterior chamber cells and a retro-endothelial plaque, were also imaged on AS-OCT scans. An imaging protocol was developed that allowed standardized serial examination and comparison of these parameters, providing objective monitoring of the disease course and response to treatment.

Study 3.2 found a unique role for AS-OCT in evaluating and monitoring PUK, with the identification of morphological qualitative and quantitative parameters. In active PUK, CT at the ulcer base was thin and the gradient of the ulcer walls steep, ranging from 21 to 87°. As the condition responded to treatment, the ulcer edges became smoother and the ulcer walls less steep. In progressive PUK, the ulcer edge became sharper, the walls developed a steeper gradient and the minimum CT decreased. Cases with risk of perforation or actual perforation had an ulcer wall gradient greater than 44°.

7.1.2 Objective Two

Study 4.1 investigated the capability of AS-OCT to quantify morphology-based parameters of the acute corneal inflammatory response in BK. Three AS-OCT parameters were examined; CT, IT and infiltrate width (IW). The CT could be measured in 97.8 to 100%, IT in 73 to 89.2% and IW in 56.8 to 73% of cases. At presentation, CT showed the highest repeatability and reproducibility of the 3 parameters with a coefficient of variation (CV) of 6.73% and 8.27% respectively. The repeatability CV for IT and IW was 20.1% and 24.6% respectively, whereas the reproducibility CV 28.2% and 31.8% respectively.

In study 4.2, AS-OCT CT measurements in the healthy cornea were found to have better repeatability and reproducibility than in BK; the repeatability CV was 1.48% for central and 1.99% for peripheral CT. Repeatability and reproducibility following DSEK surgery were also better than in BK; respective

Conclusions

CV values for central CT following DSEK were 1.51% and 5.8%. Repeatability and reproducibility of AS-OCT CT depended on the extent of corneal pathology, being poorest in BK, better in DSEK and best in healthy cornea.

Study 4.3 detected a moderate to strong correlation between AS-OCT morphological parameters of corneal inflammation and function. A larger CT at presentation correlated moderately with poorer presentation vision, and a larger presentation IT strongly with presentation vision. The AS-OCT parameters also correlated with the clinical severity of infection and inflammation. At presentation, CT showed moderate and strong correlations with the epithelial defect and infiltrate diameter respectively; correlations for IT were weaker.

7.1.3 Objective Three

In study 5.1, AS-OCT imaging quantified the differential acute corneal inflammatory response and tissue loss of Gram-ve and Gram+ve BK; presentation CT and IT were larger in Gram-ve BK. AS-OCT was found to have good diagnostic capabilities; a presentation CT ≥ 950 µm or IT ≥ 450 µm was highly indicative of Gram-ve infection. A criterion of presentation CT ≥ 950 µm or IT ≥ 450 µm had a sensitivity, specificity, positive predictive value and negative predictive value of 100%, 83.3%, 84% and 100%, respectively, as a diagnostic indicator of Gram-ve infection. The mean corneal tissue loss after resolution of infection was 75.1 µm and this was greatest in Gram-ve BK.

In study 5.2, AS-OCT quantified the corneal inflammatory response in resolving BK. The CT in the infiltrated area was largest at presentation with a mean [SD] value of 905 [206] µm and it decreased significantly to 753 [161] µm ($p<0.001$) on day 3, 678 [178] µm ($p<0.001$) on day 7 and 584 [146] µm ($p<0.001$) on day 14. The IT was also largest at presentation with a mean [SD] value of 388 [184] µm; it decreased to 320 [163] µm ($p=0.001$), 296 [135] µm ($p=0.004$) and 207 [87] µm ($p<0.001$) respectively. The IW, 1530 [1048] µm at presentation, did not change significantly during treatment. In successfully treated BK, CT was reduced in 92.3% and IT in 100% of cases on day 3 of treatment. Failure to visualise a reduction in CT and IT by day 3 could, thus, be used as an indicator of poor treatment response.

Conclusions

In studies 5.3 and 5.4, a range of pro-inflammatory cytokines was quantified in the tears of patients with BK. The levels of cytokines IL-2, IL-8, IL-12p70, IL-1β, GM-CSF, IFN-γ, IL-6, IL-10, and TNF-α were all elevated compared to controls. Their levels decreased significantly by day 3 of treatment validating the AS-OCT findings in study 5.2. In addition, levels of the cardinal cytokines of inflammation, IL-1β, IL-8 and IL-6, were greater in Gram-ve than Gram+ve BK, validating the imaging findings in study 5.1. Finally, the concentrations of cytokines IL-1β, IL-6 and IL-8 were found to correlate moderately or strongly with AS-OCT CT. The tear analysis of inflammatory parameters, thus, validated the use of AS-OCT CT as a surrogate measure of acute corneal inflammation in BK.

In study 6.1, AS-OCT was applied to investigate the effectiveness of an antibiotic regimen as prophylaxis of keratoprosthesis associated BK. Prophylactic vancomycin 1.4% drops, applied five times a day, reduced the severity of *S. aureus* BK for the first 2 days of infection compared to non-prophylaxis, but did not provide a sustainable benefit. The AS-OCT CT was greater in the non-prophylactic than the prophylactic group up to day 2 (646.2±52.6 vs. 404.7±36.2 μm, p=0.001), but no different between the two groups on day 4 (683.8±61.2 vs. 765.7±146.9 μm, p=0.645). Immunohistochemistry for CD11b and microscopy of haematoxylin and eosin stained corneal sections detected smaller levels of neutrophil infiltration in the prophylactic group on day 2, but there did not appear to be a difference on day 4, validating further the use of AS-OCT as an imaging tool for quantification of the acute corneal inflammatory response in BK. Interestingly, bacterial counts were not significantly different between non-prophylactic and prophylactic cases at any time point. Study of vancomycin pharmacokinetics with liquid chromatography–mass spectrometry showed that corneal vancomycin concentration (2.835±0.383 μg/ml) exceeded minimum inhibitory concentration (MIC) for *S. aureus* only after 16 days of vancomycin drop instillation. However, achieving MIC did not prevent the development of corneal infection.

7.2 Impact

The initial studies of this research thesis investigate the imaging capabilities of AS-OCT in corneal and conjunctival inflammation. This work is the first to be published on AS-OCT imaging and its quantification capabilities in corneal infection. Three morphology-based AS-OCT quantification parameters, CT, IT and IW, are shown to provide quantification of the acute inflammatory response in BK and an objective assessment of the condition. Qualitative features, such as anterior chamber cells or retro-endothelial plaque may also be useful for diagnosis and monitoring the condition and its response to treatment. Measurement of CT performs the best, as it can be carried out in nearly all cases of BK; it also shows the best repeatability and reproducibility. Measurement of IT with AS-OCT is slightly poorer than CT, but considerably better than IW. Both CT and IT correlate well with parameters that are used clinically in assessment of severity of infection. Finally, CT correlates well with levels of pro-inflammatory cytokines in the tears of patients with BK. As a result, the imaging capabilities and quantification capabilities in BK, with measurement of CT and IT, demonstrate that AS-OCT can provide objective clinical assessment and is a promising research tool.

Following publication of the AS-OCT application to BK (studies 3.1 and 5.2), other researchers presented the imaging capabilities of Pentacam-Scheimpflug in microbial keratitis. Corneal densitometry was used for objective assessment of corneal infection and was found elevated in patients with microbial keratitis compared to healthy controls. In addition, a reduction was observed between presentation and follow-up at 4-6 weeks after resolution of infection; however, the researchers didn't investigate the application of this parameter and imaging modality to the important early stages of treatment.[204] Also in 2012, a study reported on the use of Fourier Domain AS-OCT in microbial keratitis, as discussed in section 1.5.4.3.[238] Morphological characteristics, such as hyper-reflective stromal lesions and localized stromal thinning, were identified on the images. However, no attempt was made to quantify these parameters of infection.

The work on PUK is the first study to characterise the condition in-vivo. AS-OCT provides objective evaluation of the condition, and two quantification

parameters are identified; CT and ulcer wall gradient. Measurement of CT at the ulcer base could provide an assessment of disease severity and risk of perforation. Evaluation of the ulcer wall gradient on serial examination could be used for assessment of ulcer activity, with a reduction in gradient being a feature of decreasing activity. AS-OCT may thus have a unique role, facilitating objective documentation and monitoring of the condition.

In the remaining work of this thesis, I use AS-OCT quantification of corneal inflammation to study the diagnosis, monitoring and prevention of BK. The findings on the AS-OCT differentiation between Gram-ve and Gram+ve BK (section 5.1) may have important implications for the diagnosis of BK. A diagnostic criterion of presentation CT ≥ 950 μm or IT ≥ 450 μm is highly indicative of Gram-ve infection, with a good sensitivity and specificity. This application of AS-OCT is unique, as there is no published literature on the diagnostic potential of an alternative imaging modality in BK. It is known clinically that Gram-ve BK, especially *Pseudomonas*, presents with large infiltrates and levels of corneal oedema.[17,81] AS-OCT, however, has enabled us to objectively quantify the extent of corneal oedema and inflammation.

A limitation of this diagnostic study is that evaluation of AS-OCT in BK is based on 45 patients living exclusively on the South coast of the United Kingdom. Although the identified bacteria, mostly *Pseudomonas* and *Staphylococcus* species, are typical of Western studies,[76,77,79,85,86] there is wide geographic variation in the causative pathogens of BK.[84] The diagnostic potential of AS-OCT would need to be investigated in a larger and more heterogeneous cohort of pathogens, including fungi and *Acanthamoeba*. The ability to aid the diagnosis of atypical microbial keratitis would have huge implications, as the diagnosis and treatment of these infections can be extremely challenging.

The diagnostic potential of AS-OCT was evaluated in relatively early BK, with a mean duration of symptoms of 3.3 days, due to the novelty of the application. In addition, these are the most common cases in clinical practice and the ones clinicians may be tempted not to obtain a corneal scrape from. Its diagnostic value and the respective CT and IT figures of 950 and 450 μm may thus be applicable only to relatively early BK.

Conclusions

Study 5.1 has also shown that AS-OCT has the capability to quantify the corneal tissue loss that develops in BK. Although quantification of the differential destructive capability of Gram-ve and Gram+ve pathogens is novel, the main impact of this finding lies in the potential future application of AS-OCT to study and quantify the effect of antibiotic or immune-modulatory treatments on the outcome of BK. The use of visual acuity as an outcome measure may not be a sensitive enough measure in BK studies that investigate the extent of corneal damage, especially when considering the heterogeneity of BK. In addition, vision cannot be used as an outcome measure in animal research. This work is also the first to show in-vivo a correlation between corneal tissue loss and presentation inflammation, verifying laboratory work on animal BK and current concepts that inflammation plays of fundamental role in stromal destruction.[28,290,291]

I found that both CT and IT decrease significantly by day 3 in successfully treated BK, signifying that failure to visualise a reduction in CT and IT by day 3 can be an indicator of poor treatment response. This has huge implications for the care of BK patients, as objective criteria can now be used to assess for improvement in the condition. It may prompt a change in the antibacterial treatment or revision of the diagnosis. A reduction in CT, however, can also be observed in deteriorating BK due to associated melting of the corneal stroma. In such a case, an increase in IT will be observed, as presented in section 3.1. Both parameters should therefore be used to assess the treatment response. Qualitative morphological examination of the corneal profile for evidence of posterior surface ectasia may also assist evaluation of the treatment response.

A limitation in the investigation of AS-OCT as a quantification device in BK is that the repeatability and reproducibility of scanning and imaging the same axis of the cornea and lesion were not investigated. This represents a limitation in the methodology design but also the difficulties in carrying out such a study, as explained in section 4.1.5. Corneal infection is a dynamic and evolving condition that may develop corneal thickening, corneal thinning, or an increase or decrease in the transverse dimensions of the corneal lesion. This change in thickness or dimensions may be asymmetrical, affecting one area of the established lesion more than another. As a result, the imaging protocol used throughout this thesis, with the scan passing through the infiltrate centre

at a defined axis, may potentially result in the AS-OCT scan missing the development of an eccentric lesion. However, such developments tend to occur in atypical non-bacterial infections that were not investigated in this thesis.

The newer AS-OCT devices that have become available since the start of this PhD may potentially overcome this limitation. They provide rapid high-density raster or radial scans of the cornea and they may be able to image the entire corneal infiltrate or affected area in three dimensions. The RTVue-100 device (section 1.5.4.3) that was used during my Singapore research provides pachymetry maps with 8 high-definition meridional B-scans with 1024 A-scans per meridian, acquired in only 0.32 seconds.[319] The Spectralis (Heidelberg Engineering GmbH, Heidelberg, Germany) has a volumetric protocol with a raster scan consisting of 193 B-scans, each B-scan consisting of 512 A-lines.[320] The Topcon 3D OCT-2000 three-dimensional scan consists of 128 B-scans, each consisting of 512 A-scans.[321] However, these devices have primary been optimised for retinal OCT imaging and thus use a short wavelength scan beam in the range of 840 - 870 nm. This shorter wavelength may affect penetration through the infected opaque cornea, limiting its potential application in BK. A more recent development is Fourier domain swept light source OCT, such as the Casia SS-1000 OCT (Tomey Corporation, Nagoya, Japan). This uses the longer wavelength of 1310 nm that achieves greater penetration, but also retains the speed of the above devices as it uses Fourier domain technology. It has the greatest potential, based on specifications, in providing three-dimensional volumetric imaging in BK.

Publication of my work on AS-OCT quantification of corneal inflammation in infection led to adoption of this technique by researchers at the Singapore Eye Research Institute in Singapore. During my fellowship in Singapore, I was given the opportunity to study the role of vancomycin prophylaxis in a rabbit model of keratoprosthesis associated BK with the use Fourier-Domain AS-OCT (chapter 6).

In this animal study, the use of AS-OCT CT as a measure of acute corneal inflammation is validated further with in-vivo slit-lamp photography grading, and ex-vivo corneal microscopy and immunohistochemistry. The instillation of vancomycin 1.4% drops at a frequency that is higher than in prophylactic clinical practice may not prevent the development of BK. In addition, achieving

the vancomycin MIC in the cornea for the appropriate pathogen may not be sufficient to prevent the development of corneal infection. This indicates that the use of vancomycin drops in patients following keratoprosthesis may not provide the expected prophylaxis. Vancomycin may not be a suitable agent due to its binding to proteins of the corneal stroma and its slow bactericidal activity.[312,313] Other broad-spectrum agents, such as ofloxacin that has shown good efficacy in single agent treatment of BK,[7] need to be explored. Further research into the corneal pharmacokinetics and pharmacodynamics of antibiotic agents is required in order to improve our infection prophylaxis strategies.

A limitation of this animal work is the controversial applicability of the findings to the human condition. However, as detailed in the introduction (section 1.2.4), the rabbit cornea is very similar to the human cornea, with the presence of a stratified squamous epithelium, keratocyte-containing stroma that makes up 90% of the corneal thickness, Descemets membrane and endothelium. It has been used extensively in animal studies of BK.[42-44]

The study in section 5.3 is the first to explore and quantify in-vivo a range of cytokines over time in human BK. The findings represent the treated condition in humans, rather than an animal experiment of BK that is usually untreated and has perforation as an outcome measure. Fukuda et al in 1997 found elevated tear IL-1β levels in five patients with corneal ulcers and chemical burns.[151] Yamaguchi et al in 2014, in a study of ten patients with BK, found elevated tear levels of IL1-β, IL-6 and IL-8 at presentation.[217] My work has shown that a range of pro-inflammatory cytokines is elevated, but IL-1β, IFN-γ, IL-10, IL-6 and IL-8 show the greatest ratio compared to controls, indicating a predominant role for these cytokines in association with the neutrophil. These cytokines may be suitable targets for more specific immune-modulatory treatment than corticosteroids. My research has also provided novel insight into the time profile of the immune response in BK. A limitation of this study is that it does not investigate which cell types are producing the involved cytokines. However, human studies are inherently limited by the poor availability of material for investigation with molecular techniques, such as immunohistochemistry, immunocytochemistry or flow cytometry. Collection of

material by lavage is an effective technique that is often used in other human studies or as a clinical investigation, such as in respiratory medicine.[297,322]

This cytokine work has validated the AS-OCT findings, strongly supporting the use of AS-OCT morphological parameters, CT and IT, as markers of acute inflammation in BK. Finally, a substantial impact of this research thesis may stem from the finding that a significant improvement in morphological, molecular and cellular markers of inflammation occurs by day 3 of treatment. This strongly suggests these first 3 days of treatment may be the optimum window for immune modulation in BK.

7.3 Future direction

The future direction is guided by natural progression of my current thinking, my understanding of corneal infection and optical coherence tomography, and gaps identified the field of corneal infection during the tenure of this PhD project. I anticipate employment as an NHS consultant with the opportunity to carry out clinical research, as suggested below. I would expect the opportunity to work with the ophthalmology academic teams at the University of Southampton and the Singapore Eye Research Institute.

The following research ideas represent my plans for next 3-5 years:

1. An AS-OCT study to investigate the diagnostics and treatment response in a large cohort. In this study, 100 culture positive patients with microbial keratitis will be recruited. It will include cases of atypical microbial keratitis, particularly acanthamoebal and fungal. The aim is not only to conduct a study with greater power than my current work, but also to recruit Gram+ve cases that are less common in United Kingdom, such as *Streptococcus pneumoniae*. With the current volume of cases at University Hospital Southampton, a recruitment period of 2-3 years would be required. The ability to diagnose atypical microbial keratitis rapidly with good sensitivity is currently lacking in clinical practice and would potentially prevent the misdiagnosis and late treatment of *Acanthamoeba* and fungal cases.
2. A United Kingdom Steroids for Corneal Ulcer Trial using AS-OCT. In this study, 200-250 patients with culture positive BK will be recruited and randomised to steroid drops (dexamethasone 0.1% PF 2 hourly) or no steroid drops. The steroid drops will be started 2-3 days after starting antibiotic treatment, depending on the turnover speed of microbiology cultures. The inflammatory response will be quantified with AS-OCT CT and IT and the tissue loss with AS-OCT CTL compared to the fellow unaffected cornea. Although the Steroids for Corneal Ulcer Trial recruited 500 patients, I believe that the sensitivity of AS-OCT may allow a smaller trial to confirm or exclude a difference between the steroid and non-steroid groups. This study would also provide a more Western experience; in the Steroids for Corneal Ulcer Trial 72% of isolates were Gram+ve, of which more than two thirds were *Streptococcus pneumoniae*.[323] As discussed in section 1.4.2, the

causative pathogens in the West are considerably different. Collaboration with one or two colleagues in the UK will be required, in order to recruit a sufficiently large number of patients.

3. A study to assess imaging and quantification capabilities of FD-OCT. New faster AS-OCT devices are now commercially available that use Fourier-Domain OCT technology. At University Hospital Southampton, we have a Heidelberg SPECTRALIS® with an anterior segment module that we have been using for assessment of corneal ulcers. The aim of the proposed study is to investigate the capability of FD-OCT to measure CT, and most importantly to identify an infiltrate and measure IT. A study of 50 cases with corneal infiltration would address this aim. The abilities to accurately identify the transverse and horizontal borders, and measure the dimensions of all clinical infiltrates could transform the clinical examination and monitoring of corneal ulcers, especially in view of the widespread availability of FD-OCT devices for retinal examination.
4. A rabbit study investigating targeted immune-modulation. In my current human work, pro-inflammatory cytokines and chemokines IL-1β, IFN-γ, IL-6 and IL-8 showed the greatest increase compared to controls. The next step would be to selectively inhibit these cytokines and investigate its effect on corneal inflammation with AS-OCT, as carried out in the rabbit keratoprosthesis study of my PhD. Two groups are envisaged, one *Pseudomonas* keratitis and one *Staphylococcus aureus* keratitis. The rabbits will be treated with hourly antibiotics once infection is evident, similar to a human protocol, and anti-cytokine treatment initiated 1-2 days post bacterial inoculation. The inflammatory response and tissue loss will be quantified in-vivo with AS-OCT and slit-lamp photography. The inflammatory response will be also quantified with CD11b immunohistochemistry, cytokine quantification and bacterial counts after euthanasia at various stages of the infection.
5. On-going research into AS-OCT technology and diagnostics. Whilst in Singapore, I was involved in a study investigating the imaging capabilities of micro-OCT. Recent developments into broadband light sources have allowed for OCT systems to achieve 1–2 μm spatial resolution, termed micro-OCT, in an attempt to achieve cellular level imaging in vivo.[324-326] A prototype OCT device developed at the National University of Singapore and

Singapore Eye Research Institute showed great imaging potential. The images below illustrate its ability to image the cornea with resolution much higher than current commercial OCT imaging devices and on par with in-vivo confocal microscopy. I plan to establish collaboration with the Singaporean group in developing OCT imaging and diagnostics for corneal inflammatory conditions.

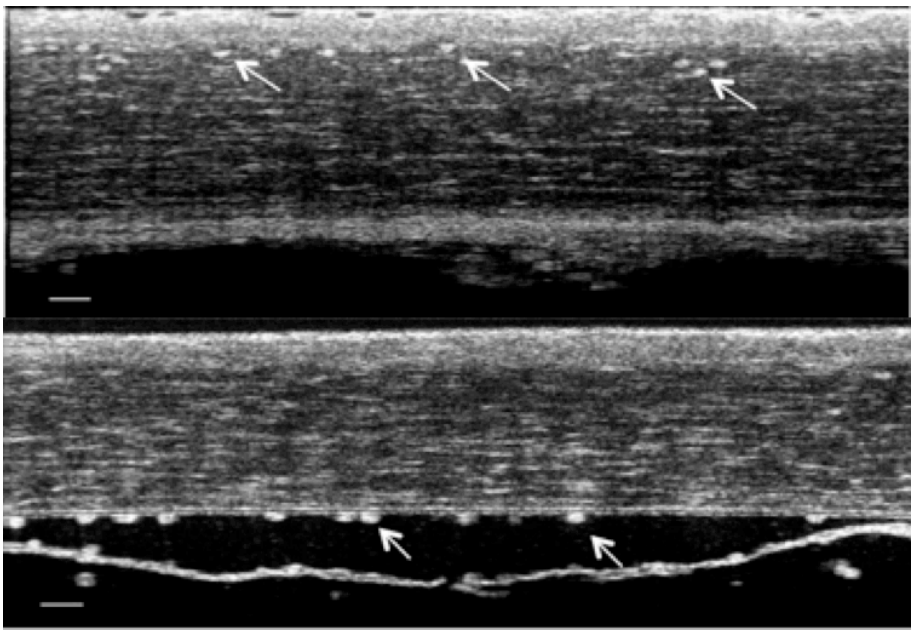

Figure 56. Micro-OCT images in a rat corneal endothelial injury model. Individual inflammatory cells (arrows) can be visualised in the anterior corneal stroma (top image) and attached to the posterior stromal surface (lower image). The Descemets membrane has detached (lower image) following cryotherapy induced injury to the endothelium.

References

1. Pascolini D, Mariotti SP. Global estimates of visual impairment: 2010. Br J Ophthalmol. 2012; 96:614-618.
2. Whitcher JP, Srinivasan M, Upadhyay MP. Corneal blindness: a global perspective. Bull World Health Organ. 2001; 79:214-21.
3. Cheng KH, Leung SL, Hoekman HW, Beekhuis WH, Mulder PG, Geerards AJ, Kijlstra A. Incidence of contact-lens-associated microbial keratitis and its related morbidity. Lancet. 1999; 354: 181-5.
4. Dart J. Extended-wear contact lenses, microbial keratitis, and public health. Lancet. 1999: 354; 174-5.
5. Kessler E, Mondino BJ, Brown SI. The corneal response to Pseudomonas aeruginosa: histopathological and enzymatic characterization. Invest Ophthalmol Vis Sci. 1977;16:116-25.
6. Steuhl KP, Doring G, Henni A, Thiel HJ, Botzenhart K. Relevance of host-derived and bacterial factors in Pseudomonas aeruginosa corneal infections. Invest Ophthalmol Vis Sci. 1987; 28:1559-1568.
7. Morlet N, Minassian D, Butcher J, and the Ofloxacin Study Group. Risk factors for treatment outcome of suspected microbial keratitis. Br J Ophthalmol. 1999; 83:1027-1031.
8. Kwong MS, Evans DJ, Ni M, Cowell BA, Fleiszig SM. Human tear fluid protects against Pseudomonas aeruginosa keratitis in a murine experimental model. Infect Immun. 2007;75:2325-32.
9. Hume EB, Dajcs JJ, Moreau JM, Sloop GD, Willcox MD, O'Callaghan RJ. Staphylococcus corneal virulence in a new topical model of infection. Invest Ophthalmol Vis Sci. 2001; 42:2904-2908.
10. Calladine D, Packard R. Clear corneal incision architecture in the immediate postoperative period evaluated using optical coherence tomography. J Cataract Refract Surg. 2007; 33:1429-35.
11. Lai MM, Tang M, Andrade EM, Li Y, Khurana RN, Song JC, Huang D, Optical coherence tomography to assess intrastromal corneal segment depth in keratoconic eyes. J Cataract Refract Surg. 2006; 32:1860-5.
12. Sorsby A, Benjamin B, Bennett AG. Steiger on refraction: a reappraisal. Br J Ophthalmol. 1981; 65:805-11.

13. Vojnikovic B, Gabriç N, Dekaris I, Juric B. Curvature analyses of the corneal front and back surface. Coll Antropol. 2013;37 Suppl 1:93-6.
14. Easty DL and Sparrow JM. Oxford Textbook of Ophthalmology. Oxford Medical Publications; 1999. Chapter 2, section 2.6, Clinical Ophthalmology, pg 373-9.
15. Azari AA, Barney NP. Conjunctivitis: a systematic review of diagnosis and treatment. JAMA. 2013;310:1721-9.
16. Miedziak AI, Miller MR, Rapuano CJ, Laibson PR, Cohen EJ. Risk factors in microbial keratitis leading to penetrating keratoplasty. Ophthalmology. 1999;106:1166-1171.
17. Bourcier T, Thomas F, Borderie V, Chaumeil C and Laroche L. Bacterial keratitis: predisposing factors, clinical and microbiological review of 300 cases. Br J Ophthalmol. 2003; 87: 834-838.
18. Stoeckelhuber M, Stoeckelhuber BM, Welsch U. Human glands of Moll: histochemical and ultrastructural characterization of the glands of Moll in the human eyelid. J Invest Dermatol. 2003;121:28-36.
19. Easty DL and Sparrow JM. Oxford Textbook of Ophthalmology. Oxford Medical Publications; 1999. Chapter 2, section 2.4, Clinical Ophthalmology, pg 327-9.
20. Hodges RR, Dartt DA. Tear film mucins: front line defenders of the ocular surface; comparison with airway and gastrointestinal tract mucins. Exp Eye Res. 2013;117:62-78.
21. Tutt R, Bradley A, Begley C, Thibos LN. Optical and visual impact of tear break-up in human eyes. Invest Ophthalmol Vis Sci. 2000;41:4117–4123.
22. Carnt NA, Willcox MD, Hau S, Keay L, Dart JK, Chakrabarti S, Stapleton F. Immune defense single nucleotide polymorphisms and recruitment strategies associated with contact lens keratitis. Ophthalmology. 2012;119:1997-2002.
23. The Eye. Basic sciences in practice. WB Saunders; 1999. Chapter 1, Anatomy of the eye and orbit, pg 72-75.
24. Dua HS, Faraj LA, Said DG, Gray T, Lowe J. Human corneal anatomy redefined: a novel pre-Descemet's layer (Dua's layer). Ophthalmology. 2013;120:1778-85.

25. Dua HS, Gomes JA, Singh A. Corneal epithelial wound healing. Br J Ophthalmol. 1994;78:401-8.
26. Wilson SL, El Haj AJ, Yang Y. Control of scar tissue formation in the cornea: strategies in clinical and corneal tissue engineering. J Funct Biomater. 2012;3:642-87.
27. West-Mays JA, Dwivedi DJ. The keratocyte: corneal stromal cell with variable repair phenotypes. Int J Biochem Cell Biol. 2006;38:1625-31.
28. Hazlett LD. Corneal response to Pseudomonas aeruginosa infection. Prog Retin Eye Res. 2004;23:1-30.
29. Bratton DL, Henson PM. Neutrophil clearance: when the party is over, clean-up begins. Trends Immunol. 2011;32:350-7.
30. Mayer WJ, Mackert MJ, Kranebitter N, Messmer EM, Grüterich M, Kampik A, Kook D. Distribution of antigen presenting cells in the human cornea: correlation of in vivo confocal microscopy and immunohistochemistry in different pathologic entities. Curr Eye Res. 2012;37:1012-8.
31. Hamrah P, Liu Y, Zhang Q, Dana MR. The corneal stroma is endowed with a significant number of resident dendritic cells. Invest Ophthalmol Vis Sci. 2003;44:581-589.
32. Zhivov A, Kraak R, Bergter H, Kundt G, Beck R, Guthoff RF. Influence of benzalkonium chloride on langerhans cells in corneal epithelium and development of dry eye in healthy volunteers. Curr Eye Res. 2010;35:762-9.
33. The Eye. Basic sciences in practice. WB Saunders; 1999 Chapter 1, Anatomy of the eye and orbit, pg. 14-17.
34. The Eye. Basic sciences in practice. WB Saunders; 1999. Chapter 1, Anatomy of the eye and orbit, pg. 75-76.
35. Riau AK, Tan NY, Angunawela RI, Htoon HM, Chaurasia SS, Mehta JS. Reproducibility and age-related changes of ocular parametric measurements in rabbits. BMC Vet Res. 2012;8:138.
36. Hayashi S, Osawa T, Tohyama K. Comparative observations on corneas, with special reference to Bowman's layer and Descemet's membrane in mammals and amphibians. J Morphol. 2002;254:247-58.
37. Joyce NC. Proliferative capacity of the corneal endothelium. Prog Retin Eye Res. 2003;22:359-89.

38. Kaye GI, Pappas GD. Studies on the cornea. I. The fine structure of the rabbit cornea and the uptake and transport of colloidal particles by the cornea in vivo. J Cell Biol. 1962;12:457-79.
39. Maurice D. The effect of the low blink rate in rabbits on topical drug penetration. J Ocul Pharmacol Ther. 1995;11:297-304.
40. Toshida H, Nguyen DH, Beuerman RW, Murakami A. Evaluation of novel dry eye model: preganglionic parasympathetic denervation in rabbit. Invest Ophthalmol Vis Sci. 2007;48:4468-75.
41. Garcia DM, Barbosa JC, Pinto CT, Cruz AA. Estimation of spontaneous blinking main sequence in normal subjects and patients with Graves' upper eyelid retraction. Invest Ophthalmol Vis Sci. 2013;54:1434-42.
42. Tan XW, Goh TW, Saraswathi P, Nyein CL, Setiawan M, Riau A, Lakshminarayanan R, Liu S, Tan D, Beuerman RW, Mehta JS. Effectiveness of antimicrobial peptide immobilization for preventing perioperative cornea implant-associated bacterial infection. Antimicrob Agents Chemother. 2014;58:5229-38.
43. Gritz DC, Kwitko S, Trousdale MD, Gonzalez VH, McDonnell PJ. Recurrence of microbial keratitis concomitant with antiinflammatory treatment in an animal model. Cornea. 1992;11:404-8.
44. Moreau JM, Sloop GD, Engel LS, Hill JM, O'Callaghan RJ. Histopathological studies of staphylococcal alpha-toxin: effects on rabbit corneas. Curr Eye Res. 1997;16:1221-8.
45. Azari AA, Barney NP. Conjunctivitis: a systematic review of diagnosis and treatment. JAMA 2013; 310:1721–1729.
46. Taylor HR, Burton MJ, Haddad D, West S, Wright H. Trachoma. Lancet. 2014;384:2142-52.
47. Schwartz RA, McDonough PH, Lee BW. Toxic epidermal necrolysis: Part I. Introduction, history, classification, clinical features, systemic manifestations, etiology, and immunopathogenesis. J Am Acad Dermatol. 2013;69:173.e1-13.
48. Schwartz RA, McDonough PH, Lee BW. Toxic epidermal necrolysis: Part II. Prognosis, sequelae, diagnosis, differential diagnosis, prevention, and treatment. J Am Acad Dermatol. 2013;69(2):187.e1-16.

49. Saw VP, Dart JK. Ocular mucous membrane pemphigoid: diagnosis and management strategies. Ocul Surf. 2008;6:128-42.
50. Bonini S, Coassin M, Aronni S, Lambiase A. Vernal keratoconjunctivitis. Eye. 2004;18:345-51.
51. Fish R, Davidson RS. Management of ocular thermal and chemical injuries, including amniotic membrane therapy. Curr Opin Ophthalmol. 2010;21:317-21.
52. Bernauer W, Broadway DC, Wright P. Chronic progressive conjunctival cicatrisation. Eye. 1993;7:371-8.
53. Wan MJ, Hunter DG. Complications of strabismus surgery: incidence and risk factors. Semin Ophthalmol. 2014;29:421-8.
54. Yeung SN, Lichtinger A, Kim P, Elbaz U, Ku JY, Amiran MD, Gorfinkle N, Wolff R, Slomovic AR. Superior versus inferior conjunctival autografts combined with fibrin glue in the management of primary pterygia. Cornea. 2013;32:1582-6.
55. Fraser SG and Wormald RP. Hospital episode statistics and changing trends in glaucoma surgery. Eye. 2008; 22:3-7.
56. Lama PJ and Fechtner RD. Antifibrotics and wound healing in glaucoma surgery. Surv Ophthalmol. 2003; 48:314-346.
57. Addicks EM, Quigley A, Green WR, Robin AL. Histological characteristics of filtering blebs in glaucomatous eyes. Arch Ophthalmol. 1983; 101:795-798.
58. Hitchings RA, Grierson I. Clinico pathological correlation in eyes with failed fistulising surgery. Trans Ophthalmol Soc UK. 1983; 103:84-88.
59. Loh RS, Chan CM, Ti SE, Lim L, Chan KS, Tan DT. Emerging prevalence of microsporidial keratitis in Singapore: epidemiology, clinical features, and management. Ophthalmology. 2009;116:2348-53.
60. Jiang C, Sun X, Wang Z, Zhang Y. Acanthamoeba keratitis: clinical characteristics and management. Ocul Surf. 2015;13:164-8.
61. Fintelmann RE, Vastine DW, Bloomer MM, Margolis TP. Thygeson superficial punctate keratitis and scarring. Cornea. 2012;31:1446-8.
62. Hassanlou M, Bhargava A, Hodge WG. Bilateral acanthamoeba keratitis and treatment strategy based on lesion depth. Can J Ophthalmol. 2006;41:71-3.
63. Ficker L, Seal D, Wright P. Staphylococcal infection and the limbus: study of the cell-mediated immune response. Eye. 1989;3:190-3.

64. Schwartz GS, Harrison AR, Holland EJ. Etiology of immune stromal (interstitial) keratitis. Cornea. 1998;17:278-81.
65. Schaefer F, Bruttin O, Zografos L, Guex-Crosier Y. Bacterial keratitis: a prospective clinical and microbiological study. Br J Ophthalmol. 2001;85:842-7.
66. Garg P. Fungal, Mycobacterial, and Nocardia infections and the eye: an update. Eye. 2012;26:245-51.
67. Koizumi N, Inatomi T, Suzuki T, Shiraishi A, Ohashi Y, Kandori M, Miyazaki D, Inoue Y, Soma T, Nishida K, Takase H, Sugita S, Mochizuki M, Kinoshita S; Japan Corneal Endotheliitis Study Group. Clinical features and management of cytomegalovirus corneal endotheliitis: analysis of 106 cases from the Japan corneal endotheliitis study. Br J Ophthalmol. 2015;99:54-8.
68. Qazi Y, Hamrah P. Corneal Allograft Rejection: Immunopathogenesis to Therapeutics. J Clin Cell Immunol. 2013;2013(Suppl 9).
69. Ezon I, Shih CY, Rosen LM, Suthar T, Udell IJ. Immunologic graft rejection in descemet's stripping endothelial keratoplasty and penetrating keratoplasty for endothelial disease. Ophthalmology. 2013;120:1360-5.
70. McKibbin M, Isaacs JD, Morrell AJ. Incidence of corneal melting in association with systemic disease in the Yorkshire Region, 1995-7. Br J Ophthalmol. 1999;83:941-3.
71. Dana MR, Qian Y, Hamrah P. Twenty-five-year panorama of corneal immunology: emerging concepts in the immunopathogenesis of microbial keratitis, peripheral ulcerative keratitis, and corneal transplant rejection. Cornea. 2000;19:625-43.
72. Messmer EM, Foster CS. Vasculitic peripheral ulcerative keratitis. Surv Ophthalmol. 1999;43:379-96.
73. Meek KM, Boote C. The use of X-ray scattering techniques to quantify the orientation and distribution of collagen in the corneal stroma. Prog Retin Eye Res. 2009;28:369-92.
74. McCally RL, Freund DE, Zorn A, Bonney-Ray J, Grebe R, de la Cruz Z, Green WR. Light-scattering and ultrastructure of healed penetrating corneal wounds. Invest Ophthalmol Vis Sci. 2007;48:157-65.

75. Varaprasathan G, Miller K, Lietman T, Whitcher JP, Cevallos V, Okumoto M, Margolis TP, Yinghui M, Cunningham ET Jr. Trends in the etiology of infectious corneal ulcers at the F. I. Proctor Foundation. Cornea. 2004; 23:360-4.
76. Liesegang TJ, Forster RK. Spectrum of microbial keratitis in South Florida. Am J Ophthalmol. 1980;90:38-47.
77. Ibrahim YW, Boase DL, Cree IA. Epidemiological characteristics, predisposing factors and microbiological profiles of infectious corneal ulcers: the Portsmouth corneal ulcer study. Br J Ophthalmol. 2009;93:1319-1324.
78. Dart JKG. Predisposing factors in microbial keratitis: the significance of contact lens wear. Br J Ophthalmol. 1988; 72:926-930.
79. Keay L, Edwards K, Naduvilath T, Taylor HR, Snibson GR, Forde K, Stapleton F. Microbial keratitis: predisposing factors and morbidity. Ophthalmology. 2006; 113:109–116.
80. Pachigolla G, Blomquist P, Cavanagh HD. Microbial keratitis pathogens and antibiotic susceptibilities: a 5-year review of cases at an urban county hospital in north Texas. Eye Contact Lens. 2007; 33:45-9.
81. Dahlgren MA, Lingappan A, Wilhelmus KR. The clinical diagnosis of microbial keratitis. Am J Ophthalmol. 2007; 143:940-944.
82. van der Meulen IJ, van Rooij J, Nieuwendaal CP, Van Cleijnenbreugel H, Geerards AJ, Remeijer L. Age-related risk factors, culture outcomes, and prognosis in patients admitted with infectious keratitis to two Dutch tertiary referral centers. Cornea. 2008;27:539-44.
83. Shah A, Sachdev A, Coggon D, Hossain P. Geographic variations in microbial keratitis: an analysis of the peer-reviewed literature. Br J Ophthalmol. 2011;95:762-7.
84. Srinivasan M, Gonzales CA, George C, Cevallos V, Mascarenhas JM, Asokan B, Wilkins J, Smolin G, Whitcher JP. Epidemiology and aetiological diagnosis of corneal ulceration in Madurai, south India. Br J Ophthalmol. 1997; 81:965-71.
85. Alexandrakis G, Alfonso EC, Miller D. Shifting trends in bacterial keratitis in south Florida and emerging resistance to fluoroquinolones. Ophthalmology. 2000;107:1497-502.

86. Lichtinger A, Yeung SN, Kim P, Amiran MD, Iovieno A, Elbaz U, Ku JY, Wolff R, Rootman DS, Slomovic AR. Shifting trends in bacterial keratitis in Toronto: an 11-year review. Ophthalmology. 2012;119:1785-90.
87. Baker H, Bloom WL. Further Studies on the Gram Stain. J Bacteriol. 1948;56:387-90.
88. Lamanna C, Mallette MF. The relation of the gram stain to the cell wall and the ribonucleic acid content of the cell. J Bacteriol. 1950;60:499-505.
89. Scheffers DJ, Pinho MG. Bacterial cell wall synthesis: new insights from localization studies. Microbiol Mol Biol Rev. 2005;69:585-607.
90. Sukhithasri V, Nisha N, Biswas L, Anil Kumar V, Biswas R. Innate immune recognition of microbial cell wall components and microbial strategies to evade such recognitions. Microbiol Res. 2013;168:396-406.
91. Zhang G, Meredith TC, Kahne D. On the essentiality of lipopolysaccharide to Gram-negative bacteria. Curr Opin Microbiol. 2013;16:779-85.
92. Brown L, Wolf JM, Prados-Rosales R, Casadevall A. Through the wall: extracellular vesicles in Gram-positive bacteria, mycobacteria and fungi. Nat Rev Microbiol. 2015;13:620-30.
93. Williams KA, Lowe M, Bartlett C, Kelly TL, Coster DJ; All Contributors. Risk factors for human corneal graft failure within the Australian corneal graft registry. Transplantation. 2008;86:1720-4.
94. Maguire MG, Stark WJ, Gottsch JD, Stulting RD, Sugar A, Fink NE, Schwartz A. Risk factors for corneal graft failure and rejection in the collaborative corneal transplantation studies. Collaborative Corneal Transplantation Studies Research Group. Ophthalmology. 1994;101:1536-47.
95. Hicks CR, Crawford GJ, Dart JK, Grabner G, Holland EJ, Stulting RD, Tan DT, Bulsara M. AlphaCor: Clinical outcomes. Cornea. 2006;25:1034-42.
96. Akpek EK, Alkharashi M, Hwang FS, Ng SM, Lindsley K. Artificial corneas versus donor corneas for repeat corneal transplants. Cochrane Database Syst Rev. 2014;11:CD009561.
97. Chew HF, Ayres BD, Hammersmith KM, Rapuano CJ, Laibson PR, Myers JS, Jin YP, Cohen EJ. Boston keratoprosthesis outcomes and complications. Cornea. 2009; 28:989-96.

98. Aldave AJ, Kamal KM, Vo RC, Yu F. The Boston type 1 keratoprosthesis: improving outcomes and expanding indications. Ophthalmology. 2009; 116:640-51.
99. Zerbe BL, Belin MW, Ciolino JB; Boston Type 1 Keratoprosthesis Study Group. Results from the multicentre Boston Type 1 Keratoprosthesis Study. Ophthalmology. 2006; 113:1779-1784.
100. Srikumaran D, Munoz B, Aldave AJ, Aquavella JV, Hannush SB, Schultze R, Belin M, Akpek EK. Long-term outcomes of boston type 1 keratoprosthesis implantation: a retrospective multicenter cohort. Ophthalmology. 2014;121:2159-64.
101. Avadhanam VS, Liu CS. A brief review of Boston type-1 and osteo-odonto keratoprostheses. Br J Ophthalmol. 2015;99:878-87.
102. Crnej A, Paschalis EI, Salvador-Culla B, Tauber A, Drnovsek-Olup B, Shen LQ, Dohlman CH. Glaucoma progression and role of glaucoma surgery in patients with Boston keratoprosthesis. Cornea. 2014;33:349-54.
103. Sivaraman KR, Hou JH, Allemann N, de la Cruz J, Cortina MS. Retroprosthetic membrane and risk of sterile keratolysis in patients with type 1 Boston keratoprosthesis. Am J Ophthalmol. 2013;155:814-22.
104. Bradley JC, Hernandez EG, Schwab IR, Mannis MJ. Boston type 1 keratoprosthesis: the University of California Davis experience. Cornea. 2009;28:321–327.
105. Magalhães FP, do Nascimento HM, Ecker DJ, Sannes-Lowery KA, Sampath R, Rosenblatt MI, de Sousa LB, de Oliveira LA. Microbiota evaluation of patients with a Boston type I keratoprosthesis treated with topical 0.5% moxifloxacin and 5% povidone-iodine. Cornea. 2013;32:407-11.
106. Kim MJ, Yu F, Aldave AJ. Microbial keratitis after Boston type I keratoprosthesis implantation: incidence, organisms, risk factors, and outcomes. Ophthalmology. 2013;120:2209-16.
107. Chan CC, Holland EJ. Infectious keratitis after Boston type 1 keratoprosthesis implantation. Cornea. 2012;31:1128-34.
108. Pepose JS, Wilhelmus KR. Divergent approaches to the management of corneal ulcers. Am J Ophthalmol. 1992; 114:630-632.
109. Garg P. Diagnosis of microbial keratitis. Br J Ophthalmol. 2010;94:961-2.

110. Brasnu E, Bourcier T, Dupas B, Degorge S, Rodallec T, Laroche L, Borderie V, Baudouin C. In vivo confocal microscopy in fungal keratitis. Br J Ophthalmol. 2007;91:588-91.
111. Das S, Samant M, Garg P, Vaddavalli PK, Vemuganti GK. Role of confocal microscopy in deep fungal keratitis. Cornea. 2009;28:11-3.
112. Yamazaki N, Kobayashi A, Yokogawa H, Ishibashi Y, Oikawa Y, Tokoro M, Sugiyama K. In vivo imaging of radial keratoneuritis in patients with Acanthamoeba keratitis by anterior-segment optical coherence tomography. Ophthalmology. 2014;121:2153-8.
113. Kobayashi A, Yokogawa H, Yamazaki N, Ishibashi Y, Oikawa Y, Tokoro M, Sugiyama K. In vivo laser confocal microscopy findings of radial keratoneuritis in patients with early stage Acanthamoeba keratitis. Ophthalmology. 2013;120:1348-53.
114. Kim E, Chidambaram JD, Srinivasan M, Lalitha P, Wee D, Lietman TM, Whitcher JP, Van Gelder RN. Prospective comparison of microbial culture and polymerase chain reaction in the diagnosis of corneal ulcer. Am J Ophthalmol. 2008;146:714-23.
115. Eleinen KG, Mohalhal AA, Elmekawy HE, Abdulbaki AM, Sherif AM, El-Sherif RH, Abdul Rahman EM. Polymerase chain reaction-guided diagnosis of infective keratitis - a hospital-based study. Curr Eye Res. 2012;37:1005-11.
116. Taravati P, Lam D, Van Gelder RN. Role of molecular diagnostics in ocular microbiology. Curr Ophthalmol Rep. 2013; 1: 181-189.
117. Matsumoto K, Ikema K, Tanihara H. Role of cytokines and chemokines in pseudomonal keratitis. Cornea 2005: 24; S43-S49.
118. Theilgaard-Mönch K, Porse BT, Borregaard N. Systems biology of neutrophil differentiation and immune response. Curr Opin Immunol. 2006;18:54-60.
119. Steuhl KP, Doring G, Henni A, Thiel HJ, Botzenhart K. Relevance of host-derived and bacterial factors in Pseudomonas aeruginosa corneal infections. Invest Ophthalmol Vis Sci. 1987; 28:1559-1568.
120. Hazlett LD, Rosen DD, Berk RS. Pseudomonas eye infections in cyclophosphamide-treated mice. Invest Ophthalmol Vis Sci. 1977;16:649-52.

121. Chusid MJ, Davis SD. Experimental bacterial keratitis in neutropenic guinea pigs: polymorphonuclear leukocytes in corneal host defense. Infect Immun. 1979;24:948-52.
122. Kernacki KA, Barrett RP, Hobden JA, Hazlett LD. Macrophage inflammatory protein-2 is a mediator of polymorphonuclear neutrophil influx in ocular bacterial infection. J Immunol. 2000;164:1037-45.
123. McClellan SA, Huang X, Barrett RP, van Rooijen N, Hazlett LD. Macrophages restrict Pseudomonas aeruginosa growth, regulate polymorphonuclear neutrophil influx, and balance pro- and anti-inflammatory cytokines in BALB/c mice. J Immunol. 2003;170:5219-27.
124. Sun Y, Karmakar M, Roy S, Ramadan RT, Williams SR, Howell S, Shive CL, Han Y, Stopford CM, Rietsch A, Pearlman E. TLR4 and TLR5 on corneal macrophages regulate Pseudomonas aeruginosa keratitis by signaling through MyD88-dependent and -independent pathways. J Immunol. 2010;185:4272-83.
125. Cruzat A, Witkin D, Baniasadi N, Zheng L, Ciolino JB, Jurkunas UV, Chodosh J, Pavan-Langston D, Dana R, Hamrah P. Inflammation and the nervous system: the connection in the cornea in patients with infectious keratitis. Invest Ophthalmol Vis Sci. 2011;52:5136-43.
126. Hazlett LD, McClellan SA, Rudner XL, Barrett RP. The role of Langerhans cells in Pseudomonas aeruginosa infection. Invest Ophthalmol Vis Sci. 2002;43:189-97.
127. Kubin M, Chow JM, Trinchieri G. Differential regulation of interleukin-12 (IL-12), tumor necrosis factor-α, and IL-1β production in human myeloid leukaemia cell lines and peripheral blood mononuclear cells. Blood. 1994;83:1847–55.
128. Kumar A, Yu FS. Toll-like receptors and corneal innate immunity. Curr Mol Med. 2006;6:327-37.
129. Mogensen TH. Pathogen recognition and inflammatory signaling in innate immune defenses. Clin Microbiol Rev. 2009;22:240-73.
130. Hirschfeld M, Ma Y, Weis JH, Vogel SN, Weis JJ. Cutting edge: repurification of lipopolysaccharide eliminates signaling through both human and murine toll-like receptor 2. J Immunol 2000;165:618–22.

131. Zhang J, Xu K, Ambati B, Yu FS. Toll-like receptor 5-mediated corneal epithelial inflammatory responses to Pseudomonas aeruginosa flagellin. Invest Ophthalmol Vis Sci. 2003;44:4247-54.
132. Malley R, Henneke P, Morse SC, Cieslewicz MJ, Lipsitch M, Thompson CM, Kurt-Jones E, Paton JC, Wessels MR, Golenbock DT. Recognition of pneumolysin by Toll-like receptor 4 confers resistance to pneumococcal infection. Proc Natl Acad Sci U S A 2003;100:1966-71.
133. Chen K, Huang J, Gong W, Iribarren P, Dunlop NM, Wang JM. Toll-like receptors in inflammation, infection and cancer. Int Immunopharmacol. 2007;7:1271-85.
134. Alexopoulou L, Holt AC, Medzhitov R, Flavell RA. Recognition of double-stranded RNA and activation of NF-kappaB by Toll-like receptor 3. Nature 2001;413:732-8.
135. Heil F, Hemmi H, Hochrein H, Ampenberger F, Kirschning C, Akira S, Lipford G, Wagner H, Bauer S. Species-specific recognition of single-stranded RNA via toll-like receptor 7 and 8. Science 2004;303:1526-9.
136. Heil F, Ahmad-Nejad P, Hemmi H, Hochrein H, Ampenberger F, Gellert T, Dietrich H, Lipford G, Takeda K, Akira S, Wagner H, Bauer S. The Toll-like receptor 7 (TLR7)-specific stimulus loxoribine uncovers a strong relationship within the TLR7, 8 and 9 subfamily. Eur J Immunol 2003;33:2987-97.
137. Bauer S, Kirschning CJ, Häcker H, Redecke V, Hausmann S, Akira S, Wagner H, Lipford GB. Human TLR9 confers responsiveness to bacterial DNA via species-specific CpG motif recognition. Proc Natl Acad Sci U S A. 2001;98:9237-42.
138. Blais DR, Vascotto SG, Griffith M, Altosaar I. LBP and CD14 secreted in tears by the lacrimal glands modulate the LPS response of corneal epithelial cells. Invest Ophthalmol Vis Sci. 2005;46:4235-44.
139. Zhang J, Xu K, Ambati B, Yu FS. Toll-like receptor 5-mediated corneal epithelial inflammatory responses to Pseudomonas aeruginosa flagellin. Invest Ophthalmol Vis Sci. 2003;44:4247-54.
140. Redfern RL, McDermott AM. Toll-like receptors in ocular surface disease. Exp Eye Res. 2010;90:679-87.

141. Ebihara N, Yamagami S, Chen L, Tokura T, Iwatsu M, Ushio H, Murakami A. Expression and function of toll-like receptor-3 and -9 in human corneal myofibroblasts. Invest Ophthalmol Vis Sci. 2007;48:3069-76.
142. Prince LR, Whyte MK, Sabroe I, Parker LC. The role of TLRs in neutrophil activation. Curr Opin Pharmacol. 2011;11:397-403.
143. Rathinam VA, Vanaja SK, Waggoner L, Sokolovska A, Becker C, Stuart LM, Leong JM, Fitzgerald KA. TRIF licenses caspase-11-dependent NLRP3 inflammasome activation by gram-negative bacteria. Cell. 2012;150:606-19.
144. Kayagaki N, Warming S, Lamkanfi M, Vande Walle L, Louie S, Dong J, Newton K, Qu Y, Liu J, Heldens S, Zhang J, Lee WP, Roose-Girma M, Dixit VM. Non-canonical inflammasome activation targets caspase-11. Nature. 2011;479:117-21.
145. Watford WT, Moriguchi M, Morinobu A, O'Shea JJ. The biology of IL-12: coordinating innate and adaptive immune responses. Cytokine Growth Factor Rev. 2003;14:361-8.
146. Dinarello CA. Biologic basis for interleukin-1 in disease. Blood 1996;87:2095-147.
147. Xue ML, Wakefield D, Willcox MD, Lloyd AR, Di Girolamo N, Cole N, Thakur A. Regulation of MMPs and TIMPs by IL-1beta during corneal ulceration and infection. Invest Ophthalmol Vis Sci. 2003;44:2020-5.
148. Hogquist KA, Unanue ER, Chaplin DD. Release of IL-1 from mononuclear phagocytes. J Immunol. 1991;147:2181-6.
149. Hazlett LD. Role of innate and adaptive immunity in the pathogenesis of keratitis. Ocul Immunol Inflamm. 2005;13:133-8.
150. Cassatella MA, Meda L, Bonora S, Ceska M, Constantin G. Interleukin 10 (IL-10) inhibits the release of proinflammatory cytokines from human polymorphonuclear leukocytes. Evidence for an autocrine role of tumor necrosis factor and IL-1 beta in mediating the production of IL-8 triggered by lipopolysaccharide. J Exp Med. 1993;178:2207-11.
151. Fukuda M, Mishima H, Otori T. Detection of interleukin-1 beta in the tear fluid of patients with corneal disease with or without conjunctival involvement. Jpn J Ophthalmol. 1997;41:63-6.

152. Cubitt CL, Tang Q, Monteiro CA, Lausch RN, Oakes JE. IL-8 gene expression in cultures of human corneal epithelial cells and keratocytes. Invest Ophthalmol Vis Sci. 1993;34:3199-206.
153. Weng J, Mohan RR, Li Q, Wilson SE. IL-1 upregulates keratinocyte growth factor and hepatocyte growth factor mRNA and protein production by cultured stromal fibroblast cells: interleukin-1 beta expression in the cornea. Cornea. 1997;16:465-71.
154. Gouwy M, Struyf S, Proost P, Van Damme J. Synergy in cytokine and chemokine networks amplifies the inflammatory response. Cytokine Growth Factor Rev. 2005;16:561-80.
155. Hume E, Sack R, Stapleton F, Willcox M. Induction of cytokines from polymorphonuclear leukocytes and epithelial cells by ocular isolates of Serratia marcescens. Ocul Immunol Inflamm. 2004;12:287-95.
156. Wei S, Blanchard DK, Liu JH, Leonard WJ, Djeu JY. Activation of tumor necrosis factor-alpha production from human neutrophils by IL-2 via IL-2-R beta. J Immunol. 1993;150:1979-87.
157. Cole N, Bao S, Willcox M, Husband AJ. TNF-alpha production in the cornea in response to Pseudomonas aeruginosa challenge. Immunol Cell Biol. 1999;77:164-6.
158. Rodrigues DR, Fernandes RK, Balderramas Hde A, Penitenti M, Bachiega TF, Calvi SA, Dias-Melicio LA, Ikoma MR, Soares ÂM. Interferon-gamma production by human neutrophils upon stimulation by IL-12, IL-15 and IL-18 and challenge with Paracoccidioides brasiliensis. Cytokine. 2014;69:102-9.
159. Spees AM, Kingsbury DD, Wangdi T, Xavier MN, Tsolis RM, Bäumler AJ. Neutrophils are a source of gamma interferon during acute Salmonella enterica serovar Typhimurium colitis. Infect Immun. 2014;82:1692-7.
160. Ma X, Chow JM, Gri G, Carra G, Gerosa F, Wolf SF, Dzialo R, Trinchieri G. The interleukin-12 p40 gene promoter is primed by interferon-g in monocytic cells. J Exp Med. 1996;183:147–57.
161. Hazlett LD, Rudner XL, McClellan SA, Barrett RP, Lighvani S. Role of IL-12 and IFN-gamma in Pseudomonas aeruginosa corneal infection. Invest Ophthalmol Vis Sci. 2002;43:419-24.
162. Locksley RM. Interleukin 12 in host defense against microbial pathogens. Proc Natl Acad Sci U S A. 1993;90:5879-80.

163. Bohn E, Autenrieth IB. IL-12 is essential for resistance against Yersinia enterocolitica by triggering IFN-gamma production in NK cells and CD4+ T cells. J Immunol. 1996;156:1458-68.
164. Akira S, Takeda K, Kaisho T. Toll-like receptors: critical proteins linking innate and acquired immunity. Nat Immunol. 2001;2:675–80.
165. Medzhitov R. Toll-like receptors and innate immunity. Nat Rev Immunol. 2001;1:135–45.
166. Sadrai Z, Hajrasouliha AR, Chauhan S, Saban DR, Dastjerdi MH, Dana R. Effect of topical azithromycin on corneal innate immune responses. Invest Ophthalmol Vis Sci. 2011;52:2525-31.
167. Xing Z, Gauldie J, Cox G, Baumann H, Jordana M, Lei XF, Achong MK. IL-6 is an anti-inflammatory cytokine required for controlling local or systemic acute inflammatory responses. J Clin Invest. 1998;101:311-20.
168. Cole N, Krockenberger M, Bao S, Beagley KW, Husband AJ, Willcox M. Effects of exogenous interleukin-6 during Pseudomonas aeruginosa corneal infection. Infect Immun. 2001;69:4116-9.
169. Xue ML, Willcox MD, Lloyd A, Wakefield D, Thakur A. Regulatory role of IL-1beta in the expression of IL-6 and IL-8 in human corneal epithelial cells during Pseudomonas aeruginosa colonization. Clin Experiment Ophthalmol. 2001;29:171-4.
170. Hoge J, Yan I, Jänner N, Schumacher V, Chalaris A, Steinmetz OM, Engel DR, Scheller J, Rose-John S, Mittrücker HW. IL-6 controls the innate immune response against Listeria monocytogenes via classical IL-6 signaling. J Immunol. 2013;190:703-11.
171. Carnt NA, Willcox MD, Hau S, Garthwaite LL, Evans VE, Radford CF, Dart JK, Chakrabarti S, Stapleton F. Association of single nucleotide polymorphisms of interleukins-1β, -6, and -12B with contact lens keratitis susceptibility and severity. Ophthalmology. 2012;119:1320-7.
172. Borish L. IL-10: evolving concepts. J Allergy Clin Immunol. 1998;101:293-7.
173. Wanidworanun C, Strober W. Predominant role of tumor necrosis factor-alpha in human monocyte IL-10 synthesis. J Immunol. 1993;151:6853-61.
174. De Santo C, Arscott R, Booth S, Karydis I, Jones M, Asher R, Salio M, Middleton M, Cerundolo V. Invariant NKT cells modulate the suppressive

activity of IL-10-secreting neutrophils differentiated with serum amyloid A. Nat Immunol. 2010;11:1039-46.

175. Mantovani A, Cassatella MA, Costantini C, Jaillon S. Neutrophils in the activation and regulation of innate and adaptive immunity. Nat Rev Immunol. 2011;11:519-31.

176. Cole N, Krockenberger M, Stapleton F, Khan S, Hume E, Husband AJ, Willcox M. Experimental Pseudomonas aeruginosa keratitis in interleukin-10 gene knockout mice. Infect Immun. 2003;71:1328-36.

177. Dai WJ, Köhler G, Brombacher F. Both innate and acquired immunity to Listeria monocytogenes infection are increased in IL-10-deficient mice. J Immunol. 1997;158:2259-67.

178. Rosenbloom AJ, Linden PK, Dorrance A, Penkosky N, Cohen-Melamed MH, Pinsky MR. Effect of granulocyte-monocyte colony-stimulating factor therapy on leukocyte function and clearance of serious infection in nonneutropenic patients. Chest. 2005;127:2139-50.

179. Karicherla P, Aras S, Aiyar A, Hobden JA. Nona-D-arginine amide suppresses corneal cytokines in Pseudomonas aeruginosa keratitis. Cornea. 2010;29:1308-14.

180. Wong Y, Sethu C, Louafi F, Hossain P. Lipopolysaccharide Regulation of Toll-Like Receptor-4 and Matrix Metalloprotease-9 in Human Primary Corneal Fibroblasts. Invest Ophthalmol Vis Sci. 2011;52:2796-2803.

181. Duan R, Remeijer L, van Dun JM, Osterhaus AD, Verjans GM. Granulocyte macrophage colony-stimulating factor expression in human herpetic stromal keratitis: implications for the role of neutrophils in HSK. Invest Ophthalmol Vis Sci. 2007;48:277-84.

182. Chegou NN, Heyckendorf J, Walzl G, Lange C, Ruhwald M. Beyond the IFN-γ horizon: biomarkers for immunodiagnosis of infection with Mycobacterium tuberculosis. Eur Respir J. 2014;43:1472-86.

183. Fehniger TA, Cooper MA, Caligiuri MA. Interleukin-2 and interleukin-15: immunotherapy for cancer. Cytokine Growth Factor Rev. 2002;13:169-83.

184. Djeu JY, Liu JH, Wei S, Rui H, Pearson CA, Leonard WJ, Blanchard DK. Function associated with IL-2 receptor-beta on human neutrophils. Mechanism of activation of antifungal activity against Candida albicans by IL-2. J Immunol. 1993;150:960-70.

185. Kellar KL, Gehrke J, Weis SE, Mahmutovic-Mayhew A, Davila B, Zajdowicz MJ, Scarborough R, LoBue PA, Lardizabal AA, Daley CL, Reves RR, Bernardo J, Campbell BH, Whitworth WC, Mazurek GH. Multiple cytokines are released when blood from patients with tuberculosis is stimulated with Mycobacterium tuberculosis Antigens. PLoS ONE 2011; 6: e26545.

186. Huang X, McClellan SA, Barrett RP, Hazlett LD. IL-18 contributes to host resistance against infection with Pseudomonas aeruginosa through induction of IFN-gamma production. J Immunol. 2002;168:5756-63.

187. Lamkanfi M, Dixit VM. Mechanisms and functions of inflammasomes. Cell. 2014;157:1013-22.

188. Bae GH, Kim JR, Kim CH, Lim DH, Chung ES, Chung TY. Corneal topographic and tomographic analysis of fellow eyes in unilateral keratoconus patients using Pentacam. Am J Ophthalmol. 2014;157:103-109.

189. Brittingham S, Tappeiner C, Frueh BE. Corneal cross-linking in keratoconus using the standard and rapid treatment protocol: differences in demarcation line and 12-month outcomes. Invest Ophthalmol Vis Sci. 2014;55:8371-6.

190. Mazzotta C, Traversi C, Baiocchi S, Caporossi O, Bovone C, Sparano MC, Balestrazzi A, Caporossi A. Corneal healing after riboflavin ultraviolet-A collagen cross-linking determined by confocal laser scanning microscopy in vivo: early and late modifications. Am J Ophthalmol. 2008;146:527-533.

191. Roberts HW, Mukherjee A, Aichner H, Rajan MS. Visual Outcomes and Graft Thickness in Microthin DSAEK-One-Year Results. Cornea. 2015;34:1345-50.

192. Mencucci R, Favuzza E, Tartaro R, Busin M, Virgili G. Descemet stripping automated endothelial keratoplasty in Fuchs' corneal endothelial dystrophy: anterior segment optical coherence tomography and in vivo confocal microscopy analysis. BMC Ophthalmol. 2015;15:99.

193. Shinton AJ, Tsatsos M, Konstantopoulos A, Goverdhan S, Elsahn AF, Anderson DF, Hossain P. Impact of graft thickness on visual acuity after Descemet's stripping endothelial keratoplasty. Br J Ophthalmol. 2012;96:246-9.

194. Garcia JP Jr, Ritterband DC, Buxton DF, De la Cruz J. Evaluation of the stability of Boston type I keratoprosthesis-donor cornea interface using anterior segment optical coherence tomography. Cornea. 2010;29:1031-5.
195. Shapiro BL, Cortés DE, Chin EK, Li JY, Werner JS, Redenbo E, Mannis MJ. High-resolution spectral domain anterior segment optical coherence tomography in type 1 Boston keratoprosthesis. Cornea. 2013;32:951-5.
196. Konstantopoulos A, Hossain PH, Anderson DF. Recent advances in ophthalmic anterior segment imaging: a new era for ophthalmic diagnosis? Br J Ophthalmol. 2007; 91: 551-557.
197. Cairns G and McGee CNJ. Orbscan computerised topography: Attributes, applications and limitations. J Cataract Refract Surg. 2005; 31:205-220.
198. Németh J, Erdélyi B, Csákány B. Corneal topography changes after a 15 second pause in blinking. J Cataract Refract Surg. 2001;27:589-92.
199. Kamiya K, Oshika T. Corneal forward shift after excimer laser keratorefractive surgery. Semin Ophthalmol. 2003;18:17–22.
200. Rao SN, Raviv T, Majmudar PA, Epstein RJ. Role of Orbscan II in screening keratoconus suspects before refractive corneal surgery. Ophthalmology. 2002;109:1642-6.
201. Khurana RN, Li Y, Tang M, Lai MM, Huang D. High-speed optical coherence tomography of corneal opacities. Ophthalmology. 2007;114:1278-1285.
202. Masters BR. Three-dimensional microscopic tomographic imaging of the cataract in a human lens in vivo. Optics Express. 1998; 3:332-338.
203. Buehl W, Stojanac D, Sacu S, Drexler W and Findl O. Comparison of three methods of measuring corneal thickness and anterior chamber depth. Am J Ophthalmol. 2006; 141:7-12.
204. Otri AM, Fares U, Al-Aqaba MA, Dua HS. Corneal densitometry as an indicator of corneal health. Ophthalmology. 2012;119:501-8.
205. Zhivov A, Stachs O, Stave J, Guthoff RF. In vivo three-dimensional confocal laser scanning microscopy of corneal surface and epithelium. Br J Ophthalmol. 2009;93:667-72.
206. Petroll WM, Weaver M, Vaidya S, McCulley JP, Cavanagh HD. Quantitative 3-dimensional corneal imaging in vivo using a modified HRT-RCM confocal microscope. Cornea. 2013;32:e36-43.

207. Labbé A, Niaudet P, Loirat C, Charbit M, Guest G, Baudouin C. In vivo confocal microscopy and anterior segment optical coherence tomography analysis of the cornea in nephropathic cystinosis. Ophthalmology. 2009;116:870-6.
208. Villani E, Galimberti D, Viola F, Mapelli C, Ratiglia R. The cornea in Sjogren's syndrome: an in vivo confocal study. Invest Ophthalmol Vis Sci. 2007;48:2017-22.
209. Lin H, Li W, Dong N, Chen W, Liu J, Chen L, Yuan H, Geng Z, Liu Z. Changes in corneal epithelial layer inflammatory cells in aqueous tear-deficient dry eye. Invest Ophthalmol Vis Sci. 2010;51:122-8.
210. Hamrah P, Sahin A, Dastjerdi MH, Shahatit BM, Bayhan HA, Dana R, Pavan-Langston D. Cellular changes of the corneal epithelium and stroma in herpes simplex keratitis: an in vivo confocal microscopy study. Ophthalmology. 2012;119:1791-7.
211. Kanavi MR, Javadi M, Yazdani S, Mirdehghanm S. Sensitivity and specificity of confocal scan in the diagnosis of infectious keratitis. Cornea. 2007; 26:782–786.
212. Tu EY, Joslin CE, Sugar J, Booton GC, Shoff ME, Fuerst PA. The relative value of confocal microscopy and superficial corneal scrapings in the diagnosis of acanthamoeba keratitis. Cornea. 2008; 27:764–772.
213. Hau SC, Dart JK, Vesaluoma M, Parmar DN, Claerhout I, Bibi K, Larkin DF. Diagnostic accuracy of microbial keratitis with in vivo scanning laser confocal microscopy. Br J Ophthalmol. 2010; 94:982–987.
214. Villani E, Baudouin C, Efron N, Hamrah P, Kojima T, Patel SV, Pflugfelder SC, Zhivov A, Dogru M. In vivo confocal microscopy of the ocular surface: from bench to bedside. Curr Eye Res. 2014;39:213-31.
215. Labbé A, Khammari C, Dupas B, Gabison E, Brasnu E, Labetoulle M, Baudouin C. Contribution of in vivo confocal microscopy to the diagnosis and management of infectious keratitis. Ocul Surf. 2009;7:41-52.
216. Lin H, Li W, Dong N, Chen W, Liu J, Chen L, Yuan H, Geng Z, Liu Z. Changes in corneal epithelial layer inflammatory cells in aqueous tear-deficient dry eye. Invest Ophthalmol Vis Sci. 2010;51:122-8.
217. Yamaguchi T, Calvacanti BM, Cruzat A, Qazi Y, Ishikawa S, Osuka A, Lederer J, Hamrah P. Correlation between human tear cytokine levels and

cellular corneal changes in patients with bacterial keratitis by in vivo confocal microscopy. Invest Ophthalmol Vis Sci. 2014;55:7457-66.

218. Amar N, Labbé A, Hamard P, Dupas B, Baudouin C. Filtering blebs and aqueous pathway an immunocytological and in vivo confocal microscopy study. Ophthalmology 2008;115:1154-1161.

219. Labbe A, Dupas B, Hamard P, Baudouin C. In vivo confocal microscopy study of blebs after filtering surgery. Ophthalmology 2005;112:1979-1986.

220. Qazi Y, Kheirkhah A, Blackie C, Cruzat A, Trinidad M, Williams C, Korb DR, Hamrah P. In vivo detection of clinically non-apparent ocular surface inflammation in patients with meibomian gland dysfunction-associated refractory dry eye symptoms: a pilot study. Eye. 2015;29:1099-110.

221. Radhakrishnan S, Goldsmith J, Huang D, Westphal V, Dueker DK, Rollins AM, Izatt JA and Smith SD. Comparison of optical coherence tomography and ultrasound biomicroscopy for detection of narrow anterior chamber angles. Arch Ophthalmol 2005; 123:1053-1059.

222. Goldsmith JA, Li Y, Chalita MR, Westphal V, Patil CA, Rollins AM, Izatt JA, Huang D. Anterior chamber width measurement by high-speed optical coherence tomography. Ophthalmology 2005; 112:238-244.

223. Fercher AF. Optical coherence tomography. J Biomed Opt. 1996;1:157-73.

224. Fercher AF. Optical coherence tomography - development, principles, applications. Z Med Phys. 2010;20:251-76.

225. Jancevski M, Foster CS. Anterior segment optical coherence tomography. Semin Ophthalmol. 2010;25:317–323.

226. Bald M, Li Y, Huang D. Anterior chamber angle evaluation with fourier-domain optical coherence tomography. J Ophthalmol. 2012;2012:103704.

227. Konstantopoulos A, Hossain P. Limitations of Fourier-domain OCT. J Cataract Refract Surg. 2010;36:534.

228. Memarzadeh F, Li Yan, Francis BA, Smith RE, Gutmark J, Huang D. Optical coherence tomography of the anterior segment in secondary glaucoma with corneal opacity after penetrating keratoplasty. Br J Ophthalmol. 2007;91:189-192.

229. Sarodia U, Sharkawi E, Hau S, Barton K. Visualisation of aqueous shunt position and patency using anterior segment optical tomography. Am J Ophthalmol. 2007; 143:1054-1056.

230. Lim LS, Aung HT, Aung T, Tan DTH. Corneal imaging with anterior segment optical coherence tomography for lamellar keratoplasty procedures. Am J Ophthalmol. 2008;145:81-90.
231. Li Y, Shekhar R and Huang D. Corneal pachymetry mapping with high-speed optical coherence tomography. Ophthalmology. 2006; 113:792-799.
232. Leung CK, Yick DW, Kwong YY, Li FC, Leung DY, Mohamed S, Tham CC, Chung-chai C, Lam DS. Analysis of bleb morphology after trabeculectomy with Visante anterior segment optical coherence tomography. Br J Ophthalmol. 2007;91:340-4.
233. Singh M, Aung T, Friedman DS, Zheng C, Foster PJ, Nolan WP, See JL, Smith SD, Chew PT. Anterior segment optical coherence tomography imaging of trabeculectomy blebs before and after laser suture lysis. Am J Ophthalmol. 2007;143:873-5.
234. Qin B, Chen S, Brass R, Li Y, Tang M, Zhang X, Wang X, Wang Q, Huang D. Keratoconus diagnosis with optical coherence tomography–based pachymetric scoring system. J Cataract Refract Surg. 2013;39:1864-71.
235. Li Y, Tan O, Brass R, Weiss JL, Huang D. Corneal epithelial thickness mapping by Fourier-domain optical coherence tomography in normal and keratoconic eyes. Ophthalmology. 2012;119:2425-33.
236. El Sanharawi M, Sandali O, Basli E, Bouheraoua N, Ameline B, Goemaere I, Georgeon C, Hamiche T, Borderie V, Laroche L. Fourier-domain optical coherence tomography imaging in corneal epithelial basement membrane dystrophy: a structural analysis. Am J Ophthalmol. 2015;159:755-63.
237. Samy El Gendy NM, Li Y, Zhang X, Huang D. Repeatability of pachymetric mapping using fourier domain optical coherence tomography in corneas with opacities. Cornea. 2012;31:418-23.
238. Soliman W, Fathalla AM, El-Sebaity DM, Al-Hussaini AK. Spectral domain anterior segment optical coherence tomography in microbial keratitis. Graefes Arch Clin Exp Ophthalmol. 2013;251:549-53.
239. Wylegała E, Teper S, Nowinska AK, Milka M, Dobrowolski D. Anterior segment imaging: Fourier-domain optical coherence tomography versus time-domain optical coherence tomography. J Cataract Refract Surg. 2009;35:1410-4.
240. World Medical Association Declaration of Helsinki: Ethical Principles for Medical Research Involving Human Subjects. JAMA. 2013;310:2191-2194.

241. Li H, Leung CK, Wong L, Cheung CY, Pang CP, Weinreb RN, Lam DS. Comparative study of central corneal thickness measurement with slit-lamp optical coherence tomography and visante optical coherence tomography. Ophthalmology. 2008;115:796-801.

242. Tan XW, Promoda A, Perera P, Tan A, Tan D, Khor KA, Beuerman RW, Mehta JS. Comparison of candidate materials for a synthetic Osteo-Odonto Keratoprosthesis (OOKP) device. Invest Ophthalmol Vis Sci. 2011;52:21–29.

243. Todani A, Ciolino JB, Ament JD, Colby KA, Pineda R, Belin MW, Aquavella JV, Chodosh J, Dohlman CH. Titanium back plate for a PMMA keratoprosthesis: clinical outcomes. Graefes Arch Clin Exp Ophthalmol. 2011;249:1515-8.

244. Johnson MK, Hobden JA, Hagenah M, O'Callaghan RJ, Hill JM, Chen S. 1990. The role of pneumolysin in ocular infections with Streptococcus pneumoniae. Curr Eye Res. 1990;9:1107-1114.

245. Calafat J, Kuijpers TW, Janssen H, Borregaard N, Verhoeven AJ, Roos D. Evidence for small intracellular vesicles in human blood phagocytes containing cytochrome b558 and the adhesion molecule CD11b/CD18. Blood. 1993;81:3122-9.

246. Thiagarajah JR, Verkman AS. Aquaporin deletion in mice reduces corneal water permeability and delays restoration of transparency after swelling. J Biol Chem. 2002;277:19139-44.

247. von Fischern T, Lorenz U, Burchard WG, Reim M, Schrage NF. Changes in mineral composition of rabbit corneas after alkali burn. Graefes Arch Clin Exp Ophthalmol. 1998;236:553-8.

248. McLeod SD, LaBree LD, Tayyanipour R, Flowers CW, Lee PP, McDonnell PJ. The importance of initial management in the treatment of severe infectious corneal ulcers. Ophthalmology. 1995;102:1943-1948.

249. Thakur A, Xue M, Stapleton F, Lloyd AR, Wakefield D, Willcox MD. Balance of pro- and anti-inflammatory cytokines correlates with outcome of acute experimental Pseudomonas aeruginosa keratitis. Infect Immun. 2002;70:2187-97.

250. Sloop GD, Moreau JM, Conerly LL, Dajcs JJ, O'Callaghan RJ. Acute inflammation of the eyelid and cornea in Staphylococcus keratitis in the rabbit. Invest Ophthalmol Vis Sci. 1999;40:385-91.

251. O'Donnell C, Maldonado-Codina C. Agreement and repeatability of central thickness measurement in normal corneas using ultrasound pachymetry and the OCULUS Pentacam. Cornea. 2005;24:920-924.
252. de Sanctis U, Missolungi A, Mutani B, Richiardi L, Grignolo FM. Reproducibility and repeatability of central corneal thickness measurement in keratoconus using the rotating Scheimpflug camera and ultrasound pachymetry. Am J Ophthalmol. 2007;144:712-718.
253. Al-Mohtaseb ZN, Wang L, Weikert MP. Repeatability and comparability of corneal thickness measurements obtained from Dual Scheimpflug Analyzer and from ultrasonic pachymetry. Graefes Arch Clin Exp Ophthalmol. 2013;251:1855-1860.
254. Williams R, Fink BA, King-Smith PE, Mitchell GL. Central corneal thickness measurements: using an ultrasonic instrument and 4 optical instruments. Cornea. 2011;30:1238-1243.
255. Tauber J, Sainz de la Maza M, Hoang-Xuan T, Foster CS. An analysis of therapeutic decision making regarding immunosuppressive chemotherapy for peripheral ulcerative keratitis. Cornea. 1990;9:66-73.
256. Sainz de la Maza M, Foster CS, Jabbur NS, Baltatzis S. Ocular characteristics and disease associations in scleritis-associated peripheral keratopathy. Arch Ophthalmol. 2002;120:15-9.
257. Konstantopoulos A, Kuo J, Anderson DF and Hossain PN. Assessment of the use of anterior segment optical coherence tomography in microbial keratitis. Am J Ophthalmol. 2008;146:534-542.
258. Shaheen BS, Bakir M, Jain S. Corneal nerves in health and disease. Surv Ophthalmol. 2014;59:263-285.
259. Statistical treatment of analytical data. By Zeev B. Alfassi. Chapter 4. Confidence limits of the mean. Pg 39. Blackwell Science Ltd.
260. Mohamed S, Lee GK, Rao SK, Wong AL, Cheng AC, Li EY, Chi SC, Lam DS. Repeatability and reproducibility of pachymetric mapping with Visante anterior segment-optical coherence tomography. Invest Ophthalmol Vis Sci. 2007;48:5499-504.
261. Motreff P, Levesque S, Souteyrand G, Sarry L, Ouchchane L, Citron B, Cassagnes J, Lusson JR. High-resolution coronary imaging by optical coherence tomography: Feasibility, pitfalls and artefact analysis. Arch Cardiovasc Dis. 2010;103:215-26.

262. Armstrong WB, Ridgway JM, Vokes DE, Guo S, Perez J, Jackson RP, Gu M, Su J, Crumley RL, Shibuya TY, Mahmood U, Chen Z, Wong BJ. Optical coherence tomography of laryngeal cancer. Laryngoscope. 2006 Jul;116:1107-13.

263. Hatta W, Uno K, Koike T, Yokosawa S, Iijima K, Imatani A, Shimosegawa T. Optical coherence tomography for the staging of tumor infiltration in superficial oesophageal squamous cell carcinoma. Gastrointest Endosc. 2010;71:899-906.

264. Sakata LM, Lavanya R, Friedman DS, Aung HT, Seah SK, Foster PJ, Aung T. Assessment of the scleral spur in anterior segment optical coherence tomography images. Arch Ophthalmol. 2008;126:181-5.

265. Tan GS, He M, Zhao W, Sakata LM, Li J, Nongpiur ME, Lavanya R, Friedman DS, Aung T. Determinants of lens vault and association with narrow angles in patients from Singapore. Am J Ophthalmol. 2012;154:39-46.

266. Fiore T, Androudi S, Iaccheri B, Lupidi M, Giansanti F, Fruttini D, Biondi L, Cagini C. Repeatability and reproducibility of retinal thickness measurements in diabetic patients with spectral domain optical coherence tomography. Curr Eye Res. 2013;38:674-9.

267. Cheng AC, Ho T, Lau S, Wong AL, Leung C, Lam DS. Measurement of LASIK flap thickness with anterior segment optical coherence tomography. J Refract Surg. 2008;24:879-84.

268. Hall RC, Mohamed FK, Htoon HM, Tan DT, Mehta JS. Laser in situ keratomileusis flap measurements: Comparison between observers and between spectral-domain and time-domain anterior segment optical coherence tomography. J Cataract Refract Surg. 2011;37:544-51.

269. Leung CK, Cheung CY, Weinreb RN, Qiu Q, Liu S, Li H, Xu G, Fan N, Huang L, Pang CP, Lam DS. Retinal nerve fiber layer imaging with spectral-domain optical coherence tomography: a variability and diagnostic performance study. Ophthalmology. 2009;116:1257-63.

270. Bourges JL, Alfonsi N, Laliberté JF, Chagnon M, Renard G, Legeais JM, Brunette I. Average 3-dimensional models for the comparison of Orbscan II and Pentacam pachymetry maps in normal corneas. Ophthalmology. 2009;116:2064-71.

271. Kim HY, Budenz DL, Lee PS, Feuer WJ, Barton K. Comparison of central corneal thickness using anterior segment optical coherence tomography vs. ultrasound pachymetry. Am J Ophthalmol. 2008;145:228-232.
272. Francoz M, Karamoko I, Baudouin C, Labbé A. Ocular surface epithelial thickness evaluation with spectral-domain optical coherence tomography. Invest Ophthalmol Vis Sci. 2011;52:9116-23.
273. Martola E-L and Baum JL. Central and peripheral corneal thickness: a clinical study. Arch Ophthalmol. 1968;79:28.
274. Chan T, Payor S, Holden BA. Corneal thickness profiles in rabbits using an ultrasonic pachometer. Invest Ophthalmol Vis Sci. 1983;24:1408-10.
275. Liu Z, Huang AJ, Pflugfelder SC. Evaluation of corneal thickness and topography in normal eyes using the Orbscan corneal topography system. Br J Ophthalmol. 1999;83:774-8.
276. Fares U, Otri AM, Al-Aqaba MA, Dua HS. Correlation of central and peripheral corneal thickness in healthy corneas. Cont Lens Anterior Eye. 2012;35:39-45.
277. Rio-Cristobal A, Martin R, Morejon A, Galarreta D. Inter-examiner agreement of the AS-OCT Visante corneal thickness. J Optom. 2011;4:95-102.
278. Srinivasan M, Mascarenhas J, Rajaraman R, Ravindran M, Lalitha P, Glidden DV, Ray KJ, Hong KC, Oldenburg CE, Lee SM, Zegans ME, McLeod SD, Lietman TM, Acharya NR; Steroids for Corneal Ulcers Trial Group. Corticosteroids for bacterial keratitis: the Steroids for Corneal Ulcers Trial (SCUT). Arch Ophthalmol. 2012;130:143-50.
279. Abadia B, Ferreras A, Calvo P, Ara M, Ferrandez B, Otin S, Frezzotti P, Pablo LE, Figus M. Relationship between spectral-domain optical coherence tomography and standard automated perimetry in healthy and glaucoma patients. Biomed Res Int. 2014;2014:514948.
280. Ballae Ganeshrao S, Turpin A, Denniss J, McKendrick AM. Enhancing Structure-Function Correlations in Glaucoma with Customized Spatial Mapping. Ophthalmology. 2015;122:1695-705.
281. Pollet-Villard F, Chiquet C, Romanet JP, Noel C, Aptel F. Structure-function relationships with spectral-domain optical coherence tomography retinal nerve fiber layer and optic nerve head measurements. Invest Ophthalmol Vis Sci. 2014;55:2953-62.

282. Lisboa R, Paranhos A Jr, Weinreb RN, Zangwill LM, Leite MT, Medeiros FA. Comparison of different spectral domain OCT scanning protocols for diagnosing preperimetric glaucoma. Invest Ophthalmol Vis Sci. 2013;54:3417-25.

283. Alasil T, Keane PA, Updike JF, Dustin L, Ouyang Y, Walsh AC, Sadda SR. Relationship between optical coherence tomography retinal parameters and visual acuity in diabetic macular edema. Ophthalmology. 2010;117:2379-86.

284. Noma H, Mimura T, Shimada K. Retinal function and morphology in central retinal vein occlusion with macular edema. Curr Eye Res. 2013;38:143-9.

285. Divaris K, Vann WF Jr, Baker AD, Lee JY. Examining the accuracy of caregivers' assessments of young children's oral health status. J Am Dent Assoc. 2012;143:1237-1247.

286. Evans, JD. Straightforward Statistics for the Behavioral Sciences. Brooks/Cole Publishing; Pacific Grove, Calif.:1996.

287. Abbouda A, Estrada AV, Rodriguez AE, Alio JL. Anterior segment optical coherence tomography in evaluation of severe fungal keratitis infections treated by corneal crosslinking. Eur J Ophthalmol 2014;24:320-4.

288. Martone G, Pichierri P, Franceschini R, Moramarco A, Ciompi L, Tosi GM, Balestrazzi A. In vivo confocal microscopy and anterior segment optical coherence tomography in a case of alternaria keratitis. Cornea 2011;30:449-53.

289. Li Q, Kumar A, Gui JF, Yu FS. Staphylococcus aureus lipoproteins trigger human corneal epithelial innate response through toll-like receptor-2. Microb Pathog. 2008; 44:426-34.

290. Zaidi TS, Zaidi T, Pier GB. Role of neutrophils, MyD88-mediated neutrophil recruitment, and complement in antibody-mediated defense against Pseudomonas aeruginosa keratitis. Invest Ophthalmol Vis Sci. 2010; 51:2085-2093.

291. Hazlett LD and Hendricks RL. Reviews for immune privilege in the year 2010: immune privilege and infection. Ocul Immunol & Inflamm. 2010; 18:237–243.

292. Riau AK, Liu YC, Lwin NC, Ang HP, Tan NY, Yam GH, Tan DT, Mehta JS. Comparative study of nJ- and μJ-energy level femtosecond lasers: evaluation of flap adhesion strength, stromal bed quality, and tissue responses. Invest Ophthalmol Vis Sci. 2014;55:3186-3194.

293. Chusid MJ, Nelson DB, Meyer LA. The role of the polymorphonuclear leukocyte in the induction of corneal edema. Invest Ophthalmol Vis Sci. 1986; 27:1466-9.

294. Hindman HB, Huxlin KR, Pantanelli SM, Callan CL, Sabesan R, Ching SS, Miller BE, Martin T, Yoon G. Post-DSAEK optical changes: a comprehensive prospective analysis on the role of ocular wavefront aberrations, haze, and corneal thickness. Cornea. 2013;32:1567-77.

295. Marquart ME. Animal models of bacterial keratitis. J Biomed Biotechnol. 2011:680642.

296. Wallin A, Sue-Chu M, Bjermer L, Ward J, Sandström T, Lindberg A, Lundbäck B, Djukanović R, Holgate S, Wilson S. Effect of inhaled fluticasone with and without salmeterol on airway inflammation in asthma. J Allergy Clin Immunol. 2003;112:72-8.

297. Uddin M, Nong G, Ward J, Seumois G, Prince LR, Wilson SJ, Cornelius V, Dent G, Djukanovic R. Prosurvival activity for airway neutrophils in severe asthma. Thorax. 2010;65:684-9.

298. Haslett C. Granulocyte apoptosis and inflammatory disease. Br Med Bull 1997;53:669–83.

299. Allan BD, Dart JK. Strategies for the management of microbial keratitis. Br J Ophthalmol. 1995;79:777-86.

300. Ray KJ, Srinivasan M, Mascarenhas J, Rajaraman R, Ravindran M, Glidden DV, Oldenburg CE, Sun CQ, Zegans ME, McLeod SD, Acharya NR, Lietman TM. Early addition of topical corticosteroids in the treatment of bacterial keratitis. JAMA Ophthalmol. 2014;132:737-41.

301. Cohen EJ. The case against the use of steroids in the treatment of bacterial keratitis. Arch Ophthalmol. 2009;127:103-4.

302. Lee HS, Hattori T, Park EY, Stevenson W, Chauhan SK, Dana R. Expression of toll-like receptor 4 contributes to corneal inflammation in experimental dry eye disease. Invest Ophthalmol Vis Sci. 2012;53:5632-40.

303. Karthikeyan RS, Priya JL, Leal SM Jr, Toska J, Rietsch A, Prajna V, Pearlman E, Lalitha P. Host response and bacterial virulence factor expression in

Pseudomonas aeruginosa and Streptococcus pneumoniae corneal ulcers. PLoS One. 2013;8:e64867.

304. Jin X, Qin Q, Tu L, Qu J. Glucocorticoids inhibit the innate immune system of human corneal fibroblast through their suppression of toll-like receptors. Mol Vis. 2009;15:2435-41.

305. Ellis TN, Beaman BL. Interferon-gamma activation of polymorphonuclear neutrophil function. Immunology. 2004;112:2-12.

306. Hume EB, Cole N, Garthwaite LL, Khan S, Willcox MD. A protective role for IL-6 in staphylococcal microbial keratitis. Invest Ophthalmol Vis Sci. 2006;47:4926-30.

307. Ramchandran RS, Diloreto DA Jr, Chung MM, Kleinman DM, Plotnik RP, Graman P, Aquavella JV. Infectious endophthalmitis in adult eyes receiving Boston type I keratoprosthesis. Ophthalmology. 2012;119:674-81.

308. Durand ML, Dohlman CH. Successful prevention of bacterial endophthalmitis in eyes with the Boston keratoprosthesis. Cornea. 2009;28:896-901.

309. Barnes SD, Dohlman CH, Durand ML. Fungal colonization and infection in Boston keratoprosthesis. Cornea. 2007;26:9-15.

310. Dohlman CH, Dudenhoefer EJ, Khan BF, Morneault S. Protection of the ocular surface after keratoprosthesis surgery: the role of soft contact lenses. CLAO J. 2002;28:72-4.

311. Harissi-Dagher M, Khan BF, Schaumberg DA, Dohlman CH. Importance of nutrition to corneal grafts when used as a carrier of the Boston Keratoprosthesis. Cornea. 2007;26:564-8.

312. Rybak MJ. The pharmacokinetic and pharmacodynamic properties of vancomycin. Clin Infect Dis. 2006;42:Suppl 1:S35-9.

313. LaPlante KL, Rybak MJ. Impact of high-inoculum Staphylococcus aureus on the activities of nafcillin, vancomycin, linezolid, and daptomycin, alone and in combination with gentamicin, in an in vitro pharmacodynamic model. Antimicrob Agents Chemother. 2004;48:4665-72.

314. Cahane M, Ben Simon GJ, Barequet IS, Grinbaum A, Diamanstein-Weiss L, Goller O, Rubinstein E, Avni I. Human corneal stromal tissue concentration after consecutive doses of topically applied 3.3% vancomycin. Br J Ophthalmol. 2004;88:22-24.

315. Olthoff CM, Schouten JS, van de Borne BW, Webers CA. Noncompliance with ocular hypotensive treatment in patients with glaucoma or ocular hypertension an evidence-based review. Ophthalmology. 2005;112:953-61.
316. Okeke CO, Quigley HA, Jampel HD, Ying GS, Plyler RJ, Jiang Y, Friedman DS. Adherence with topical glaucoma medication monitored electronically the Travatan Dosing Aid study. Ophthalmology. 2009;116:191-9.
317. Natarajan JV, Darwitan A, Barathi VA, Ang M, Htoon HM, Boey F, Tam KC, Wong TT, Venkatraman SS. Sustained drug release in nanomedicine: a long-acting nanocarrier-based formulation for glaucoma. ACS Nano. 2014;8:419-29.
318. Alves D, Olívia Pereira M. Mini-review: Antimicrobial peptides and enzymes as promising candidates to functionalize biomaterial surfaces. Biofouling. 2014;30:483-99.
319. Li Y, Tang M, Zhang X, Salaroli CH, Ramos JL, Huang D. Pachymetric mapping with Fourier-domain optical coherence tomography. J Cataract Refract Surg. 2010;36:826-831.
320. Tsikata E, Lee R, Shieh E, Simavli H, Que CJ, Guo R, Khoueir Z, de Boer J, Chen TC. Comprehensive Three-Dimensional Analysis of the Neuroretinal Rim in Glaucoma Using High-Density Spectral-Domain Optical Coherence Tomography Volume Scans. Invest Ophthalmol Vis Sci. 2016;57:5498-5508.
321. Akashi A, Kanamori A, Nakamura M, Fujihara M, Yamada Y, Negi A. Comparative assessment for the ability of Cirrus, RTVue, and 3D-OCT to diagnose glaucoma. Invest Ophthalmol Vis Sci. 2013;54:4478-4484.
322. Radha S, Afroz T, Prasad S, Ravindra N. Diagnostic utility of bronchoalveolar lavage. J Cytol. 2014;31:136-8.
323. Srinivasan M, Mascarenhas J, Rajaraman R, Ravindran M, Lalitha P, Glidden DV, Ray KJ, Hong KC, Oldenburg CE, Lee SM, Zegans ME, McLeod SD, Lietman TM, Acharya NR; Steroids for Corneal Ulcers Trial Group. The steroids for corneal ulcers trial: study design and baseline characteristics. Arch Ophthalmol. 2012;130:151-7.
324. Liu L, Chu KK, Houser GH, Diephuis BJ, Li Y, Wilsterman EJ, Shastry S, Dierksen G, Birket SE, Mazur M, Byan-Parker S, Grizzle WE, Sorscher EJ, Rowe SM, Tearney GJ. Method for quantitative study of airway functional microanatomy using micro-optical coherence tomography. PloS one. 2013;8:e54473.

325. Liu L, Gardecki JA, Nadkarni SK, Toussaint JD, Yagi Y, Bouma BE, Tearney GJ. Imaging the subcellular structure of human coronary atherosclerosis using micro-optical coherence tomography. Nat Med. 2011;17:1010-1014.
326. Liu L, Shastry S, Byan-Parker S, Houser G, K Chu K, Birket SE, Fernandez CM, Gardecki JA, Grizzle WE, Wilsterman EJ, Sorscher EJ, Rowe SM, Tearney GJ. An autoregulatory mechanism governing mucociliary transport is sensitive to mucus load. Am J Respir Cell Mol Biol. 2014;51:485-493.

Publications arising during this PhD work

Konstantopoulos A, Kuo J, Anderson DF and Hossain PN. Assessment of the use of anterior segment optical coherence tomography in microbial keratitis. Am J Ophthalmol 2008; 146:534-542.

Konstantopoulos A and Hossain PN. Limitations of Fourier Domain OCT. J Cataract and Refractive Surgery 2010; 36:534.

Konstantopoulos A, Yadegarfar G, Fievez M, Anderson D, Hossain P. In-vivo quantification of bacterial keratitis with optical coherence tomography. Invest Ophthalmol Vis Sci 2011; 52:1093–1097.

Konstantopoulos A, Yadegardar M, Yadegarfar G, Stinghe A, Macleod A, Jacob A, Hossain P. Deep sclerectomy versus trabeculectomy: a morphological study with anterior segment optical coherence tomography. Br J Ophthalmol 2013;97:708-14.

Konstantopoulos A, Tan XW, Goh GT, Saraswathi P, Chen L, Nyein CL, Zhou L, Beuerman R, Tan DT, Mehta J. Prophylactic Vancomycin Drops Reduce the Severity of Early Bacterial Keratitis in Keratoprosthesis. PLoS One. 2015;10(10):e0139653. doi: 10.1371/journal.pone.0139653.

Ang M, Konstantopoulos A, Goh G, Htoon HM, Seah X, Lwin NC, Liu X, Chen S, Liu L, Mehta JS. Evaluation of a Micro-Optical Coherence Tomography for the Corneal Endothelium in an Animal Model. Sci Rep. 2016 Jul 15;6:29769. doi: 10.1038/srep29769.

Assessment of the Use of Anterior Segment Optical Coherence Tomography in Microbial Keratitis

ARIS KONSTANTOPOULOS, JENNIFER KUO, DAVID ANDERSON, AND PARWEZ HOSSAIN

• PURPOSE: **To investigate the imaging capabilities of anterior segment optical coherence tomography (AS OCT) in microbial keratitis and to assess whether measurements of the quantitative parameters, infiltrate thickness and corneal thickness, were possible.**

• DESIGN: **Prospective, noncomparative, observational case series.**

• METHODS: **The study was conducted at a university hospital clinical setting. Seven patients (eyes) with suspected microbial keratitis underwent standard clinical examination and treatment based on slit-lamp clinical findings. AS OCT scanning was performed on presentation and at two follow-up appointments. All scans were carried out with the scanning beam passing through the center of the infiltration and at a specific meridian. Examination was carried out by the same operator.**

• RESULTS: **Corneal infiltration was imaged as a hyperreflective area in the corneal stroma on high-resolution AS OCT scans. Retrocorneal pathologic features and anterior chamber inflammatory cells could be imaged. Corneal and infiltrate thickness could be measured with calipers in six cases. In one case, corneal and infiltrate thickness could not be measured because of a thick inflammatory plaque attached to the endothelium. In this case, the width of the plaque was measured on serial scans.**

• CONCLUSIONS: **AS OCT imaging provides a range of parameters that can be used to assess microbial keratitis and the treatment response objectively.** (Am J Ophthalmol 2008;146:534–542. © 2008 by Elsevier Inc. All rights reserved.)

MICROBIAL KERATITIS IS A POTENTIALLY SERIOUS corneal infection that can lead to severe visual loss.[1] It often is associated with contact lens wear, trauma, and ocular surface disease.[2] Diagnosis usually is based on the clinical features of the corneal epithelial defect and stromal infiltration, as assessed with the slit-lamp. Assessment of the depth and extent of pathologic features is subjective and depends significantly on the experience of the examiner. Evaluation of the response to treatment traditionally is carried out by measurement of the epithelial defect dimensions on the slit-lamp[3] and less commonly with the aid of serial anterior segment photography.

Anterior segment optical coherence tomography (AS OCT) is a new imaging method of the anterior segment of the eye. It produces high-resolution cross-sectional images of the cornea, making it a promising device for imaging corneal anatomic and pathologic features.[4–6] It has been used to analyze the architecture of clear corneal incisions after cataract surgery and to assess the depth of intrastromal corneal rings in keratoconic eyes.[5,6] Because of its noncontact examination, it may be an ideal method for evaluating and monitoring corneal ulcers that are suspected to be microbial in origin.

We present a prospective, longitudinal AS OCT study of patients with suspected microbial keratitis. The aim of this study was to investigate the imaging capabilities of AS OCT in microbial keratitis and to assess whether measurements of the quantitative parameters, infiltrate thickness (IT) and corneal thickness (CT), were possible.

METHODS

PATIENTS WHO SOUGHT TREATMENT AT THE SOUTHAMPton Eye Unit during the previous four months with a suspected microbial corneal ulcer and who were interested in participating in the study were included. Patients with no corneal infiltration on clinical examination were not included.

Patients underwent treatment based on slit-lamp examination and clinical findings. In addition, they underwent imaging with AS OCT (Visante OCT; Carl Zeiss Meditec Inc, Dublin, California, USA). Imaging was carried out at presentation and subsequently at two follow-up appointments. At all visits, cross-sectional AS OCT scans were carried out through the same area of the corneal infiltration with the scanning beam running through the meridian that crossed the center of the infiltration.

Measurements of CT and IT were obtained on high-resolution corneal images with caliper tools provided by the Visante OCT software (version 1.1.2). CT was measured in the center of the infiltrated area by placing one caliper arm on the most anterior hyperreflective corneal surface, whether stromal or epithelial, and the second arm on the hyperreflective layer of the endothelium. Infiltration was defined as a hyperreflective area in the corneal stroma. IT was measured in the center of the infiltrate by placing one caliper arm on

Accepted for publication May 20, 2008.

From the Southampton Eye Unit, Southampton General Hospital, Southampton, United Kingdom.

Inquiries to Parwez Hossain, University of Southampton, Eye Unit, MP104, Southampton General Hospital, Tremona Road, Southampton S016 6YD, United Kingdom; e-mail: parwez@soton.ac.uk

0002-9394/08/$34.00
doi:10.1016/j.ajo.2008.05.030

TABLE. Summary of Corneal Infiltrate Characteristics

Case No.	Patient Age (yrs)	Risk Factor	Location	Presentation AS OCT Infiltrate Thickness (μm)	Presentation AS OCT Corneal Thickness at Infiltrated Area (μm)	Final AS OCT Infiltrate Thickness (μm)	Final AS OCT Corneal Thickness at Infiltrated Area (μm)
1	29	CL wear	ST	190	800	110	650
2	63	CL wear	Inferior	130	670	120	590
3	35	RCES	IT	370	910	250	610
4	57	CL wear	Central	530	1180	170	450
5	60	CL wear	Temporal	590	1560	160	540
6	72	Trichiasis, lagophthalmos	Central	3640[a]	NP[b]	0[a]	190
7	61	CL wear	Central	370	800	630	630

AS OCT = anterior segment optical coherence tomography; CL = contact lens; IT = inferior temporal; RCES = recurrent corneal erosion syndrome; ST = superior temporal; yrs = years.

[a]In Case 6, measurements refer to AS OCT inflammatory plaque width; infiltrate thickness could not be measured.

[b]In Case 6, measurement of corneal thickness was not possible at presentation, because the endothelium could not be distinguished clearly from the endothelial inflammatory plaque.

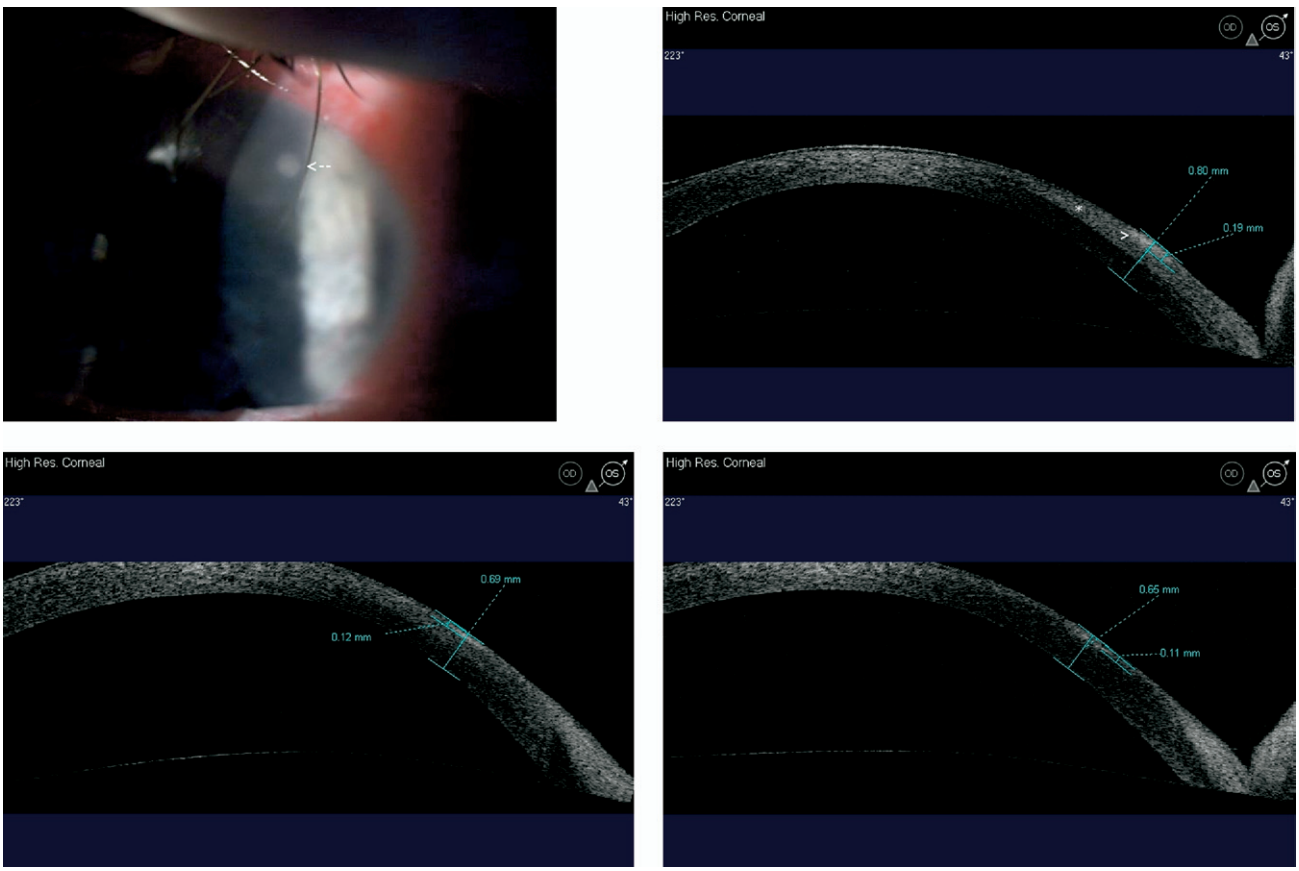

FIGURE 1. Images demonstrating contact lens-associated keratitis, including serial high-resolution anterior segment optical coherence tomography (AS OCT) images at the 43-degree meridian. (Top left) Anterior segment photograph obtained at presentation showing small corneal infiltrate (arrow). (Top right) AS OCT image obtained at presentation showing superficial stromal infiltrate (>) with edema in the anterior stroma (*). (Bottom left) AS OCT image obtained two days after presentation showing reduction of infiltrate and corneal thickness (CT). (Bottom right) AS OCT image obtained two weeks after presentation showing further reduction of CT and the presence of superficial stromal scarring.

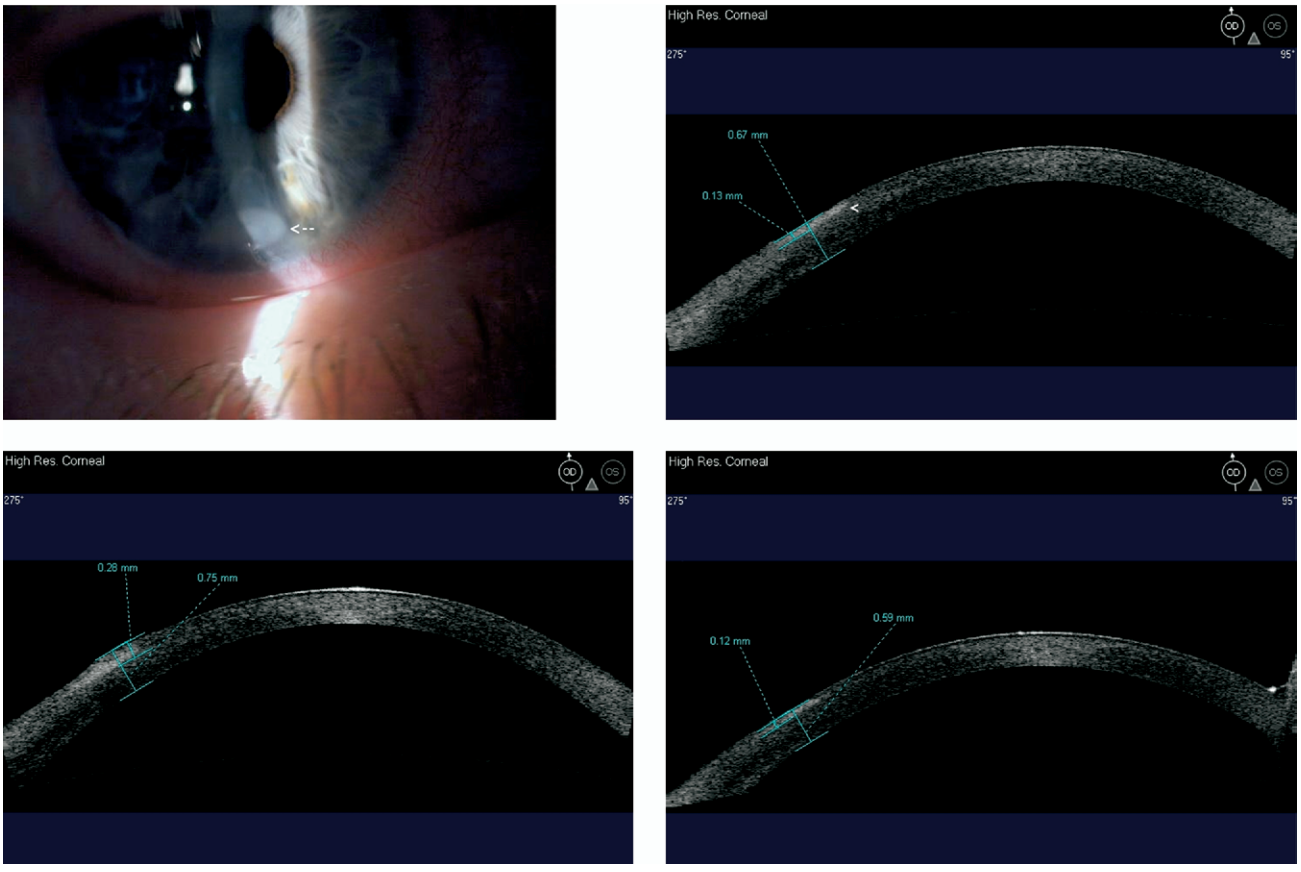

FIGURE 2. Images demonstrating contact lens-associated keratitis, including serial high-resolution AS OCT images at the 95-degree meridian. (Top left) Anterior segment photograph obtained at presentation showing inferior corneal infiltrate (arrow). (Top right) AS OCT image obtained at presentation showing an epithelial defect and a superficial anterior stromal infiltrate (<). (Bottom left) AS OCT image obtained four days after presentation showing resolution of epithelial defect and raised epithelial surface. (Bottom right) AS OCT image obtained two weeks after presentation showing reduction of CT and the development of scar tissue.

the most anterior hyperreflective corneal surface, whether stromal or epithelial, and the second arm on the posterior border of the hyperreflective area. Scans and measurements were carried out by the same investigator (A.K.).

RESULTS

SEVEN PATIENTS (EYES) WERE INCLUDED IN THE STUDY (Table). The imaging capabilities of the AS OCT are described in the individual case reports. Serial measurements of quantitative parameters were possible in all cases. CT and IT were measured in six cases. In one case (Case 6), this was not possible because the endothelium could not be distinguished from an attached endothelial inflammatory plaque. In this case, the width of the inflammatory plaque was measured on serial examination.

• **CASE 1:** A 29-year-old male contact lens wearer sought treatment for a painful left eye. Slit-lamp examination showed mild conjunctival injection and a small epithelial defect associated with stromal infiltration (Figure 1, Top left). An AS OCT scan at the 43-degree meridian showed a superficial stromal infiltrate associated with corneal edema (Figure 1, Top right). The CT in the infiltrated area measured 800 μm; the IT was 190 μm. Intensive topical ofloxacin was commenced. Two days later, the conjunctival injection was reduced and the epithelial defect had resolved clinically. Microbiologic cultures showed negative results. On an AS OCT scan, CT and IT both were reduced to 690 and 120 μm, respectively (Figure 1, Bottom left). Twelve days later, the infiltrate had resolved clinically with mild corneal scarring. On an AS OCT scan, the CT in the affected region was 650 μm (Figure 1, Bottom right).

• **CASE 2:** A 63-year-old female contact lens wearer sought treatment for a painful right eye. Slit-lamp examination showed conjunctival injection associated with an inferior epithelial defect and infiltration (Figure 2, Top left). The AS OCT scan at the 95-degree meridian showed superficial infiltration measuring 130 μm thick; the CT in the infiltrated area measured 670 μm (Figure 2, Top right). Intensive topical

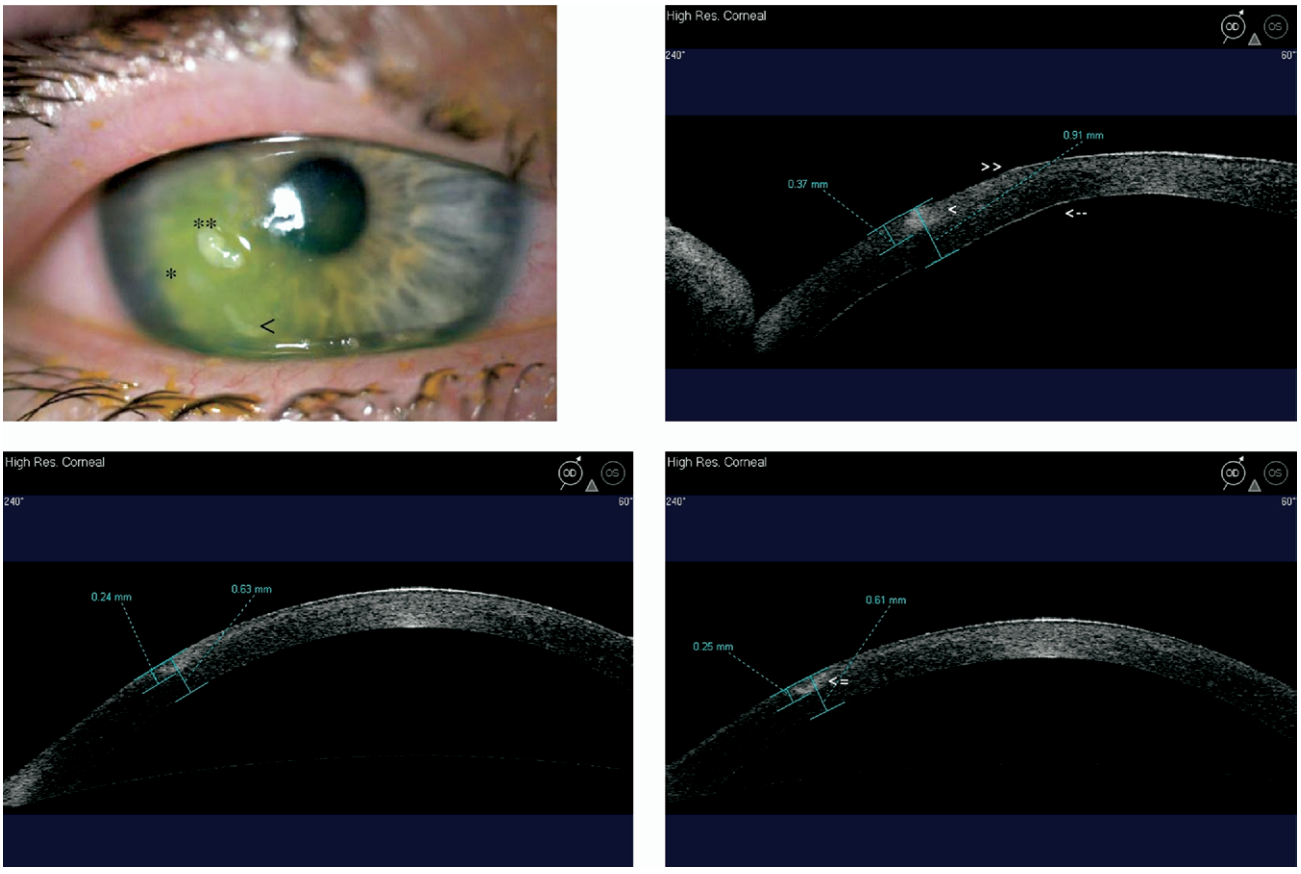

FIGURE 3. Images demonstrating microbial keratitis in a patient with recurrent corneal erosion syndrome, including serial high-resolution AS OCT images at the 60-degree meridian. (Top left) Anterior segment photograph obtained at presentation showing corneal infiltrates (* and <) and mucus (**). (Top right) AS OCT images obtained at presentation through the lower infiltrate (<) showing corneal infiltration (<) and loss of epithelial continuity (>>). The lower border of the epithelial defect cannot be seen because of the underlying hyperreflective stromal infiltration. Stromal edema has resulted in a change in convexity of the posterior corneal surface (arrow). (Bottom left) AS OCT image obtained 10 days after initiation of treatment showing reduction of infiltrate and CT; an intact epithelial surface is now present. (Bottom right) AS OCT image obtained 17 days after initiation of treatment showing further reduction of CT and the development of scar tissue (arrow).

ofloxacin was commenced. Four days later, the epithelial defect had resolved clinically with the presence of an irregular and slightly raised epithelial surface. Microbiologic cultures showed negative results. On repeat AS OCT, an intact epithelium was present over the infiltrate; the IT and CT had increased to 280 and 750 μm, respectively (Figure 2, Bottom left). Inclusion of the raised epithelium in the thickness measurements most likely accounted for this. Topical ofloxacin six times daily was continued. Clinical examination 10 days later showed a quiet eye with no epithelial defect and the development of scar tissue in the infiltrated area. The CT, as demonstrated on AS OCT, had decreased, measuring 590 μm (Figure 2, Bottom right).

• **CASE 3:** A 35-year-old woman with a history of recurrent corneal erosion syndrome sought treatment for a painful right eye. Slit-lamp examination showed a corneal epithelial defect associated with three small superficial infiltrates (Figure 3, Top left). High-resolution AS OCT imaging through the inferior infiltrate at the 60-degree meridian showed that the infiltrate measured 370 μm in thickness and that the CT was 910 μm. Intensive topical ofloxacin and cefuroxime 5% were commenced, with a good response. *Staphylococcus aureus* was grown on culture. Ten days after presentation, the epithelial defect had healed and the infiltrates were resolving clinically. Repeat AS OCT showed that the IT was reduced, measuring 240 μm, as was the CT at 630 μm. One week later, the infiltrates had resolved clinically and scar tissue had developed. On AS OCT, the CT was reduced further and scar tissue was imaged to a depth of 250 μm.

• **CASE 4:** A 57-year-old male contact lens wearer sought treatment for a two-day history of a painful right eye. Slit-lamp examination showed moderate conjunctival injection with an epithelial defect and stromal infiltration associated with a hypopyon (Figure 4, Top left). On an AS OCT scan at the 90-degree meridian, the IT measured 530

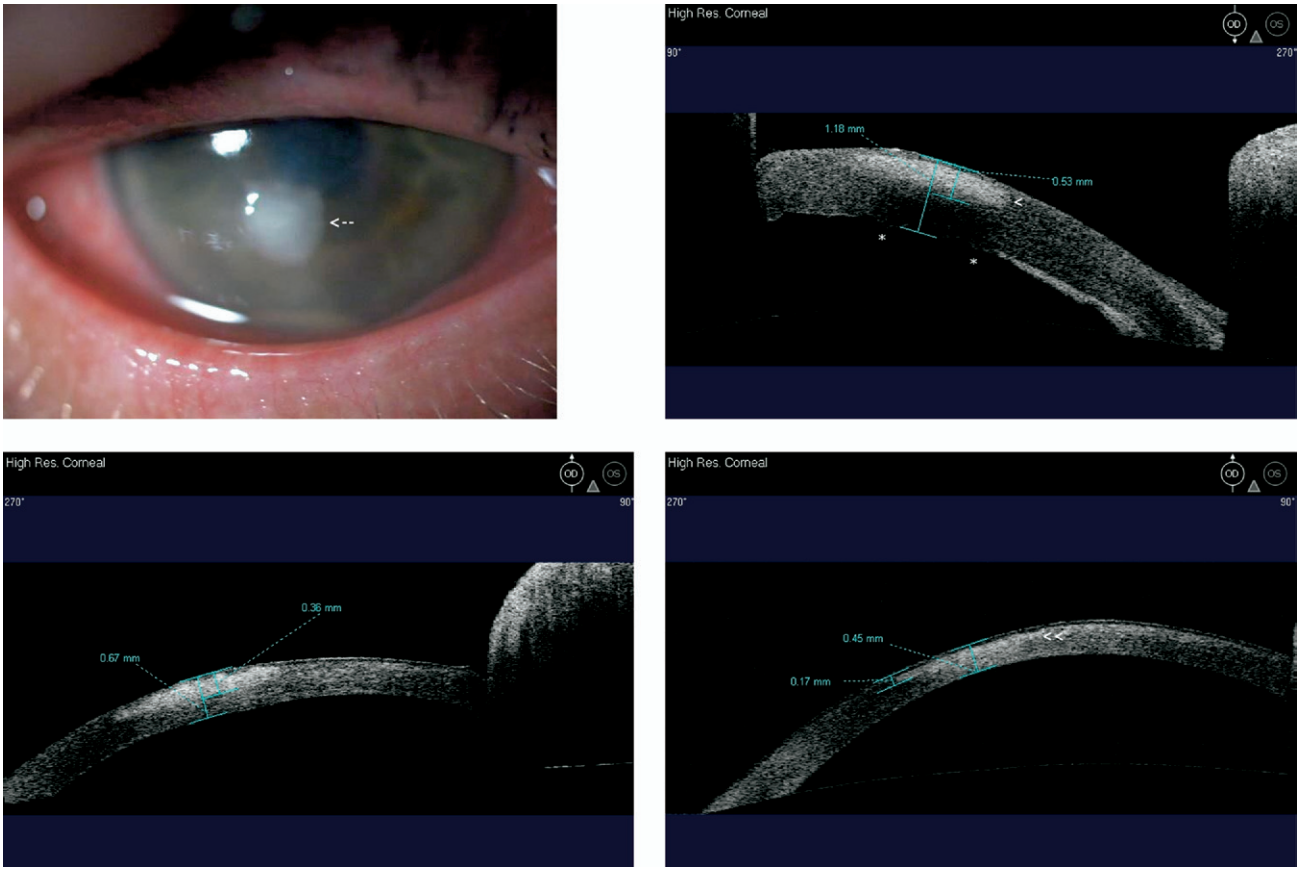

FIGURE 4. Images demonstrating microbial keratitis in a contact lens wearer, including serial high-resolution AS OCT images at the 90-degree meridian. (Top left) Anterior segment photograph obtained at presentation showing corneal infiltrate (arrow). (Top right) AS OCT image obtained at presentation showing an epithelial defect and a thick stromal infiltrate (<). Descemet folds (*) are present because of associated edema. (Bottom left) AS OCT image obtained two weeks after presentation showing reduction of infiltrate and CT with a smoother endothelial surface. (Bottom right) AS OCT image obtained eight weeks after presentation showing further reduction of CT and anterior stromal scarring (<<).

μm; and the CT in the infiltrated area measured 1180 μm (Figure 4, Top right). Intensive topical cefuroxime 5% and ofloxacin were commenced. Two days later, the epithelial defect size and hypopyon height were smaller on slit-lamp examination. *Pseudomonas aeruginosa* was grown on culture. One week after presentation, the epithelial defect had decreased in size, the hypopyon had resolved, and the infiltrate was less dense clinically. Repeat AS OCT showed that the IT and CT both were reduced, measuring 490 and 920 μm, respectively. Topical ofloxacin six times daily was continued, and one week later, the epithelial defect had resolved clinically. On AS OCT, the IT and CT were reduced further, measuring 360 and 670 μm, respectively (Figure 4, Bottom left). Topical ofloxacin was continued four times daily. On clinical examination six weeks later, the eye was quiet with the development of scar tissue in the infiltrated area. The CT, as shown on AS OCT, measured 450 μm (Figure 4, Bottom right).

• **CASE 5:** A 60-year-old female contact lens wearer sought treatment for a two- to three-day history of increasing pain and redness of right eye. Slit-lamp examination showed moderate conjunctival injection and a large epithelial defect associated with stromal infiltration (Figure 5, Top left). Anterior chamber (AC) inflammation was present with a hypopyon. An AS OCT scan at the 180-degree meridian showed a thick stromal infiltrate with significant edema (Figure 5, Top right). The CT in the infiltrated area measured 1560 μm, and the IT measured 590 μm. Corneal scrapes were carried out and intensive topical ofloxacin and cefuroxime 5% were commenced. An examination two days later showed reduction of hypopyon height and epithelial defect size. On AS OCT scan, the CT and IT had decreased to 900 and 390 μm, respectively (Figure 5, Bottom left). *P. aeruginosa* was cultured. Clinical improvement continued, and four days later, the CT in the infiltrated area, as measured by AS OCT, measured 820 μm. One week later, the corneal ulcer had resolved clinically with the development of scar tissue. The CT on AS OCT measured 540 μm (Figure 5, Bottom right).

• **CASE 6:** A 72-year-old man sought treatment for a three- to four-week history of discomfort and decreasing vision in his

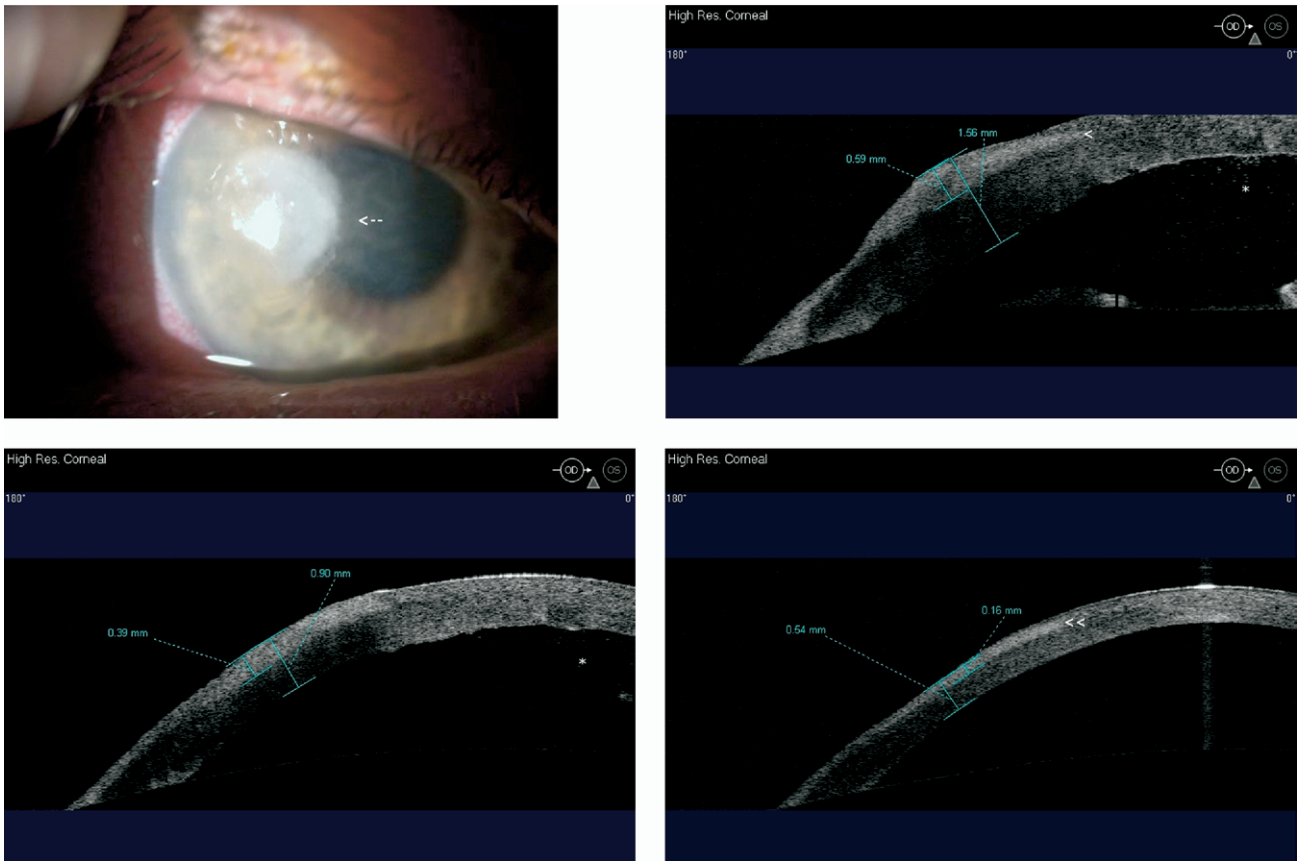

FIGURE 5. Images demonstrating microbial keratitis in a contact lens wearer, including serial high-resolution AS OCT images at the 180-degree meridian. (Top left) Anterior segment photograph obtained at presentation showing a dense corneal infiltrate (arrow). (Top right) AS OCT image obtained at presentation showing a thick anterior stromal infiltrate (<) with associated edema; anterior chamber (AC) inflammatory cells are visible (*). (Bottom left) AS OCT image obtained two days after presentation showing reduction of infiltrate and CT; AC inflammatory cells are still present (*). (Bottom right) AS OCT image obtained two weeks after presentation showing further reduction of CT and the presence of anterior stromal scar tissue (<<).

left eye. He had a history of trichiasis and lagophthalmos. Slit-lamp examination showed conjunctival injection and a corneal epithelial defect associated with corneal thinning and deep stromal infiltration (Figure 6, Top left). Posterior synechiae and mild AC inflammation also were present. AS OCT imaging through the center of the ulceration at the 110-degree meridian (Figure 6, Top right) showed significant corneal thinning. A large plaque of organized inflammatory cells was attached to the endothelium, measuring 3.64 mm in width. The CT could not be measured in the thinned area, because the endothelium could not be distinguished from the inflammatory plaque. Corneal scrapes were carried out and intensive topical ofloxacin and cefuroxime 5% were commenced. Over the next three days, conjunctival injection diminished, but there was no clinically detectable change in the epithelial defect or infiltration. However, repeat AS OCT (Figure 6, Bottom left) showed that the inflammatory plaque was smaller, measuring 3.09 mm wide. Diphtheroids were grown on culture. The frequency of antibiotics was reduced, and during the following week, the size of the epithelial defect and infiltration diminished clinically. At 10 days after presentation, the risk of perforation was raised, because a very thin cornea was present clinically. AS OCT (Figure 6, Bottom right) showed that the inflammatory plaque had resolved completely. The CT in the ulcerated area could be assessed and measured 190 μm.

• **CASE 7:** A 61-year-old male contact lens wearer was referred to the corneal clinic with a three-week history of a poorly responding corneal ulcer in the right eye. Slit-lamp examination showed marked conjunctival injection and a central epithelial defect associated with stromal infiltration (Figure 7, Top left). AC inflammation with a hypopyon was present. An AS OCT scan through the center of the infiltrate at the 180-degree meridian showed a stromal infiltrate with corneal edema (Figure 7, Top right). The CT in the infiltrated area was 800 μm, and the IT was 370 μm. Corneal scrapes were carried out and intensive topical ofloxacin and cefuroxime 5% commenced. Two days later, coagulase-negative Staphylococcus was grown on culture and topical dexamethasone 0.1% every two hours was added. Four days

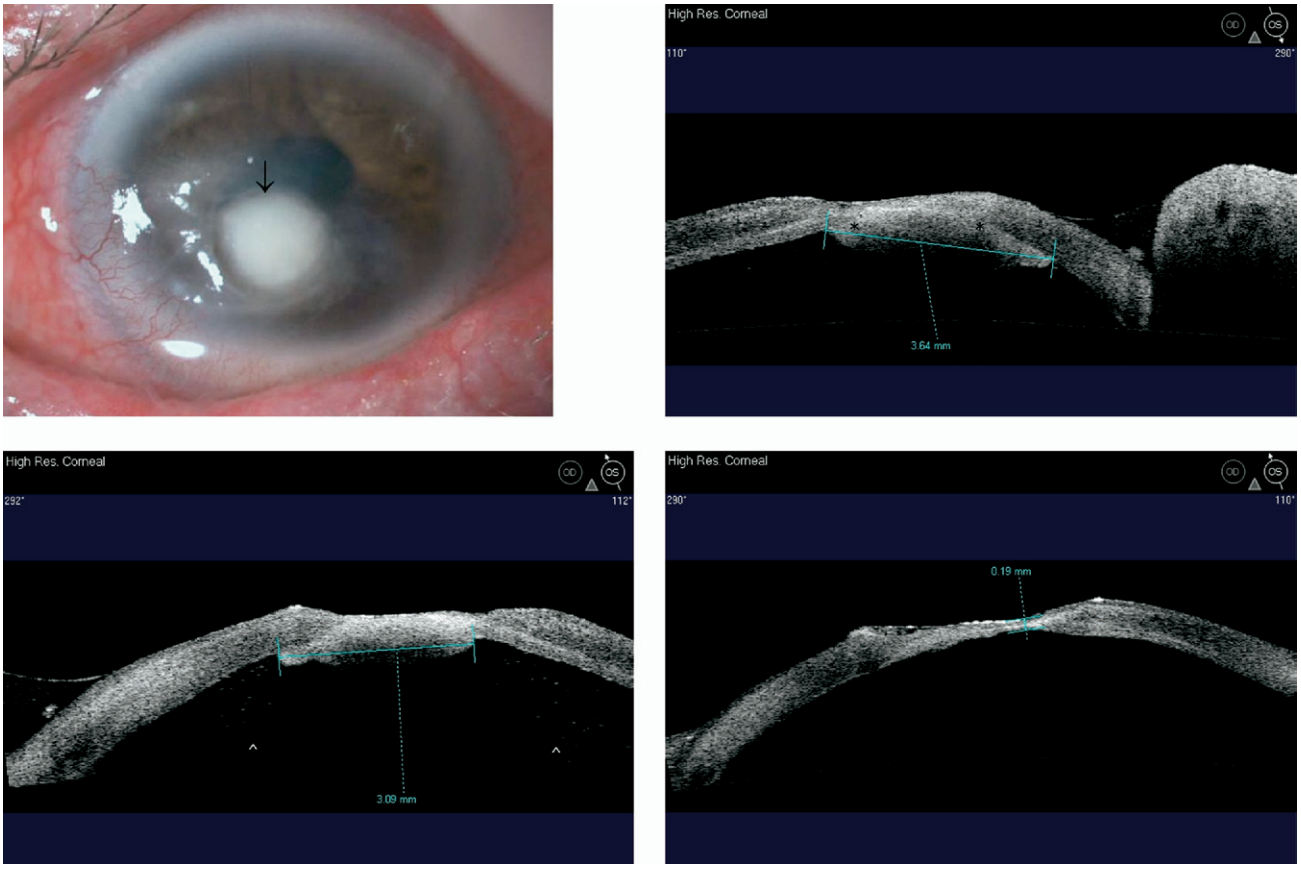

FIGURE 6. Images demonstrating microbial keratitis in a patient with trichiasis and lagophthalmos, including serial high-resolution AS OCT images at the 110-degree meridian. (Top left) Anterior segment photograph obtained at presentation showing corneal infiltrate (arrow). (Top right) AS OCT image obtained at presentation showing sloping ulcer edges with corneal thinning and a plaque of organized inflammatory cells attached to the endothelium (*). (Bottom left) AS OCT image obtained three days after initiation of treatment showing reduction of the inflammatory plaque width. Individual inflammatory cells (^) can be seen in the AC. (Bottom right) AS OCT image obtained 10 days after initiation of treatment showing resolution of inflammatory plaque; CT can now be measured.

after presentation, his condition remained unchanged on slit-lamp examination; on AS OCT, the CT was unchanged but the infiltrate was thicker, measuring 480 μm (Figure 7, Middle left). Repeat AS OCT three days later showed that the infiltration was even thicker. In addition, the CT had decreased, measuring 630 μm (Figure 7, Middle right). Because a fungal cause was highly suspected, lamellar corneal biopsy was carried out and Fusarium species fungus subsequently were cultured. Despite systemic and topical antifungal treatment, corneal thinning with descemetocele developed (Figure 7, Bottom). The patient subsequently underwent penetrating keratoplasty (PK).

DISCUSSION

WE DEMONSTRATED THE IMAGING CAPABILITIES OF AS OCT in microbial keratitis. AS OCT provides a range of qualitative and quantitative information; serial standardized examination allows objective assessment of microbial keratitis and monitoring of the disease course. Six cases responded well to standard topical antibiotic treatment, and one required PK.

Corneal and anterior segment parameters can be measured with caliper tools provided by software. Our study shows that the CT at the infiltrated area can be measured on high-resolution corneal scans. At the initial stages of microbial keratitis, even mild cases have a thickened cornea at the infiltrated area. The epithelium and endothelium normally are imaged as hyperreflective layers compared with the stroma, facilitating placement of the calipers. In one case (Case 6), CT measurement was not possible. This patient had a chronic bacterial infection in which the endothelium could not be distinguished from an attached endothelial inflammatory plaque.

Serial, reiterative scans can be carried out through the same area of the cornea by adhering to a scanning protocol. CT, therefore, can be monitored objectively during the course of the disease. As the infection and inflammation resolve, CT decreases. At the later stages of the disease, scar tissue develops and the affected cornea may become thinner than adjacent healthy tissue. How-

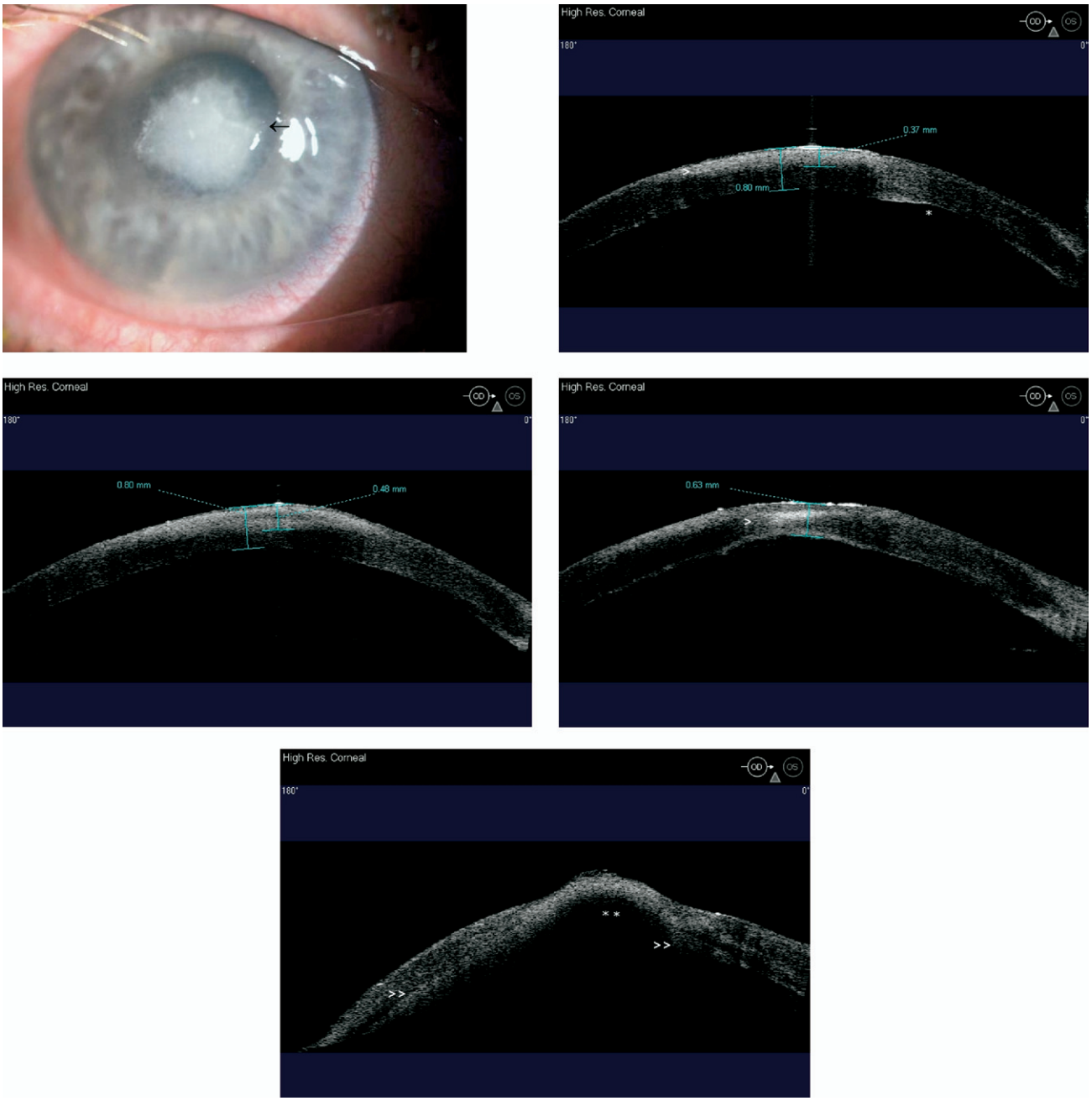

FIGURE 7. Images demonstrating fungal keratitis in a contact lens wearer, including serial high-resolution AS OCT images at the 180-degree meridian. (Top left) Anterior segment photograph obtained at presentation showing dense corneal infiltrate (arrow). (Top right) AS OCT image obtained at presentation showing anterior stromal infiltrate (>) and edema resulting in change in curvature of posterior corneal surface (*). (Middle left) AS OCT image obtained four days after presentation showing an increase in infiltrate thickness. (Middle right) AS OCT image obtained seven days after presentation showing further increase in infiltrate thickness (>) and reduction of CT. (Bottom) AS OCT image obtained two weeks after presentation showing corneal thinning with descemetocele formation (**); inflammatory plaque can be seen attached to endothelial surface (>>).

ever, as demonstrated by Case 7, CT reduction is not always associated with resolution of infection. Fungal infection or chronic bacterial infection may result in tissue necrosis and severe corneal thinning with risk of perforation. Case 7 demonstrates that such corneal thinning may be detected earlier on AS OCT than on clinical examination. Scans always have to be interpreted in the context of the clinical situation and examination. AS OCT cannot replace slit-lamp examination, but it does provide information that may aid assessment.

Infiltration thickness also can be measured with caliper tools, because AS OCT images stromal infiltration as a

hyperreflective area in the stroma. This was possible in all cases except for the patient who sought treatment with advanced thinning (Case 6). In the early stages of microbial keratitis, clinical improvement is associated with reduction of IT on serial scans. Cases 2 and 7 demonstrate that an increase in IT also may be detected. This change may be detected on AS OCT before deterioration becomes clinically apparent. In the later stages of the disease, measurement of IT may become more difficult, because the infiltration becomes replaced by scar tissue. Qualitative assessment of the infiltration also is possible, because the intensity of hyperreflectivity corresponds to the density of the infiltration on slit-lamp examination. Serial, reiterative scans therefore may aid objective evaluation of the infiltration and response to treatment.

Anterior segment OCT provides additional qualitative and quantitative information that may be useful in the assessment of microbial keratitis. Inflammatory cells may appear to be hyperreflective and floating in the AC or may be imaged as aggregates on the endothelial surface forming keratic precipitates. Case 6 illustrates that retrocorneal pathologic features, such as an endothelial inflammatory plaque, also can be imaged and measured. Measurement of the width of this plaque on serial scans allowed objective assessment of the disease course, despite the fact that CT or IT could not be measured. AS OCT also can image and monitor the extent of stromal edema associated with the ulceration. Edema is visualized as diffuse thickening of the corneal stroma, resulting in a change in convexity of the posterior corneal surface. In more severe cases (Cases 4 and 5), Descemet folds can be imaged as ruffles in the normally smooth endothelial surface.

The value of AS OCT in imaging and studying corneal and anterior segment pathologic features increasingly is being explored.[5–10] The use of 1310-nm wavelength light allows high scan rates and penetration through opaque tissues with limited light scatter.[4,11] AS OCT has been used to evaluate the anterior segment in secondary glaucoma with corneal opacity after PK and to visualize the patency and position of aqueous shunt devices in the presence of poor corneal transparency.[7,8] It has shown excellent imaging capabilities in analyzing clear corneal incisions after cataract surgery and corneal architecture after lamellar corneal transplantation.[5,9] Recently, it also has been demonstrated to have good repeatability and reproducibility in the study of CT in keratoconus.[10]

Until the advent of AS OCT, it had not been possible to measure such a range of parameters readily in microbial keratitis. This study has shown that serial, reiterative AS OCT examination allows objective assessment of the disease and treatment response. A larger study will confirm the full clinical significance of the available measurements and test repeatability. Our early investigations strongly suggest that AS OCT has a valuable role in the clinical assessment of patients with microbial keratitis.

THE AUTHORS INDICATE NO FINANCIAL SUPPORT OR FINANCIAL CONFLICT OF INTEREST. INVOLVED IN DESIGN OF STUDY (A.K., D.A., P.H.); conduct of study and data collection (A.K., J.K.); management, analysis, and interpretation of data (A.K., P.H.); and preparation (A.K., P.H.), review, and approval of the manuscript (A.K., D.A., P.H.). The NHS Berkshire Research Ethics Committee provided ethical approval for this study. Informed consent was obtained from each patient.

REFERENCES

1. McLeod SD, LaBree LD, Tayyanipour R, et al. The importance of initial management in the treatment of severe infectious corneal ulcers. Ophthalmology 1995;102:1943–1948.
2. Bourcier T, Thomas F, Borderie V, Chaumeil C, Laroche L. Bacterial keratitis: predisposing factors, clinical and microbiological review of 300 cases. Br J Ophthalmol 2003;87:834–838.
3. Morlet N, Minassian D, Butcher J, the Ofloxacin Study Group. Risk factors for treatment outcome of suspected microbial keratitis. Br J Ophthalmol 1999;83:1027–1031.
4. Konstantopoulos A, Hossain PH, Anderson DF. Recent advances in ophthalmic anterior segment imaging: a new era for ophthalmic diagnosis? Br J Ophthalmol 2007;91:551–557.
5. Calladine D, Packard R. Clear corneal incision architecture in the immediate postoperative period evaluated using optical coherence tomography. J Cataract Refract Surg 2007;33:1429–1435.
6. Lai MM, Tang M, Andrade EM, et al. Optical coherence tomography to assess intrastromal corneal segment depth in keratoconic eyes. J Cataract Refract Surg 2006;32:1860–1865.
7. Memarzadeh F, Li Yan, Francis BA, Smith RE, Gutmark J, Huang D. Optical coherence tomography of the anterior segment in secondary glaucoma with corneal opacity after penetrating keratoplasty. Br J Ophthalmol 2007;91:189–192.
8. Sarodia U, Sharkawi E, Hau S, Barton K. Visualization of aqueous shunt position and patency using anterior segment optical tomography. Am J Ophthalmol 2007;143:1054–1056.
9. Lim LS, Aung HT, Aung T, Tan DTH. Corneal imaging with anterior segment optical coherence tomography for lamellar keratoplasty procedures. Am J Ophthalmol 2008;145:81–90.
10. Mohamed S, Lee GK, Rao SK, et al. Repeatability and reproducibility of pachymetric mapping with Visante anterior segment optical coherence tomography. Invest Ophthalmol Vis Sci 2007;48:5499–5504.
11. Radhakrishnan S, Goldsmith J, Huang D, et al. Comparison of optical coherence tomography and ultrasound biomicroscopy for detection of narrow anterior chamber angles. Arch Ophthalmol 2005;123:1053–1059.

plus-power and minus-power IOLs and ask manufacturers to supply this information.—*Wolfgang Haigis, MS, PhD*

REFERENCES

1. Haigis W. The Haigis formula. In: Shammas HJ, eds, Intraocular Lens Power Calculations. Thorofare, NJ, Slack, 2004; 41–57
2. Haigis W, Duzanec Z, J. Kammann J, Fischer A. Klinische Individualisierung von IOL-Konstanten. In: Vörösmahrty D, Duncker G, Hartmann C, eds, 10. Kongreß der Deutschsprachigen Gesellschaft für Intraokularlinsen-Implantation und refraktive Chirurgie, März 1996. Budapest. Berlin, Springer-Verlag, 1997; 281–287
3. User Group for Laser Interference Biometry. Optimized IOL constants for the Zeiss IOLMaster. Available at: http://www.augenklinik.uni-wuerzburg.de/ulib/c1.htm. Accessed November 14, 2009

Limitations of Fourier-domain OCT

At the time of writing this letter, the RTVue-100 (Optovue, Inc.) used by Wylęgala et al.[1] is the only commercially available Fourier-domain optical coherence tomography (OCT) device that can scan the anterior segment without "personal" modifications. Similar to all commercially available Fourier-domain OCT devices, it uses shorter wavelength light than the Visante-OCT (Carl Zeiss Meditec) (840 nm versus 1310 nm). It scans at a faster rate (26 000 A-scans/s) than time-domain OCT devices (2048 A-scans/s for Visante-OCT). This improves image quality by achieving higher resolution and also reducing motion artifact.

We agree with the authors that Fourier-domain OCT can image Bowman layer as a distinct entity in a healthy cornea (Figure 1, *A*, in article). However, Figures 3, *A*, and 4, *A*, suggest that visualization of Bowman layer may be limited in the presence of corneal pathology. The use of short wavelength light may be a contributing factor. Using a modified Fourier-domain OCT, the Cirrus high-definition OCT (Carl Zeiss Meditec), Wong et al.[2] imaged the termination of the Descemet/endothelium layer at the Schwalbe line. As this may potentially be important in analyzing the angle, do the authors have any information regarding the capabilities of the RTVue-100 in imaging this landmark?

Wavelength light of 1310 nm has a good depth of penetration, including through nontransparent structures such as limbus and corneal opacity.[3,4] Figure 6 illustrates the poor penetration of shorter wavelength light. Fourier-domain OCT visualization of the Ahmed valve and ocular structures deeper than this is inferior to that with the Visante OCT. Similarly, in Figure 2, the root of the angle is not imaged adequately with the Fourier-domain OCT. We would not necessarily agree with the authors' statement that "all angle structures can be visualized" with the Fourier-domain OCT. Wong et al.[2] have recently highlighted this limitation of Fourier-domain OCT.

It is well recognized that the scleral spur can be visualized in 70% to 80% of cases with the Visante OCT.[2,5] In Figure 2, the scleral spur is identified with the Visante OCT, but not with the RTVue-100. It would be interesting to know in what percentage of cases the scleral spur was visualized with the RTVue-100. In addition, how did the authors define and measure the angle-opening distance?

Aris Konstantopoulos, MSc, MRCOphth
Parwez Hossain, PhD, FRCOphth, FRCS(Ed)
Southampton, United Kingdom

REFERENCES

1. Wylęgala E, Teper S, Nowińska AK, Milka M, Dobrowolski D. Anterior segment imaging: Fourier-domain optical coherence tomography versus time-domain optical coherence tomography. J Cataract Refract Surg 2009; 35:1410–1414
2. Wong H-T, Lim MC, Sakata LM, Aung HT, Amerasinghe N, Friedman DS, Aung T. High-definition optical coherence tomography imaging of the iridocorneal angle of the eye. Arch Ophthalmol 2009; 127:256–260
3. Radhakrishnan S, Rollins AM, Roth JE, Yazdanfar S, Westphal V, Bardenstein DS, Izatt JA. Real-time optical coherence tomography of the anterior segment at 1310 nm. Arch Ophthalmol 2001; 119:1179–1185
4. Konstantopoulos A, Kuo J, Anderson D, Hossain P. Assessment of the use of anterior segment optical coherence tomography in microbial keratitis. Am J Ophthalmol 2008; 146:534–542
5. Sakata LM, Lavanya R, Friedman DS, Aung HT, Seah SK, Foster PJ, Aung T. Assessment of the scleral spur in anterior segment optical coherence tomography images. Arch Ophthalmol 2008; 126:181–185

REPLY: We can definitely claim that anterior segment OCT is a noncontact, high-resolution imaging technique with many possible clinical applications: keratoplasty, keratorefractive surgery, Descemet membrane detachment, ocular injury; even corneal infectious diseases.[1–5] As far as we know, there are 3 commercially available spectral domain anterior segment modalities that do not require personal modifications: RTVue-100 (Optovue Inc.), Cirrus HD-OCT model 4000 (Carl Zeiss Meditec), and SOCT Copernicus HR (Optopol Technology SA).

In comparing anterior segment morphology by time-domain and spectral-domain OCT, we focused on 2 aspects: visualization of anatomical anterior segment structures and overall anterior segment evaluation. Because of higher resolution, the Fourier-domain OCT allows visualization of structures not visible during time-domain OCT examination; for example, Bowman layer, trabecular meshwork, Schlemm canal, early subepithelial changes in cases of transforming

In Vivo Quantification of Bacterial Keratitis with Optical Coherence Tomography

Aristides Konstantopoulos,[1] *Ghasem Yadegarfar,*[2] *Marina Fievez,*[1] *David F. Anderson,*[1] *and Parwez Hossain*[1,3]

Purpose. To quantify the human corneal inflammatory response in treated bacterial keratitis with long-wavelength anterior segment optical coherence tomography (AS-OCT).

Methods. Patients with clinically suspected bacterial keratitis were recruited from the corneal service at Southampton Eye Unit, UK. Patients underwent AS-OCT and slit-lamp examination on presentation (day 0) and days 3, 7, and 14 of treatment. Corneal thickness (CT) in the infiltrated area, infiltrate thickness (IT), and infiltrate width (IW) were measured on high-resolution AS-OCT scans. Mean values for each day and rates of change for each interval were calculated and compared (one-way ANOVA, paired *t*-test).

Results. Twenty-six eyes of 26 patients were recruited. Mean CT and IT on presentation were 905 μm and 388 μm, respectively. On days 3, 7, and 14, CT and IT decreased to 753 μm and 320 μm ($P < 0.01$), 678 μm and 296 μm ($P < 0.01$), and 584 μm and 207 μm ($P < 0.01$), respectively. Mean IW, 1498 μm on presentation, did not change during treatment ($P > 0.30$). Mean daily rate of CT reduction was faster in the early (days 0–3) compared to late (days 7–14) phase (4.49% vs. 1.33%, $P = 0.006$). Mean daily rate of IT reduction was no different in early, middle, and late phases (5.41% vs. 1.19% vs. 3.38%, $P > 0.01$). In the late phase, IT decreased faster than CT (3.38% vs. 1.33%, $P = 0.003$).

Conclusions. CT and IT decreased significantly by day 3 in resolving bacterial keratitis. The rapid early phase reduction in IT and CT was followed by rapid late phase IT reduction. This study demonstrates that serial AS-OCT examination can be used to monitor in vivo the clinical course of inflammatory disease. (*Invest Ophthalmol Vis Sci.* 2011;52:1093–1097) DOI: 10.1167/iovs.10-6067

Corneal disease is a major cause of blindness, with its epidemiology encompassing a spectrum of corneal infections and inflammatory diseases.[1–4] Bacterial keratitis, an infective and inflammatory condition of the cornea, is characterized by corneal epithelial ulceration, corneal edema and stromal infiltration with inflammatory cells.[5–8] Animal studies have confirmed these morphologic changes with histopathology.[6,9,10]

In clinical practice, bacterial keratitis is routinely assessed with slit-lamp biomicroscopy, an examination and imaging modality that is primarily limited by the physical properties of light. The location of corneal infiltration can be assessed and the horizontal and vertical dimensions of epithelial ulceration and infiltration measured.[11] However, the depth of pathology and associated corneal edema cannot be measured with the slit-lamp. As a result, in vivo information regarding corneal inflammation in bacterial keratitis and the response to treatment is limited.

Objective clinical assessment of bacterial keratitis and the treatment response is difficult, especially during the early treatment phase. Subjective features, such as improvement of patient symptoms, are therefore also used as indicators of resolving infection. Recently, however, in vivo assessment of microbial keratitis has become possible with long wavelength anterior segment optical coherence tomography (AS-OCT). This modality provides cross-sectional scans of the cornea and assessment of the depth of inflammation with measurements of stromal infiltration thickness and corneal thickness in the infiltrated area.[12]

In this study we aim to quantify corneal inflammation in resolving bacterial keratitis by measuring the temporal in vivo change of corneal thickness (CT), infiltrate thickness (IT), and infiltrate width (IW) with a commercially available AS-OCT device.

Methods

Recruitment of Patients

This study was approved by the local NHS Research Ethics Committee and informed consent was obtained from all patients. The research was performed in accordance with the tenets of the Declaration of Helsinki. Subjects with a clinical diagnosis of presumed bacterial keratitis were recruited from the corneal service at Southampton Eye Unit, Southampton University Hospitals NHS Trust, UK. A clinical diagnosis of bacterial keratitis was made in the presence of a typical history and an epithelial ulceration with underlying stromal infiltration associated with signs of inflammation.[13–15] Patients with a history and clinical findings suggestive of a viral keratitis or hypersensitivity type corneal ulceration were not recruited. Bacterial keratitis was considered resolved if the epithelial defect and signs of inflammation resolved completely. Recruited patients who did not respond to antibacterial treatment were excluded.

Examination and Scanning Protocol

Anterior segment imaging was carried out by OCT tomography (Visante OCT; Carl Zeiss Meditec Inc, Dublin, CA). AS-OCT imaging

From the [1]Southampton Eye Unit, Southampton University Hospitals NHS Trust, Southampton, United Kingdom; the [2]Biostat & Epidemiology Department, School of Public Health Sciences, Isfahan University of Medical Sciences, Isfahan, Iran; and the [3]Division of Infection, Inflammation & Immunity, University of Southampton, Southampton General Hospital, Southampton, United Kingdom.

Submitted for publication June 16, 2010; revised August 21, 2010; accepted August 29, 2010.

Disclosure: **A. Konstantopoulos**, None; **G. Yadegarfar**, None; **M. Fievez**, None; **D.F. Anderson**, None; **P. Hossain**, None

Presented at the annual meeting of the Association for Research in Vision and Ophthalmology, Fort Lauderdale, Florida, May 2009 and the XXVII Congress of the European Society of Cataract and Refractive Surgeons.

Corresponding author: Parwez Hossain, University of Southampton, Eye Unit, MP104, Southampton General Hospital, Tremona Road, Southampton, SO16 6YD, UK; parwez@soton.ac.uk.

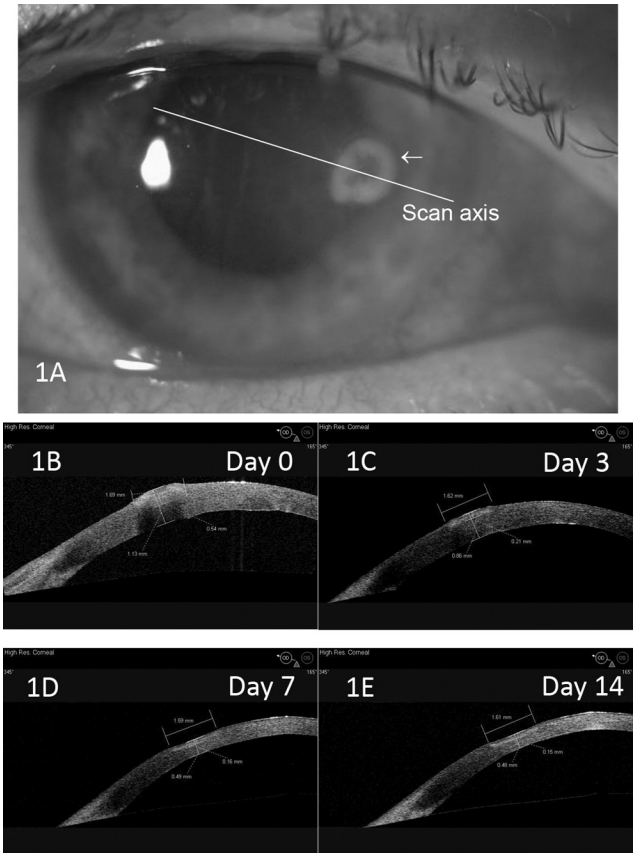

FIGURE 1. AS-OCT imaging of bacterial keratitis. (**A**) A corneal ulcer with inflammatory infiltration (←) due to *Pseudomonas aeruginosa* keratitis. (**B**) The high-resolution AS-OCT image through the center of the infiltrated area at the 165° axis on presentation. The hyper-reflective area in the anterior corneal stroma corresponds to the clinical infiltration. The epithelium and endothelium have lost the smooth profile, reflecting the increased stromal thickness due to stromal infiltration and edema. Corneal thickness, infiltrate thickness and infiltrate width measure 1130, 540, and 1690 μm respectively. (**C**), (**D**), and (**E**) illustrate the reduction of corneal and infiltrate thickness on days 3, 7, and 14 respectively. Infiltrate width does not change considerably.

and clinical slit-lamp examination were carried out on presentation (day 0) and subsequently on days 3, 7, and 14 of treatment. All patients underwent treatment based on clinical findings and requirements. Standard antibacterial treatment was intensive guttae ofloxacin 0.3% and guttae cefuroxime 5% to the affected eye. Antibiotics were instilled at an hourly frequency for 48 hours, then reduced to two hourly for a further 48 hours. The frequency was then reduced to six hourly for a total treatment period of two weeks.

A standardized scanning protocol was used. At all visits high-resolution AS-OCT scans were carried out through the same area of corneal infiltration with the scanning beam running through the center of the infiltration at a defined axis. Corneal infiltration on the AS-OCT images was defined as the hyper-reflective area that corresponded to the clinical corneal infiltration. CT, IT, and IW were measured with caliper tools of the OCT tomography software (Visante, version 1.1.2; Carl Zeiss MediTec, Inc.). CT was measured in the center of the infiltration with one caliper arm on the most anterior hyper-reflective corneal surface and the second arm on the hyper-reflective endothelium. IT, also in the center of the infiltration, was measured with one caliper arm on the most anterior hyper-reflective corneal surface and the second arm on the posterior border of the hyper-reflective area. IW was measured by placement of the caliper arms on the transverse borders of the hyper-reflective area. The scanning protocol is illustrated in Figure 1.

CT, IT and IW were measured on days 0 (presentation), 3, 7, and 14 of treatment. Mean values were calculated for each day and compared. For parameters that showed statistically significant change, the daily rate of change was calculated for the early (days 0 to 3), middle (days 3 to 7), and late (days 7 to 14) phases of treatment. Daily rate of change of each parameter was calculated for each eye according to the formula: [*X* day B − *X* day A] /*X* day A /time interval in days, where *X* is the parameter value and A and B are the first and last day of the treatment phase, respectively. Mean values were calculated and compared.

Statistical Analysis

Power of the study to detect rate of change in IT and CT, at 5% significance level, using one-way analysis of variance (ANOVA) was 93% and 92%, respectively. Mean values of CT, IT, IW and their daily rate of change were compared for statistical difference using paired *t*-test and one-way ANOVA. P values < 0.01 were considered statistically significant. Statistical Analysis was performed with analysis software (The Statistical Package for Social Science, version 15; SPSS Inc, Chicago, IL).

RESULTS

Twenty seven patients (27 eyes) with a clinical diagnosis of bacterial keratitis were recruited. One patient who did not respond to standard antibacterial treatment had fungal keratitis and was excluded. In the remaining 26 patients with bacterial keratitis the infection resolved. Patient and keratitis characteristics are summarized in Table 1. Serial AS-OCT imaging and the change in CT, IT and IW with treatment are illustrated in Figures 1 and 2.

CT in the infiltrated area was largest on presentation (day 0) with a mean [SD] value of 905 [206] μm. On days 3, 7, and 14 mean [SD] CT had decreased significantly to 753 [161] μm

TABLE 1. Characteristics of Patients and Bacterial Keratitis

Patients, *n*	26
Sex, *n*	
Male	13
Female	13
Age, y	
Mean	48.4
Range	21–80
Eyes, *n*	26
Laterality	
Left	8
Right	18
Risk factor	
Contact lens wear	20
Recurrent corneal erosion syndrome	2
Lagophthalmos	2
Atopy with dry eye	1
Corneal surgery—limbal relaxing incisions	1
Presentation OCT measurements	
Corneal thickness	
Mean, μm	905
Range, μm	540–1490
Infiltrate thickness	
Mean, μm	388
Range, μm	130–840
Microbiology, *n*	
Pseudomonas aeruginosa	9
Diphtheroids	1
Coagulase-negative staphylococcus	1
Staphylococcus aureus	1
Negative	8
Not performed	6

OCT, optical coherence tomography.

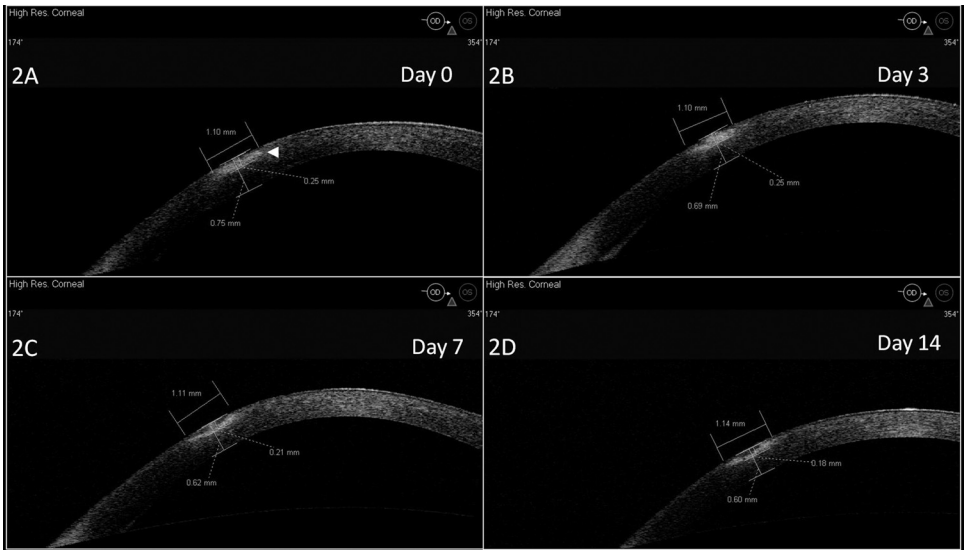

FIGURE 2. Culture-negative keratitis imaged serially with AS-OCT showing the change in corneal parameters in a contact lens wearer with presumed bacterial keratitis. Serial high-resolution AS-OCT scans have been carried out through the center of the corneal infiltration at the 174° axis. (**A**) The stromal infiltration ◀ at presentation associated with posterior bowing of the endothelium due to infiltration and edema. Corneal thickness, infiltrate thickness and infiltrate width measure 750, 250, and 1100 μm respectively. (**B**), (**C**), and (**D**) illustrate the reduction of corneal and infiltrate thickness on days 3, 7, and 14 of treatment. Infiltrate width does not decrease.

($P < 0.001$), 678 [178] μm ($P < 0.001$) and 584 [146] μm ($P < 0.001$), respectively. CT measurements were possible in all 26 (100%) eyes. The temporal change of CT is illustrated in Figure 3.

IT was also largest on presentation with a mean [SD] value of 388 [184] μm. On days 3, 7, and 14, mean [SD] IT had decreased to 320 [163] μm ($P = 0.001$), 296 [135] μm ($P = 0.004$), and 207 [87] μm ($P < 0.001$), respectively. IT measurements could be carried out in 21 (80.8%) of cases. The temporal change of IT is illustrated in Figure 4.

Mean [SD] IW on presentation was 1530 [1048] μm. IW did not change significantly during treatment with mean [SD] values of 1498 [855] μm ($P = 0.591$), 1547 [956] μm ($P = 0.878$), and 1680 [1014] μm ($P = 0.308$), on days 3, 7, and 14 respectively. IW measurements were possible in 13 (50%) eyes (Fig. 5).

CT decreased most rapidly in the early phase of treatment, with a mean [SD] daily rate of 4.49 [3.78]%. The mean [SD] daily rate of CT reduction in the middle phase was 2.69 [3.62]% (4.49 vs. 2.69, $P = 0.21$) and decreased in the late phase to 1.33 [2.29]% per day (4.49 vs. 1.33, $P = 0.006$).

IT also decreased most rapidly in the early phase of treatment, with a mean [SD] daily rate of 5.41 [5.13]%. In the middle phase, the mean [SD] daily rate of IT reduction was slower at 1.19 [6.80]% (5.41 vs. 1.19, $P = 0.042$), but accelerated again in the late phase to 3.38 [3.08]% per day (5.41 vs. 3.38, $P = 0.70$).

The mean daily rates of CT and IT reduction were not significantly different in the early (4.49% vs. 5.41%, $P = 0.49$) and middle phases of treatment (2.69 vs. 1.19, $P = 0.40$). In the late phase, however, IT decreased at a significantly faster rate than CT (3.38% vs. 1.33%, $P = 0.003$; Table 2).

Pseudomonas aeruginosa was cultured in 9 cases. A subgroup analysis was therefore carried out to compare pseudomonas to non-pseudomonas keratitis. CT on presentation was larger in the pseudomonas group (mean CT [SD]: 1072 [196] vs. 807 [142] μm, $P = 0.001$), as was IT (mean IT [SD]: 501 [117] vs. 344 [189] μm, $P = 0.057$), and IW (mean IW [SD]: 2628 [1057] vs. 1035 [565] μm, $P = 0.003$). CT and IT differences between the two pathogen groups did not persist on days 3, 7, and 14. The IW difference persisted on day 3 (mean IW [SD]: 2460 [894] vs. 1138 [566] μm, $P = 0.009$), day 7 (mean IW [SD]: 2660 [927] vs. 1052 [391] μm, $P = 0.001$), and day 14 (mean IW [SD]: 2655 [873] vs. 1167 [649] μm, $P = 0.005$) of treatment.

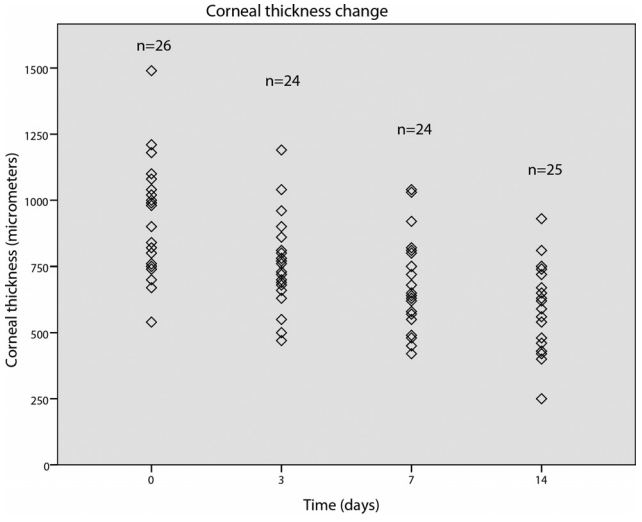

FIGURE 3. Corneal thickness reduction during treatment of bacterial keratitis.

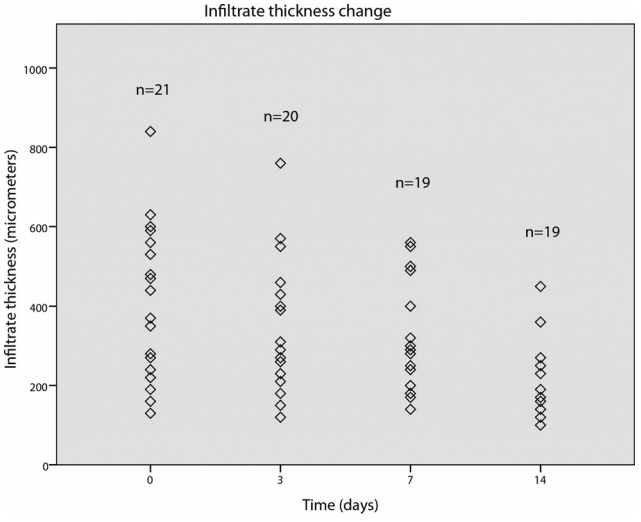

FIGURE 4. Infiltrate thickness reduction during treatment of bacterial keratitis.

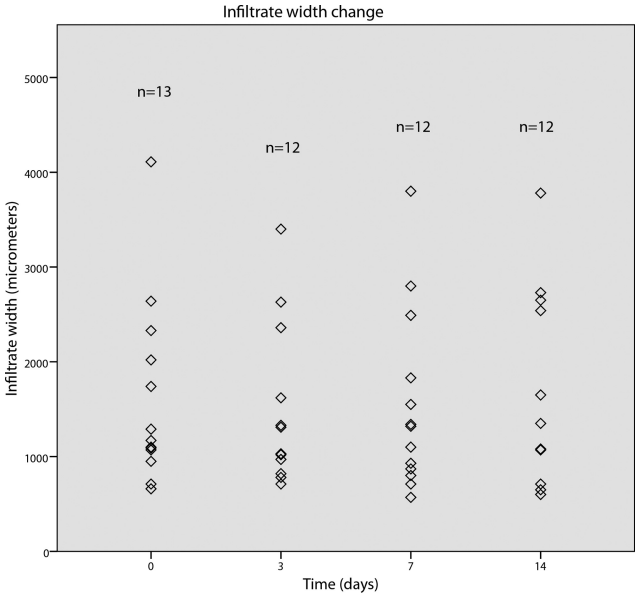

FIGURE 5. Infiltrate width in resolving bacterial keratitis.

The rate of decrease of CT was statistically larger in the pseudomonas group during the early treatment phase (mean [SD] daily rate: 7.58 [4.57] vs. 3.22 [2.61]%, $P = 0.007$), but of borderline statistical difference in the middle (mean [SD] daily rate: 4.48 [3.66] vs. 1.74 [3.32]%, $P = 0.09$) and late (mean [SD] daily rate: 2.18 [1.61] vs. 0.78 [2.54] %, $P = 0.16$) phases. The rate of decrease of IT was not statistically different in the two groups.

DISCUSSION

In this quantification study of human bacterial keratitis both CT and IT decreased significantly within three days of starting treatment, providing objective evidence that successful treatment results in an early reduction in corneal edema and inflammation. In contrast, IW did not change. This study has also shown that AS-OCT can be applied to the in vivo quantification of the course of an inflammatory condition, providing serial measurements of CT, IT, and IW in bacterial keratitis.

In addition to this early phase reduction in IT and CT, resolving bacterial keratitis showed a late phase reduction in IT. During the early and middle phases of treatment, IT and CT decreased at similar rates, indicating that a similar process may be taking place in the infiltrated and deeper non-infiltrated cornea. Reduction in corneal edema is the most likely explanation for these early changes. In the late phase, however, the reduction of CT decelerated significantly compared to the early phase and IT decreased at a significantly faster rate than CT. This suggests a different biological process to the early phase. We hypothesize that resolution of inflammatory cells and other components of the stromal infiltrate takes place in this late phase.

Pseudomonas keratitis had a larger corneal inflammatory response than non-pseudomonas keratitis. All parameters, CT, IT, and IW, were larger in corneal infection due to pseudomonas. In addition, early CT reduction was more rapid in this group. Histopathology studies have shown that inflammation in bacterial keratitis is characterized by stromal infiltration and corneal edema.[6,9,10] Experimental animal models of pseudomonas keratitis have shown intense PMN infiltration and edema on light microscopy.[10,16] The in vivo quantitative and morphologic information provided by AS-OCT is consistent with these microscopy examinations. AS-OCT technology, however, does not have the capability to distinguish inflammatory infiltration from scarring, as both appear hyper-reflective on AS-OCT.

In animal studies of keratitis, in vivo assessment of the infection severity and course is carried out with slit-lamp grading. Ocular parameters, such as conjunctival injection, chemosis, corneal infiltration, corneal edema, and iritis are quantified on a grading scale of 0 to 4 to produce a total severity score.[6] Enucleation of the eye and microscopy examination are often required to objectively assess the extent and depth of corneal infection.[9,10] The development of a portable AS-OCT device may overcome these limitations and provide objective in vivo quantification information without the requirement for enucleation.

We found that IW, as defined in this study, did not decrease with resolution of the infection. This may be explained by the proximity of the superficial margins of the infiltrated area to the immune laden tear film and limbus. In the early phase of treatment, any reduction in edema is offset by a waning immune response that is more likely to infiltrate the superficial margins rather than the compact deeper stroma. In the later phases, as the inflammatory components are gradually replaced with collagen and scar tissue, the measured width of the infiltrate would not change, as co-existing scar tissue and inflammatory infiltration both appear hyper-reflective on AS-OCT.

We could measure CT in all cases and IT in 80.8% of cases. However, IW could only be measured in 50% of cases, as the transverse margins of the infiltrate could not be identified in the remaining cases. This is most likely due to two factors. First, infiltrations have soft, ill-defined transverse margins from ongoing inflammatory activity, and second, the AS-OCT transverse imaging resolution (60 μm) is lower than the axial resolution (18 μm).[17]

This study has also demonstrated the application of AS-OCT to monitoring bacterial keratitis in clinical practice. Reiterative scans and measurements of CT, IT, and IW can be used for objective and quantitative assessment of disease severity and treatment response. Although slit-lamp biomicroscopy is the gold standard in clinical practice, evaluation of corneal inflammation is subjective and assessment of the treatment response is difficult in the early stages. AS-OCT showed a mean IT reduction of 68 μm in the early phase, a change that cannot be

TABLE 2. Rate of Change of Corneal Thickness and Infiltrate Thickness in Resolving Bacterial Keratits

Rate of Change (% per day)	Days 0–3	Days 3–7	Days 7–14
Mean daily CT decrease [SD]	4.49 [3.78]	2.69 [3.62]	1.33 [2.29]
Mean daily IT decrease [SD]	5.41 [5.13]	1.19 [6.80]	3.38 [3.08]
*P**	0.49	0.40	0.003

CT, corneal thickness; IT, infiltrate thickness.
* *P*: 2-tailed *t*-test.

detected or measured with slit-lamp biomicroscopy. The use of long wavelength light (1310 nm) in AS-OCT achieved good penetration through structures that highly scatter light, such as corneal infiltration and opacification, by non-contact examination.[12,18,19] Alternative imaging modalities, such as ultrasound biomicroscopy and Scheimpflug imaging (Pentacam), have a limited role in corneal inflammation.

In summary, AS-OCT can directly visualize, measure and monitor in vivo parameters of corneal inflammation in bacterial keratitis. Resolving corneal infection is characterized by an early reduction in corneal edema, followed by a later reduction in infiltration. Serial standardized AS-OCT scanning can be used in clinical practice to quantify and objectively assess bacterial keratitis.

References

1. Dart JKG. Predisposing factors in microbial keratitis: the significance of contact lens wear. *Br J Ophthalmol.* 1988;72:926–930.
2. McLeod SD, LaBree LD, Tayyanipour R, Flowers CW, Lee PP, McDonnell PJ. The importance of initial management in the treatment of severe infectious corneal ulcers. *Ophthalmology.* 1995; 102:1943–1948.
3. Whitcher JP, Srinivasan M, Upadhyay MP. Corneal blindness: a global perspective. *Bull World Health Organ.* 2001;79:214–221.
4. Srinivasan M. Infective keratitis: a challenge to Indian ophthalmologists. *Indian J Ophthalmol.* 2007;55:5–6.
5. Schaefer F, Bruttin O, Zografos L, Guex-Crosier Y. Bacterial keratitis: a prospective clinical and microbiological study. *Br J Ophthalmol.* 2001;85:842–847.
6. Hume EB, Dajcs JJ, Moreau JM, Sloop GD, Willcox MD, O'Callaghan RJ. Staphylococcus corneal virulence in a new topical model of infection. *Invest Ophthalmol Vis Sci.* 2001;42:2904–2908.
7. Bourcier T, Thomas F, Borderie V, Chaumeil C, Laroche L. Bacterial keratitis: predisposing factors, clinical and microbiological review of 300 cases. *Br J Ophthalmol.* 2003;87:834–838.
8. Erie JC, Nevitt MP, Hodge DO, Ballard DJ. The incidence of ulcerative keratitis in a defined population from 1950 through 1988. *Arch Ophthalmol.* 1993;111:1665–1671.
9. Girgis DO, Sloop GD, Reed JM, O'Callaghan RJ. Effects of toxin production in a murine model of Staphylococcus aureus keratitis. *Invest Ophthalmol Vis Sci.* 2005;46:2064–2070.
10. Kessler E, Mondino BJ, Brown SI. The corneal response to Pseudomonas aeruginosa: histopathological and enzymatic characterization. *Invest Ophthalmol Vis Sci.* 1977;16:116–125.
11. Efron N, Morgan PB, Hill EA, Raynor MK, Tullo AB. The size, location and clinical severity of corneal infiltrative events associated with contact lens wear. *Optom Vis Sci.* 2005;82:519–527.
12. Konstantopoulos A, Kuo J, Anderson DF, Hossain PN. Assessment of the use of anterior segment optical coherence tomography in microbial keratitis. *Am J Ophthalmol.* 2008;146:534–542.
13. Morlet N, Minassian D, Butcher J, and the Ofloxacin Study Group. Risk factors for treatment outcome of suspected microbial keratitis. *Br J Ophthalmol.* 1999;83:1027–1031.
14. Srinivasan M, Gonzales CA, George C, et al. Epidemiology and aetiological diagnosis of corneal ulceration in Madurai, South India. *Br J Ophthalmol.* 1997;81:965–971.
15. Bharathi MJ, Ramakrishnan R, Meenakshi R, Mittal S, Shivakumar C, Srinivasan M. Microbiological diagnosis of infective keratitis: comparative evaluation of direct microscopy and culture results. *Br J Ophthalmol.* 2006;90:1271–1276.
16. Steuhl KP, Doring G, Henni A, Thiel HJ, Botzenhart K. Relevance of host-derived and bacterial factors in Pseudomonas aeruginosa corneal infections. *Invest Ophthalmol Vis Sci.* 1987;28:1559–1568.
17. Konstantopoulos A, Hossain PH, Anderson DF. Recent advances in ophthalmic anterior segment imaging: a new era for ophthalmic diagnosis? *Br J Ophthalmol.* 2007;91:551–557.
18. Memarzadeh F, Li Yan, Francis BA, Smith RE, Gutmark J, Huang D. Optical coherence tomography of the anterior segment in secondary glaucoma with corneal opacity after penetrating keratoplasty. *Br J Ophthalmol.* 2007;91:189–192.
19. Radhakrishnan S, Rollins AM, Roth JE, et al. Real-time optical coherence tomography of the anterior segment at 1310nm. *Arch Ophthalmol.* 2001;119:1179–1185.

BJO Online First, published on April 5, 2013 as 10.1136/bjophthalmol-2012-301926

Deep sclerectomy versus trabeculectomy: a morphological study with anterior segment optical coherence tomography

Aris Konstantopoulos,[1,2] Mohammad E Yadegarfar,[3] Ghasem Yadegarfar,[4,5] Alina Stinghe,[1] Alex Macleod,[1] Aby Jacob,[1] Parwez Hossain[1,2]

[1]Southampton Eye Unit, University Hospital Southampton NHS Foundation Trust, Southampton, UK
[2]Clinical and Experimental Sciences, University of Southampton, Southampton, UK
[3]Commissioning Department, Wolverhampton Primary Care Trust, Wolverhampton, UK
[4]Department of Primary Care and Public Health, School of Public Health, Imperial College London, London, UK
[5]School of Public Health, Isfahan University of Medical Sciences, Isfahan, Iran

Correspondence to
Dr Parwez Hossain, Southampton Eye Unit, MP104, Southampton General Hospital, Tremona Road, Southampton SO16 6YD, UK; p.n.hossain@soton.ac.uk

Received 18 April 2012
Revised 31 January 2013
Accepted 2 March 2013

ABSTRACT

Purpose To investigate the intraocular pressure (IOP) lowering mechanisms of deep sclerectomy (DS) with anterior segment optical coherence tomography (AS-OCT).

Methods In a prospective cross-sectional study, AS-OCT parameters were compared between DS, trabeculectomy and control cases. Association with IOP and success (IOP≤16 mm Hg without medication) was investigated.

Results 18 DS (15 patients), 17 trabeculectomy (16 patients) and 15 controls (15 patients) were examined. Successful had a taller intrascleral lake (IL) and thicker conjunctival/Tenon's layer (CTL) than non-successful cases (513.3 vs 361.1 μm, p=0.027 and 586.7 vs 251.1 μm, p<0.001, respectively). CTL thickness correlated with IOP (r=−0.6407, p=0.004). CTL thickness was significantly different between controls, DS and trabeculectomy (mean (SD): 203.3 (62.6) vs 418.9 (261.9) vs 604.1 (220.7) μm, p<0.0001). Successful trabeculectomy cases had a taller bleb cavity (BC) than non-successful cases (607.5 vs 176.7 μm, p=0.041). CTL microcysts were detected in 50% of DS and 52.9% of trabeculectomy cases (p=1).

Conclusions Trans-conjunctival aqueous percolation was identified as a novel DS drainage route. DS had a fluid reservoir below the scleral flap, the IL, in analogy to the trabeculectomy BC. A postoperative tall IL and a thick CTL were associated with good outcome.

INTRODUCTION

Filtration surgery for glaucoma is usually carried out when medical and laser treatment fail to control progression of the disease. Deep sclerectomy (DS) is a non-penetrating filtration procedure that has a better safety profile than trabeculectomy.[1–4] The incidence of postoperative complications such as hypotony, flat anterior chamber, choroidal detachment, intraocular inflammation and endophthalmitis is lower than with trabeculectomy.[1–4]

The intraocular pressure (IOP) lowering mechanisms in DS are not yet fully understood. Aqueous egress through the trabeculo-Descemet's membrane (TDM) into the intrascleral lake (IL), removal of juxtacanalicular tissue, aqueous drainage via the uveoscleral pathway and through Schlemm's canal have been suggested.[5–8] In trabeculectomy, IOP reduction relies on aqueous drainage through a sclerostomy to the subconjunctival space, formation of a subconjunctival bleb cavity (BC) and trans-conjunctival aqueous percolation.[9–11]

Bleb morphology is an important indicator of bleb function and may predict the functional outcome of surgery.[12] Filtration procedure morphology has been extensively studied with ultrasound biomicroscopy (UBM) and confocal microscopy.[5 6 8–11 13] Recently, anterior segment optical coherence tomography (AS-OCT) has been used to analyse trabeculectomy characteristics, such as bleb height, bleb wall thickness and bleb wall microcysts.[14 15] AS-OCT provides higher image resolution than UBM (18 vs 25 μm) without contact examination that may alter morphology.[16]

In this prospective study, we investigate the IOP lowering mechanisms of DS and correlate AS-OCT parameters with IOP. We compare morphological features of DS to trabeculectomy and control eyes.

MATERIALS AND METHODS

Local National Health Service (NHS) Research Ethics Committee and patient informed consent were obtained. The research adhered to the tenets of the Declaration of Helsinki.

Recruitment

Consecutive trabeculectomy and DS patients with primary glaucoma at Southampton Eye Unit were invited and recruited. Procedures with follow-up less than 3 months were excluded in order to avoid potential confounders in the early postoperative stages. Postoperative needling or laser goniopuncture was not exclusion criteria. Control glaucoma patients on IOP lowering treatment were recruited in order to compare the conjunctival/Tenon's layer (CTL) of non-surgery and surgery eyes. Cataract surgery within 6 months and prior filtration surgery were exclusion criteria.

Surgery

DS procedures were carried out by one surgeon (AJ). The CTL was retracted with a fornix base at the 90° position and a 4×4 mm limbus-based scleral flap was dissected. Sclera was deep-dissected forwards to enter Schlemm's canal and expose the juxtacanalicular tissue. The dissection was continued forward to de-roof Schlemm's canal and expose a thin TDM. The deep scleral block was excised and juxtacanalicular tissue peeled from the opened Schlemm's canal. The intrascleral space was filled with viscoelastic (VISCOAT) but no implant. Finally, the scleral flap and CTL were sutured with 10/0 vicryl sutures.

In trabeculectomy (surgeons AJ and AM), the CTL was retracted with a fornix base at the 90°

To cite: Konstantopoulos A, Yadegarfar ME, Yadegarfar G, *et al*. *Br J Ophthalmol* Published Online First: [*please include* Day Month Year] doi:10.1136/bjophthalmol-2012-301926

position and mitomycin-C 0.2 mg/ml or 5-fluorouracil 50 mg/ml was applied for 2–3 min and then thoroughly washed. A 4×3 mm limbus-based scleral flap was dissected and a sclerostomy performed using the Kelly punch. The scleral flap was sutured watertight with fixed and releasable 10/0 nylon sutures, the opening pressure titrated via a paracentesis. The CTL was sutured with 10/0 nylon sutures.

AS-OCT imaging

AS-OCT imaging (Visante OCT, Carl Zeiss Meditec Inc, Dublin, California, USA) was carried out with the upper eyelid elevated and the patient looking down. The rotating scanning beam of the four-quadrant high-resolution mode was centred on the scleral flap by direct visualisation on the integrated camera. Multiple scans were carried out and the scan that was best centred on the scleral flap was analysed. For control patients, the scanning beam was centred 2–3 mm posterior to the limbus at the 90° position. The AS-OCT user (AK) who carried out image acquisition, analysis and measurements was masked to the outcome of each case (figures 1–4). Interesting AS-OCT filtration procedure parameters are presented in figure 5.

Analysis

Images were analysed for the presence of a BC, CTL microcysts, posterior drainage, drainage under the trabeculectomy scleral flap and suprachoroidal drainage. The BC was defined as a hyporeflective area above the sclera, CTL microcysts as small (at least 10 μm diameter) hyporeflective spaces within the CTL, posterior drainage as a hyporeflective area at or behind the posterior scleral flap edge, drainage under the trabeculectomy scleral flap as a hyporeflective area under the flap and suprachoroidal drainage as a hyporeflective area between sclera and choroid. The maximum height of the BC was measured. Height of filtration procedure and CTL thickness were measured at the posterior scleral flap edge on the 90° scan. Height of filtration procedure was defined as the distance from the superior surface of the scleral flap to the outer surface of the CTL, and CTL thickness as the distance between the inner and outer surfaces of the CTL. For DS cases, maximum IL height, perpendicular to the TDM, was measured. The IL was defined as the hyporeflective space between the lower surface of the scleral flap and the superior surface of the TDM. The TDM thickness, defined as the distance between the superior and inferior surfaces of the TDM, was measured at the centre of the TDM on the 90° scan. In control patients, CTL thickness was measured 3 mm posterior to the irido-corneal angle on the 90° scan. Software callipers were used for measurements.

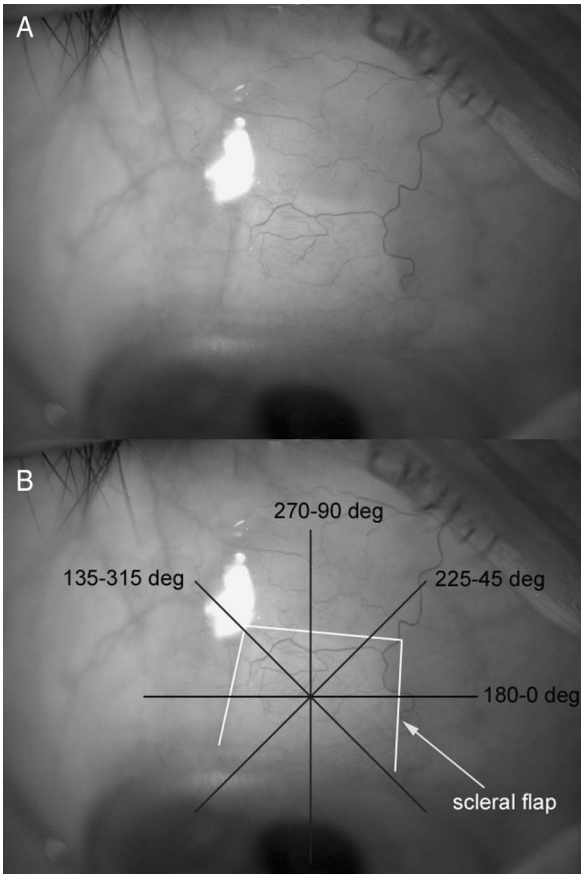

Figure 1 The anterior segment optical coherence tomography (AS-OCT) scanning protocol is illustrated. (A) A photo of a deep sclerectomy. (B) Illustrates that the AS-OCT rotating scanning beam of the four-quadrant high-resolution mode is centred on the scleral flap of the filtration procedure.

Patient age, type of glaucoma, preoperative Goldmann IOP, number of preoperative IOP lowering agents, type of filtration procedure and antimetabolite use, postoperative IOP and number of IOP lowering agents at the time of the AS-OCT scan were recorded. IOP≤16 mm Hg at the time of the scan without glaucoma medication was used to define a successful and a non-successful group. A strict success criterion was chosen in order to avoid random allocation due to IOP fluctuation.

AS-OCT parameters were compared between the DS, trabeculectomy and control groups. They were examined for association with IOP and success in the surgical groups. In addition, the DS and trabeculectomy procedures were grouped together and analysed collectively as the 'filtration group'.

Normality distribution of data was assessed by Kolmogorov–Smirnov statistics, normal distribution plots and histograms. All variables had a skewed distribution; therefore, the Kruskal–Wallis test, Mann–Whitney U test, Wilcoxon signed-rank test and Spearman correlation coefficient were used to analyse numerical outcomes. Fisher's exact test was used to compare categorical outcomes. Differences were considered statistically significant when $p<0.05$. SAS V.9.1 (SAS Institute Inc, Cary, North Carolina, USA) was used.

RESULTS

Eighteen DS, 17 trabeculectomy and 15 control cases were examined. Three DS and 11 trabeculectomy procedures had been augmented with preoperative mitomycin-C, and 6 trabeculectomy procedures with 5-fluorouracil. There was no difference in patient age, glaucoma type and IOP on the scan day between the three groups (table 1). Both DS and trabeculectomy groups had a significant IOP reduction compared with before surgery (22.3 vs 16.9 mm Hg, $p<0.001$ and 22.5 vs 14.4 mm Hg, $p<0.001$ respectively). Results are summarised in tables 2–4.

Bleb cavity and intrascleral lake

A BC was detected more frequently in trabeculectomy than DS procedures (64.7% vs 22.2%, $p=0.018$). In the glaucoma 'filtration group' (n=35), eyes with a BC had lower IOP than eyes without a BC (mean (SD):13.1 (4.3) vs 17.7 (5.0) mm Hg, $p=0.006$). The presence of BC was also associated with success ($p=0.005$). Trabeculectomy procedures with a BC had a borderline significantly lower IOP than eyes without BC (mean (SD):12.4 (4.7) vs 18.2 (6.3) mm Hg, $p=0.077$). The presence of BC also showed a borderline association with success ($p=0.109$). Successful trabeculectomy procedures had a

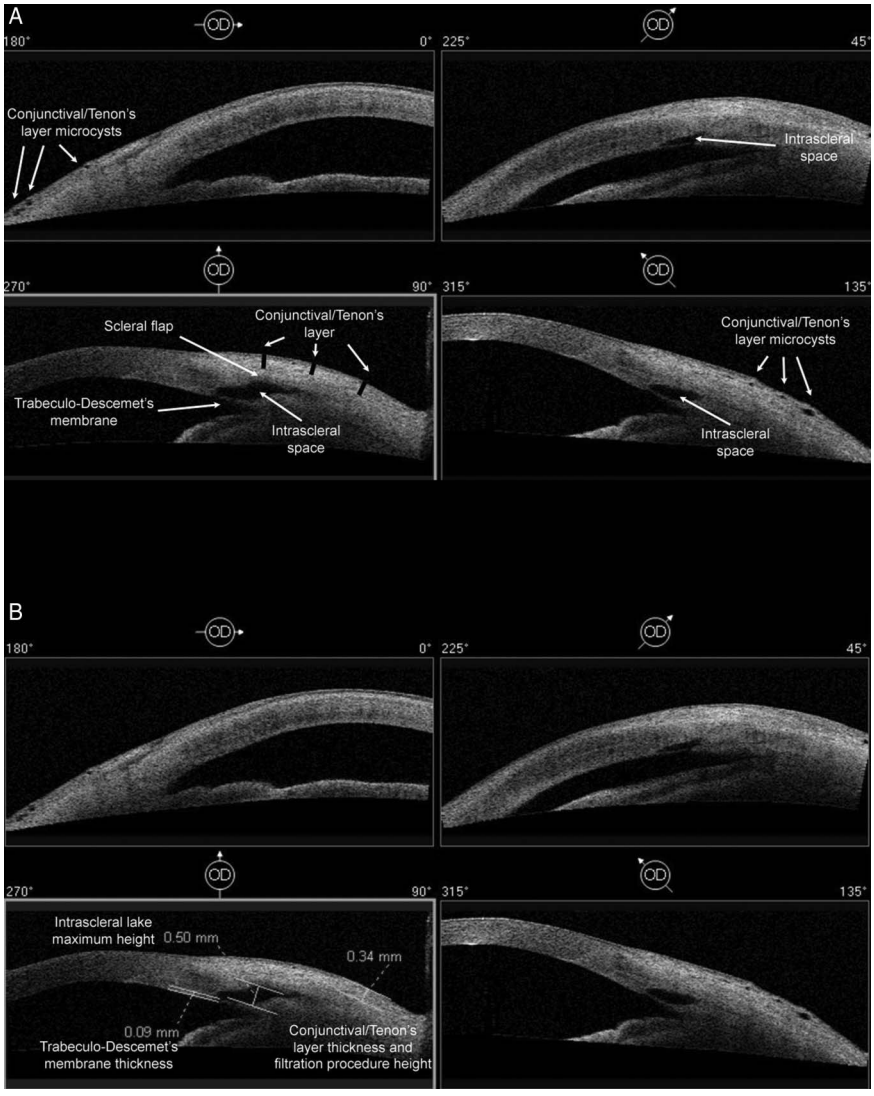

Figure 2 Anterior segment optical coherence tomography scan of a deep sclerectomy. (A) Illustrates the morphology of the filtration procedure and (B) the measurement of the filtration procedure parameters.

significantly taller BC than non-successful eyes (607.5 vs 176.7 μm, p=0.041). However, maximum BC height was not associated with IOP (r=0.235, p=0.488). Maximum IL height in DS did show a negative correlation with IOP (r=−0.493, p=0.038) and successful eyes had a significantly taller IL than non-successful eyes (513.3 vs 361.1 μm, p=0.027).

Height of filtration procedure

Height of filtration procedure was smaller in DS than trabeculectomy (418.9 vs 699.4 μm, p=0.005). In the 'filtration group' successful procedures were taller than non-successful procedures (713.5 vs 344 μm, p<0.001); height correlated negatively with IOP (r=−0.455, p=0.006).

Successful DS procedures were taller than non-successful cases (586.7 vs 251.1 μm, p<0.001) and height of filtration procedure correlated negatively with IOP (r=−0.641, p=0.004). Successful trabeculectomy procedures were taller than non-successful cases (817.3 vs 483.3 μm, p=0.021), but height did not correlate with IOP (r=−0.368, p=0.147).

Conjunctival/Tenon's layer

CTL thickness in the 'filtration group' correlated negatively with IOP (r=−0.397, p=0.018) and successful procedures had a thicker CTL than non-successful cases (632.5 vs 344 μm, p<0.001).

Successful DS procedures had a thicker CTL than non-successful cases (586.7 vs 251.1 μm, p<0.001) and CTL thickness correlated negatively with IOP (r=−0.641, p=0.004). Successful trabeculectomy procedures had borderline significantly thicker CTL than non-successful cases (670 vs 483.3 μm, p=0.107); CTL thickness did not correlate with IOP (r=−0.254, p=0.325).

In control eyes, CTL thickness did not correlate with IOP on the scan day (r=0.137, p=0.627). There was a significant difference in CTL thickness between control, DS and trabeculectomy groups (mean (SD): 203.3 (62.6) vs 418.9 (261.9) vs 604.1 (220.7) μm, p<0.0001). The CTL of non-successful procedures in the 'filtration group' was thicker than in control cases (mean (SD): 344 (194.2) vs 203.3 (62.6) μm, p=0.004).

CTL microcysts were detected in 50% of DS and 52.9% of trabeculectomy cases (p=1), but absent in control eyes. In the 'filtration group', eyes with CTL microcysts did not have lower IOP than eyes without CTL (mean (SD): 15.1 (5.2) vs 16.3 (5.2) mm Hg, p=0.547). The presence of CTL microcysts was not associated with success either (p=0.092).

Drainage posterior to and under the flap

Successful procedures in the 'filtration group' showed posterior drainage with borderline higher frequency than non-successful cases (p=0.057). Eyes with posterior drainage did not have

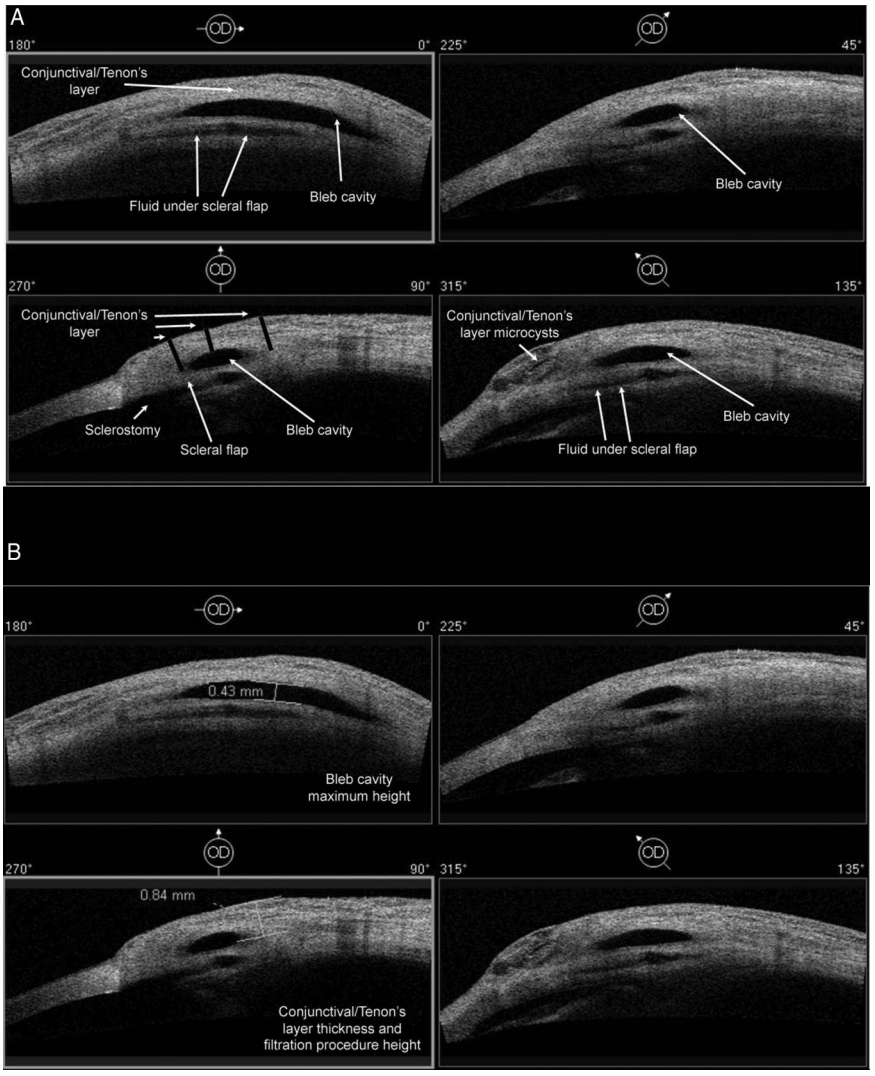

Figure 3 Anterior segment optical coherence tomography scan of a trabeculectomy. (A) Illustrates the morphology of the filtration procedure and (B) the measurement of the filtration procedure parameters.

lower IOP than eyes without IOP (mean (SD): 13 (3.2) vs 16.1 (5.3) mm Hg, p=0.121).

DS cases and trabeculectomy eyes with posterior drainage did not have lower IOP than cases without IOP (mean (SD): 14 (2.8) vs 17.3 (4.2) mm Hg, p=0.218 and 12.3 (3.8) vs 14.9 (6.2) mm Hg, p=0.447 respectively). In trabeculectomy, IOP was not lower in eyes with drainage under the flap than eyes without (mean (SD): 12.7 (5.2) vs 15.6 (6.3) mm Hg, p=0.404).

Drainage posterior to and under the flap were not associated with success (table 4).

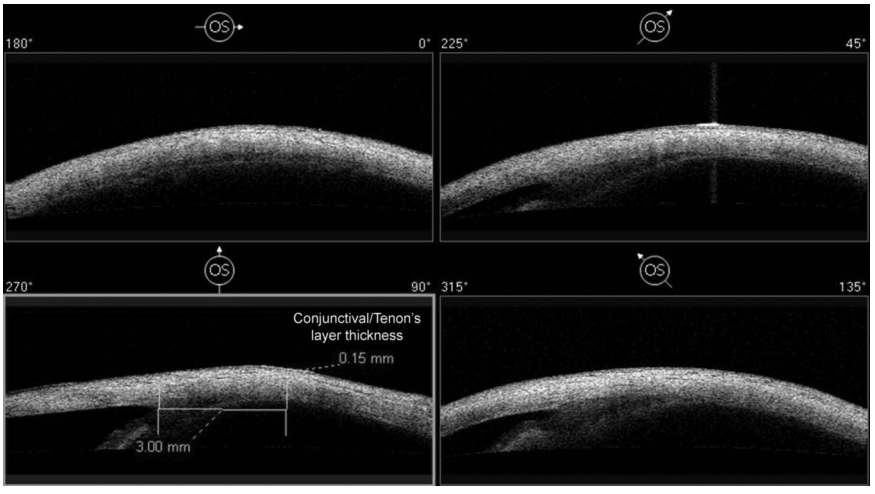

Figure 4 Anterior segment optical coherence tomography scan of a non-operated eye. Measurement of the conjunctival/Tenon's layer 3 mm posterior to the angle on the 90° scan is illustrated.

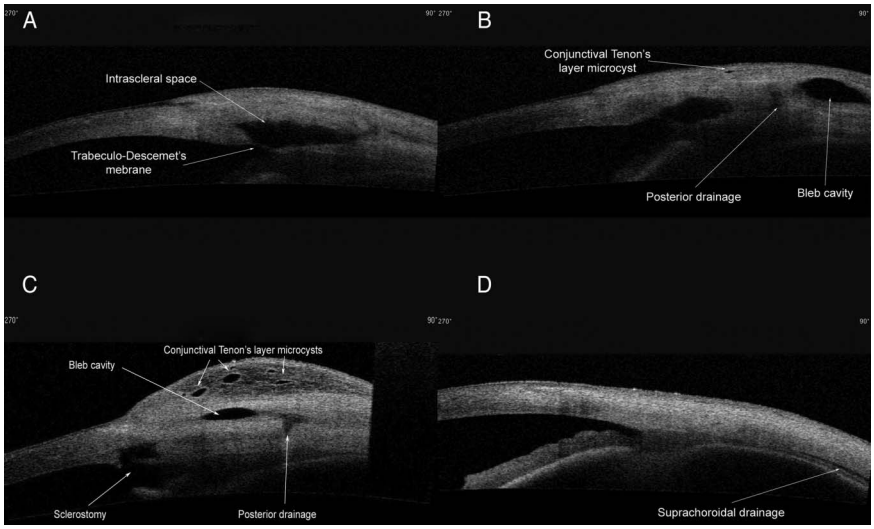

Figure 5 Anterior segment optical coherence tomography scan of interesting filtration procedure parameters. (A) Shows the very tall intrascleral lake of a successful deep sclerectomy. (B) Illustrates a deep sclerectomy with the presence of a bleb cavity. (C) Illustrates a trabeculectomy with high aqueous outflow; a thick conjunctival/Tenon's layer with numerous microcysts is present. (D) Shows the presence of suprachoroidal drainage in a control patient using latanoprost 0.005% (Xalatan).

Suprachoroidal drainage

Suprachoroidal drainage was detected in one control case but no surgical case.

Trabeculo-Descemet's membrane

TDM thickness (mean 56.7 μm) did not show an association with IOP or success.

DISCUSSION

This study has demonstrated in-vivo morphological differences between DS and trabeculectomy. DS developed a fluid reservoir below the scleral flap, the IL, whereas trabeculectomy developed a reservoir above the flap, the BC. The height of IL and BC was associated with good outcome. CTL microcysts were present equally in DS and trabeculectomy, indicating that trans-conjunctival aqueous percolation also takes place in DS.

The importance of IL height, and possibly reservoir dimensions, is only becoming clearer with the advent of AS-OCT. The IL height in DS correlated negatively with IOP and was larger in successful cases, confirming findings by Mavracanas *et al*.[17] UBM has previously failed to find this association,[8] most likely due to its inferior resolution. AS-OCT imaging provides evidence that aqueous egress via the TDM is an important drainage

Table 1 Patient characteristics

Parameter	Deep sclerectomy	Trabeculectomy	Controls	p Value
Patients	15	16	15	
Eyes	18	17	15	
Patient age				
Mean (SD) (years)	76.4 (12.1)	71.5 (11.6)	78.8 (8.0)	0.198*
Glaucoma type (eyes)				
POAG	15 (83.3%)	11 (64.7%)	10 (66.7%)	0.454†
PACG	2	3	1	
NTG	0	1	1	
Other	1	2	3	
Preoperative IOP				
Mean (SD) (mm Hg)	22.3 (3.6)	22.5 (3.2)		0.727‡
Preoperative IOP agents				
Mean (SD)	2.67 (1.14)	3.41 (1.00)		0.069‡
Follow-up on scan day				
Mean (SD) (days)	482.2 (218.6)	372.2 (143.5)	NA	0.171‡
Range (days)	108–869	128–631		
IOP on scan day				
Mean (SD) (mm Hg)	16.9 (4.2)	14.4 (5.9)	17.6 (3.5)	0.093*
Success§				
Yes	9 (50%)	11 (64.7%)	NA	0.499†
IOP agents on scan day				
Mean (SD)	0.56 (0.86)	0.29 (0.77)	2.47 (0.92)	<0.001*

*Kruskal–Wallis test.
†Fisher's exact test.
‡Mann–Whitney U test.
§IOP≤16 mm Hg without glaucoma medication.
IOP, intraocular pressure; NTG, normal tension glaucoma; PACG, primary angle closure glaucoma; POAG, primary open angle glaucoma.

Table 2 Anterior Segment Optical Coherence Tomography comparison of deep sclerectomy and trabeculectomy

Bleb parameter	Deep sclerectomy	Trabeculectomy	p Value
Bleb cavity presence			
Yes	4 (22.2%)	11 (64.7%)	0.018*
CTL microcyst presence			
Yes	9 (50%)	9 (52.9%)	1*
Height of filtration procedure			
Mean (SD) (μm)	418.9 (261.9)	699.4 (280.9)	0.005†
CTL thickness			
Mean (SD) (μm)	418.9 (261.9)	604.1 (220.7)	0.016†
Bleb cavity maximum height			
Mean (SD) (μm)		490 (367.4)	
Intrascleral lake maximum height			
Mean (SD) (μm)	437.2 (155.8)		
TDM thickness			
Mean (SD) (μm)	56.7 (17.2)		

*Fisher's exact test.
†Mann–Whitney U test.
CTL, conjunctival/Tenon's layer; TDM, trabeculo-Descemet's membrane.

mechanism and that good aqueous outflow is associated with a large fluid reservoir in DS.

The higher aqueous outflow in trabeculectomy compared to the slower aqueous egress in DS was associated with BC development, as a BC was present more frequently in trabeculectomy. BC height was larger in successful procedures, suggesting that the BC acts as an aqueous reservoir. The IL in DS may also function as a fluid reservoir, analogous to the trabeculectomy BC. In agreement with Tominaga *et al*,[15] we found that BC height did not correlate with IOP. The difference between the two outcome measures, IOP and success, may reflect the confounding effect of IOP lowering agents on IOP correlation analyses.

Excessive conjunctival scarring at the filtration site is a major cause of poor outcome.[18–20] In DS, the CTL thickness correlated negatively with IOP and successful cases had a thicker CTL than non-successful eyes. Similarly in trabeculectomy, successful procedures had a thicker CTL, although of borderline statistical significance. Previous AS-OCT studies have found that successful trabeculectomy procedures have a thicker wall than non-successful cases.[14 15] This suggests that in both filtration procedures, good drainage is associated with increased CTL thickness.

Table 3 Correlation of anterior segment optical coherence tomography filtration parameters with intraocular pressure

Bleb parameter	Spearman correlation coefficient	p Value
Filtration group (n=35)		
Height of filtration procedure	−0.455	0.006
CTL thickness	−0.397	0.018
Deep sclerectomy (n=18)		
CTL thickness	−0.641	0.004
Intrascleral lake maximum height	−0.493	0.038
Height of filtration procedure	−0.641	0.004
TDM thickness	−0.0502	0.843
Trabeculectomy (n=17)		
CTL thickness	−0.254	0.325
Height of filtration procedure	−0.368	0.147
Bleb cavity maximum height	0.235	0.488

CTL, conjunctival/Tenon's layer; TDM, Trabeculo-Descemet's membrane.

Table 4 Association of anterior segment optical coherence tomography filtration parameters with success

Bleb parameter	Successful*	Non-successful	p Value
Deep sclerectomy (n=18)			
Posterior drainage			
Yes/no	2/7	0/9	0.471†
Bleb cavity presence			
Yes/no	4/5	0/9	0.082†
Height of filtration procedure			
Mean (SD) (μm)	586.7 (280.8)	251.1 (60.1)	<0.001‡
CTL thickness			
Mean (SD) (μm)	586.7 (280.8)	251.1 (60.1)	<0.001‡
Intrascleral lake maximum height			
Mean (SD) (μm)	513.3 (147.8)	361.1 (129.2)	0.027‡
TDM thickness			
Mean (SD) (μm)	60 (22.4)	53.3 (10)	0.784‡
Trabeculectomy (n=17)			
Posterior drainage			
Yes/no	3/8	0/6	0.515†
Drainage under flap			
Yes/no	6/5	4/2	1.0†
Bleb cavity presence			
Yes/no	9/2	2/4	0.109†
Height of filtration procedure			
Mean (SD) (μm)	817.3 (229.0)	483.3 (247.0)	0.021‡
CTL thickness			
Mean (SD) (μm)	670 (184.1)	483.3 (247.0)	0.107‡
Bleb cavity maximum height			
Mean (SD) (μm)	607.5 (359.2)	176.7 (143.6)	0.041‡

*Intraocular pressure ≤16 mm Hg without glaucoma medication.
†Fisher's exact test.
‡Mann–Whitney U test.
CTL, conjunctival/Tenon's layer; TDM, Trabeculo-Descemet's membrane.

No study to date had examined CTL thickness in DS. The CTL was thinner than in trabeculectomy and success was associated with thicker CTL. Trabeculectomy confocal microscopy studies have shown that functioning blebs have a loose arrangement of subepithelial connective tissue.[10 11] Well-functioning DS procedures may have a similar loose subepithelial connective tissue resulting in a relatively thick CTL, whereas less well-draining procedures may have dense connective tissue with a thinner CTL.

A histological study by Addicks *et al*[18] has found that the subepithelial connective tissue was thicker in failed blebs than in normal eyes or functioning blebs. Our findings support that failed filtration procedures have a thicker subepithelial connective tissue than normal eyes. However, our in-vivo CTL measurements, supported by other OCT studies,[14 15 21] suggest that failed blebs have a thinner connective tissue layer than functioning blebs.

We did not find a significant association between drainage posterior to or under the scleral flap and success or IOP. Decreasing image resolution as AS-OCT penetrates the thickened CTL may limit investigation of the role of resistance by the scleral flap. The small number of cases may have also contributed, as posterior drainage in the larger 'filtration group' showed borderline association (p=0.057) with success.

Height of filtration procedure in DS was associated with success and correlated with IOP. In DS, the height depends

almost exclusively on CTL thickness. Successful trabeculectomy procedures were taller than non-successful cases. This is most likely due to the fact that height in trabeculectomy is a measure of CTL thickness and BC height, both parameters found in our study to be larger in successful cases. Previous AS-OCT work has not found an association between trabeculectomy height and success or IOP.[14 15] A three-dimensional OCT study, however, did show that trabeculectomy height correlated with IOP and was associated with success.[21] In our study, height of filtration procedure in trabeculectomy did not correlate with IOP. The lack of correlation may be due to the confounding effect of pressure lowering agents on correlation analyses with IOP as an outcome measure.

CTL microcysts were present in DS and trabeculectomy procedures equally while absent from control eyes, providing in-vivo anatomical evidence that trans-conjunctival aqueous drainage is an important drainage mechanism in DS. Our findings suggest that trans-conjunctival aqueous percolation from their respective reservoirs occurs equally in DS and trabeculectomy. Confocal microscopy and three-dimensional OCT studies on trabeculectomy have documented the important drainage role of CTL microcysts with the number of microcysts correlating with good bleb function.[9–11 21 22]

We used the Visante OCT four-quadrant high-resolution mode for imaging. The four scans provide information on the anterior–posterior and medial–lateral extension of the drainage area. This scanning mode provides an easy, quick and objective assessment of the drainage area that can readily be integrated into clinical practice.

In conclusion, visualisation and comparison of morphology of glaucoma filtration procedures with AS-OCT have provided novel insight into the drainage mechanisms of surgery, especially for non-penetrating DS. A tall, and therefore, large fluid reservoir, either IL or BC, is important to success. A thicker CTL in the postoperative period is also associated with low IOP. Focusing research on these two important parameters may guide the evolution of modern glaucoma surgery.

Contributors AK, AJ and PH designed the study; AK, AS and AJ conducted the study; AK and AS performed data collection; AK, MEY and GY performed data management; AK, MEY and GY performed data analysis; AK, AJ and AM performed data interpretation; AK, AJ and PH prepared the manuscript; AK, AM, AJ and PH reviewed the manuscript; AK, AJ, AM and PH performed approval of manuscript.

Competing interests None.

Ethics approval NHS Berkshire Research Ethics Committee.

Provenance and peer review Not commissioned; externally peer reviewed.

REFERENCES

1 Mermoud A, Schnyder CC, Sickenberg M, *et al*. Comparison of deep sclerectomy with collagen implant and trabeculectomy in open angle glaucoma. *J Cataract Refract Surg* 1999;25:323–31.
2 El Sayyad F, Helal M, El-Kholify H, *et al*. Nonpenetrating deep sclerectomy versus trabeculectomy in bilateral primary open angle glaucoma. *Ophthalmology* 2000;107:1671–4.
3 Dupas B, Fardeau C, Cassoux N, *et al*. Deep sclerectomy and trabeculectomy in uveitic glaucoma. *Eye* 2010;24:310–14.
4 Ang GS, Varga Z, Shaarawy T. Postoperative infection in penetrating versus non-penetrating glaucoma surgery. *Br J Ophthalmol* 2010;94:1571–6.
5 Chiou AG, Mermoud A, Hediguer SE, *et al*. Ultrasound biomicrosopy of eyes undergoing deep sclerectomy with collagen implant. *Br J Ophthalmol* 1996;80:541–4.
6 Roters S, Luke C, Jonescu-Cuypers CP, *et al*. Ultrasound biomicroscopy and its value in predicting the long term outcome of viscocanalostomy. *Br J Ophthalmol* 2002;86:997–1001.
7 Delarive T, Rossier A, Rossier S, *et al*. Aqueous dynamic and histological findings after deep sclerectomy with collagen implant in an animal model. *Br J Ophthalmol* 2003;87:1340–4.
8 Khairy HA, Atta HR, Green FD, *et al*. Ultrasound biomicroscopy in deep sclerectomy. *Eye* 2005;19:555–60.
9 Ciancaglini M, Carpineto P, Agnifili L, *et al*. Conjunctival characteristics in primary open angle glaucoma and modifications induced by trabeculectomy with mitomycin C: an in vivo confocal microscopy study. *Br J Ophthalmol* 2009;93:1204–9.
10 Labbe A, Dupas B, Hamard P, *et al*. In vivo confocal microscopy study of blebs after filtering surgery. *Ophthalmology* 2005;112:1979–86.
11 Amar N, Labbé A, Hamard P, *et al*. Filtering blebs and aqueous pathway an immunocytological and in vivo confocal microscopy study. *Ophthalmology* 2008;115:1154–61.
12 Azuara-Blanco A, Katz LJ. Dysfunctional filtering blebs. *Surv Ophthalmol* 1998;43:93–126.
13 Yamamoto T, Sakuma T, Kitakawa Y. An ultrasound biomicroscopic study of filtering blebs after mitomycin C trabeculectomy. *Ophthalmology* 1995;102:1770–6.
14 Singh M, Chew PT, Friedman DS, *et al*. Imaging of trabeculectomy blebs using anterior segment optical coherence tomography. *Ophthalmology* 2007;114:47–53.
15 Tominaga A, Miki A, Yamazaki Y, *et al*. The assessment of the filtering bleb function with anterior segment optical coherence tomography. *J Glaucoma* 2010;9:551–5.
16 Konstantopoulos A, Hossain PH, Anderson DF. Recent advances in ophthalmic anterior segment imaging: a new era for ophthalmic diagnosis? *Br J Ophthalmol* 2007;91:551–7.
17 Mavracanas N, Mendrinos E, Shaarawy T. Postoperative IOP is related to intrascleral bleb height in eyes with clinically flat blebs following deep sclerectomy with collagen implant and mitomycin. *Br J Ophthalmol* 2010;94:410–13.
18 Addicks EM, Quigley A, Green WR, *et al*. Histological characteristics of filtering blebs in glaucomatous eyes. *Arch Ophthalmol* 1983;101:795–8.
19 Lama PJ, Fechtner RD. Antifibrotics and wound healing in glaucoma surgery. *Surv Ophthalmol* 2003;48:314–46.
20 Hitchings RA, Grierson I. Clinico pathological correlation in eyes with failed fistulising surgery. *Trans Ophthalmol Soc UK* 1983;103:84–8.
21 Kawana K, Kiuchi T, Yasuno Y, *et al*. Evaluation of trabeculectomy blebs using 3-dimensional cornea and anterior segment optical coherence tomography. *Ophthalmology* 2009;116:848–55.
22 Messmer EM, Zapp DM, Mackert MJ, *et al*. In vivo confocal microscopy of filtering blebs after trabeculectomy. *Arch Ophthalmol* 2006;124:1095–103.

PLOS | ONE

RESEARCH ARTICLE

Prophylactic Vancomycin Drops Reduce the Severity of Early Bacterial Keratitis in Keratoprosthesis

Aris Konstantopoulos[1,2], Xiao Wei Tan[1], Gwendoline Tze Wei Goh[1], Padmanabhan Saraswathi[1], Liyan Chen[1], Chan Lwin Nyein[1], Lei Zhou[1], Roger Beuerman[1], Donald Tiang Hwee Tan[1,2,3], Jod Mehta[1,2,3,4]*

1 Singapore Eye Research Institute, Singapore, **2** Singapore National Eye Centre, Singapore, **3** Department of Clinical Sciences, Duke-NUS Graduate Medical School, Singapore, **4** Nanyang Technological University, Singapore

* jodmehta@gmail.com

OPEN ACCESS

Citation: Konstantopoulos A, Tan XW, Goh GTW, Saraswathi P, Chen L, Nyein CL, et al. (2015) Prophylactic Vancomycin Drops Reduce the Severity of Early Bacterial Keratitis in Keratoprosthesis. PLoS ONE 10(10): e0139653. doi:10.1371/journal.pone.0139653

Editor: Rajiv R. Mohan, University of Missouri-Columbia, UNITED STATES

Received: May 29, 2015

Accepted: August 16, 2015

Published: October 13, 2015

Data Availability Statement: All relevant data are within the paper and its Supporting Information files.

Funding: This research was supported by the Singapore National Research Foundation under its Translational and Clinical Research (TCR) Programme (NMRC/TCR/008-SERI/2013) and administered by the Singapore Ministry of Health's National Medical Research Council. Authors that received funding: LZ, RWB, DTT, JSM. The funders had no role in study design, data collection and analysis, decision to publish, or preparation of the manuscript.

Abstract

Background

Artificial cornea transplantation, keratoprosthesis, improves vision for patients at high risk of failure with human cadaveric cornea. However, post-operative infection can cause visual loss and implant extrusion in 3.2–17% of eyes. Long-term vancomycin drops are recommended following keratoprosthesis to prevent bacterial keratitis. Evidence, though, in support of this practice is poor. We investigated whether prophylactic vancomycin drops prevented bacterial keratitis in an animal keratoprosthesis model.

Methodology

Twenty-three rabbits were assigned either to a prophylactic group (n = 13) that received vancomycin 1.4% drops 5 times/day from keratoprosthesis implantation to sacrifice, or a non-prophylactic group (n = 10) that received no drops. All rabbits had *Staphylococcus aureus* inoculation into the cornea at 7–12 days post-implantation and were sacrificed at predetermined time-points. Prophylactic and non-prophylactic groups were compared with slit-lamp photography (SLP), anterior segment optical coherence tomography (AS-OCT), and histology, immunohistochemistry and bacterial quantification of excised corneas. Corneal vancomycin pharmacokinetics were studied in 8 additional rabbits.

Results

On day 1 post-inoculation, the median SLP score and mean±SEM AS-OCT corneal thickness (CT) were greater in the non-prophylactic than the prophylactic group (11 vs. 1, p = 0.049 and 486.9±61.2 vs. 327.4±37.1 μm, p = 0.029 respectively). On days 2 and 4, SLP scores and CT were not significantly different. Immunohistochemistry showed a greater CD11b+ve/non-CD11b+ve cell ratio in the non-prophylactic group (1.45 vs. 0.71) on day 2. Bacterial counts were not significantly different between the two groups. Corneal

Competing Interests: The authors have declared that no competing interests exist.

vancomycin concentration (2.835±0.383 μg/ml) exceeded minimum inhibitory concentration (MIC) for *Staphylococcus aureus* only after 16 days of vancomycin drops. Two of 3 rabbits still developed infection despite bacterial inoculation after 16 days of prophylactic drops.

Conclusions

Prophylactic vancomycin drops provided short-term benefit, but did not prevent infection. Achieving MIC in the cornea was not sufficient to prevent *Staphylococcus aureus* keratitis. Patients should continue to be counselled regarding the risk of infection following keratoprosthesis.

Introduction

Corneal infection and inflammatory disorders are significant causes of global visual impairment and blindness. According to the World Health Organisation, corneal disease predominantly in association with infection and scarring is a major cause of blindness in the world, second only to cataract.[1] Globally, 2.85 million people are estimated to be visually impaired and 1.56 million blind due to corneal opacities.[2] In addition to limited worldwide availability of high quality corneal material, the prognosis of corneal grafts, even in developed countries, is relatively poor in the presence of ocular surface disease, inflammation or failed previous graft.[3,4] Artificial corneas have the potential to eliminate immune mediated rejection and failure, especially in higher risk cases.

Results with fully synthetic corneas have been poor;[5,6] the AlphaCor artificial cornea had a retention rate of 80% and 62% at 1 and 2 years respectively.[5] Devices that use a hybrid of synthetic and biological tissue, such as the Boston keratoprosthesis (Kpro), have recently gained in popularity, as they provide visual improvement with a low extrusion rate.[7–9] In a large multi-centre study, the Boston type 1 retention rate was 67% at 7 years.[10] Limitations, however, such as the requirement for cadaveric cornea, the development of glaucoma, retroprosthetic membrane and infection limit more widespread use.[7,11–13]

Infection in Kpro is a devastating complication that can cause acute deterioration of vision. Published rates vary depending on follow-up, ranging between 3.2–17% of eyes.[14–17] Prophylactic vancomycin drops following Boston Kpro have been accredited with a reduction in rate of bacterial endophthalmitis.[18,19] However, they have not been found to reduce bacterial keratitis rates in Boston Kpro.[16] Studies on Kpro associated infection should be interpreted within the context of their retrospective nature, small cohorts and heterogeneity of patients and causative microbial pathogens.

In this prospective study we investigated whether regular application of vancomycin drops could prevent the development of *Staphylococcus aureus* keratitis in an established animal model of Kpro associated microbial keratitis.[20]

Materials and Methods

The study adhered to the Statement for Use of Animals in Ophthalmic Vision and Research by the Association for Research in Vision and Ophthalmology. The protocol was approved by the Institutional Animal Care and Use Committee and Institutional Biosafety Committee at Singapore Eye Research Institute. Thirty-one New Zealand White rabbits were used.

Rabbit model

New Zealand White rabbits, aged 1 to 2 months and weighing 2 to 2.5 kg, were anaesthetised using an intramuscular injection of ketamine hydrochloride (35 mg/kg; Parnell Laboratories, Alexandria, Australia) and xylazine hydrochloride (5 mg/kg; Troy Laboratories, Smithfield, Australia). The right eye was chosen for surgery and a titanium film implanted, as previously described.[20] Briefly, a 7 mm diameter and 75% deep corneal stromal pocket was created using the Visumax^{TM} femtosecond laser (Carl Zeiss Meditec, Jena, Germany). A 5 mm wide superior arcuate incision was made by a guarded diamond blade (Storz, Bausch and Lomb, USA), the pocket opened up with a Seibel spatula (Rhein Medical Inc., Petersburg, FL) and a 4 mm diameter titanium film implanted into the pocket.

Twenty-three rabbits, used for the prophylactic versus non-prophylactic study, had a 25 μl bacterial solution (*Staphylococcus aureus* ATCC29213, 2X10^4 CFU/ml) inoculated with a 29 G needle into the corneal pocket above the titanium film at 7–12 days post-implantation and were sacrificed at predetermined time-points (Fig 1). Euthanasia was carried out with intravenous pentobarbitone (85 mg/kg) in anaesthetized rabbits.

Eight rabbits were used exclusively to study the corneal pharmacokinetics of vancomycin and the effectiveness of the corneal vancomycin minimum inhibitory concentration (MIC) for *S. aureus*; 3 rabbits without an implant were sacrificed after 4 days of bilateral vancomycin drop instillation, 2 rabbits with a titanium film implant were sacrificed after 10 days of vancomycin drop instillation and 3 rabbits with a titanium film implant had a 25 μl bacterial solution (*Staphylococcus aureus* ATCC29213, 2X10^4 CFU/ml) inoculated 16 days post-implantation and were sacrificed once corneal infection had developed.

Prophylactic versus non-prophylactic study

Twenty-three rabbits were assigned either to a prophylactic group or a non-prophylactic group. The prophylactic group (13 rabbits) received one drop of vancomycin 1.4% (Singapore General Hospital, SingHealth) to the right eye 5 times a day from titanium film implantation to sacrifice; 6 rabbits were sacrificed on day 2 post-inoculation and 7 on day 4 post-inoculation. The non-prophylactic group (10 rabbits) received no drops to the right eye after surgery; 5 rabbits were sacrificed on day 2 post-inoculation and 5 on day 4 post-inoculation.

Slit-lamp photography and anterior segment optical coherence tomography (AS-OCT) were carried out before and after bacterial inoculation. The corneas of sacrificed rabbits were examined for histology, immunohistochemistry and quantification of viable bacteria. The clinical imaging and laboratory parameters were compared between prophylactic and non-prophylactic groups. The study design is illustrated in Fig 1.

Slit lamp photography and anterior segment optical coherence tomography. Slit-lamp photographs (Zoom Slit Lamp NS-2D, Righton, Tokyo, Japan) and AS-OCT scans (RTVue; Optovue, Inc, Fremont, CA) were taken before and after titanium film implantation, immediately before bacterial inoculation, and on days 1, 2 and 4 after bacterial inoculation. Serial slit-lamp photographs in Fig 2 illustrate the progression of infection.

Post-inoculation slit-lamp photographs were graded, using a condensed version of a previously described scale.[21] Briefly, the photos were graded in a blind manner using a scale of 0 to 4 for each of 4 parameters: conjunctival injection, conjunctival chemosis, corneal oedema and corneal infiltration. The individual parameter scores were added to give a total slit-lamp photography (SLP) score ranging from 0 to 16.

Pre-inoculation and post-inoculation corneal thickness (CT) measurements were carried out between the anterior corneal and implant surfaces on AS-OCT scans through the implant

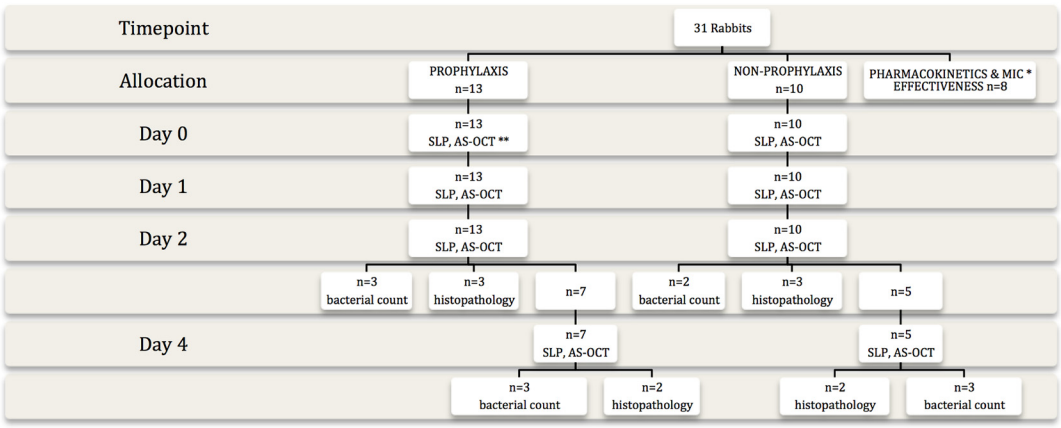

Fig 1. Study design. The flow chart demonstrates allocation to prophylactic and non-prophylactic groups, follow-up and investigations carried out at each time point. (* MIC: minimum inhibitory concentration, ** SLP: slit-lamp photography, AS-OCT: anterior segment optical coherence tomography)

doi:10.1371/journal.pone.0139653.g001

centre. Five measurements, all perpendicular to the anterior corneal surface, were carried out and the mean CT was calculated (Fig 3).

Quantification of viable bacteria. On days 2 and 4 post-inoculation, rabbit corneas were removed by trephination. They were individually homogenized in sterile phosphate buffered saline (PBS) using plastic pestles followed by fine homogenization with bead beating using sterile glass beads (2 mm). The homogenate then underwent serial dilution plating using Tryptic Soy Agar (TSA) plates (Beckman, USA). The plates were incubated at 35°C for 48 hours. The numbers of colonies were counted and the results expressed as $\log_{10}$ number of CFU/cornea.

Histology and immunohistochemistry. Excised corneas of rabbits that were sacrificed on days 2 and 4 were fixed in 4% paraformaldehyde followed by dehydration with a serial concentration of ethanol. After dehydration, tissue blocks were embedded into paraffin and cut at 5 μm thickness using a microtome. The sections were stained with Hematoxylin (Sigma

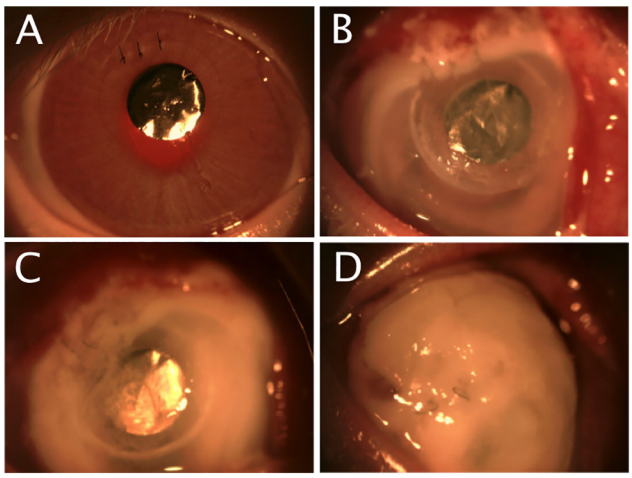

Fig 2. Serial slit-lamp photography for clinical grading. A. A quiet eye with a clear cornea and the titanium keratoprosthesis in-situ before bacterial inoculation. B. On day 1 following inoculation, the conjunctiva is injected and the cornea oedematous with early infiltration. C. On day 2, moderate corneal infiltration has developed. D. On day 4, severe corneal infiltration is present.

doi:10.1371/journal.pone.0139653.g002

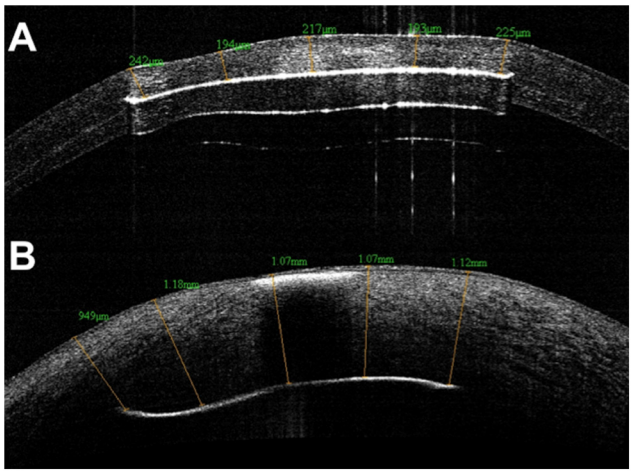

Fig 3. Anterior Segment Optical Coherence Tomography. Corneal thickness between implant and anterior corneal surface was measured at 5 locations before (A) and after (B) bacterial inoculation.

doi:10.1371/journal.pone.0139653.g003

Aldrich, St. Louis, MO, USA) and Eosin (Sigma Aldrich, St. Louis, MO, USA) and then viewed under a light microscope.

Tissue blocks were also embedded in optimum cutting temperature (OCT) cryo-compound (Leica Microsystems, Nussloch, Germany) for immunohistochemistry studies. Frozen tissue blocks were stored at −80°C until sectioning. Serial sagittal corneal 10 μm sections were cut using a cryostat (Microm HM550; Microm, Walldorf, Germany). Sections were placed on poly-lysine-coated glass slides and air dried for 15 minutes.

For Hematoxylin and Eosin (H&E) staining, tissue sections were immersed in hematoxylin and eosin solutions for 10–20 seconds before cleaning with pure xylene. For immunohistochemistry, tissue sections were post-fixed with 4% paraformaldehyde for 15 minutes, washed with PBS and blocked with 10% normal goat serum in 1X PBS and 0.15% Triton X-100 for 1 hour. The sections were incubated with rat monoclonal antibody against CD11b (Abcam, San-Francisco CA) diluted 1:100 at 4°C overnight. After washing with 1X PBS, the sections were incubated with goat anti-rat Alexa Fluor 488 conjugated secondary antibody (Invitrogen, Carlsbad, CA) at room temperature for 1 hour. Slides were then mounted with UltraCruz Mounting Medium containing 4′, 6-diamidino-2-phenylindole (DAPI; Santa Cruz Biotechnology, Santa Cruz, CA). For negative controls, non-immune serum was used in place of the specific primary antibody. Sections were observed and imaged with a fluorescence microscope (Carl Zeiss).

Microscopic qualitative assessment was carried out on H&E stained sections. Immunostaining for CD11b positive (+ve) cells was quantitatively compared between prophylactic and non-prophylactic cases. Five random corneal sections from each rabbit were examined for the ratio of CD11b positive/non-CD11b positive cells.

Pharmacokinetics and effectiveness of minimum inhibitory concentration of vancomycin

Two rabbits with a titanium film implant had corneal and aqueous vancomycin quantification of the right eye after 10 days of instillation of one drop of vancomycin 1.4% 5 times a day. The left eye of 6 rabbits was used for corneal and aqueous vancomycin quantification; 3 rabbits had one drop of vancomycin 1.4% instilled 5 times a day for 10 days before sacrifice and 3 rabbits for 16 days.

Three rabbits had bilateral vancomycin quantification following 4 days of vancomycin 1.4% drop instillation 5 times a day. Prior to starting the antibiotic regimen, the cornea of the right eye had complete epithelial debridement following application of 20% alcohol for 60 seconds, whereas the epithelium of the left cornea was not debrided.

A further 3 rabbits with a titanium film implant to the right eye had bacterial inoculation, as described above, in order to investigate the effectiveness of vancomycin prophylaxis once the corneal vancomycin MIC for *Staphylococcus aureus* (2.0 μg/ml) had been achieved. Inoculation was carried out after 16 days of vancomycin 1.4% drop instillation 5 times a day, as corneal vancomycin quantification at the different time intervals showed that the MIC was achieved by day 16 of antibiotic use. Following bacterial inoculation, development of infection was assessed clinically with SLP and AS-OCT imaging.

Liquid Chromatography–Mass Spectrometry. Quantification of corneal vancomycin was carried out by Liquid Chromatography–Mass Spectrometry (LC-MS). Vancomycin standards (Vancomycin hydrochloride, Hospira, Lake Forest, Illinois, USA) were prepared by dissolution of a single dose vial and serial dilution with water. Aqueous humour samples (120–150 μL) were extracted with three equivalents of methanol (Merck, Darmstadt, Germany). The samples were shaken for 5 min at 1200 rpm (20°C) and centrifuged for 10 min at 16,000 g (4°C). The supernatants were transferred to fresh tubes and dried in a vacuum concentrator. Cornea samples were cut and ground with a pestle while frozen. They were next homogenized on ice with 300 μL of 3:1 methanol/water with 0.1% formic acid (Sigma Aldrich, St. Louis, MO, USA) for 1 min. The homogenates were then spun down briefly on a capsule centrifuge and supernatants transferred to fresh tubes. The residues were homogenized and spun down a second time. The extracts were combined and centrifuged for 10 min at 16,000 g (4°C). The supernatants were transferred to fresh tubes and dried in a vacuum concentrator. Samples were reconstituted in water (Ultrapure water, Millipore purification unit) and centrifuged for 5 min at 16,000 g (10°C) before transferring to autosampler vials for LC-MS/MS analysis.

Chromatographic separation was performed on a Waters 2695 Separations Module (Milford, MA, USA) with a Thermo Scientific Hypersil Gold C18 column (Whaltham, MA, USA) (2.1 × 50 mm, 3 μm). The mobile phase was A: 0.1% formic acid in water and B: 0.1% formic acid in acetonitrile. The gradient profile was 2% B at 0 min, 25% B at 6 min, 90% B from 6.5 to 8.5 min and 2% B from 9 to 13 min. The flow rate was 0.3 ml/min. The autosampler and column heater temperatures were maintained at 10 and 30°C, respectively. Detection was performed by an AB Sciex API 2000 triple quadrupole mass spectrometer (Concord, Canada) with an electrospray ionization source operating in the positive ionization mode. The ion source voltage was set to 5 kV. Vancomycin was detected by monitoring the transition 725.5/144.0 with collision energy of 25 V.

Calculation of the corneal vancomycin concentration was based on the amount of vancomycin detected in the cornea by LC-MS, the gross weight of the cornea and the assumptions that 1 ml of water weighs 1 gram and that the water content of the cornea was 78%.[22,23]

Statistical analysis

Normality distribution of data was assessed by Shapiro-Wilk statistics and histograms. Mean or median values were compared between the prophylactic and non-prophylactic groups. The CT values were compared with the t-test and ANOVA, the total SLP scores with the Kruskal-Wallis and Mann-Whitney U-tests. Bacterial counts and vancomycin concentrations were compared with the t-test. The Statistical Package for Social Science (SPSS), version 15, was used; statistical significance was considered $p<0.05$.

Table 1. Slit-lamp photography score comparison between prophylactic and non-prophylactic groups.

Parameter	Day	Prophylactic	Non-prophylactic	P value
		Slit-Lamp Photography score [median (IQR)]		
Conjunctival injection	1	0 (0, 3)	3 (0, 3.25)	0.166
Conjunctival chemosis	1	0 (0, 3)	3 (0.75, 3.25)	0.148
Corneal infiltration	1	0 (0, 1)	1.5 (0, 3)	0.232
Corneal oedema	1	1 (0, 3)	3 (1, 3.25)	0.115
Total	1	1 (0, 10.5)	11 (1, 13)	0.049
Conjunctival injection	2	2.5 (1, 3)	3 (1, 4)	0.539
Conjunctival chemosis	2	2.5 (1, 3)	3 (1, 4)	0.497
Corneal infiltration	2	2.5 (1, 3.75)	3 (1, 4)	0.418
Corneal oedema	2	3 (1.25, 4)	3.5 (2, 4)	0.628
Total	2	10.5 (4.25, 13.75)	12.5 (5.75, 16)	0.456
Conjunctival injection	4	4 (2, 4)	4 (2.5, 4)	0.648
Conjunctival chemosis	4	4 (2, 4)	4 (2.5, 4)	0.648
Corneal infiltration	4	3 (2, 4)	4 (1.75, 4)	0.527
Corneal oedema	4	4 (3, 4)	4 (2.5, 4)	0.788
Total	4	15 (10, 16)	16 (9.25, 16)	0.527

doi:10.1371/journal.pone.0139653.t001

Results

Slit-lamp photography

Overall, the median total SLP score increased from 4.0 (Inter-quartile range [IQR] 1,12) on day 1 to 12 (IQR 5,14.5) on day 2 and 16 (10,16) on day 4 (p = 0.004).

On day 1, the median total SLP score was greater in the non-prophylactic group compared to the prophylactic group (p = 0.049). On days 2 and 4, the scores were not significantly different between non-prophylactic and prophylactic groups (p = 0.456 and p = 0.527 respectively). The SLP scores are detailed in Table 1.

Anterior segment optical coherence tomography

Pre-inoculation (mean±SEM) CT was not significantly different between non-prophylactic and prophylactic groups (229.9±9.1 vs. 219.3±12.9 μm, p = 0.533). On day 1 post-inoculation, CT in the non-prophylactic group was significantly greater than in the prophylactic group (486.9±61.2 vs. 327.4±37.1 μm, p = 0.029). On day 2 post-inoculation, CT was also greater in the non-prophylactic group (646.2±52.6 vs. 404.7±36.2 μm, p = 0.001). On day 4, however, there was no significant difference between the non-prophylactic and prophylactic groups (683.8±61.2 vs. 765.7±146.9 μm, p = 0.645). The CT comparison between the two groups is illustrated in Fig 4.

In the non-prophylactic group, CT increased from 229.9±9.1 μm pre-inoculation to 486.9±61.2, 646.2±52.6 and 683.8±61.2 μm on days 1, 2 and 4 respectively ($p<0.001$). Bonferroni post-hoc tests showed that the difference was significant between pre-inoculation and day 1 CT (p = 0.003), but not between day 1 and day 2 CT (p = 0.128) or between day 2 and 4 (p = 1).

In the prophylactic group, CT increased from 219.3±12.9 μm pre-inoculation to 327.4±37.1, 400.4.7±36.2 and 765.7±146.9 μm on days 1, 2 and 4 respectively ($p<0.001$). Bonferroni post-hoc tests showed that, compared to before inoculation, the average CT was not significantly different on day 1 (p = 0.590) but became significantly different on day 2 (p = 0.050). Average

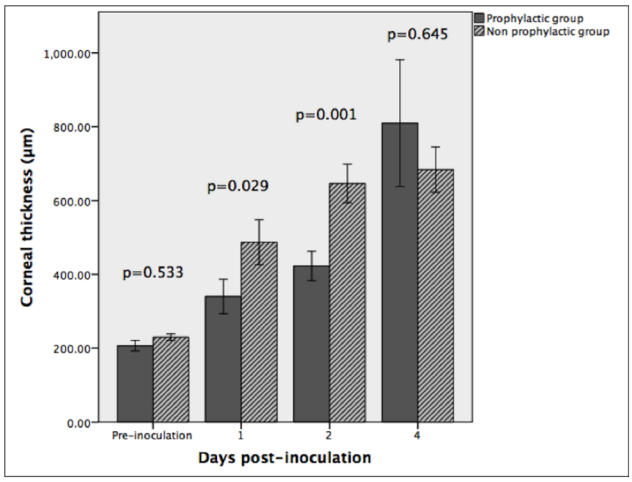

Fig 4. Corneal thickness. Comparison of corneal thickness between the prophylactic and non-prophylactic group. (error bars represent ± 1 standard error of mean)

doi:10.1371/journal.pone.0139653.g004

CT was not significantly different between days 1 and 2 ($p = 1.0$) but was between days 2 and 4 ($p<0.001$).

Bacterial quantification

Log10 mean (±SEM) bacterial counts were not significantly different between non-prophylactic and prophylactic cases on day 2 (4.6±1.0 vs. 5.6±0.4 CFU/cornea, $p = 0.474$) and day 4 (5.7±0.2 vs. 5.4±0.5 CFU/cornea, $p = 0.574$). This is illustrated in Fig 5.

Histology and immunohistochemistry

The corneal stroma of rabbits that were euthanized on day 2 was thickened in both groups, with greater thickness present in the non-prophylactic group (Fig 6). The epithelial and endothelial surfaces appeared irregular and the stroma less densely populated by keratocytes compared to the healthy cornea. Numerous polymorphonuclear neutrophil (PMN) cells were present throughout the corneal stroma in both infection groups. The corneas of rabbits that were sacrificed on day 4 showed similar microscopic features but the stromal thickening and oedema appeared to be approximately equal in prophylactic and non-prophylactic cases.

Immunostaining of day 2 corneal sections showed that the CD11b +ve/non-CD11b +ve cell ratio was greater in the non-prophylactic than in the prophylactic cases (1.45 vs. 0.71) (Fig 7). On day 4, the ratio was slightly larger in the non-prophylactic than prophylactic cases but the difference between the two was small (1.71 vs. 1.30).

Pharmacokinetics and effectiveness of minimum inhibitory concentration of vancomycin

Corneal vancomycin concentration (mean±SEM) of rabbits that were sacrificed on days 2, 10 and 16 after initiation of vancomycin drops was 0.027±0.008, 0.975±0.215 and 2.835±0.383 μg/ml respectively ($p = 0.007$) (Fig 8). Vancomycin was not detected in the aqueous humour after 2 days of antibiotics; although it was detected in the day 10 and day 16 rabbits, it was below the level of quantification.

In the experiment that investigated the effect of removing the epithelium on corneal vancomycin concentration, the concentration after 4 days was 1.36±0.45 μg/ml without epithelial

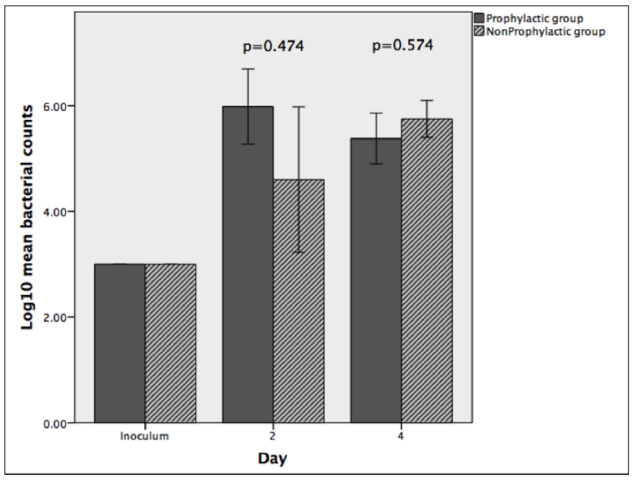

Fig 5. Bacterial quantification. Comparison of bacterial counts between the prophylactic and non-prophylactic group. (error bars represent ± 1 standard error of mean)

doi:10.1371/journal.pone.0139653.g005

removal and 2.57±0.40 μg/ml with epithelial removal (p = 0.115). The aqueous humour vancomycin concentration was 0.04±0.005 μg/ml without epithelial removal and 0.43±0.15 μg/ml with epithelial removal (p = 0.063).

In the experiment that investigated the effectiveness of vancomycin prophylaxis once corneal vancomycin MIC for *Staphylococcus aureus* had been achieved, 2 of the 3 rabbits showed evidence of corneal infection with the development of an injected, sticky eye and a corneal infiltrate by day 2 post-inoculation. In the 3 rabbits, the CT (mean±SEM) increased from 228.8±5.7 μm before inoculation to 336.9±40.9 μm on day 1 and 431.7±47.2 μm on day 2 post-inoculation (p = 0.021).

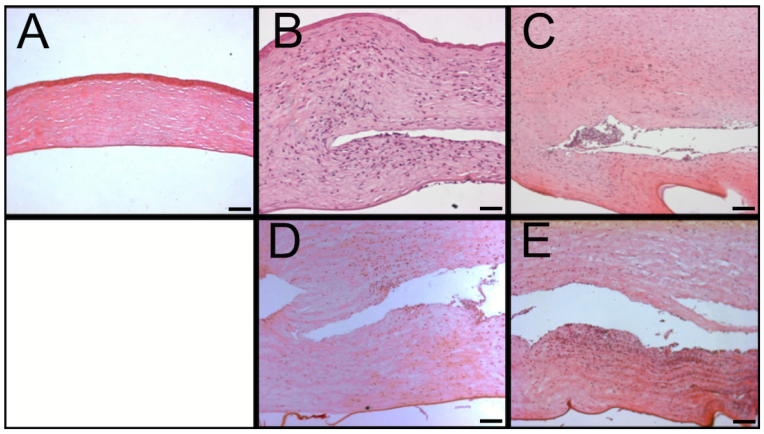

Fig 6. Histology. Haematoxylin and eosin stained corneal sections, comparing vancomycin prophylaxis to non-prophylaxis cases. A. Healthy cornea. B (day 2, prophylaxis). A rich infiltration of neutrophils is present throughout the stroma. The epithelial and endothelial surfaces are irregular due to stromal oedema. C (day 2, non-prophylaxis). The stroma appears more oedematous than in image B. A rich neutrophilic infiltration is also present, mostly in the pocket, but the neutrophils appear to be less densely arranged in the stroma than in image B, most likely reflecting the presence of more oedema. D (day 4, prophylaxis). The stroma is more oedematous than in image B and the Descemets membrane is detached, reflecting greater levels of infection. The neutrophilic infiltration is not as dense as in image B, most likely due to more stromal oedema. E (day 4, non-prophylaxis). The stroma appears similarly oedematous to that in image D and slightly richer in neutrophilic infiltration. (Scale bar 100μm)

doi:10.1371/journal.pone.0139653.g006

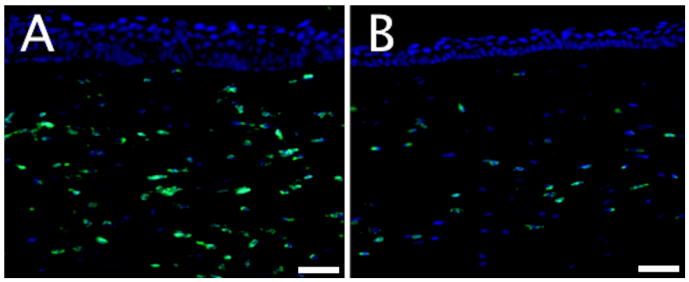

Fig 7. Immunohistochemistry. Comparison between prophylaxis and non-prophylaxis on day 2 following bacterial inoculation. More CD11b +ve neutrophils (fluorescing green) are present in the non-prophylactic case (A) than the prophylactic case (B). (Scale bar 50μm).

doi:10.1371/journal.pone.0139653.g007

Discussion

Prophylactic vancomycin 1.4% drops, applied five times a day, reduced the severity of *S. aureus* bacterial keratitis for the first 2 days of infection compared to non-prophylaxis. However, they did not provide a sustainable benefit and they did not reduce the corneal bacterial counts. Corneal vancomycin levels remained below MIC for *Staphylococcus aureus* following 10 continuous days of vancomycin drop instillation, but did reach MIC by day 16. Achieving MIC did not prevent the development of corneal infection.

In this study we investigated the effectiveness of vancomycin drop prophylaxis, as patients with Boston type-1 Kpro typically receive once or twice daily prophylactic vancomycin drops with or without a fluoroquinolone.[17, 24] However, bacterial keratitis can still develop in patients receiving prophylaxis,[17] and the risk of fungal keratitis may even be increased.[24] The recommendation for the use of postoperative prophylactic vancomycin drops stems from the beneficial effect vancomycin drops have been found to have on the rate of endophthalmitis.[18,19] This potential benefit, however, may be confounded by other modifications to the treatment of Boston type-1 patients, such as the use of a bandage contact lens to keep the corneal surface hydrated,[18,19,25] and the redesign of the Kpo back-plate to include holes with the aim of improving nutrition of the corneal graft carrier.[26] Our study, although an animal model of Kpro infection involving a higher frequency of vancomycin drop use than typical

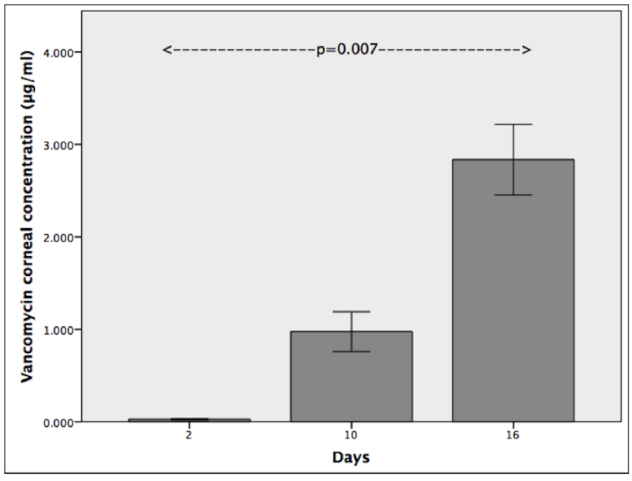

Fig 8. Vancomycin pharmacokinetics. Corneal vancomycin concentration increases with duration of vancomycin drop administration. (error bars represent ± 1 standard error of mean)

doi:10.1371/journal.pone.0139653.g008

regimens for Boston type-1 patients, suggests that vancomycin drops may only provide a limited prophylactic benefit.

The use of prophylactic vancomycin drops reduced the severity of the early corneal inflammatory response, but the efficacy was lost by day 4 following inoculation. Anterior segment optical coherence tomography provides morphology-based quantification of corneal inflammation. It can quantify the corneal inflammatory response in microbial keratitis with measurements of CT and monitor the progress of bacterial keratitis with serial measurements.[27,28] The AS-OCT CT was less in the prophylactic than the non-prophylactic group on days 1 and 2, but was not different between the groups on day 4. The initial efficacy of the prophylactic regimen is also supported by the fact that CT in the prophylactic group on day 1 was not significantly increased compared to pre-inoculation, but day 1 CT was increased in the non-prophylactic group. The SLP scores also showed an initial prophylactic benefit, as the day 1 total score was 1 in the prophylactic group compared to 11 in the non-prophylactic, but this was lost by day 2.

Immunohistochemistry and H&E microscopy also detected smaller levels of PMN infiltration in the prophylactic group on day 2, but there did not appear to be a difference on day 4. We found that the counts of viable bacteria were not reduced by vancomycin prophylaxis on days 2 and 4, providing further evidence that prophylactic drops may not provide a sustainable benefit. It is well documented that bacteria stimulate an innate immune response, rich in PMNs, via the interaction of their pathogen-associated molecular patterns with Toll-like receptors on corneal epithelial cells and stromal fibroblasts.[29–31]

Vancomycin drop instillation did not prevent the development of infection despite MIC levels for *S. aureus* being achieved by day 16 of drop use. In-vivo inhibition of bacteria may require a much higher concentration than the nominal MIC that is based on in-vitro tests, as the protease rich microenvironment of the cornea may degrade the vancomycin. Although there are no data for the cornea, it is known that vancomycin, a glycopeptide antibiotic, shows moderate binding to proteins. It may therefore bind to lectin-like proteins of the stromal extracellular matrix, reducing its bioavailability further.[32] These factors, combined with the slow bactericidal activity of vancomycin,[33] may account for its poor prophylactic effectiveness in our study. In view of this discrepancy between laboratory efficacy and clinical effectiveness for vancomycin, other broad-spectrum antibiotics may need to be investigated as suitable alternatives for prophylaxis.

Study of the corneal vancomycin pharmacokinetics showed that a period of 16 days with a strict drop instillation regimen of five times a day and 100% compliance was required to achieve MIC, unless the epithelium was debrided in which case MIC was achieved within 4 days. This raises the question whether the typical prophylactic use of antibiotic drops once or twice daily [17,24] would actually achieve MIC for a range of pathogens. Even if more frequent instillation was recommended, it is unlikely patients would remain compliant with a more intensive use over the long-term. There is good evidence from glaucoma studies that non-compliance with drops can be as high as 80%.[34] At only 3 months after starting treatment, just over half (55.6%) of patients took greater than 75% of the expected doses, even though once daily dosing was recommended.[35] Future developments, such as sustained drug release systems with liposomes and anti-infective or anti-adhesive biomaterials, may address these limitations.[36,37]

In conclusion, our animal model study of keratoprosthesis and corneal infection has shown that vancomycin drop instillation at a frequency that is higher than prophylactic clinical practice provided a short term benefit but did not prevent the development of *S. aureus* keratitis. In addition, even after the vancomycin MIC in the cornea was achieved, this was not sufficient to prevent corneal infection. Investigation of alternative antibiotic agents and of the discrepancy

been laboratory efficacy and clinical effectiveness is required to improve our infection prophylaxis strategies in keratoprosthesis surgery. Despite the use of post-operative antibiotics, patients should continue to be counselled regarding the long-term risk of infection following keratoprosthesis surgery.

Author Contributions

Conceived and designed the experiments: AK XWT JSM. Performed the experiments: AK GTWG CLN PS LC LSM. Analyzed the data: AK GTWG PS LC JSM. Contributed reagents/materials/analysis tools: LZ RWB DTT JSM. Wrote the paper: AK GTWG LZ RWB DTT JSM.

References

1. Whitcher JP, Srinivasan M, Upadhyay MP. Corneal blindness: a global perspective. Bull World Health Organ 2001: 79:214–21. PMID: 11285665
2. Pascolini D, Mariotti SP. Global estimates of visual impairment: 2010. Br J Ophthalmol 2012; 96:614–618. doi: 10.1136/bjophthalmol-2011-300539 PMID: 22133988
3. Williams KA, Lowe M, Bartlett C, Kelly TL, Coster DJ; All Contributors. Risk factors for human corneal graft failure within the Australian corneal graft registry. Transplantation. 2008; 86:1720–4. doi: 10.1097/TP.0b013e3181903b0a PMID: 19104411
4. Maguire MG, Stark WJ, Gottsch JD, Stulting RD, Sugar A, Fink NE, et al. Risk factors for corneal graft failure and rejection in the collaborative corneal transplantation studies. Collaborative Corneal Transplantation Studies Research Group. Ophthalmology. 1994; 101:1536–47. PMID: 8090456
5. Hicks CR, Crawford GJ, Dart JK, Grabner G, Holland EJ, Stulting RD, et al. AlphaCor: Clinical outcomes. Cornea. 2006; 25:1034–42. PMID: 17133049
6. Akpek EK, Alkharashi M, Hwang FS, Ng SM, Lindsley K. Artificial corneas versus donor corneas for repeat corneal transplants. Cochrane Database Syst Rev. 2014; 11:CD009561. [Epub ahead of print] doi: 10.1002/14651858.CD009561.pub2 PMID: 25372407
7. Chew HF, Ayres BD, Hammersmith KM, Rapuano CJ, Laibson PR, Myers JS, et al. Boston keratoprosthesis outcomes and complications. Cornea. 2009; 28:989–96. doi: 10.1097/ICO.0b013e3181a186dc PMID: 19724214
8. Aldave AJ, Kamal KM, Vo RC, Yu F. The Boston type 1 keratoprosthesis: improving outcomes and expanding indications. Ophthalmology. 2009; 116:640–51. doi: 10.1016/j.ophtha.2008.12.058 PMID: 19243830
9. Zerbe BL, Belin MW, Ciolino JB; Boston Type 1 Keratoprosthesis Study Group. Results from the multicentre Boston Type 1 Keratoprosthesis Study. Ophthalmology. 2006; 113:1779–1784. PMID: 16872678
10. Srikumaran D, Munoz B, Aldave AJ, Aquavella JV, Hannush SB, Schultze R, et al. Long-term outcomes of boston type 1 keratoprosthesis implantation: a retrospective multicenter cohort. Ophthalmology. 2014; 121:2159–64. doi: 10.1016/j.ophtha.2014.05.030 PMID: 25017414
11. Avadhanam VS, Liu CS. A brief review of Boston type-1 and osteo-odonto keratoprostheses. Br J Ophthalmol. 2015; 99:878–87. doi: 10.1136/bjophthalmol-2014-305359 PMID: 25349081
12. Crnej A, Paschalis EI, Salvador-Culla B, Tauber A, Drnovsek-Olup B, Shen LQ, et al. Glaucoma progression and role of glaucoma surgery in patients with Boston keratoprosthesis. Cornea. 2014; 33:349–54. doi: 10.1097/ICO.0000000000000067 PMID: 24531120
13. Sivaraman KR, Hou JH, Allemann N, de la Cruz J, Cortina MS. Retroprosthetic membrane and risk of sterile keratolysis in patients with type 1 Boston keratoprosthesis. Am J Ophthalmol. 2013; 155:814–22. doi: 10.1016/j.ajo.2012.11.019 PMID: 23352344
14. Bradley JC, Hernandez EG, Schwab IR, Mannis MJ. Boston type 1 keratoprosthesis: the University of California Davis experience. Cornea. 2009; 28:321–327. doi: 10.1097/ICO.0b013e31818b8bfa PMID: 19387235
15. Magalhães FP, do Nascimento HM, Ecker DJ, Sannes-Lowery KA, Sampath R, Rosenblatt MI, et al. Microbiota evaluation of patients with a Boston type I keratoprosthesis treated with topical 0.5% moxifloxacin and 5% povidone-iodine. Cornea. 2013; 32:407–11. doi: 10.1097/ICO.0b013e31824a8b9b PMID: 22488148
16. Kim MJ, Yu F, Aldave AJ. Microbial keratitis after Boston type I keratoprosthesis implantation: incidence, organisms, risk factors, and outcomes. Ophthalmology. 2013; 120:2209–16. doi: 10.1016/j.ophtha.2013.05.001 PMID: 23747162

17. Chan CC, Holland EJ. Infectious keratitis after Boston type 1 keratoprosthesis implantation. Cornea. 2012; 31:1128–34. doi: 10.1097/ICO.0b013e318245c02a PMID: 22960647

18. Ramchandran RS, Diloreto DA Jr, Chung MM, Kleinman DM, Plotnik RP, Graman P, et al. Infectious endophthalmitis in adult eyes receiving Boston type I keratoprosthesis. Ophthalmology. 2012; 119:674–81. doi: 10.1016/j.ophtha.2011.10.009 PMID: 22266108

19. Durand ML, Dohlman CH. Successful prevention of bacterial endophthalmitis in eyes with the Boston keratoprosthesis. Cornea. 2009; 28:896–901. doi: 10.1097/ICO.0b013e3181983982 PMID: 19654525

20. Tan XW, Goh TW, Saraswathi P, Nyein CL, Setiawan M, Riau A, et al. Effectiveness of antimicrobial peptide immobilization for preventing perioperative cornea implant-associated bacterial infection. Antimicrob Agents Chemother. 2014; 58:5229–38. doi: 10.1128/AAC.02859-14 PMID: 24957820

21. Johnson MK, Hobden JA, Hagenah M, O'Callaghan RJ, Hill JM, Chen S. The role of pneumolysin in ocular infections with Streptococcus pneumoniae. Curr Eye Res. 1990; 9:1107–1114. PMID: 2095322

22. Thiagarajah JR, Verkman AS. Aquaporin deletion in mice reduces corneal water permeability and delays restoration of transparency after swelling. J Biol Chem. 2002; 277:19139–44. PMID: 11891232

23. von Fischern T, Lorenz U, Burchard WG, Reim M, Schrage NF. Changes in mineral composition of rabbit corneas after alkali burn. Graefes Arch Clin Exp Ophthalmol. 1998; 236:553–8. PMID: 9672803

24. Barnes SD, Dohlman CH, Durand ML. Fungal colonization and infection in Boston keratoprosthesis. Cornea. 2007; 26:9–15. PMID: 17198007

25. Dohlman CH, Dudenhoefer EJ, Khan BF, Morneault S. Protection of the ocular surface after keratoprosthesis surgery: the role of soft contact lenses. CLAO J. 2002; 28:72–4. PMID: 12054373

26. Harissi-Dagher M, Khan BF, Schaumberg DA, Dohlman CH. Importance of nutrition to corneal grafts when used as a carrier of the Boston Keratoprosthesis. Cornea. 2007; 26:564–8. PMID: 17525653

27. Konstantopoulos A, Kuo J, Anderson DF, Hossain PN. Assessment of the use of anterior segment optical coherence tomography in microbial keratitis. Am J Ophthalmol 2008; 146:534–542. doi: 10.1016/j.ajo.2008.05.030 PMID: 18602080

28. Konstantopoulos A, Yadegarfar G, Fievez M, Anderson DF, Hossain P. In vivo quantification of bacterial keratitis with optical coherence tomography. Invest Ophthalmol Vis Sci. 2011; 52:1093–7. doi: 10.1167/iovs.10-6067 PMID: 20926816

29. Tullos NA, Thompson HW, Taylor SD, Sanders M, Norcross EW, Tolo I, et al. Modulation of immune signaling, bacterial clearance, and corneal integrity by toll-like receptors during streptococcus pneumoniae keratitis. Curr Eye Res. 2013; 38:1036–48. doi: 10.3109/02713683.2013.804094 PMID: 23841825

30. Jin X, Qin Q, Tu L, Qu J. Glucocorticoids inhibit the innate immune system of human corneal fibroblast through their suppression of toll-like receptors. Mol Vis. 2009; 15:2435–41. PMID: 19956406

31. Li Q, Kumar A, Gui JF, Yu FS. Staphylococcus aureus lipoproteins trigger human corneal epithelial innate response through toll-like receptor-2. Microb Pathog. 2008; 44:426–34. doi: 10.1016/j.micpath.2007.11.006 PMID: 18191935

32. Rybak MJ. The pharmacokinetic and pharmacodynamic properties of vancomycin. Clin Infect Dis. 2006; 42:Suppl 1:S35–9. PMID: 16323118

33. LaPlante KL, Rybak MJ. Impact of high-inoculum Staphylococcus aureus on the activities of nafcillin, vancomycin, linezolid, and daptomycin, alone and in combination with gentamicin, in an in vitro pharmacodynamic model. Antimicrob Agents Chemother. 2004; 48:4665–72. PMID: 15561842

34. Olthoff CM, Schouten JS, van de Borne BW, Webers CA. Noncompliance with ocular hypotensive treatment in patients with glaucoma or ocular hypertension an evidence-based review. Ophthalmology. 2005; 112:953–61. PMID: 15885795

35. Okeke CO, Quigley HA, Jampel HD, Ying GS, Plyler RJ, Jiang Y, et al. Adherence with topical glaucoma medication monitored electronically the Travatan Dosing Aid study. Ophthalmology. 2009; 116:191–9. doi: 10.1016/j.ophtha.2008.09.004 PMID: 19084273

36. Natarajan JV, Darwitan A, Barathi VA, Ang M, Htoon HM, Boey F, et al. Sustained drug release in nanomedicine: a long-acting nanocarrier-based formulation for glaucoma. ACS Nano. 2014; 8:419–29. doi: 10.1021/nn4046024 PMID: 24392729

37. Alves D, Olívia Pereira M. Mini-review: Antimicrobial peptides and enzymes as promising candidates to functionalize biomaterial surfaces. Biofouling. 2014; 30:483–99. doi: 10.1080/08927014.2014.889120 PMID: 24666008

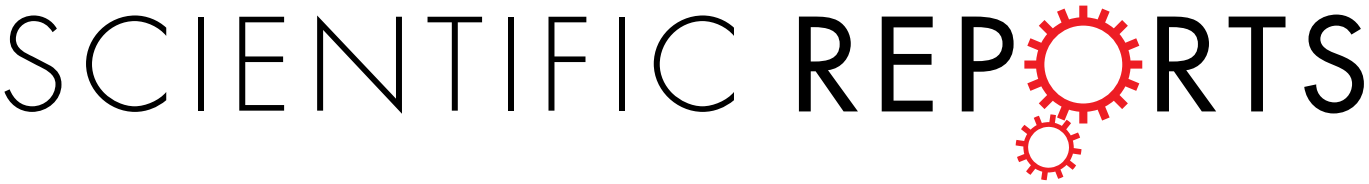

OPEN

Evaluation of a Micro-Optical Coherence Tomography for the Corneal Endothelium in an Animal Model

Received: 23 March 2016
Accepted: 14 June 2016
Published: 15 July 2016

Marcus Ang[1,2,3], Aris Konstantopoulos[1,2], Gwendoline Goh[2], Hla M. Htoon[2], Xinyi Seah[2], Nyein Chan Lwin[2], Xinyu Liu[4], Si Chen[4], Linbo Liu[4] & Jodhbir S. Mehta[1,2,3]

Recent developments in optical coherence tomography (OCT) systems for the cornea have limited resolution or acquisition speed. In this study we aim to evaluate the use of a 'micro-OCT' (μOCT ~1 μm axial resolution) compared to existing imaging modalities using animal models of corneal endothelial disease. We used established cryoinjury and bullous keratopathy models in Sprague Dawley rats comparing *ex vivo* μOCT imaging in normal and diseased eyes to (1) histology; (2) *in vivo* confocal microscopy (IVCM); and (3) scanning electron microscopy (SEM). Qualitative and quantitative comparisons amongst imaging modalities were performed using mean endothelial cell circularity [(4π × Area)/Perimeter^2] with coefficient of variation (COV). We found that μOCT imaging was able to delineate endothelial cells (with nuclei), detect inflammatory cells, and corneal layers with histology-like resolution, comparable to existing imaging modalities. The mean endothelial cell circularity score was 0.88 ± 0.03, 0.87 ± 0.04 and 0.88 ± 0.05 (P = 0.216) for the SEM, IVCM and μOCT respectively, with SEM producing homogenous endothelial cell images (COV = 0.028) compared to the IVCM (0.051) and μOCT (0.062). In summary, our preliminary study suggests that the μOCT may be useful for achieving non-contact, histology-like images of the cornea for endothelial cell evaluation, which requires further development for *in vivo* imaging.

Corneal diseases are the second most common cause of vision loss[1,2], with over 180 million people worldwide estimated to be suffering from secondary visual impairment[1]. Corneal transplantation still remains the main method for restoring vision once corneal clarity is affected[3]. Thus, evaluation and imaging of the cornea is important for early diagnosis, to allow for timely intervention and prevention of permanent corneal damage. Recent developments in surgical techniques have enabled surgeons to perform selective replacement of the diseased layer of the cornea – which may lead to improved corneal graft survival and surgical outcomes[3]. In particular, selective replacement of both the endothelial layer[4], and the stromal layer[5], may confer advantages such as tectonic stability or a rapid visual recovery, compared to replacing the entire cornea during transplantation. Thus, the role of imaging to delineate corneal layers is becoming increasingly important in the pre-operative, intra-operative and post-operative assessment of patients requiring corneal transplantation.

Current imaging techniques such as confocal microscopy and high-frequency ultrasound have limitations such as a narrow field of view or limited resolution respectively[6]. Optical coherence tomography (OCT) has emerged as a promising technique for high-resolution, cross-sectional and en face imaging of the cornea[7]. Existing commercial anterior segment OCT (AS-OCT) systems obtain cross-sections of the cornea with 5–20 μm axial resolution, at a variety of widths (6–16 mm) and depths (2–6 mm)[7]. However, current available AS-OCT technology is unable to clearly image cells within the cornea and may be affected by factors such as scars, artifacts and light scatter that often reduce image quality[8,9].

Recent developments into broadband light sources have allowed for OCT systems to achieve 1–2 μm spatial resolution, termed micro-OCT or μOCT, in an attempt to achieve cellular level imaging *in vivo*[10–12]. By use of a

[1]Singapore National Eye Centre, Singapore. [2]Singapore Eye Research Institute, Singapore. [3]Department of Ophthalmology and Visual Science, Duke-NUS Graduate Medical School, Singapore. [4]School of Electrical & Electronic Engineering and School of Chemical & Biomedical Engineering, Nanyang Technological University, Singapore. Correspondence and requests for materials should be addressed to J.S.M. (email: jodmehta@gmail.com)

supercontinuum source, μOCT achieves 2 μm × 2 μm × 1 μm resolution (in tissue) at 8 frames per second[13,14]. This first μOCT system was shown to provide visualization of many key cellular and sub-cellular features associated with coronary artery diseases[14], and pulmonary airway diseases *ex vivo*[13]. However, the light source contains pulsed radiations in the visible spectrum (650 nm–700 nm) which is subject to stricter safety constrains in input power. More recently, we have developed a μOCT system using NIR superluminescent diode arrays (SLDs) which make it more suitable for ocular imaging *in vivo* imaging[15]. We had previously described the visualization of corneal endothelial cells using a spectral estimation OCT, which has a 4.7 times better axial resolution compared to spectral domain OCT[16]. However, the image processing speed was too slow for translation to clinical use.

Therefore, in this study we evaluated the SLD array based μOCT system for 'micro' (~1 μm) axial resolution, specifically to image the cornea. To the best of our knowledge, this is the first time that three dimensional visualization of corneal endothelium by OCT is validated against gold standard methods. The μOCT imaging system has a spectral bandwidth of 350 nm centered at 930 nm, in order to achieve the best possible axial resolution using near infared (NIR) light. In order to assess the ability of the μOCT system to adequately image the microstructures of the cornea, and in particular, endothelial cells - we used established models to assess normal and damaged cornea. In this preliminary animal study, we compared the μOCT imaging to histology images; and existing imaging modalities such as *in vivo* confocal microscopy (IVCM) and scanning electron microscopy (SEM).

Materials and Methods

In this study, we used 12 Sprague Dawley rats (aged 8–10 weeks) bred and maintained at the SingHealth Experimental Medical Centre (Singapore General Hospital, Singapore). We utilized two established techniques to induce corneal endothelial injury in one eye of each rat, with the fellow eye serving as the control. First, we used a cryoinjury model previously described[17], with a cryoprobe made of stainless steel (2.5 mm in diameter; flat tip; ERBE Elektromedizin GmbH, Tübingen, Germany), precooled to −80 °C and gently placed on the central cornea of the rat eye (3 eyes). The cryoprobe was kept on the corneal surface until an ice ball covered the entire corneal surface (approximately 3 seconds duration)[17]. Immediately after freezing, the cryoprobe was freed from the corneal surface with irrigation with a balanced salt solution, and the cornea was allowed to thaw spontaneously. The second model we used to induce bullous keratopathy[18], was performed with benzalkonium chloride (BAK) 0.05%, which was injected into the anterior chamber of the rat eyes (3 eyes). Briefly, the anterior chamber of one eye was punctured using a 30 G needle under anesthesia and rinsed with BAK for 90 seconds, followed by rinsing with 0.9% sodium chloride for another 90 seconds. The corneal puncture was sealed with a small air bubble. Antibiotic ointment was applied to the eyes at the end of each procedure. Our study was conducted with approval from the Institutional Animal Care and Use Committee of Singapore Health Services; and all animals were treated according to tenets of the Association for Research in Vision and Ophthalmology's statement for the Use of Animals in Ophthalmic and Vision Research.

Micro-Optical Coherence Tomography (μOCT). Optical coherence tomography measures the electric field amplitude of light that is elastically scattered from within tissue in three dimensions. Depth or axial (z) ranging is achieved by interferometric measurement of the optical delay of light returned from the sample. The μOCT system we have described here is a spectral-domain OCT, implemented with several key improvements to standard OCT that yields high resolution in both lateral and axial directions as previously described[15]. In brief, the combined output of two SLD arrays (Superlum Broadlighters T-850-HP and Exalos Ultra-Broadband EBS4C32) provides the high-bandwidth (755–1105 nm), short coherence length light necessary for high axial resolution of 1.3 μm in air. A typical OCT system includes an interferometer with the reference and sample arms intersecting at a beamsplitter. The device is equipped with a 10X objective lens and a 20X objective lens, which provides a lateral resolution of 2.5 μm and 1.3 μm respectively. The effective beam diameter at the the back aperture of the objective lens was 2.6 mm (1% power level) so that it was under-filled. A telecentric scanning configureation was assumed to perform a sectional scan across a transverse range of 0.872 mm by 0.872 mm. The total power incident on the sample was less than 2 mW. Custom software was employed to control the galvanometer scanning motors while acquiring spectral data from the two-line scan cameras. In order to detect the spectral interference signal across the entire illumination bandwidth, we employed two spectrometers based on an InGaAs camera (Sensors Unlimited GL2048L) and a Si camera (E2V, AViiVA EM4) respectively. The system operates with a user-configurable line and frame rates and customizable scan geometry; typical settings are 60 frames per second, 1024 A-lines per frame in a linear scan, and 0.872 mm by 0.872 mm (X by Z) for a cross-sectional image. The transverse scanning step size was 0.85 μm is less than half of the μOCT beam spot size (2.5 μm) to satisfy the requirement set by Nyquist sampling therom. A three dimensional image could be formed by acquiring a time-series stack of 1024 B-mode (cross-sectional) μOCT images within 17 seconds.

Anterior segment evaluation and histology. Preoperatively and 3 days after the interventions, examinations including AS-OCT (RTvue, Optovue, Fremont, CA), *in vivo* confocal microscopy i.e. IVCM (HRT3 Rostock module; Heidelberg Engineering GmbH, Heidelberg, Germany) and slit-lamp photography (FS-3V Zoom Photo Slit Lamp, Nikon, Tokyo, Japan) were performed. All animals were then sacrificed and *ex vivo* imaging was performed with the μOCT system, before flat mount preparations of treated and untreated corneas to evaluate endothelial cells and cross-sectional histology. Corneas were fixed in 4% paraformaldehyde, dehydrated and embedded in paraffin blocks for sectioning at 5 μm for haematoxylin and eosin (H&E) staining as previously described[19]. In brief, sections were immersed in hematoxylin (Sigma Aldrich, St. Louis, MO, USA) for 2 minutes and counter stained with eosin (Sigma Aldrich, St. Louis, MO, USA) solutions for another 2 minutes before soaking with pure xylene to remove traces of ethanol, dried and imaged using a light microscope (Nikon C2 confocal microscope). The corneal buttons excised from the enucleated eyes were placed endothelial side up and stained with alizarin red S (0.50%; pH 4.2) for 3 minutes, and then were washed in wash buffer solution twice

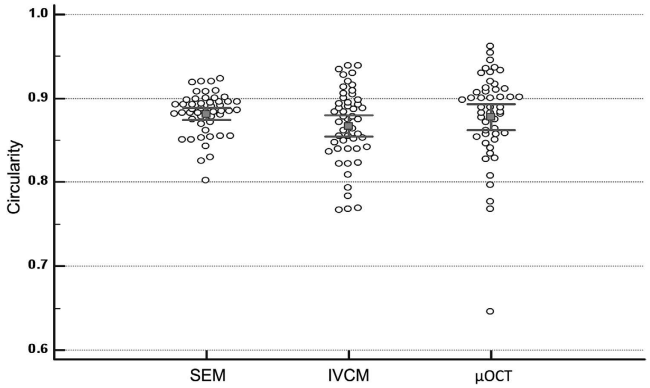

Figure 1. Endothelial cell circularity score i.e. $(4\pi \times \text{Area})/\text{Perimeter}^2$ where a value approaching 1.0 indicated a more circular and hexagonal profile, compared amongst the three imaging techniques using scanning electron microscopy (SEM), *vivo* confocal microscopy (IVCM), and micro-optical coherence tomography (μOCT); P = 0.216.

for 2 minutes. The corneas were then mounted on a glass slide endothelial side up under a cover slip, and were imaged using an inverted light microscope (Nikon C2 Confocal microscope).

Scanning electron microscopy (SEM). We also evaluated the changes in the corneal endothelium by performing SEM in both the diseased eyes and control eyes. The globes were immersed in a fixative solution, containing 2.5% glutaraldehyde in 0.1 M sodium cacodylate (pH 7.4; Electron Microscopy Sciences, Hatfield, PA) overnight at 4 °C. The corneas were excised from the globes, washed three times in distilled water for 10 min each, and were kept in 1% osmium tetroxide (FMB, Singapore) at 22 °C for 2 h for final fixation. The corneas were then dehydrated through serial dilutions of ethanol (25%, 50%, 75%, 95%, and 100% each for 10 min, with the 100% twice). The samples were then dried in a critical point dryer (BALTEC, Balzers, Liechtenstein) and mounted on SEM stubs using carbon adhesive tabs. Samples were then sputter-coated with a 10 nm thick layer of gold (BALTEC) and examined with a scanning electron microscope (JSM-5600; JEOL, Tokyo, Japan).

Statistical Analysis. All numeric data obtained were expressed as mean ± standard deviation. Comparisons of mean endothelial cell circularity with coefficient of variation (COV) were statistically analyzed using two-way ANOVA followed by post-hoc Bonferroni test for multiple comparisons. Two masked assessors obtained morphometric data of the area and perimeter of fifty randomly selected cells from scans of each imaging technique (μOCT, IVCM and SEM) were manually outlined by point-to-point tracing of the cell borders using the National Institutes of Health Image J 1.38X (NIH, Bethesda, MD) software. Cell circularity was then determined using the formula:

$$\text{Circularity} = (4\pi \times \text{Area})/\text{Perimeter}^2$$

where a value approaching 1.0 indicated a circular profile[20]. Hence, normal hexagonal endothelial cells will have a profile closer to 1.0 as opposed to damaged endothelial cells. Alpha was set at a significance level of 5%. All analyses were performed using STATA version 11 (StataCorp LP, College Station, Texas, USA).

Results

We found that the circularity scores were comparable between all 3 imaging modalities in the normal endothelial cell analysis of control eyes (n = 12). The mean circularity score was 0.88 ± 0.03, 0.87 ± 0.04 and 0.88 ± 0.05 (P = 0.216) for the SEM, IVCM and μOCT image analysis respectively – Fig. 1. Each imaging modality was able to outline the normal endothelial cells, with the SEM producing homogenous endothelial cell images (COV = 0.028) compared to the IVCM (0.051) and μOCT (0.062). When compared to histology images, the en face μOCT imaging were able to delineate the endothelial cells clearly without artifacts from fixing techniques; while B-scan μOCT images successfully demonstrated distinct layers of normal cornea i.e. epithelium, Bowman's layer, stromal layers and Descemet's membrane (DM). The high-resolution μOCT was also able to delineate the endothelial cell nuclei, which are not usually visible when imaged by IVCM or specular microscopy – Fig. 2.

We also found that the μOCT was able to image the endothelial cell surface in the central cornea in all the samples, using the coronal reconstruction or en face view of the serial scans in the cryoinjury (n = 6) and BAK injury (n = 6) eyes. The μOCT images reflected the loss of hexagonality, disruption of the endothelial cell layer and signs of inflammation in the same central cornea, which was also detected in the IVCM and SEM images – representative examples in Fig. 3. After 3 days from endothelial injury, we observed an increase in central corneal thickness in the cryoinjury model (n = 6, mean ± standard deviation: 320 ± 60 μm, P = 0.047) and BAK injury model (n = 6, 371 ± 90 μm, P = 0.004) compared to the control eyes (n = 12, 169 ± 10 μm) as measured by AS-OCT, which is optimized and validated for measuring corneal thickness. While the conventional AS-OCT was able to detect the gross changes in the cornea, we found that the μOCT was better able to delineate the layers of the cornea in the control eyes, especially the epithelium, Bowman's layer, and Descemet membrane; as well as

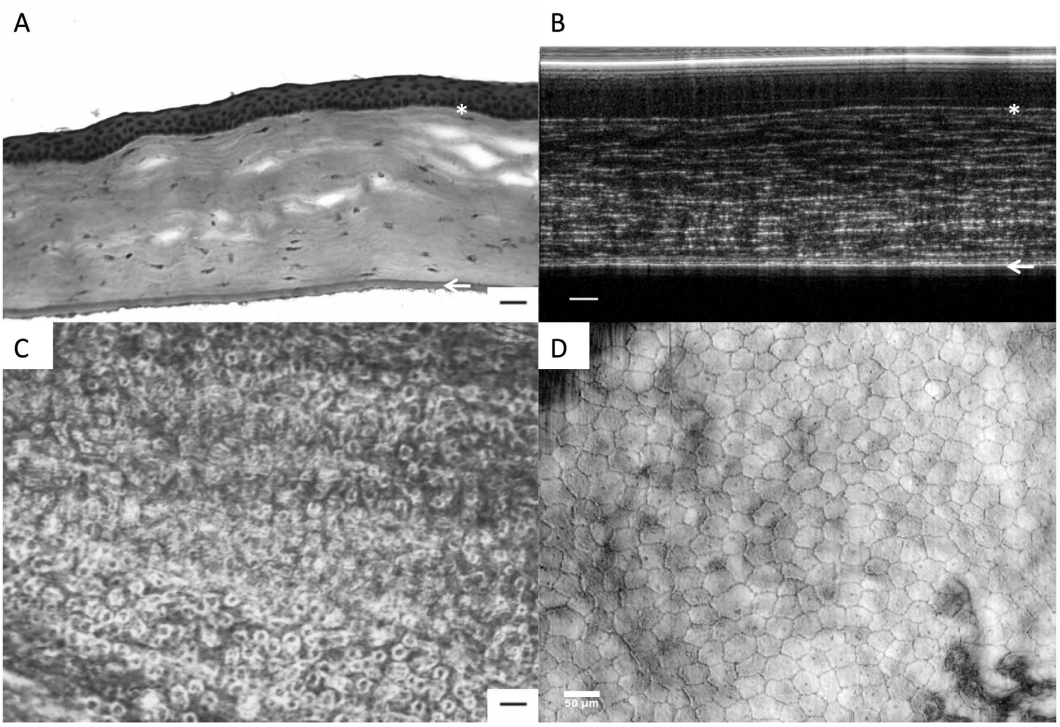

Figure 2. Histology images compared to μOCT scan images of the normal mouse cornea. (**A**) Cross-sectional histology sections using H&E stain (20x magnification, scale bar = 20 μm). *Indicates Bowman's layer. Epithelium lies above the Bowman's layer. Arrow indicates Descemet membrane, corneal stromal layer lies in between. Endothelial cell layer can be seen just below the Descemet membrane. (**B**) Cross-sectional B-scan μOCT images were able to delineate the corresponsing distinct layers of the cornea with similar resolution to histology images i.e. *Bowman's layer, collagen fibrils in stroma, Descemet membrane (arrow) and endothelial cell layer below (scale bar = 40 μm). Epithelium lies above the Bowman's layer. Arrow indicates Descemet membrane, corneal stromal layer lies in between. Endothelial cell layer can be seen just below the Descemet membrane. (**C**) Endothelial cell layer histology image using Alizarin S Red (20x magnification, scale bar = 20 μm). (**D**) En face μOCT scan of the normal endothelial cells without artifacts from histology fixing and staining (scale bar = 40 μm) was able to detect the presence of nuclei and villi.

that seen in the injury model eyes – Fig. 4. The μOCT also detected subtle changes in the stromal layer where the cryoinjury eyes had anterior stromal scarring with cells seen on the damaged DM; while the BAK injured eyes had more edema with minimal stromal haze and more inflammatory cells on the DM surface.

Discussion

In this preliminary study, we describe the use of a new μOCT system that utilizes a very broad bandwidth light source and common-path spectral-domain OCT (SD-OCT) technology to provide 1-μm-axial resolution (in tissue) scans of the cornea. We found that the novel μOCT system was able to produce 'histology-resolution' images using both the cross-sectional views of the cornea, as well as en face views of the endothelial surface – without suffering from the artifacts usually introduced by histology fixing techniques. With this micro-resolution of 1-μm, accurate measurements of the corneal layers, as well as finer detail of structures such as inflammatory cells within the stroma; or epithelial and DM damage, may be obtained directly from a time-series stack of B-mode (cross-sectional) μOCT images – potentially a significant improvement over current commercial ASOCT imaging. Moreover, coronal reconstruction from rapid serial μOCT scans also allowed rapid non-contact imaging of the endothelial cell layer compared to the 'contact' IVCM and time consuming *in vitro* SEM – but with a much larger field of view (IVCM: 400 × 400 μm; SEM: 200 × 1300 μm). We found that the μOCT produced endothelial cell imaging with homogenous circularity scores as a surrogate for hexagonality, as we recognize that direct comparisons using endothelial cell density was not possible due to the artifacts from histology fixing and the lack of a reference across imaging modalities. The high-resolution μOCT was able to delineate the endothelial cell nuclei, which are not usually visible when imaged by IVCM or specular microscopy, which may have potential clinical applications such as detection of early endothelial damage, as we continue to develop the μOCT for *in vivo* use[21].

Since its first *in vivo* use for the retina, OCT imaging has revolutionized our ability to evaluate the eye and its structures on a microscopic level[22]. Currently, commercially available ultrahigh-resolution OCT may provide a potential improvement in performance, enabling imaging of corneal cells or even delineation of micro-vascular structures, which had previously only been possible with IVCM or histopathology[23,24]. In combination with image processing and segmentation techniques, we describe a further improved μOCT that permits the quantitative measurement of corneal microanatomy and morphology, i.e. non-contact visualization of endothelial

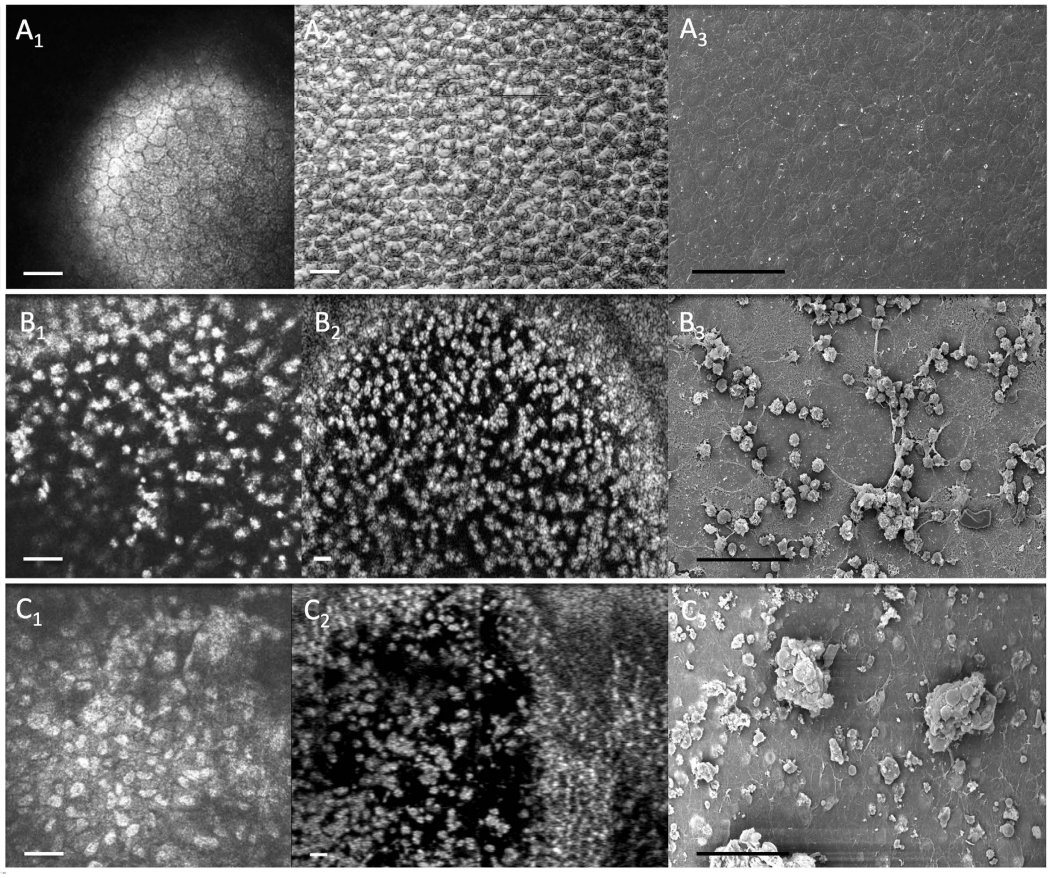

Figure 3. Endothelial cell imaging using *in vivo* confocal microscopy (left), micro-optical coherence tomography (center) and scanning electron microscopy (right) in control eyes (**A**), cryoinjury model eyes (**B**) and benzakolnium chloride injury model (**C**). A_1, B_1 and C_1: En-face images of rats cornea pre (A_1) and post-injury (B_1, C_1) using *In vivo* confocal Microscopy (scale bar = 50 μm). A_2, B_2 and C_2: En-face images of rats cornea pre (A_2) and post-injury (B_2,C_2) using micro-OCT (Scale bar = 40 μm). A_3, B_3, and C_3: Cross sectional images of rats cornea Pre (A_3) and post-injury (B_3,C_3) using Scanning Electron Microscopy (2000X magnification) (scale bar = 50 μm).

cells using en face OCT reconstruction[25]. Previous studies have examined the correlation of conventional resolution OCT and histology of the retina in animals, but found discrepancies due to image resolution and histology fixation changes[26]. Here, we compared our μOCT images with SEM and IVCM to show that μOCT provided rapid, non-contact *ex vivo* histology-like images for the cornea and endothelium. Moreover, while previous prototype high-resolution OCT systems were able to visualize corneal layers[27], the system described here was able to produce images with a similar axial resolution and field of view, but with additional cellular detail such as the presence of inflammatory cells within the stromal and endothelial layer. The potential clinical applications of *in vivo* imaging of the corneal endothelial cells include monitoring corneal endothelial cell count and morphology to guide surgery[28], improving corneal endothelial cell imaging to compare endothelial keratoplasty techniques[29], or even early detection of post-keratoplasty rejection by looking at inflammatory cells to differentiate rejection from infection[30].

The advantages of OCT are well known[31], with image resolution improving over time to achieve histology-like images; and non-contact *in vivo* images obtained in real time that potentially allows surgical guidance and functional imaging[32]. However, the disadvantages of OCT, especially μOCT, include the trade-off between lateral resolution and depth of focus limited axial imaging range, and imaging speed[11]. The maximum depth of focus of μOCT used in this study is limited by confocal parameter to approximately 150 μm, which can be mitigated by use of depth of focus extension techniques[33–35]. Likewise, the axial imaging range (ranging depth) was 0.5 mm, which could be solved by use of a line scan camera of larger pixel numbers and/or full-range OCT imaging[36]. While IVCM generally achieves an axial resolution of 4–10 μm and a transverse resolution of 2–6 μm, while a previously described full-field OCT offered a axial and transverse resolution of 2–3 μm, image acquisition time was relatively lengthy (1.5 s/image), requiring the samples to be completely immobile[37]. Full-field optical coherence microscopy (FF-OCM) has also been used to visualize endothelial cells, but requires acquisition times of ~20–100 times longer than that of spectral domain OCT, which makes it difficult to translate it for clinical use[27]. In the current system, we achieved 1 μm axial resolution with a higher image acquisition speed of 60 kHz A-line. Since high-speed imaging is important to reduce motion artifact and enable clinical imaging applications, the future development of μOCT will be focused on improving image acquisition speed and motion tracking. One

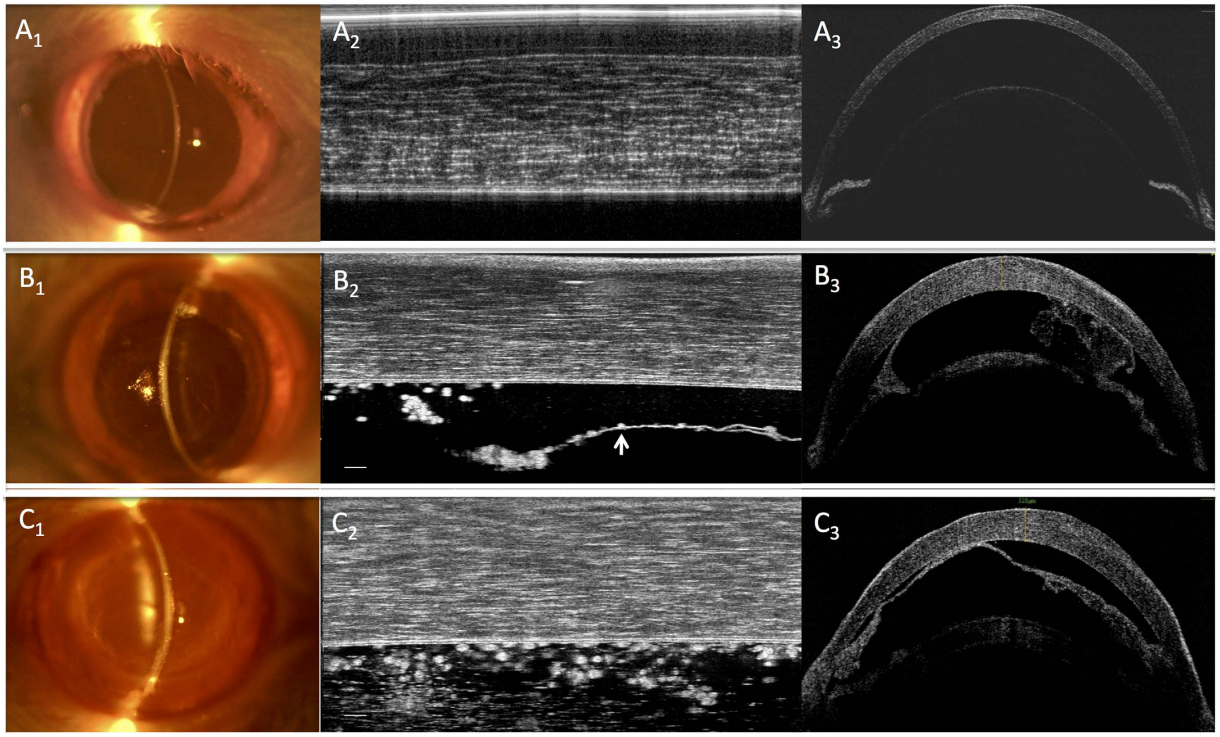

Figure 4. Slit lamp follow up and Cross sectional images of (**A**) normal rat cornea (**B**) Cryo-injury rat cornea (**C**) Chemical (BAK) injury rat cornea. A_1, B_1 and C_1: Slit lamp examination of rats cornea Pre (A_1) and post-injury (B_1,C_1) (30X magnification). A_2, B_2 and C_2: Cross sectional images of rats cornea Pre (A_2) and post-injury (B_2,C_2) using micro-OCT (Scale bar = 40 μm). A_3, B_3, and C_3: Cross sectional images of rats cornea Pre (A_3) and post-injury (B_3,C_3) using Optovue OCT.

promising solution to the speed issue may be to develop a swept source μOCT system which can achieve an A-line speed up to 4 MHz[38].

We recognize that our results are from a pilot study in a small number of eyes where this novel technology was tested in *ex vivo* rat eyes. Ideally, a larger number of eyes with *in vivo* analysis of corneal endothelial cell parameters such as that from specular microscopy could have been performed, but we used an *in vivo* animal model to evaluate both normal and damaged endothelial cells, where such parameters are not applicable. Nonetheless, we provide promising results from this preliminary study that used a novel μOCT system to provide rapid non-contact en face views of the corneal endothelium, with comparative repeatability compared to other conventional imaging techniques. The ability to delineate the endothelial nuclei and inflammatory cells have potential clinical applications, and future developments in image processing will improve image resolution and the depth of penetration will also allow us to perform *in vivo* imaging in human corneas. In summary, we described a novel μOCT system using a high-resolution spectral domain OCT imaging technique with established methods and algorithms, to potentially achieve histology-like images within the rat cornea. This preliminary study suggests that the μOCT system is able to obtain endothelial cell imaging with adequate resolution compared to histology and other existing techniques. Further *in vivo* studies, and ultimately, translation for human use *in vivo* would be required to establish this promising μOCT system for clinical applications.

References

1. Whitcher, J. P., Srinivasan, M. & Upadhyay, M. P. Corneal blindness: a global perspective. *Bull World Health Organ* **79,** 214–221 (2001).
2. Foster, A. & Resnikoff, S. The impact of Vision 2020 on global blindness. *Eye* (*Lond*) **19,** 1133–1135 (2005).
3. Tan, D. T., Dart, J. K., Holland, E. J. & Kinoshita, S. Corneal transplantation. *Lancet* **379,** 1749–1761 (2012).
4. Ang, M. *et al.* Endothelial cell loss and graft survival after Descemet's stripping automated endothelial keratoplasty and penetrating keratoplasty. *Ophthalmology* **119,** 2239–2244 (2012).
5. Han, D. C., Mehta, J. S., Por, Y. M., Htoon, H. M. & Tan, D. T. Comparison of outcomes of lamellar keratoplasty and penetrating keratoplasty in keratoconus. *Am J Ophthalmol* **148,** 744–751 e741 (2009).
6. Rio-Cristobal, A. & Martin, R. Corneal assessment technologies: current status. *Surv Ophthalmol* **59,** 599–614 (2014).
7. Ang, M. *et al.* Anterior segment optical coherence tomography study of the cornea and anterior segment in adult ethnic South Asian Indian eyes. *Invest Ophthalmol Vis Sci.* **53,** 120–125 (2012).
8. Girard, M. J., Strouthidis, N. G., Ethier, C. R. & Mari, J. M. Shadow removal and contrast enhancement in optical coherence tomography images of the human optic nerve head. *Invest Ophthalmol Vis Sci.* **52,** 7738–7748 (2011).
9. Mari, J. M., Strouthidis, N. G., Park, S. C. & Girard, M. J. Enhancement of lamina cribrosa visibility in optical coherence tomography images using adaptive compensation. *Invest Ophthalmol Vis Sci.* **54,** 2238–2247 (2013).
10. Liu, L. *et al.* Method for quantitative study of airway functional microanatomy using micro-optical coherence tomography. *PloS one* **8,** e54473 (2013).

11. Liu, L. *et al.* Imaging the subcellular structure of human coronary atherosclerosis using micro-optical coherence tomography. *Nature Medicine* **17,** 1010–1014 (2011).
12. Liu, L. *et al.* An autoregulatory mechanism governing mucociliary transport is sensitive to mucus load. *American journal of respiratory cell and molecular biology* **51,** 485–493 (2014).
13. Liu, L. *et al.* Method for Quantitative Study of Airway Functional Microanatomy Using Micro-Optical Coherence Tomography. *Plos One* **8,** e54473 (2013).
14. Liu, L. *et al.* Imaging the subcellular structure of human coronary atherosclerosis using micro-optical coherence tomography. *Nat Med.* **17,** 1010–1014 (2011).
15. Cui, D., Liu, X. & Zhang, J. *et al.* Dual spectrometer system with spectral compounding for 1-μm optical coherence tomography *in vivo*. *Opt. Lett.* **39(23),** 6727–30 (2014).
16. Liu, X., Chen, S., Cui, D., Yu, X. & Liu, L. Spectral estimation optical coherence tomography for axial super-resolution. *Optics Express* **23,** 26521–26532 (2015).
17. Han, S. B. *et al.* A mouse model of corneal endothelial decompensation using cryoinjury. *Mol Vis* **19,** 1222–1230 (2013).
18. Bredow, L., Schwartzkopff, J. & Reinhard, T. Regeneration of corneal endothelial cells following keratoplasty in rats with bullous keratopathy. *Mol Vis.* **20,** 683–690 (2014).
19. Han, S. B. *et al.* Mice with a Targeted Disruption of Slc4a11 Model the Progressive Corneal Changes of Congenital Hereditary Endothelial Dystrophy. *Invest Ophthalmol Vis Sci.* (2013).
20. Peh, G. S. *et al.* Optimization of human corneal endothelial cell culture: density dependency of successful cultures *in vitro*. *BMC Res Notes* **6,** 176 (2013).
21. Patel, D. V., Phua, Y. S. & McGhee, C. N. Clinical and microstructural analysis of patients with hyper-reflective corneal endothelial nuclei imaged by *in vivo* confocal microscopy. *Exp Eye Res.* **82,** 682–687 (2006).
22. Swanson, E. A. *et al. In vivo* retinal imaging by optical coherence tomography. *Opt Lett* **18,** 1864–1866 (1993).
23. Ang, M. *et al.* Optical Coherence Tomography Angiography for Anterior Segment Vasculature Imaging. *Ophthalmology* **122,** 1740–1747 (2015).
24. Ang, M., Cai, Y., Shahipasand, S. *et al.* En face optical coherence tomography angiography for corneal neovascularisation. *Br J Ophthalmol* **100(5)**, 616–21 (2016).
25. Girard, M. J. *et al.* Enhancement of Corneal Visibility in Optical Coherence Tomography Images Using Corneal Adaptive Compensation. *Transl Vis Sci Technol* **4,** 3 (2015).
26. Drexler, W. *et al.* Ultrahigh-resolution ophthalmic optical coherence tomography. *Nat Med.* **7,** 502–507 (2001).
27. Christopoulos, V. *et al. In vivo* corneal high-speed, ultra high-resolution optical coherence tomography. *Arch Ophthalmol* **125,** 1027–1035 (2007).
28. Ang, M. *et al.* Endothelial keratoplasty after failed penetrating keratoplasty: an alternative to repeat penetrating keratoplasty. *Am J Ophthalmol* **158,** 1221-1227 e1221 (2014).
29. Ang, M., Wilkins, M. R., Mehta, J. S. & Tan, D. Descemet membrane endothelial keratoplasty. *Br J Ophthalmol* **100,** 15–21 (2016).
30. Ang, M., Sng, C. C., Chee, S. P., Tan, D. T. & Mehta, J. S. Outcomes of corneal transplantation for irreversible corneal decompensation secondary to corneal endotheliitis in Asian eyes. *Am J Ophthalmol* **156,** 260–266 e262 (2013).
31. Fujimoto, J. G. Optical coherence tomography for ultrahigh resolution *in vivo* imaging. *Nature Biotechnology* **21,** 1361–1367 (2003).
32. Jia, Y. *et al.* Split-spectrum amplitude-decorrelation angiography with optical coherence tomography. *Optics Express* **20,** 4710–4725 (2012).
33. Leitgeb, R. A., Villiger, M., Bachmann, A. H., Steinmann, L. & Lasser, T. Extended focus depth for Fourier domain optical coherence microscopy. *Opt. Lett.* **31,** 2450–2452 (2006).
34. Yu, X. *et al.* Depth extension and sidelobe suppression in optical coherence tomography using pupil filters. *Optics Express* **22,** 26956–26966 (2014).
35. Liu, L., Liu, C., Howe, W. C., Sheppard, C. J. R. & Chen, N. Binary-phase spatial filter for real-time swept-source optical coherence microscopy. *Optics Letters* **32,** 2375–2377 (2007).
36. Sarunic, M., Choma, M. A., Yang, C. & Izatt, J. A. Instantaneous complex conjugate resolved spectral domain and swept-source OCT using 3x3 fiber couplers. *Optics Express* **13,** 957–967 (2005).
37. Akiba, M. *et al.* Ultrahigh-resolution imaging of human donor cornea using full-field optical coherence tomography. *J Biomed Opt.* **12,** 041202 (2007).
38. Fechtig, D. J., Schmoll, T., Grajciar, B. *et al.* Line-field parallel swept source interferometric imaging at up to 1 MHz. *Opt. Lett.* **39(18),** 5333–6 (2014).

Acknowledgements

Singapore National Medical Research Council (NMRC/CNIG/1128/2015), National Research Foundation Singapore (NRFCRP13-2014-05), Ministry of Education Singapore (MOE2013-T2-2-107).

Author Contributions

All authors contributed to the design, conduct, data collection and preparation of the manuscript. Design and conduct of the study (M.A., A.K., G.G., H.M.H., X.S., N.C.L., X.L., S.C., L.L. and J.S.M.); collection (M.A., A.K., G.G., H.M.H., X.S., N.C.L., X.L., S.C., L.L. and J.S.M.); management (M.A. and J.S.M.); analysis (M.A., H.M.H., L.L. and J.S.M.) and interpretation of the data (M.A., A.K., G.G., H.M.H., X.S., N.C.L., X.L., S.C., L.L. and J.S.M.); and preparation of the manuscript (M.A., A.K., G.G., H.M.H., X.S., N.C.L., X.L., S.C., L.L. and J.S.M.).

Additional Information

Competing financial interests: The authors declare no competing financial interests.

How to cite this article: Ang, M. *et al.* Evaluation of a Micro-Optical Coherence Tomography for the Corneal Endothelium in an Animal Model. *Sci. Rep.* **6**, 29769; doi: 10.1038/srep29769 (2016).

Imaging Capabilities of Anterior Segment Optical Coherence Tomography in Conjunctival Inflammation

Introduction

Glaucoma is the commonest cause of preventable visual impairment in England and Wales.[1] The International Glaucoma Association estimates that more than 500000 people suffer from glaucoma in England and Wales. When medical and laser treatment fail to control progression of the disease, filtration surgery is usually carried out. Therefore, an excess of 4000 trabeculectomy procedures are performed in England alone per year.[2]

Bleb morphology is an important indicator of bleb function and outcome of glaucoma filtration surgery.[3] Excessive conjunctival scarring at the filtration site is considered the major cause for poor outcome.[4-6] Cytotoxic agents, such as mitomycin-C and 5-fluorouracil, are, therefore, used during surgery in order to reduce the conjunctival and Tenon's capsule fibrosis; both agents inhibit fibroblast growth.[4] Post-operative steroid drops are also used routinely in order to reduce the post-operative conjunctival inflammation and scarring.

Filtration procedure morphology has been extensively studied with ultrasound biomicroscopy (UBM) and in vivo confocal microscopy.[7-13] However, AS-OCT provides higher image resolution than UBM (18 vs. 25μm) without the requirement for contact examination that may alter the morphology of the filtration procedure.[14] It has been used to analyse the characteristics of trabeculectomy procedures, such as the height of the bleb, the thickness of the bleb wall and the presence of bleb wall microcysts.[15,16]

Understanding the post-operative conjunctival healing response may help us improve the procedure and outcomes for patients. In addition, studying the drainage and intraocular pressure (IOP) lowering mechanisms in trabeculectomy and deep sclerectomy (DS), the two most common glaucoma filtration procedures, may guide the evolution of filtration surgery.

Appendix - AS-OCT imaging capabilities in conjunctival inflammation

Hypothesis

In this study, the capabilities of AS-OCT to image the conjunctiva and Tenon's layer (CoTL) are explored, using filtration surgery as a model of conjunctival inflammation and scarring. I hypothesise that AS-OCT imaging following trabeculectomy and DS filtration surgery will identify differences in qualitative and quantitative parameters of the CoTL between the two procedures.

Materials and methods

Recruitment of patients and controls

Thirty-five consecutive filtration procedure patients with primary glaucoma were recruited at University Hospital Southampton NHS Foundation Trust. Procedures with follow-up less than 3 months were excluded in order to avoid potential confounders in the early postoperative stages. Postoperative needling or laser goniopuncture were not exclusion criteria.

Fifteen control glaucoma patients on IOP lowering medication were also recruited, aiming to explore the capabilities of AS-OCT to image the healthy CoTL and, in addition, to compare the CoTL characteristics of non-surgery and surgery eyes. Cataract surgery within 6 months and prior filtration surgery were exclusion criteria for control patients.

Filtration surgery

Surgery was carried out by two consultant ophthalmologists with a specialist interest in glaucoma. In DS procedures, the CoTL was retracted with a fornix base at the 90^{o} position and a 4x4mm limbus-based scleral flap was dissected. Sclera was deep-dissected forwards to enter Schlemm's canal and expose the juxta-canalicular tissue. The dissection was then continued forward to de-roof Schlemm's canal and expose a thin trabeculo-Descemet's membrane (TDM). The deep scleral block was excised and juxta-canalicular tissue peeled from the opened Schlemm's canal. The intrascleral space was filled with viscoelastic (VISCOAT®, Alcon Laboratories, Inc). Finally, the scleral flap and CoTL were sutured in their normal anatomical position with 10/0 vicryl sutures.

In trabeculectomy surgery, the CoTL was retracted with a fornix base at the 90^{o} position and mitomycin-C 0.2 mg/ml or 5-fluorouracil 50 mg/ml applied for 2-3 minutes, then thoroughly washed. A 4x3mm limbus-based scleral flap was dissected and a sclerostomy performed using the Kelly punch. The scleral flap was sutured watertight with fixed and releasable 10/0 nylon sutures, the opening pressure titrated via a paracentesis. The CoTL was sutured with 10/0 nylon sutures.

Scanning methodology

Visante OCT imaging of glaucoma filtration surgery cases was carried out with the upper eyelid elevated and the patient looking down in order to expose the surgical site. The rotating scanning beam of the four-quadrant high-resolution mode was centred on the scleral flap by direct visualisation on the integrated camera (figure A1). Multiple scans were carried out and the scan that was best centred on the scleral flap was analysed.

Visante OCT imaging of control participants was also carried out with the upper eyelid elevated and the patient looking down. The rotating beam of the four-quadrant high-resolution mode was centred 2-3 mm posterior to the limbus at the 90^{o} position.

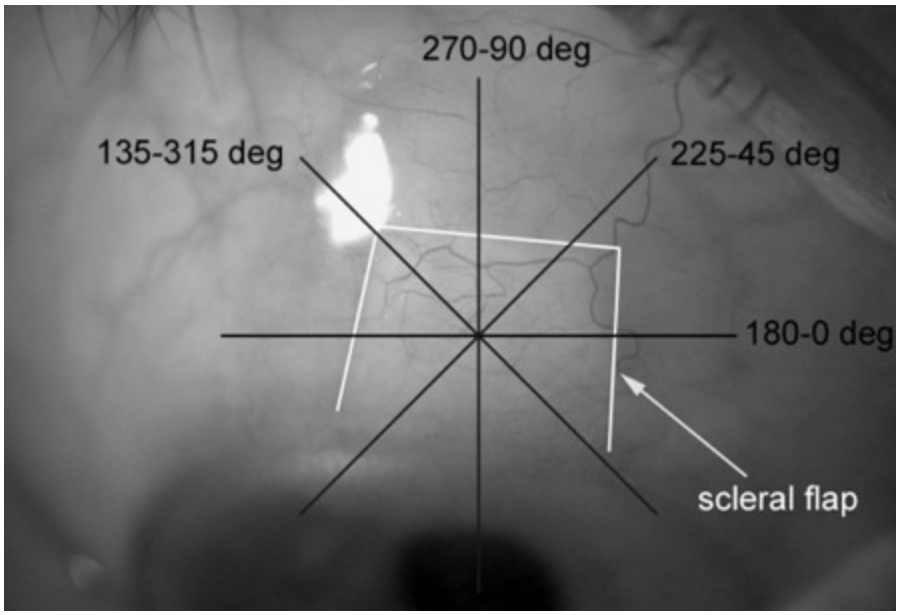

Figure A1. The scanning protocol in glaucoma filtration surgery. The Anterior Segment Optical Coherence Tomography (AS-OCT) rotating scanning beam of the four-quadrant high-resolution mode is centred on the scleral flap of the filtration procedure.

Image analysis

Images were analysed for the presence of a bleb cavity (BC), CoTL microcysts and posterior drainage. The maximum height of the BC and the maximum height of the intrascleral lake (IL) were measured. The height of the filtration procedure and the CoTL thickness were measured at the posterior scleral flap edge on the 90^{o} scan (figures A2 and A3). In control cases, the CoTL thickness was measured 3mm posterior to the irido-corneal angle on the image of the 90^{o} scan (figure A4).

Definitions of the AS-OCT parameters are presented in table A1. Software callipers (software version 1.1.2) were used for measurements.

Appendix - AS-OCT imaging capabilities in conjunctival inflammation

AS-OCT parameter	Definition
Bleb cavity	A hypo-reflective area above the sclera and below the CoTL
CoTL microcysts	Small, at least 10 μm in diameter, hypo-reflective spaces within the CoTL
Posterior drainage	A hypo-reflective area at or behind the posterior scleral flap edge
Height of filtration procedure	The distance from the superior surface of the scleral flap to the outer surface of the CoTL
CoTL thickness	The distance between the inner and outer surfaces of the CoTL
Intrascleral lake height	The hypo-reflective space between the lower surface of the scleral flap and the superior surface of the trabeculo-Descemet's membrane
CoTL: conjunctival/Tenon's layer	

Table A1. Definition of AS-OCT filtration procedure parameters.

Data analysis

Patient age, type of glaucoma, pre-operative Goldmann IOP, number of pre-operative IOP lowering agents, type of filtration procedure and antimetabolite use, post-operative IOP and number of IOP lowering agents at the time of the AS-OCT scan were recorded. IOP≤16mmHg at the time of the scan without glaucoma medication was used to define a successful group; the remaining cases were classified as non-successful. A strict success criterion was chosen in order to avoid random allocation due to IOP fluctuation.

AS-OCT parameters were quantified and compared between the filtration and control groups. They were examined for association with IOP and success in

the surgical groups. DS and trabeculectomy procedures were analysed as individual groups and also as a collective ‘filtration group’.

Normality distribution of data was assessed by Kolmogorov-Smirnov statistics, normal distribution plots and histograms. All variables had a skewed distribution; therefore, the Kruskal Wallis test, Mann-Whitney U test, Wilcoxon signed-rank test and Spearman correlation coefficient were used to analyse numerical outcomes. Fisher’s exact test was used to compare categorical outcomes. Statistical Analysis Software (SAS) version 9.1 (SAS Institute Inc., Cary, NC, USA) was used and differences were considered statistically significant when $p<0.05$.

Results

Fifty cases in total were scanned and analysed. Thirty-five filtration procedures, consisting of 18 DS and 17 trabeculectomy procedures, and 15 control cases were examined. There was no difference in patient age, glaucoma type and IOP on the scan day between the three groups (table A2). Three DS and 17 trabeculectomy procedures had been augmented with per-operative mitomycin-C or 5-fluorouracil.

Both DS and trabeculectomy groups had a significant IOP reduction compared to before surgery (22.3 vs. 16.9mmHg, $p<0.001$ and 22.5 vs. 14.4mmHg, $p<0.001$ respectively). The results are summarized in tables A3-A5.

Parameter	DS	Trab	Controls	P value
Patients (eyes)	15 (18)	16 (17)	15 (15)	
Patient age				
-mean [SD] (years)	76.4 [12.1]	71.5 [11.6]	78.8 [8.0]	0.198
Glaucoma type (eyes)				
-POAG	15 (83.3%)	11 (64.7%)	10 (66.7%)	0.454
-PACG	2	3	1	
-NTG	0	1	1	
-Other	1	2	3	
Pre-operative IOP				
-mean [SD] (mmHg)	22.3 [3.6]	22.5 [3.2]	NA	0.727
Pre-operative agents				
-mean [SD]	2.67 [1.14]	3.41 [1.00]	NA	0.069
Follow-up on scan day				
-mean [SD] (days)	482.2 [218.6]	372.2 [143.5]	NA	0.171
-range (days)	108 - 869	128 - 631		
IOP on scan day				
-mean [SD] (mmHg)	16.9 [4.2]	14.4 [5.9]	17.6 [3.5]	0.093
Success [a]				
-yes	9 (50%)	11 (64.7%)	NA	0.499
IOP agents on scan day				
-mean [SD]	0.56 [0.86]	0.29 [0.77]	2.47 [0.92]	<0.001

[a]IOP ≤ 16mmHg without drops, DS: deep sclerectomy, trab: trabeculectomy, POAG: primary open angle glaucoma, PACG: primary angle closure glaucoma, NTG: normal tension glaucoma, IOP: intraocular pressure, NA: not applicable

Table A2. Filtration procedure and control patient characteristics.

Appendix - AS-OCT imaging capabilities in conjunctival inflammation

Conjunctival/Tenon's layer

Filtration procedure scans

The CoTL could be visualised and measured on the images of all filtration group cases. The CoTL thickness in the filtration group correlated negatively with IOP (r=-0.397, p=0.018) and successful procedures had a thicker CoTL than non-successful cases (632.5 vs. 344 μm, p<0.001).

Successful DS procedures had a thicker CoTL than non-successful cases (586.7 vs. 251.1 μm, p<0.001) and CoTL thickness correlated negatively with IOP (r=-0.641, p=0.004). Successful trabeculectomy procedures had a thicker CoTL than non-successful cases, though of borderline statistical significance (670 vs. 483.3 μm, p=0.107); CoTL thickness did not correlate with IOP (r=-0.254, p=0.325).

Microcysts in the CoTL were detected in 51.4% of the filtration group cases. They were present in 50% of DS and 52.9% of trabeculectomy cases (p=1), but absent in control eyes. In the filtration group, eyes with CoTL microcysts did not have a lower IOP than eyes without (mean [SD]: 15.1[5.2] vs. 16.3[5.2] mmHg, p= 0.547). The presence of CoTL microcysts had a borderline association with success (p=0.092).

In the trabeculectomy group, eyes with microcysts didn't have a lower IOP than eyes without (mean [SD]: 13.1[5.3] vs. 15.9[6.4] mmHg, p=0.370) and the presence of microcysts was not associated with success (p=0.335). In DS cases also, eyes with microcysts didn't have a lower IOP than eyes without (mean [SD]: 17.1[4.4] vs. 16.7[4.2] mmHg, p=0.931) and the presence of microcysts was not associated with success (p=0.347).

Control scans

In control eyes, the CoTL thickness did not correlate with IOP on the scan day (r=0.137, p=0.627). There was a significant difference in CoTL thickness between control, DS and trabeculectomy groups (mean [SD]: 203.3[62.6] vs. 418.9[261.9] vs. 604.1[220.7] μm, p<0.001). The CoTL of non-successful procedures in the filtration group was thicker than in control cases (mean [SD]: 344[194.2] vs. 203.3[62.6] μm, p=0.004).

Appendix - AS-OCT imaging capabilities in conjunctival inflammation

Height of filtration procedure

Filtration procedure height could be measured on the images of all filtration group cases. In the filtration group, successful procedures were taller than non-successful procedures (713.5 vs. 344 μm, $p<0.001$); height correlated negatively with IOP ($r=-0.455$, $p=0.006$). Height of filtration procedure was smaller in DS than trabeculectomy images (418.9 vs. 699.4 μm, $p=0.005$).

Successful DS procedures were taller than non-successful cases (586.7 vs. 251.1μm, $p<0.001$) and height of filtration procedure correlated negatively with IOP ($r=-0.641$, $p=0.004$). Successful trabeculectomy procedures were taller than non-successful cases (817.3 vs. 483.3 μm, $p=0.021$), but height did not correlate with IOP ($r=-0.368$, $p=0.147$).

Appendix - AS-OCT imaging capabilities in conjunctival inflammation

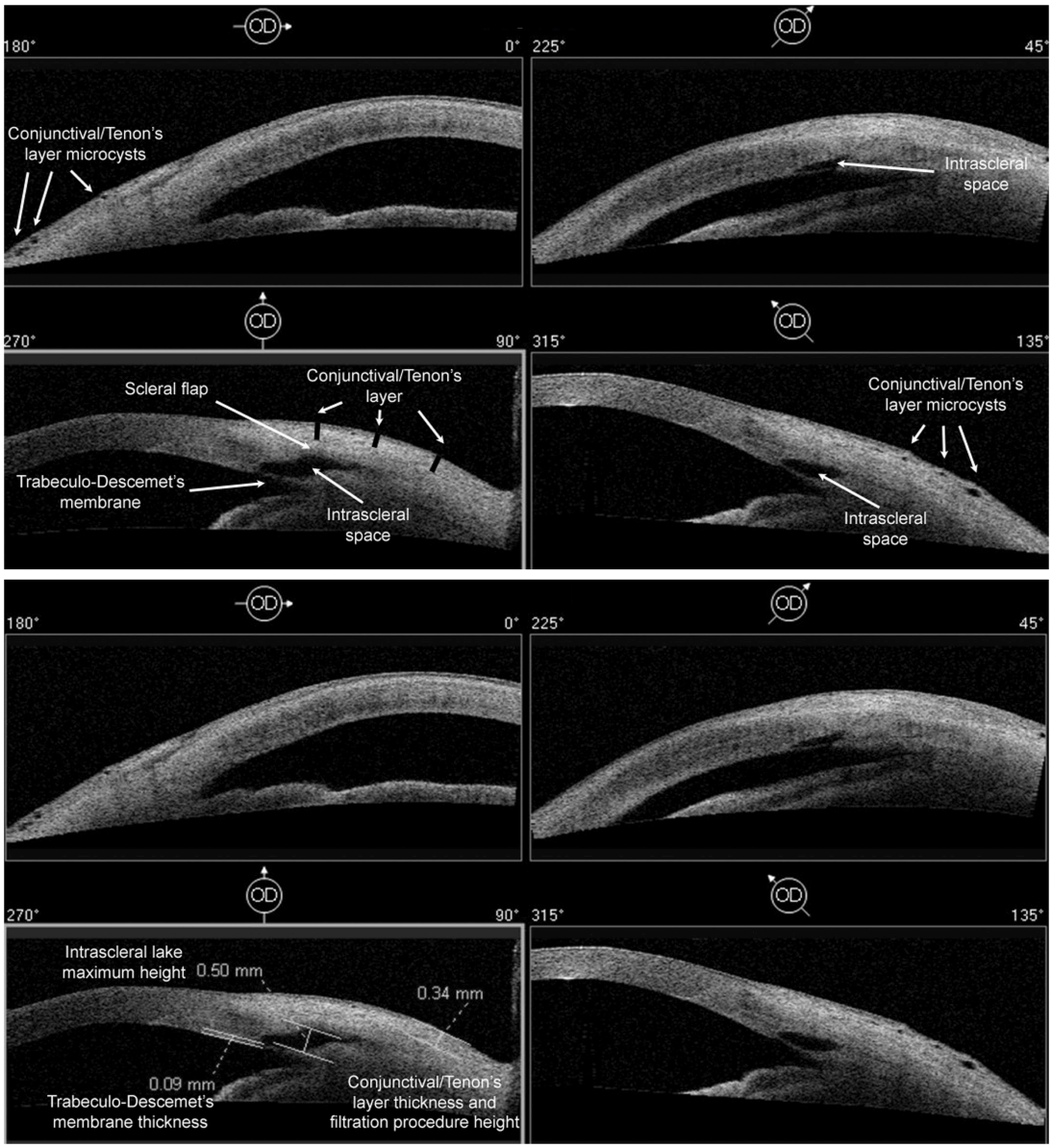

Figure A2. AS-OCT of a deep sclerectomy. The top image illustrates the morphology of the filtration procedure; the lower image the measurement of the filtration procedure parameters.

Bleb cavity and intrascleral lake

A BC was detected on 42.9% of the filtration group images. It was detected more frequently in trabeculectomy than DS procedures (64.7% vs. 22.2%, p=0.018). In the filtration group, eyes with a BC had a lower IOP than eyes

without a BC (mean [SD]: 13.1[4.3] vs. 17.7[5.0] mmHg, p=0.006). The presence of a BC was also associated with success (p=0.005).

Trabeculectomy procedures with a BC had a borderline significantly lower IOP than eyes without (mean [SD]: 12.4[4.7] vs. 18.2[6.3] mmHg, p= 0.077). The presence of a BC had a borderline association with success (p=0.109). Successful trabeculectomy procedures had a significantly taller BC than non-successful eyes (607.5 vs. 176.7 µm, p=0.041). However, maximum BC height was not associated with IOP (r= 0.235, p=0.488).

The maximum IL height in DS procedures showed a significant negative correlation with IOP (r=-0.493, p=0.038) and successful eyes had a significantly taller IL than non-successful eyes (513.3 vs. 361.1µm, p=0.027).

Drainage posterior to the flap

Posterior drainage was identified on 14.3% of the filtration group images. Successful procedures in the filtration group had evidence of posterior drainage with borderline higher frequency than non-successful cases (p=0.057). Eyes with posterior drainage on the scans did not have a significantly lower IOP than eyes without (mean [SD]: 13[3.2] vs. 16.1[5.3] mmHg, p=0.121).

The DS cases and trabeculectomy eyes with posterior drainage did not have a significantly lower IOP than cases without (mean [SD]: 14[2.8] vs. 17.3[4.2] mmHg, p=0.218 and 12.3[3.8] vs. 14.9[6.2] mmHg, p=0.447 respectively). Drainage posterior to the flap was not associated with success either.

Appendix - AS-OCT imaging capabilities in conjunctival inflammation

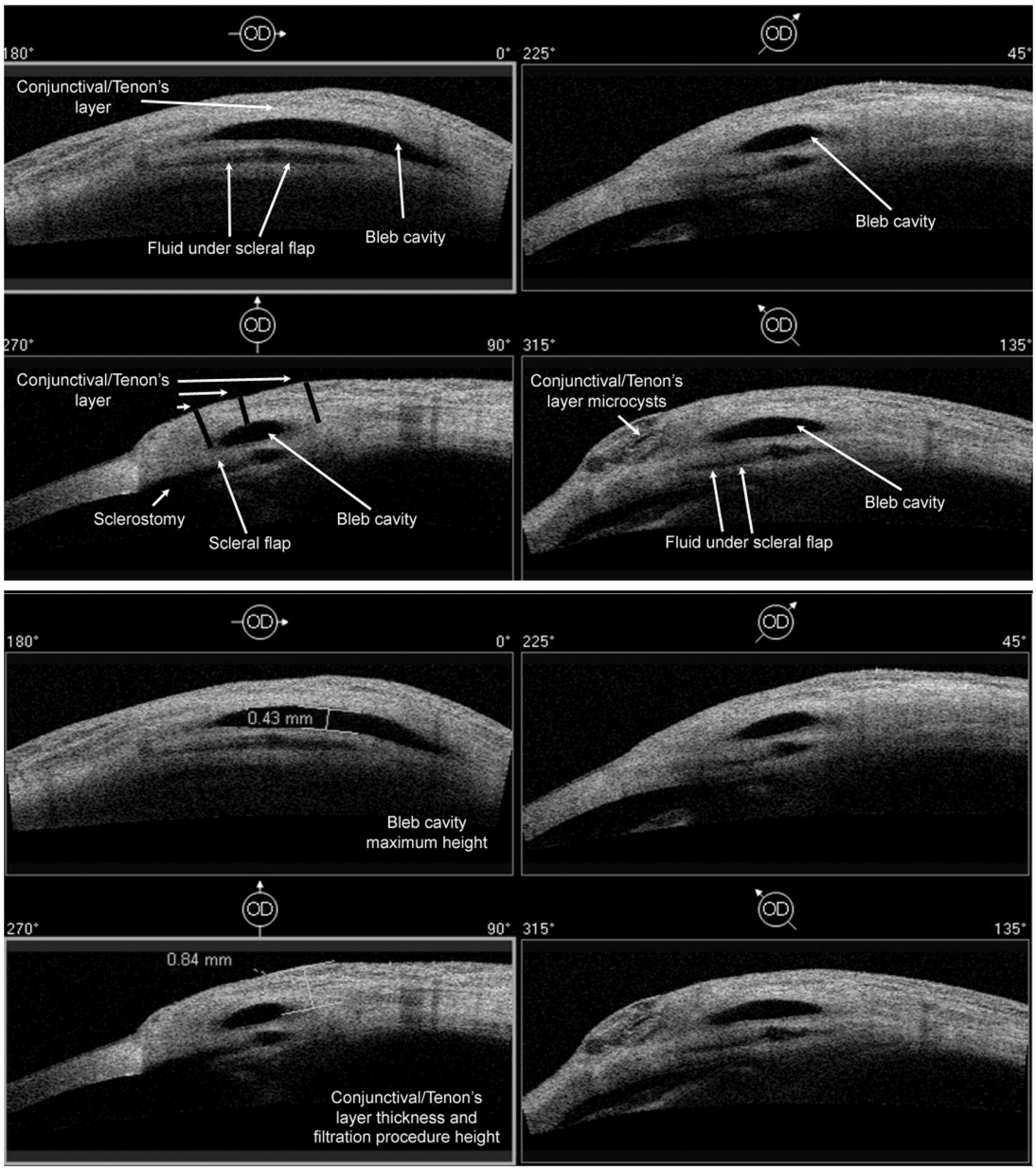

Figure A3. AS-OCT of a trabeculectomy. The top image illustrates the morphology of the filtration procedure; the lower image the measurement of filtration procedure parameters.

Bleb parameter	DS	Trab	P-value
Bleb cavity presence			
-yes	4 (22.2%)	11 (64.7%)	0.018
CoTL microcyst presence			
-yes	9 (50%)	9 (52.9%)	1
Height of filtration procedure			
-mean [SD] (µm)	418.9 [261.9]	699.4 [280.9]	0.005
CoTL thickness			
-mean [SD] (µm)	418.9 [261.9]	604.1 [220.7]	0.016
Bleb cavity maximum height			
-mean [SD] (µm)		490.0 [367.4]	
Intrascleral lake maximum height			
-mean [SD] (µm)	437.2 [155.8]		

DS: deep sclerectomy, trab: trabeculectomy, CoTL: conjunctival/Tenon's layer

Table A3. AS-OCT comparison of DS and trabeculectomy.

AS-OCT parameter	Spearman r	P-value
Filtration group (n=35)		
Height of filtration procedure	-0.455	0.006
CoTL thickness	-0.397	0.018
Deep Sclerectomy (n=18)		
CoTL thickness	-0.641	0.004
Intrascleral lake maximum height	-0.493	0.038
Height of filtration procedure	-0.641	0.004
Trabeculectomy (n=17)		
CoTL thickness	-0.254	0.325
Height of filtration procedure	-0.368	0.147
Bleb cavity maximum height	0.235	0.488

IOP: intraocular pressure, r: correlation coefficient, CoTL: conjunctival/Tenon's layer

Table A4. Correlation of AS-OCT filtration parameters with IOP.

Appendix - AS-OCT imaging capabilities in conjunctival inflammation

Bleb parameter	Successful [a]	Non successful	P-value
Deep Sclerectomy (n=18)			
Posterior drainage -yes/no	2/7	0/9	0.471
Bleb cavity presence -yes/no	4/5	0/9	0.082
Height of filtration procedure -mean [SD] (µm)	586.7 [280.8]	251.1 [60.1]	<0.001
CoTL thickness -mean [SD] (µm)	586.7 [280.8]	251.1 [60.1]	<0.001
IL maximum height -mean [SD] (µm)	513.3 [147.8]	361.1 [129.2]	0.027
Trabeculectomy (n=17)			
Posterior drainage -yes/no	3/8	0/6	0.515
Bleb cavity presence -yes/no	9/2	2/4	0.109
Height of filtration procedure -mean [SD] (µm)	817.3 [229.0]	483.3 [247.0]	0.021
CoTL thickness -mean [SD] (µm)	670 [184.1]	483.3 [247.0]	0.107
BC maximum height -mean [SD] (µm)	607.5 [359.2]	176.7 [143.6]	0.041

[a]intraocular pressure ≤ 16mmHg without glaucoma medication, CoTL: conjunctival/Tenon's layer, IL: intrascleral lake, BC: bleb cavity

Table A5. Association of AS-OCT filtration parameters with success.

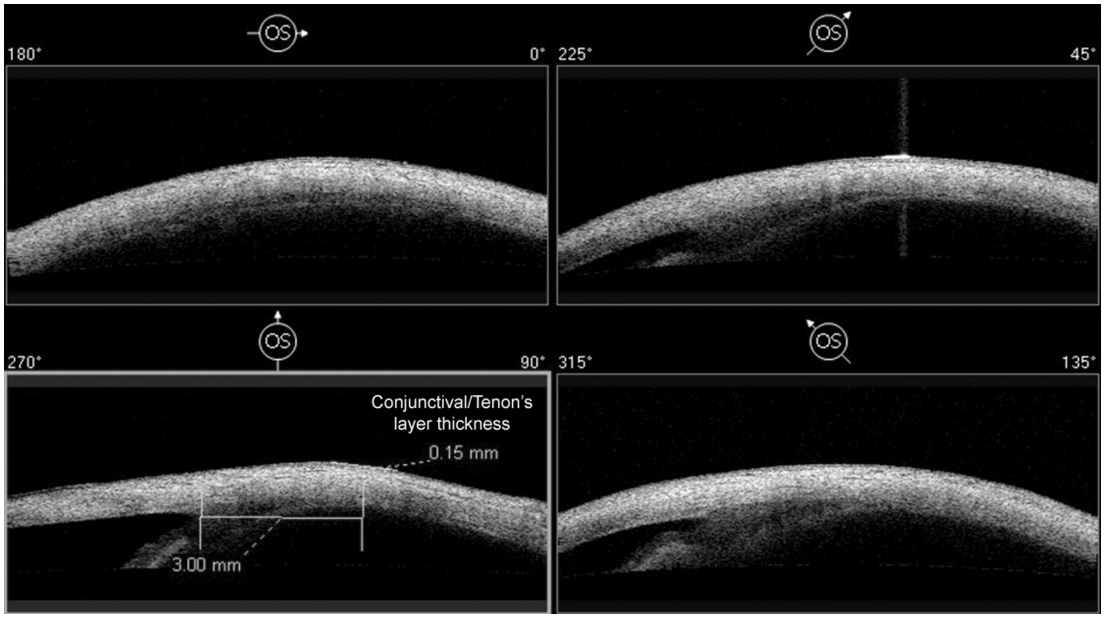

Figure A4. AS-OCT of the healthy conjunctiva/Tenon's layer. Measurement of the conjunctival/Tenon's layer thickness 3mm posterior to the angle on the 90° scan is illustrated.

Discussion

This study investigated the capabilities of AS-OCT to image and quantify characteristics of the CoTL after trabeculectomy and DS filtration surgery. The CoTL was distinguished from the underlying sclera and its thickness measured on all the AS-OCT images. It was also possible to visualise microcysts within the CoTL and drainage posterior to the scleral flap. In addition, the BC and IL of trabeculectomy and DS procedures, respectively, could be imaged and their height measured.

AS-OCT imaging identified the in-vivo morphological differences between DS and trabeculectomy. The CoTL was thicker in trabeculectomy than DS and the height of the filtration procedure was greater for trabeculectomy. A BC was present more frequently in trabeculectomy than DS images, whereas the IL was visualised only in DS images.

The post-operative response of the CoTL is important in glaucoma, as excessive conjunctival scarring at the filtration site is a major cause of poor

outcome.[4-6] The CoTL thickness in DS correlated negatively with IOP and successful cases had a thicker CoTL than non-successful eyes. In trabeculectomy, successful procedures also had a thicker CoTL, although of borderline statistical significance (p=0.107). Previous AS-OCT studies have found successful trabeculectomy procedures to have a thicker wall than non-successful cases.[15,16] This suggests that, in both DS and trabeculectomy procedures, good drainage is associated with increased CoTL thickness.

No study to date had examined the CoTL and its thickness in DS. The CoTL in DS was thinner than in trabeculectomy and success was associated with a thicker CoTL. Trabeculectomy confocal microscopy studies have shown that functioning blebs have a loose arrangement of subepithelial connective tissue.[7,8] Well functioning DS procedures may also have a similar loose subepithelial connective tissue resulting in a relatively thick CoTL, whereas less well draining procedures may have dense connective tissue with a thinner CoTL.

Non-successful filtration procedures were shown to have a thicker CoTL than non-surgery eyes with glaucoma. This is in keeping with a histological study that found that the subepithelial connective tissue was thicker in failed blebs than in normal eyes or functioning blebs.[5] However, my in-vivo measurements, supported by numerous other OCT studies,[15-17] suggested that failed blebs have a thinner CoTL than functioning blebs.

Microcysts of the CoTL were present in 50% of DS and 52.9% of trabeculectomy images, whilst absent from control eyes, providing in-vivo anatomical evidence that trans-conjunctival aqueous drainage is an important drainage mechanism in both DS and trabeculectomy. Kawana et al, using a long wavelength Fourier-domain three-dimensional OCT, identified microcysts in 86.8% of trabeculectomy cases.[17] Other research teams have identified microcysts using the Visante OCT, but did not present quantification results.[15,18] Confocal microscopy and three-dimensional OCT studies on trabeculectomy have found that the number of microcysts correlated with good bleb function.[7,8,17,19,20] My study only found a borderline association between the presence of microcysts and success. This may be due to the inferior imaging resolution and modes of the Visante OCT compared to confocal microscopy and newer three-dimensional OCT devices.

Appendix - AS-OCT imaging capabilities in conjunctival inflammation

A BC was detected in 64.7% of trabeculectomy scans and 22.2% of DS scans. Leung et al detected a supra-scleral fluid space in 57.1% of trabeculectomy cases.[18] The higher aqueous outflow in trabeculectomy compared to the slower aqueous egress in DS was associated with BC development, as a BC was present more frequently in trabeculectomy. Trabeculectomy BC height was larger in successful procedures, suggesting that the BC acted as an aqueous reservoir. In agreement with Tominaga et al, the BC height did not correlate with IOP.[16] The difference between the two outcome measures, IOP and success, may reflect the confounding effect of IOP lowering agents on IOP correlation analyses.

The IL, visualised in all DS images, may also function as a fluid reservoir, analogous to the trabeculectomy BC. The IL height in DS correlated negatively with IOP and was larger in successful cases, confirming previous AS-OCT findings by Mavracanas et al.[21] UBM has previously failed to find this association,[11] most likely due to inferior imaging resolution or compression of the tissues by the imaging probe. The importance of IL height, and possibly reservoir dimensions, is only becoming clearer with the advent of AS-OCT.

The height of filtration procedure could be measured on all images. In DS, it was associated with success and correlated with IOP. In trabeculectomy, it was associated with success but not IOP. The height in DS is a similar parameter to CoTL thickness, as it depends almost exclusively on CoTL thickness. Successful trabeculectomy procedures were taller than non-successful cases. This is most likely due to the fact that height in trabeculectomy is a measure of CoTL thickness and BC height, both parameters found to be larger in successful cases. Although previous Visante OCT work has not found an association between trabeculectomy height and success or IOP,[15,16] a three dimensional OCT study did show that trabeculectomy height correlated with IOP and was associated with success.[17]

Drainage posterior to the scleral flap was detected only in 14.3% of filtration group scans and showed a borderline association (p=0.057) with success. No significant association was found in either trabeculectomy or DS group. Kawana et al, using Fourier-domain three-dimensional OCT, identified fluid under the flap in 94.7% of trabeculectomy cases, but didn't investigate for drainage posterior to the flap.[17] Decreasing image resolution of the Visante

OCT, as the OCT signal penetrates the thickened CoTL, or its lack of a three-dimensional scanning mode may limit identification of fluid posterior to the flap compared to Fourier-domain OCT.

This AS-OCT study has provided novel insight into the drainage mechanisms of surgery, especially for non-penetrating DS. A tall and therefore large fluid reservoir, either IL or BC, was important to success. A thicker CoTL in the post-operative period was also associated with low IOP. Further research on these two important parameters, especially with serial longitudinal AS-OCT imaging, may improve our understanding of filtration surgery outcomes.

Conclusions

The CoTL could be identified and its thickness measured on all Visante OCT scans of filtration procedures; CoTL microcysts and drainage posterior to the scleral flap could be visualised. In addition, the BC and IL of trabeculectomy and DS procedures, respectively, could be imaged and their height measured. Interestingly, morphological parameters identified with AS-OCT, specifically CoTL thickness, BC height and IL height, were associated with function.

The Visante OCT identified in-vivo morphological differences between DS and trabeculectomy. The CoTL was thicker in trabeculectomy than DS and the height of the filtration procedure was greater for trabeculectomy. A BC was more common in trabeculectomy than DS, whereas the IL was an exclusive feature of DS.

References

1. Bunce C and Wormald R. Leading causes of certification for blindness and partial sight in England and Wales. BMC Public Health. 2006; 6:58.
2. Fraser SG and Wormald RP. Hospital episode statistics and changing trends in glaucoma surgery. Eye. 2008; 22:3-7.
3. Azuara-Blanco A and Katz LJ. Dysfunctional filtering blebs. Surv Ophthalmol. 1998; 43:93-126.
4. Lama PJ and Fechtner RD. Antifibrotics and wound healing in glaucoma surgery. Surv Ophthalmol. 2003; 48:314-346.
5. Addicks EM, Quigley A, Green WR, Robin AL. Histological characteristics of filtering blebs in glaucomatous eyes. Arch Ophthalmol. 1983; 101:795-798.
6. Hitchings RA, Grierson I. Clinico pathological correlation in eyes with failed fistulising surgery. Trans Ophthalmol Soc UK. 1983; 103:84-88.
7. Amar N, Labbé A, Hamard P, Dupas B, Baudouin C. Filtering blebs and aqueous pathway an immunocytological and in vivo confocal microscopy study. Ophthalmology 2008;115:1154-1161.
8. Labbe A, Dupas B, Hamard P, Baudouin C. In vivo confocal microscopy study of blebs after filtering surgery. Ophthalmology 2005;112:1979-1986.
9. Chiou AG, Mermoud A, Hediguer SE, Schnyder CC, Faggioni R. Ultrasound biomicrosopy of eyes undergoing deep sclerectomy with collagen implant. Br J Ophthalmol. 1996;80:541-544.
10. Roters S, Luke C, Jonescu-Cuypers CP, Engels BF, Jacobi PC, Konen W, Krieglstein GK. Ultrasound biomicroscopy and its value in predicting the long term outcome of viscocanalostomy. Br J Ophthalmol. 2002;86:997-1001.
11. Khairy HA, Atta HR, Green FD, van der Hoek J, Azuara-Blanco A. Ultrasound biomicroscopy in deep sclerectomy. Eye. 2005;19:555-560.
12. Ciancaglini M, Carpineto P, Agnifili L, Nubile M, Fasanella V, Mattei PA, Mastropasqua L. Conjunctival characteristics in primary open angle glaucoma and modifications induced by trabeculectomy with mitomycin C: an in vivo confocal microscopy study. Br J Ophthalmol. 2009;93:1204-1209.
13. Yamamoto T, Sakuma T, Kitakawa Y. An ultrasound biomicroscopic study of filtering blebs after mitomycin C trabeculectomy. Ophthalmology. 1995;102:1770-1776.

14. Konstantopoulos A, Hossain PH, Anderson DF. Recent advances in ophthalmic anterior segment imaging: a new era for ophthalmic diagnosis? Br J Ophthalmol. 2007; 91: 551-557.
15. Singh M, Chew PT, Friedman DS, Nolan WP, See JL, Smith SD, Zheng C, Foster PJ, Aung T. Imaging of trabeculectomy blebs using anterior segment optical coherence tomography. Ophthalmology. 2007; 114:47-53.
16. Tominaga A, Miki A, Yamazaki Y, Matsushita K, Otori Y. The assessment of the filtering bleb function with anterior segment optical coherence tomography. J Glaucoma. 2010;9:551-5.
17. Kawana K, Kiuchi T, Yasuno Y, Oshika T. Evaluation of trabeculectomy blebs using 3-dimensional cornea and anterior segment optical coherence tomography. Ophthalmology. 2009;116:848-55.
18. Leung CK, Yick DW, Kwong YY, Li FC, Leung DY, Mohamed S, Tham CC, Chung-chai C, Lam DS. Analysis of bleb morphology after trabeculectomy with Visante anterior segment optical coherence tomography. Br J Ophthalmol. 2007;91:340-4.
19. Li Y, Shekhar R and Huang D. Corneal pachymetry mapping with high-speed optical coherence tomography. Ophthalmology. 2006; 113:792-799.
20. Messmer EM, Zapp DM, Mackert MJ, Thiel M, Kampik A. In vivo confocal microscopy of filtering blebs after trabeculectomy. Arch Ophthalmol. 2006;124:1095-103.
21. Mavracanas N, Mendrinos E, Shaarawy T. Postoperative IOP is related to intrascleral bleb height in eyes with clinically flat blebs following deep sclerectomy with collagen implant and mitomycin. Br J Ophthalmol. 2010;94:410-413.